UC Irvine
UC Irvine Electronic Theses and Dissertations

Title
Boundary Layer Flashback of Turbulent Premixed Jet Flames at Elevated Pressures and Temperatures

Permalink
https://escholarship.org/uc/item/5386b8gx

Author
Kalantari, Alireza

Publication Date
2018

Peer reviewed|Thesis/dissertation

eScholarship.org Powered by the California Digital Library
University of California

UNIVERSITY OF CALIFORNIA,
IRVINE

Boundary Layer Flashback of Turbulent Premixed Jet Flames at Elevated Pressures and Temperatures

DISSERTATION

submitted in partial satisfaction of the requirements
for the degree of

DOCTOR OF PHILOSOPHY

in Mechanical and Aerospace Engineering

by

Alireza Kalantari

Dissertation Committee:
Professor G. Scott Samuelsen, Chair
Professor Vincent McDonell
Professor Derek Dunn-Rankin

2018

© 2018 Alireza Kalantari
Chapter 2 © 2017 Elsevier Ltd. All rights reserved

DEDICATION

To my beloved parents, Farzaneh and Manouchehr, and my brother, Mohammad

Words cannot express how grateful I am for your endless love, support, and encouragement. You have always inspired me and stood behind me throughout my life.

To my lovely wife, Razieh for your unconditional love, support, and care

You have always been on my side and I am grateful to have you in my life.

Table of Contents

LIST OF FIGURES

LIST OF TABLES

NOMENCLATURE

Latin Symbols

D	Burner head diameter
Da	Damköhler number
f	Darcy friction factor
F	Fraction of stoichiometric
g	Velocity gradient
g_c	Critical velocity gradient
l_t	Turbulence length scale
Le	Lewis number
m	Pressure exponent of equivalence ratio
n	Reaction order
P_0	Reference pressure, 1 atm
P_u	Ambient pressure
Pe	Peclet number
Pr	Prandtl number
r	Radial distance
R	Burner head radius
Re	Reynolds number
Re_τ	Friction Reynolds number
S_f	Laminar flame velocity profile
S_L	Laminar flame speed
T_0	Reference temperature, 300 K
T_u	Unburned reactants temperature
u_τ	Shear velocity
u^+	Dimensionless velocity
$\overline{U}$	Mean axial velocity
$\overline{U}_f$	Mean flashback velocity
u_t'	Integral velocity fluctuations

y^+	Wall units

Greek Symbols

α	Thermal conductivity
δ	Flame thickness
δ_p	Penetration distance
δ_q	Quenching distance
θ	Angle between two beams
λ	Wavelength
μ_u	Unburned reactants viscosity
ν	Kinematic viscosity
Π	Non-dimensional group
τ_w	Wall shear stress
ϕ	Equivalence ratio
ϕ_f	Equivalence ratio at flashback

Acronyms

BR	Blockage Ratio
CFD	Computational Fluid Dynamics
CIVB	Combustion Induced Vortex Breakdown
DNS	Direct Numerical Simulation
LDV	Laser Doppler Velocimetry
LES	Large Eddy Simulation
MTG	MTG Micro Turbine Generator
Nd:YAG	Neodymium-Doped Yttrium Aluminum Garnet
NG	Natural Gas
PIV	Particle Image Velocimetry
PLIF	Planar Laser-Induced Fluorescence
RANS	Reynolds-Averaged Navier–Stokes
rms	Root Mean Square

ACKNOWLEDGMENTS

I would like to acknowledge the support from the U.S. Department of Energy through a University Turbine Systems Research grant (Contract No. DE-FE0011948).

I would like to express my deepest gratitude to my advisors at the UCI Combustion Laboratory Professors G. Scott Samuelsen and Vincent McDonell. Besides offering great academic advising, they have been supportive, understanding, and encouraging throughout my Ph.D. This work would have not been possible without their guidance.

I also thank Professor Derek Dunn-Rankin for serving on my dissertation committee and providing valuable comments.

I want to appreciate the assistance of Dr. Elliot Sullivan-Lewis regarding the experiment setup and test plan. Special thanks to Dr. Zhixuan Duan for his contribution to the data interpretation and overall work. Thanks to Richard Hack and Max Venaas for ensuring the safe operation of UCI combustion facilities.

CURRICULUM VITAE

Alireza Kalantari

UCI Combustion Laboratory
Department of Mechanical and Aerospace Engineering
University of California, Irvine
alirezak@uci.edu

Educational Background

- **University of California Irvine** **(2013-2018)**
  Department of Mechanical and Aerospace Engineering
  Ph.D. in Mechanical and Aerospace Engineering
  Total cumulative **GPA: 4 / 4**
  Title of Dissertation: "*Boundary Layer Flashback of Turbulent Premixed Jet Flames at Elevated Pressures and Temperatures"*
  Under supervision of *Prof. Scott Samuelsen and Prof. Vince McDonell*

- **University of Tehran, Iran** **(2010-2012)**
  Department of Mechanical Engineering
  M.Sc. Student in Mechanical Engineering (Thermal-Fluid Sciences)
  Total cumulative **GPA: 4 / 4**
  Title of M.Sc. Thesis: "*Numerical Investigation of Peristaltic Flow in Curved Channels Considering Non-Newtonian Fluids*"
  Under supervision of *Prof. Kayvan Sadeghy and Prof. Alireza Riasi*

- **University of Tehran, Iran** **(2005-2010)**
  Department of Mechanical Engineering
  B.Sc. in Mechanical Engineering
  Total cumulative **GPA: 3.9 / 4**

Honors & Awards

- **Best Paper Award**, American Society of Mechanical Engineers, Turbomachinery Technical Conference **(2017)**
- **Student Award**, American Society of Mechanical Engineers, International Gas turbine Institute **(2016)**
- **Student Scholarship**, Combustion Energy Frontier Research Center, Combustion Summer School, Princeton University **(2015, 2016)**
- **Graduate Student Fellowship**, University of California Irvine, Department of Mechanical Engineering **(2013)**
- **Ranked 1st** among the **M.Sc. students** in Mechanical Engineering, University of Tehran **(2012)**
- **Ranked 19th** in the national **Ph.D.** qualification exam for Mechanical Engineering, Energy Conversion, Iran (**2012)**

- Awarded **Full Scholarship** for B.Sc. and M.Sc. Study, University of Tehran, Department of Mechanical Engineering **(2005-2012)**
- **Ranked 100th** among more than 20000 participants in **the National Graduate Study Exam** in the field of Mechanical Engineering, Iran **(2010)**
- Obtained **the Highest Total Cumulative GPA** out of 130 of **B.Sc. students** in Mechanical Engineering, University of Tehran **(2010)**
- **Ranked 17th** in Fourteenth **National Scientific Olympiad** in Mechanical Engineering, Iran **(2009)**

Journal Articles & Conference Papers

- **Kalantari, A.**, McDonell, V., "*Boundary Layer Flashback of Non-Swirling Premixed Flames: Mechanisms, Fundamental Research, and Recent Advances*", Journal of Progress in Energy and Combustion Science, 2017.
- **Kalantari, A.**, Sullivan-Lewis, E., McDonell, V., "*Application of a Turbulent Jet Flame Flashback Propensity Model to a Commercial Gas Turbine Combustor*", Journal of Engineering for Gas Turbines and Power, 2017.
- Hoferichter, V., Hirsch, C., Sattelmayer, T., **Kalantari, A.**, Sullivan-Lewis, E., and McDonell, V., "*Comparison of Two Methods to Predict Boundary Layer Flashback Limits of Turbulent Hydrogen-Air Jet Flames*", Journal of Flow, Turbulence and Combustion, 2018.
- **Kalantari, A.**, Sullivan-Lewis, E., McDonell, V., "*Flashback Propensity of Turbulent Hydrogen-Air Jet Flames at Gas Turbine Premixer Conditions*" Journal of Engineering for Gas Turbines and Power, 2016.
- **Kalantari, A.**, McDonell, V., Samuelsen, S., "*Towards Improved Boundary Layer Flashback Resistance of a 65kW Gas Turbine with a Retrofittable Injector Concept*", Proceedings of ASME Turbo Expo 2018, GT2018-75834.
- **Kalantari A.**, Sullivan-Lewis E., McDonell V., "*Application of a Turbulent Jet Flame Flashback Propensity Model to a Commercial Gas Turbine Combustor*", Proceedings of ASME Turbo Expo 2016, GT2016-58059.
- Duan, Z., **Kalantari, A.**, Mcdonell, V., "*Parametric Analysis on Flashback Propensity with Various Fuel Compositions and Burner Materials*", Proceedings of ASME Turbo Expo 2015, GT2015-43629.
- **Kalantari, A.**, Sullivan-Lewis, E., Mcdonell, V., "*Analytical and Experimental Analysis of Flashback Propensity at Elevated Pressures and Temperatures*", 9th U. S. National Combustion Meeting.
- **Kalantari, A.**, Riasi, A., and Sadeghy, K., "*Peristaltic Flow of Giesekus Fluids through Curved Channels: an Approximate Solution*", Journal of Society of Rheology: Japan, 2014.
- **Kalantari, A.**, Sadeghy, K., and Sadeqi, S., "*Peristaltic Flow of Non-Newtonian Fluids through Curved Channels: a Numerical Study*", Annual Transactions of the Nordic Rheology Society, 2013.

Technical Reports

- **Kalantari, A.**, Sullivan-Lewis, E., McDonell, V., "*Development of Criteria for Flashback Propensity in Jet Flames for High Hydrogen Content and Natural Gas Type Fuels*", US Department of Energy Office of Fossil Energy, Contract Number: FE0011948, Technical Report, 2016.
- **Kalantari, A.**, Colorado, A., McDonell, V., "*Effect of Variable Fuel Composition on Emissions and Lean Blowoff Stability Performance*", California Energy Commission, Publication Number: CEC-500-2017-026, Technical Report, 2017.

ABSTRACT OF THE DISSERTATION

Boundary Layer Flashback of Turbulent Premixed Jet Flames at Elevated Pressures and Temperatures

By

Alireza Kalantari

Doctor of Philosophy in Mechanical and Aerospace Engineering

University of California, Irvine, 2018

Professor G. Scott Samuelsen, Chair

Carbon emissions from the combustion of fossil fuels are a concern within the power generation sector. As a result, while natural gas is currently plentiful, strategies for using fuels derived from renewable sources (i.e., alternative fuels) must still be pursued if a reduction in carbon signature is to be achieved. Many of these potential fuels contain some level of hydrogen. The combustion of high hydrogen content fuels reduces carbon-containing pollutants. However, NOx emissions are still an inevitable result of fuel/air combustion. Hence, lean premixed combustion of hydrogen-rich fuels has been implemented along with a precise control of combustion temperatures to achieve a reduction in all pollutant species. This technology is well established for gas turbines operating on natural gas, while the combustion of alternative fuels faces additional challenges. Hydrogen-rich fuels are particularly prone to flashback.

Boundary layer flashback of a premixed jet flame has been investigated experimentally under turbulent flow conditions at elevated pressures and temperatures (i.e., 3 to 8 atm and 300 to 600 K). The data presented in this study are for hydrogen fuel at various Reynolds numbers, which are representative of gas turbine premixer conditions and are significantly higher than results currently available in the literature. Three burner heads constructed of different materials (stainless steel, copper, and zirconia ceramic) were used to evaluate the effect of tip temperature, a parameter found to be an important factor

in triggering flashback. This study adds insight towards understanding of boundary layer flashback at high pressures. To confirm the accuracy and consistency of the results, similar experiments were conducted at the same operating conditions for a commercially available injector from a micro turbine combustor. In addition, this study characterizes flashback systematically by developing a comprehensive non-dimensional model which takes into account all effective parameters in boundary layer flashback propensity. The model developed using the high pressure test rig is able to predict flashback tendencies for the new data as well as the existing data in the literature, including a commercial gas turbine engine and can thus serve as a design tool for identifying when flashback is likely to occur for a given geometry and condition.

Chapter 1 - Introduction

1.1 Overview

Pollutant emission from combustion engines is currently a concern for industry and is a primary factor in engine design. Premixed lean combustion is a practical method to reduce emissions through precisely controlling combustion temperatures. Modern premixed gas turbines operate over a relatively narrow range of primary zone combustion temperatures (often close to the lean blow off limit) in order to avoid conditions with high rates of pollutant production. At such lean conditions, fuel variability is a significant operational problem for gas turbine engines. Hence, flame stability and operating range are important issues in the gas turbine industry. Due to the high degree of mixing required to minimize primary zone temperature variations, the premixer design plays a key role in the resulting emission performance.

Syngas compositions substantially change the flame behavior. Considering the narrow operating range of the combustor to meet all requirements, further attention needs to be given to addressing the operability issues (e.g. lean blow off, flashback, dynamic stability) associated with alternative fuels. In the case of high hydrogen content fuels, curtailing the high propensity for flashback is of primary concern. Gas turbines fed by high hydrogen content fuels are especially prone to flashback due to high flame speed and small quenching distance associated with these fuels. Flashback occurs when the flame propagates from the combustion zone into premixing section of combustor. Flashback causes significant damage to the premixer, and if it is not arrested immediately, can deteriorate the entire combustor. Flame flashback into a premixer is characterized by at least four mechanisms: flashback in the core flow, flashback due to flame instabilities, combustion induced vortex breakdown (CIVB), and flashback in the wall boundary layer. The boundary layer mechanism is considered the primary mode of flashback for jet flames, which are the focus of this research.

1.2 Goals and Objectives

In a gas turbine engine, the combustor operates at elevated pressures and temperatures as well as high Reynolds number, which are primarily determined by the compressor exit. To incorporate the use of hydrogen-rich fuels in gas turbines, flashback needs to be well understood at gas turbine premixer conditions. The prior studies conducted under atmospheric pressure cannot be generally applied to gas turbines without validation. Indeed, the combustion characteristics of hydrogen-rich fuels are strongly affected at high pressure and high turbulent Reynolds number. In addition, designing a robust combustion system operating on hydrogen-rich fuels cannot be achieved without predicting flashback tendencies. Hence, developing a criteria for flashback propensity of hydrogen-rich fuels is also required.

It is noted that despite extensive experimental studies in the past, no comprehensive study has fully examined the boundary layer flashback of turbulent hydrogen jet flames at high pressures. The present research addresses the boundary layer flashback of hydrogen-air premixed jet flames at gas turbine premixer conditions. Burner heads constructed from different materials are investigated and effects of thermal coupling between the burner and flame is also considered. Hence, the goals of the present work are to (1) address this knowledge gap by obtaining new data at gas turbine relevant conditions, (2) develop and apply a comprehensive design tool for predicting boundary layer flashback based on applying generalized non-dimensional analysis. The goals of this project were achieved by carrying out the following tasks:

Task 1: Experimental setup

Task 2: Flashback data acquisition

Task 3: Data analysis and correlation development

Chapter 2 - Background and Motivation[1]

The combustion of fossil fuels is expected to play a key role as a power generation source in the foreseeable future. Petroleum and natural gas are an essential part of total power generation in many countries worldwide. Combustion driven engines are utilized to produce the required energy consumption by residential, commercial and manufacturing sectors. Combustion engines, including gas turbines, not only have high reliability, but also offer an excellent load following ability [1,2]. Given the inherent advantages of gas turbines, they have been consistently evolving to improve efficiency while also using an increasingly variable fuel composition [1,3]. As manufacturers develop more robust gas turbines in terms of performance and stability, pollutant emission remains a key concern. Environmental awareness has prompted development of combustion systems with remarkably low pollutant emission levels [4,5]. To achieve this goal, premixed combustion is implemented along with a precise control of the temperature inside the combustor [1,3,6]. The pollutant emission of a gas turbine is significantly controlled by decreasing temperature spatial variation and operating within the lean combustion limit. However, operability issues including lean blow-off, auto-ignition, flashback, and dynamic stability are challenging due to the intrinsic characteristics of premixed flames [1,3,6]. Current gas turbines operate within a narrow range of fuel/air ratio to avoid these aforementioned problems. As a result, the operating range of an engine must be determined for various fuels prior to its design and development. Experimental data, theories, and numerical modeling can effectively contribute to evaluate the combustion characteristics under various operating conditions. Operability issues in an engine can cause severe damage to the engine and the stability of the combustion system has been extensively studied in past few decades to address this problem [6,7].

[1] Portions from https://doi.org/10.1016/j.pecs.2017.03.001, © 2017 Elsevier Ltd. All rights reserved

In recent years, the ability to extract natural gas using advanced hydraulic fracturing technology has led to an abundance of this fuel [8,9]. Natural gas is appealing due to its inherently low emissions compared to liquid and solid fossil fuels. However, the combustion of all fossil derived hydrocarbons generates pollutants including CO, unburned hydrocarbons (UHC), particular matter (C), and especially CO_2, a greenhouse gas produced by complete combustion of fuel. As a result, while natural gas is currently plentiful, near term strategies for using fuel derived from renewable sources (e.g., alternative fuels) must still be pursued if a reduction in carbon signature is to be achieved [10]. Using alternative fuels is an important step providing a realistic solution toward resolving a long term problem. For example, the combustion of hydrogen eliminates the direct generation of carbon species. Steam reforming of natural gas is a common method of hydrogen production [11,12] in which hydrogen-rich content fuels can be derived and combusted in a gas turbine while allowing management of the associated carbon [13]. In terms of coal as a fuel, integrated gasification combined cycle (IGCC) represents a technology to manage CO_2 emission for clean coal applications [14,15]. The synthesis gas produced through the IGCC process contains mainly hydrogen and carbon monoxide, the latter of which can be further shifted to H_2 and CO_2 through reactions with water [13]. The captured CO_2 can be transported and stored in suitable places, playing an important role in reducing greenhouse emission and mitigating climate change [16,17]. Hydrogen can also be produced renewably via electrolysis of water using electricity generated by wind or photovoltaic [18]. This hydrogen can be added to the existing natural gas infrastructure or combusted directly.

In light of these developments with increased consideration for carbon management, it is apparent that fuel flexibility remains a key consideration for gas turbine systems. It also underscores the importance of high hydrogen content fuels [19] for which the fuel/air mixture preparation and subsequent combustion behavior needs to be well understood. It is clear that syngas composition changes the flame behavior [6].

Of particular relevance to lean premixed gas turbines combustion systems is determination of how fuel composition impacts flashback propensity.

Flashback has been the subject of many studies in the past few decades. This section summarizes the major findings from research dating to the 1940's, when a systematic experiment was developed to investigate boundary layer flashback. Furthermore, recent progress, technical challenges, and recommendations for future studies are discussed. Despite the fact that prediction of flashback propensity is crucial to overcome the operability issues associated with gas turbines, the lack of a comprehensive study to summarize all observations, conclusions, and theories developed in the past is still apparent.

2.1 Flashback Mechanisms

Flashback occurs when the flame propagates from the combustion zone into the premixing section of the combustor. Flame flashback significantly increases the temperature inside the premixer, which is not originally designed for this purpose. Furthermore, if the flame anchors within the wake of existing geometric features inside the premixer passage ways, it can cause serious damage to the engine. Flashback in gas turbine premixers can occur as a result of at least four mechanisms [6,20,21]: (1) core flow flashback, (2) combustion instability induced flashback, (3) combustion induced vortex breakdown (CIVB), and (4) boundary layer flashback. Each is briefly introduced for context.

2.1.1 Core Flow Flashback

Flame propagation in the core flow occurs when the turbulent burning velocity exceeds the local flow velocity in the core flow [6,20]. The turbulent burning velocity magnitude plays the main role in triggering the core flow flashback and is a function of turbulent-flame interaction as well as chemical kinetics [22]. As a result, the fuel composition and turbulence structure are essential parameters for determining the core flow flashback limits [23,24]. A typical combustor is designed to avoid core flashback by simply

increasing the axial velocity. However, common flame stabilization methods used in practical devices may lead to core flashback. For instance, swirl significantly decreases the local axial velocity component. In addition, flame stretching caused by the vortex-flame interaction increases the turbulent flame speed [25–27]. Consequently, these two effects, higher turbulent flame speed and lower flow axial velocity, can lead to core flow flashback.

The key characteristics of core flashback is the turbulent burning velocity which has been extensively studied in the literature and is often presented as a function of laminar flame speed and turbulence characteristics [28–31]. Fuels with higher flame speed, such as hydrogen, increase the potential risk of flashback compared to natural gas. Several correlations for turbulent burning velocity have shown promise as a prediction tool for core flow flashback [22,32]. However, these correlations cannot be generally extended to various fuels since the turbulent burning velocity is strongly dependent upon fuel compositions [23,24]. In addition, different concepts associated with the definition of turbulent burning velocity result in different values, which also contributes to inconsistency among the existing data in the literature and challenges in interpretation [22].

2.1.2 Combustion Instability Induced Flashback

Flashback due to combustion instability occurs as a result of large amplitude fluctuations of the flow field [6,21]. Instabilities can be generated by the interaction of the acoustic modes, unsteady heat release, and flow structure. Pressure and velocity oscillations associated with the instability can induce the flame movement and generate large vortices leading to the flow reversal [33], which can potentially result in flashback. Figure 2.1 indicates the instability of the flame stabilized by backward-facing step [33]. The pulsation cycle of the flow structure leads to the lifting of the flame from the edge of step and eventually triggers flashback. A large eddy simulation (LES) performed by Thibaut et al. [21] investigated the flashback induced by the flame instability. The interactions between acoustic, turbulence, and combustion

were effectively captured by imposing an external velocity modulation at the inlet of the computational domain, illustrated in Figure 2.2. As the flow reversal is enhanced by the instability process, the flame propagates upstream of the step.

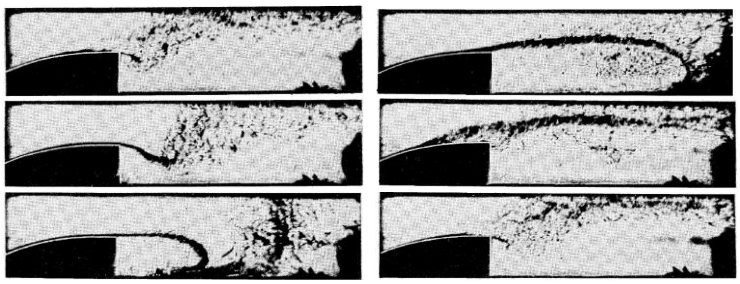

Figure 2.1: Combustion instability of a backward-facing step and cyclic process of the flame-flow interaction investigated by Keller et al. [33].

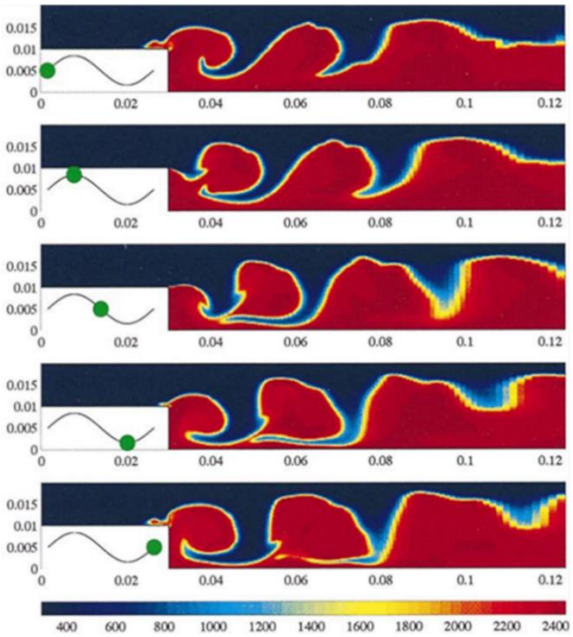

Figure 2.2: Temperature distribution of premixed flames stabilized by a backward-facing step obtained from two-dimensional LES [21].

2.1.3 Combustion Induced Vortex Breakdown

CIVB flashback is a prevalent mechanism in swirl stabilized gas turbine combustors. Vortex breakdown is a unique characteristic of swirling flows and depends on the swirl number, which describes the relative amount of swirl strength. If the swirl number is above a critical value, it leads to generation of vortex

breakdown [34,35]; otherwise reverse flow would not occur. An increase in azimuthal velocity relative to axial velocity causes vortex breakdown and creation of a reverse flow region. Vortex break down is an abrupt change in the vortex structure leading to the formation of a stagnation point and recirculation region downstream of it. In a study by Konle et al. [36], particle image velocimetry (PIV)-laser induced fluorescence (LIF) measurements with high temporal resolution identified the formation of a closed bubble at the tip of the internal recirculation zone, which is induced by small changes of the flow field as indicated in Figure 2.3. Positive vorticity generated by the volumetric expansion tends to move the bubble downstream and stabilizes the flame; however, the baroclinic torque produces negative vorticity, enhancing the negative axial velocity and causing the upstream propagation of the bubble [37–40].

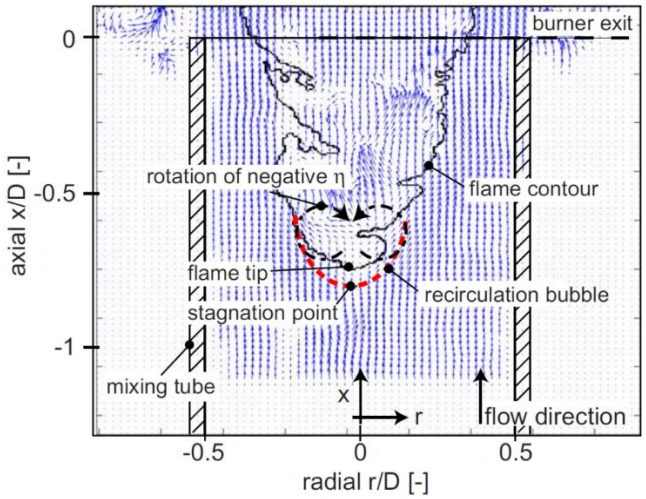

Figure 2.3: Instantaneous image showing the location of the flame front relative to the recirculation bubble studied by Konle et al. [36,41].

A competition between the volume expansion and baroclinic toques dictates the movement of the bubble and determines whether fast flame propagation occurs. The position of flame front relative to the recirculation bubble was observed to be a critical parameter in triggering CIVB flashback [36]. A flame front located downstream of the stagnation point provides a favorable condition for the generation of reverse flow caused by baroclinic torque. However, if the flame anchors upstream of the stagnation point, the volume expansion term compensates for an increase of baroclinc torque. Indeed, the flame tip

location needs to be downstream of the stagnation point in order to propagate upstream; otherwise, the flame remains stable. For the former case, the bubble propagates upstream under special circumstances and moves the flame front into the premixing zone, which can then lead to flashback.

A number of experimental studies investigated the effects of syngas compositions on CIVB flashback. Various fuel compositions, representing actual syngas mixtures [42] have been considered, and the results indicate that fuels with higher hydrogen concentration tends to have higher propensity for flashback via the CIVB mechanism. In general, for swirl stabilized systems, it is noted that (1) flashback characteristics depends on the swirl number and (2) multiple flashback mechanisms may result depending on swirl strength which creates some challenges in interpreting flashback for these systems. Some work has also been directed at this issue by varying the swirl number and indicated that the upstream flame propagation speed was significantly different based on flashback mechanisms [43].

2.1.4 Boundary Layer Flashback

Boundary layer flashback is considered the primary mechanism of flashback in jet/Bunsen flames and has been studied extensively in the literature. The free stream velocity of a gas turbine premixer during regular operating conditions exceeds the turbulent flame speed. As a result, the upstream flame propagation cannot occur in the core flow region. But the flow velocity decreases close to the wall due to no-slip boundary condition and this can be a potential route for the onset of flashback. The burning velocity also decreases near the so called “quenching distance” where the reaction cannot sustain itself due to heat loss or flame stretch [44–46]. Hence, flashback occurs at a location where the local burning velocity is large enough to overcome the local flow velocity near the wall. Boundary layer flashback has been characterized by the “critical velocity gradient” concept in the literature [47]. The critical velocity gradient corresponds to the bulk flow velocity at the condition of flashback and thus is an indicator of the flashback propensity of a mixture for a given condition. Boundary layer flashback has been studied under laminar

and turbulent flow conditions for different parameters including fuel/oxidizer composition, preheat temperature, operating pressure, burner material, and geometrical burner configuration. It is noted that the most recent research has focused on high hydrogen content fuels as interest in the use of low carbon fuels increases.

With a brief overview of known flashback mechanisms now provided, emphasis is now focused on the boundary layer mechanism which is the primary mechanism considered in this review.

2.2 Boundary Layer Flashback Mechanism

Figure 2.4 summarizes studies from 1943 to 2017 that address boundary layer flashback in non-swirling premixed flames, including published papers and technical reports.

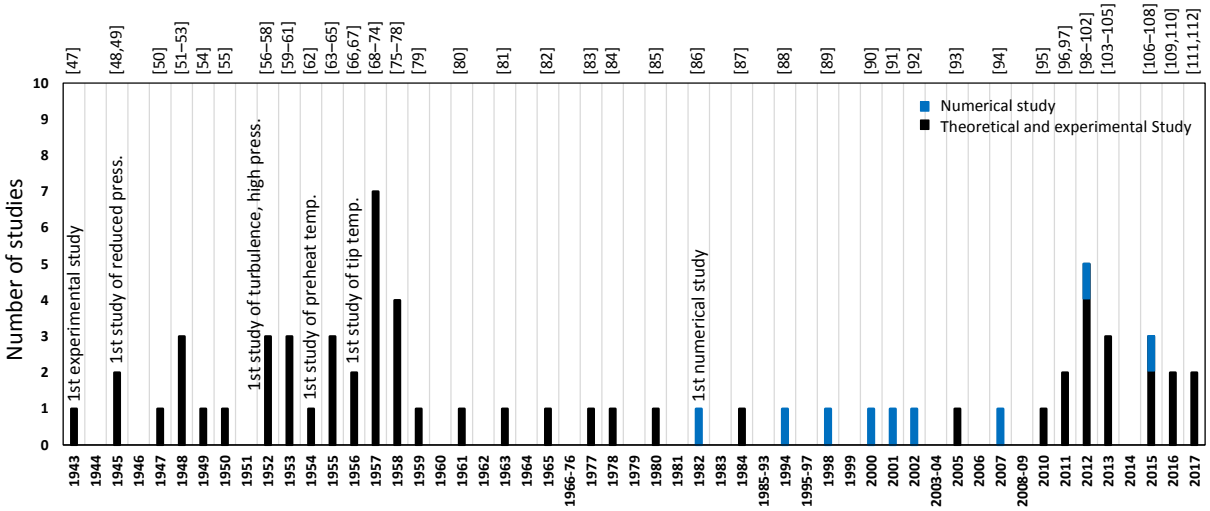

Figure 2.4: Number of studies per year addressing boundary layer flashback.

Lewis and Von Elbe first conducted a systematic experiment and developed a prediction model for boundary layer flashback [47]. Garside et al. carried out the first flashback experiment at sub-atmospheric pressure [49], while Edse first studied the turbulent boundary layer flashback at high pressure [56]. The effect of preheat temperature and tip temperature were first investigated by Grumer and Harris [62] and Bollinger and Edse [66], respectively. The first numerical study was conducted by Lee and T'ien [86] for propagation of a premixed laminar flame through a tube.

2.2.1 Simple Model for Boundary Layer Flashback Prediction

The critical velocity gradient model neglects the flame-flow interaction and assumes that the flow velocity remains undisturbed. Figure 2.5 indicates the flame front stabilized inside a burner close to the wall. The velocity profile of the unburned mixture $u(y)$ represents a laminar flow approaching the flame front. The flame speed denoted by $S_f(y)$ decreases close to the wall due to the heat loss and quenching of radicals. The flame is quenched at a certain distance from the wall and part of the flame close to the wall trails behind the central position as indicated in Figure 2.5 [47,48,63]. The quenching distance in Figure 2.5 is denoted by δ_q. The velocity gradient g at the wall in Eq. 2.1 is used to describe the flashback, in which τ_w is the shear stress and μ_u is the viscosity of the unburned mixture.

$$g = \left|\frac{\partial u}{\partial y}\right| = \frac{|\tau_w|}{\mu_u} \qquad \text{Eq. 2.1}$$

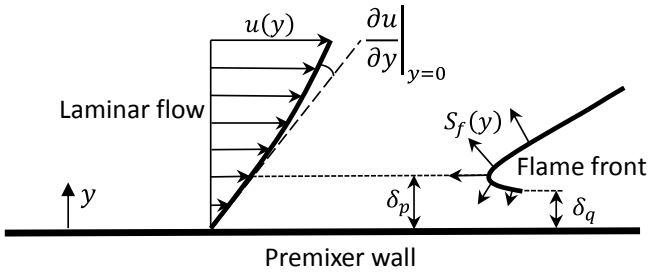

Figure 2.5: Schematic of the critical velocity gradient prediction model.

Based on this theory, flashback occurs when the flow velocity drops below the burning velocity somewhere in the flow field close to the wall. The location at which the burning velocity is equal to the flow velocity is defined as the penetration distance δ_p [113], indicated in Figure 2.5. The magnitude of the flow bulk velocity at the onset of flashback corresponds to the critical velocity gradient at the wall, g_c. Hence, the flame does not propagate as long as the velocity gradient is higher than this critical value (i.e., g_c).

To explain this concept in more detail, a tube burner is considered in which the flame stabilizes downstream of the burner rim. Figure 2.6 represents several flow conditions relative to the propagation of the flame into the tube [47]. The burning velocity is zero within the quenching distance and it gradually increases to its constant normal value corresponding to the one-dimensional laminar flame speed. Both quenching and penetration distances are indicated in Figure 2.6. Line (2) indicates the critical velocity gradient condition at which flashback is possible. As the flow velocity is decreased (line (1)), the flame flashes back and propagates upstream. However, if the flow velocity is further increased than the critical value (line (3)), the flame is swept out of the tube.

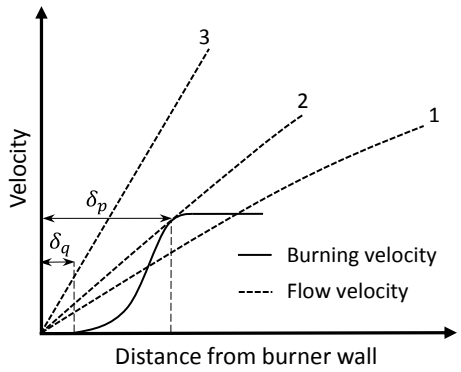

Figure 2.6: Critical velocity gradient model showing the flow velocity and burning velocity profiles at flashback condition, adapted from [47].

The velocity gradient at the wall is approximated by the ratio of the flow velocity to the penetration distance as follows in Eq. 2.2. This is based on the assumption that the flow velocity remains linear close to the wall.

$$g_c = \frac{u|_{y=\delta_p}}{\delta_p} \qquad \text{Eq. 2.2}$$

The flow velocity at the penetration distance is equal to the burning velocity at the critical condition. Furthermore, the burning velocity magnitude at the penetration distance is assumed to be close to its normal value and can thus be approximated by the laminar flame speed S_L [47]. The laminar flame speed

is calculated based on the one-dimensional steady flow assumption. With these simplifications, Eq. 2.2 reduces to:

$$g_c = \frac{S_L}{\delta_p} \qquad \text{Eq. 2.3}$$

For fully developed laminar flow in a pipe with the radius of *R*, the velocity gradient can be analytically determined from Eq. 2.4.

$$u(r) = 2\overline{U}\left(1 - \left(\frac{r}{R}\right)^2\right) \qquad \text{Eq. 2.4}$$

in which *r* is radial distance and $\overline{U}$ is the bulk flow velocity. Combining Eq. 2.3 with the derivative of Eq. 2.4 at the tube wall ($r = R$), Eq. 2.5 is obtained at flashback condition (see, also [53]):

$$g_c = \frac{S_L}{\delta_p} = \frac{4\overline{U}}{R} \qquad \text{Eq. 2.5}$$

The critical velocity gradient concept has been frequently used in the literature to characterize boundary layer flashback. It was used as a means to evaluate flashback propensity of a given fuel at different operating conditions. Regarding fuel composition impacts, it is evident that the influence of fuel composition on laminar flame speed and penetration distance can capture the effects.

While Eq. 2.3 was originally proposed to predict the flashback propensity of laminar flames [47], the concept was extended to turbulent conditions. For fully developed turbulent flow in a pipe upstream of location which the flame stabilizes, the velocity gradient is estimated from the Blasius correlations for smooth pipes with the diameter of D at a given Reynolds number Re [114]:

$$g = \frac{1}{8}\frac{f\overline{U}^2}{\nu} \qquad \text{Eq. 2.6}$$

$$f = \frac{0.3164}{Re^{0.25}}, \qquad 4 \times 10^3 < Re < 10^5 \qquad \text{Eq. 2.7}$$

$$g = 0.03955\, Re^{0.75} \frac{\overline{U}}{D} \qquad \text{Eq. 2.8}$$

in which f and ν are friction factor and kinematic viscosity, respectively. Eq. 2.3 and Eq. 2.8 are used together to determine the flashback propensity of turbulent flames [63].

The only parameter not fully described in this simple analysis is the penetration distance for a specific fuel or distance from the wall at which the flow velocity is equal to the burning velocity. Indeed, the penetration distance in Eq. 2.3 needs to be determined in order to predict flashback propensity of different fuel compositions. The overall variation of penetration distance is considered to be proportional to the quenching distance, as frequently reported in the literature [48,51,61,69,76,82,85]. Flame quenching near the wall can be categorized into three situations: (1) quenching between two parallel plates or inside a tube, (2) head-on quenching, and (3) sidewall quenching. The first quenching type is defined as a minimum distance between two parallel plates (or minimum tube diameter) at which the flame can propagate through the channel (or tube). Many experimental studies have been conducted to investigate the relation between the passage characteristic dimension as a function of fuel variation, equivalence ratio, pressure, wall temperature, and material. It is difficult to isolate the effect of one variable since all parameters are coupled and cannot be changed independently. Nevertheless, different studies have tried to address this problem by investigating various parameters [44,115–117] and finding empirical relations [118–121].

The measurement of quenching distance for a single wall is more complicated. Head-on quenching is defined as the flame propagates perpendicular to the wall (studied in [122–125]) as indicated in Figure 2.7, while for sidewall quenching, the flame propagates parallel to the cold wall [45,46,126]. In boundary layer flashback, the flame propagates upstream along the wall in which the sidewall quenching plays an

important role. However, it is noted that the quenching distance between two parallel plates (or inside a tube) has been used in the literature to characterize boundary layer flashback [48,51,69,76,85].

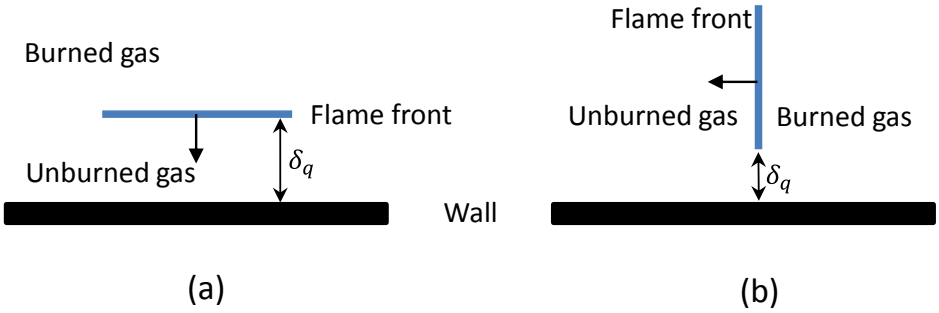

Figure 2.7: Flame-wall interaction: (a) head-on quenching and (b) sidewall quenching.

The critical velocity gradient model originally developed neglects flame-flow interaction which is a significant simplification. As suggested in Figure 2.6, the flow velocity profile at the onset of flashback was assumed to not be influenced by the flame. In addition, the burning velocity profile is assumed to only be affected by the wall and consideration of quenching distance. Yet this approach has been widely implemented in the literature and has proven capable of correlating the experimental data for laminar and certain types of turbulent flames, as will be shown in Sections 2.3 and 2.4, respectively.

2.2.2 Underlying Physics of Boundary Layer Flashback

More recent experimental and numerical simulations reveal that the flame-flow interaction near the wall can have a significant effect on flow velocity distribution for both laminar and turbulent flows at the onset of flashback [99,100,106,108]. In practical devices, the premixed fuel/air mixture is injected into the combustor by the burner premixer. At normal operating conditions, the flame stabilizes past the burner rim due to the sudden expansion as the flow is injected from the burner into the combustion chamber. The schematic of the stable flame front is shown in Figure 2.8(a). When the boundary layer flashback limit is reached, the flame propagates upstream into premixed reactants, indicated in Figure 2.8(b).

As a result, it is apparent that two regimes must be considered for physical interpretation and modeling. The first is the regime prior to transition of the stabilized flame at the burner rim into the injector. This regime is labeled as an “unconfined flame” situation. Once the flame enters the premixer/injector and propagates upstream along the wall, the underlying physics of the problem are different. This second regime is labeled as a “confined flame” throughout this chapter.

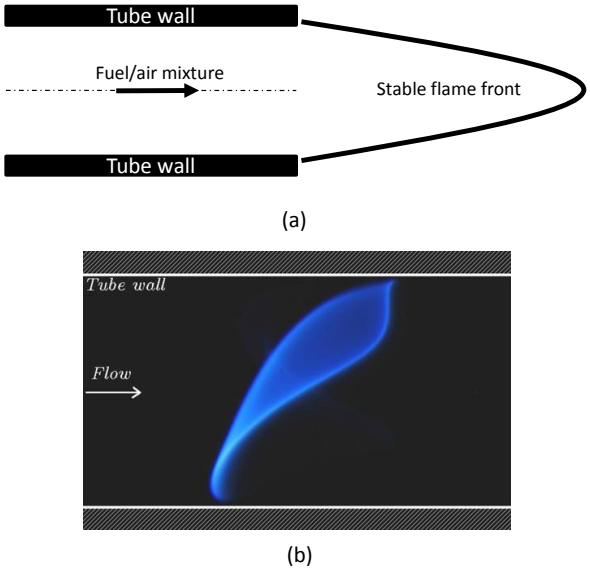

Figure 2.8: Flame configuration: (a) unconfined flame stabilized downstream of the premixer tube and (b) confined flame stabilized in a tube [94].

Until the transition of the unconfined flame from the burner rim into the premixer tube, the flame does not strongly affect the velocity distribution of the incoming flow and the flow velocity profile upstream of the flame front remains approximately undisturbed as experimentally observed and discussed in [106]. This is the main reason why the critical velocity gradient concept originally conceived was able to characterize boundary layer flashback propensity, especially under laminar conditions.

However, once the flame propagates into the burner (confined flames), the basic assumption of the critical velocity gradient concept is not valid [99,100]. The flow-flame interaction near the wall-region for confined flames cannot be neglected. The flame is strongly curved towards the unburned mixture as flame

propagates upstream leading to a divergence of streamlines and adverse pressure gradient. When the gas expansion is large enough relative to the local flow velocity near the wall, it can cause the boundary layer separation as discussed in more detail in Section 2.4.4.

2.2.3 Parameters Impacting Boundary Layer Flashback

Many parameters impact flashback propensity; as a result, isolating the effect of a specific variable is difficult. In general, all parameters can be categorized into the following groups:

- Flow and combustion characteristics
- Operating conditions
- Flame configuration and boundary layer heating

How each impacts flashback propensity is discussed in the sections below.

2.2.3.1 Flow and Combustion Characteristics

The flow bulk velocity directly impacts boundary layer flashback by changing the streamwise momentum near the wall-region. As the mean flow velocity increases, the local flame speed must increase in order to propagate upstream. Hence, flashback propensity occurs at fuel/air ratios nearer to those associated with the highest flame speed as the bulk flow velocity increases. Furthermore, the velocity profile of the incoming flow, where the flame stabilizes, affects the flashback limits. For instance, it was noted experimentally that when the incoming flow is not fully developed, the flashback propensity decreases due to the higher wall shear stress, which is a function of entrance length [83].

The boundary layer flashback limit is quite different under laminar and turbulent boundary conditions. The flame-wall interaction is more complex under turbulent conditions [127,128]. Depending on the turbulent Reynolds number, the turbulent combustion regime dictates the flame structure and defines

how the small scale eddies interact with the flame [129,130]. Hence, the turbulent flame speed is also a function of turbulence intensity and consequently higher turbulence intensity results in higher flashback propensity [22].

Combustion characteristics of premixed flames are dependent upon the fuel composition. The mixture burning velocity plays a key role in triggering the flashback and is largely a function of chemical kinetic mechanisms. Furthermore, the thermal and radical quenching by the wall varies significantly with different fuel compositions which, in turn, leads to different flashback limits [48,57,65,69]. The high flashback propensity of hydrogen mixtures is a result of high burning velocity and small quenching distance. The flame propagation is enhanced for low Lewis number premixed flames as verified for various fuel compositions by experimental and numerical studies [131–136].

2.2.3.2 Operating Conditions

Pressure and preheat temperature are two important factors in boundary layer flashback. An increase in preheat temperature increases the burning velocity significantly [137]. Consequently, boundary layer flashback propensity increases for higher preheat temperatures, which will be discussed in detail in Section 2.3.3 and 2.4.3.

Boundary layer flashback experiments at high pressure are especially germane to gas turbine applications. Conclusions and results drawn from atmospheric pressure tests must be further verified at high pressure prior to any general conclusion for systems operated at elevated pressure. It is noted that the effect of sub-atmospheric pressures on flashback has been studied [67,70,76], but these results cannot be extended to elevated pressures as will be discussed in Section 2.4.3.

2.2.3.3 Flame Configuration and Boundary Layer Heating

Experimental results have indicated that the flame-flow interaction near the wall-region cannot be neglected for flames propagating through a channel (confined flames) [99,100]. As will be discussed in

Section 2.4.4.1, confined flames are more prone to flashback and the flame-wall interaction for confined flames has received considerable attention in recent years in both experimental and numerical modeling studies. When the flame propagates upstream in the confined configuration, the flame leading edge is convex towards the reactants, enhancing the flame stretch effect and causing the approach flow to decelerate.

Burner heads constructed from different materials show varying flashback propensity [66,98,103,104]. The effect of thermal coupling between the burner head and flame on flashback propensity has been found to be an important parameter. A qualitative relationship has been observed between flashback and the variables involved in the construction and operation of the burners [66,98,103,104]. The flame temperature and product species also vary with fuel composition, in turn influencing the heat transfer between the burner rim and flame front (see Figure 2.8(a)). This can cause the burner tip temperature to change depending on the fuel compositions for a given equivalence ratio. The heat is conducted upstream along the burner, causing the heat addition from the wall into the incoming reactants. The boundary layer heating leads to a point of inflection in the velocity profile, which can induce flow separation. As a result, flashback propensity is more pronounced for uncooled burners. Unsteady transitions in operating conditions (e.g. a sudden drop in reactant flow rates) can also trigger boundary layer flashback [138]. It is also noted that the flame, which does not initially flash back at a given condition, can eventually flash back after long periods of operation due to small perturbations which may lead to an increase in the premixer wall temperature.

Using an enclosure about an unconfined flame can also change the flashback propensity limits due to resulting recirculation regions in the sudden expansion region and change in the local heat transfer characteristics which will be explained in Section 2.4.2 [98,104].

2.3 Laminar Flames

Determination of limits for boundary layer flashback of laminar flames received much attention in the early literature. Different basic models and correlations, including Lewis and von Elbe's critical velocity concept, were developed in order to characterize the flashback propensity. These prediction models were used to compare the experimental results with various fuel compositions, preheat temperatures, and operating pressures. In addition, the sensitivity of flashback limit to the burner diameter, ranging from quenching limit to large values, was evaluated for different fuel/oxidizer mixtures. Numerical simulations of laminar flame provided more detail regarding the flame-flow interaction and have been used to reproduce the flashback limits obtained from experimental results. The detailed discussion is presented in following sections.

2.3.1 Prediction Models

As mentioned previously, Lewis and Von Elbe [47] developed the critical velocity gradient model to predict the flashback propensity of jet flames. The penetration distance of the flame near the wall calculated from Eq. 2.3 was found to be about the half of quenching distance of a flame through plane parallel plates and predicted to be one-third of quenching distance for cylindrical tubes. This concept was further developed by using non-dimensional parameters. Putnam et al. used Peclet numbers to present the critical velocity gradient model in non-dimensional form [52]. Peclet number represents the balance between the characteristic time scales of the flow and chemical reaction [52,139,140]. Based on this approach, flow and flame Peclet numbers are defined for a tube diameter of D in Eq. 2.9 and Eq. 2.10:

$$Pe_{flow} = \frac{D\bar{U}}{\alpha} \qquad \text{Eq. 2.9}$$

$$Pe_{flame} = \frac{DS_L}{\alpha} \qquad \text{Eq. 2.10}$$

where α is thermal diffusivity and $\overline{U}$ is the flow bulk velocity. In this model, the penetration distance (δ_p) is considered to be a multiple of the laminar flame thickness calculated from one-dimensional steady analysis as follows [141]:

$$\delta_p = K\frac{\alpha}{S_L} \qquad \text{Eq. 2.11}$$

in which *K* is an arbitrary constant. Substituting Eq. 2.11 in Eq. 2.5 and using *D* for the burner diameter, this equation is written as:

$$\frac{8\overline{U}}{D} = \frac{S_L^2}{K\alpha} \qquad \text{Eq. 2.12}$$

Multiplying both side of Eq. 2.12 by D^2 and dividing by α, this equation can be simplified to the non-dimensional form [52]:

$$Pe_{flow} = \frac{1}{8K}\left(Pe_{flame}\right)^2 \qquad \text{Eq. 2.13}$$

This approach assumes a linear velocity profile near the wall. Furthermore, the burning velocity is assumed to be equal to the one-dimensional laminar flame speed, which is not affected by the quenching in the vicinity of the tube wall. These assumptions were relaxed to improve the prediction model developed in [52]. Indeed, the penetration distance δ_p at which the flow velocity equals the flame speed is an unknown parameter and must be determined. Figure 2.9 illustrates the flow and flame velocity profiles at the onset of flashback. Parameter e denotes the distance from the wall at which the burning velocity starts falling as a parabolic curve to zero value at the distance, d. Therefore, the flame velocity profile close to the wall can be written as [52]:

$$S_f\,(r) = S_L\left(1 - \frac{(r+e-R)^2}{d^2}\right) \qquad \text{Eq. 2.14}$$

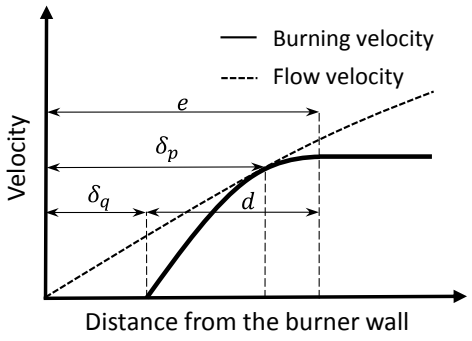

Figure 2.9. Schematic of the flame and flow velocity profiles for boundary layer flashback, adapted from [52].

in which r is the radial distance from the center of the tube with a radius of R. At the penetration distance, the flow velocity and flame speed are equal [52]:

$$u\left(r|_{\delta_p}\right) = 2\overline{U}\left(1-\left(\frac{r}{R}\right)^2\right) = S_f\ \left(r|_{\delta_p}\right) = S_L\left(1-\frac{(r+e-R)^2}{d^2}\right) \qquad \text{Eq. 2.15}$$

In addition, the flame and velocity profiles are tangent at the penetration distance as indicated in Figure 2.9 [52]:

$$\left.\frac{du}{dr}\right|_{\delta_p} = -4\frac{\overline{U}}{R^2}r = \left.\frac{dS_f}{dr}\right|_{\delta_p} = -2S_L\left(\frac{r+e-R}{d^2}\right) \qquad \text{Eq. 2.16}$$

The critical velocity at which flashback occurs is obtained by eliminating the r coordinate between Eq. 2.15 and Eq. 2.16, resulting in the following equation:

$$\left(\frac{2\overline{U}d}{S_L R}\right)^2 - \left(\frac{2\overline{U}d}{S_L R}\right)\left(\frac{d^2-e^2+2eR}{Rd}\right)+1=0 \qquad \text{Eq. 2.17}$$

If the ratio of *d/e* is assumed to be β and the distance *e* is approximated by the planar flame thickness ($K\alpha/S_L$), Eq. 2.17 is simplified to the non-dimensional form as:

$$Pe_{flow} = \frac{Pe_{flame}^2}{4K\beta^2}\left(1 - \frac{K}{Pe_{flame}}(1-\beta^2) - \sqrt{\left(1 - \frac{K}{Pe_{flame}}(1-\beta^2)\right)^2 - \beta^2}\right) \qquad \text{Eq. 2.18}$$

In this equation, it is assumed that $e \leq R \; or \; Pe_{flame}/K \geq 2$ and the flame velocity in the vicinity of the wall (e) is affected by the quenching effect. For the special case where β equals zero (meaning that the burning velocity abruptly drops to zero from the normal value), Eq. 2.18 is simplified to:

$$Pe_{flow} = \frac{Pe_{flame}^2}{8K}\left(\frac{1}{1 - \frac{K}{Pe_{flame}}}\right) \qquad \text{Eq. 2.19}$$

A similar equation was developed in [52] for $e > R \; or \; Pe_{flame}/K < 2$ in which the burning velocity at the centerline of the tube burner is influenced by the wall quenching.

Figure 2.10 shows the performance of the Peclet number analysis, Eq. 2.13, for ethylene/air [50], acetylene/oxygen [49], and natural gas [48]. The solid line in this figure represents $Pe_{flow} = 0.0125\left(Pe_{flame}\right)^2$ variation in logarithmic scales, where the slope of the trend line is equal to 2. As shown in Figure 2.10, good agreement between the model and data obtained using various fuels is apparent. However, for the simplified case (Eq. 2.19), the slope of log plot is always smaller than 2, depending on Pe_{flame}/K (see Eq. 2.20).

$$\frac{d\left(log\left(Pe_{flow}\right)\right)}{d\left(log\left(Pe_{flame}\right)\right)} = 2 - \frac{1}{Pe_{flame}/K - 1} \qquad \text{Eq. 2.20}$$

The Peclet number analysis can predict the limited data for the laminar flame stabilized beyond a tube burner exit. However, significant deviation is observed at small Peclet numbers in Figure 2.10. The authors mention several effects as the main reasons for the observed deviation [52]. Namely that the equations

derived do not take into account the difference between one-dimensional and two-dimensional heat transfer from the flame, the change in the flame front, and the change of the flow direction at the flame front. Furthermore, the quenching distance is dependent on the tube size and increases as the tube size decreases. A group of data at high Peclet numbers also deviates from the trend line in Figure 2.10 and this was associated with turbulent effects previously identified by von Elbe and Menster [48].

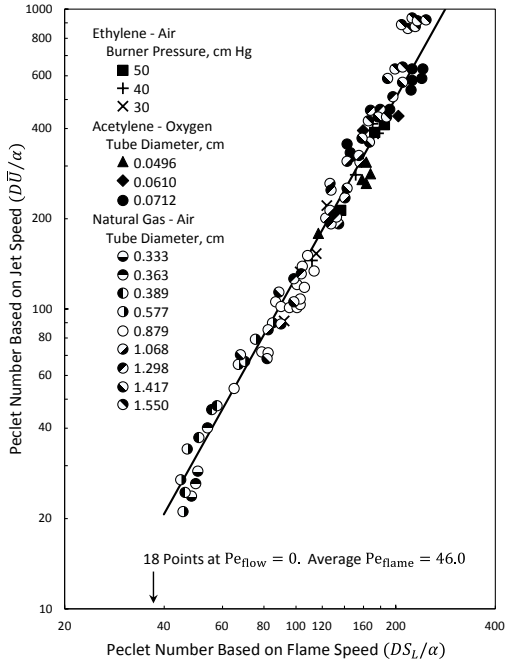

Figure 2.10: Peclet number non-dimensional analysis for boundary layer flashback, reproduced from [52].

Based on the conclusion made by Wohl et al. [61] who state that the penetration distance is proportional to flame thickness and quenching distance, Berlad et al. presented the critical velocity gradient model as a function of the quenching distance as follows [69]:

$$g_c = C\left(\frac{S_L}{\delta_q}\right) \qquad \text{Eq. 2.21}$$

The penetration distance used by Von Elbe and Mentser [48] is about the half of the quenching distance for flame quenching between parallel plates. Assuming the quenching distance of circular tube is about

1.5 times that of parallel plates, the constant *C* should be 3 from Von Elbe and Mentser [48]. The application of Eq. 2.21 was further examined using a wide variety of published experimental data for various fuels [44,47,48,60,61,63,142]. Figure 2.11 presents the variation of critical velocity gradient versus the ratio of laminar flame speed to the quenching distance for various fuels at different pressures, preheat temperatures, and equivalence ratios. Based on this study, the value of *C* is not constant and increases from 2.5 to 5 as g_c increases from 10 to 10^5 *1/s*. Hence, the constant *C* can be represented as function of g_c itself, resulting in a power law variation suggested in [69] (Eq. 2.22). This correlation is indicated by the solid line in Figure 2.11.

$$g_c = 14.125\left(\frac{S_L}{\delta_q}\right)^{1.168} \qquad \text{Eq. 2.22}$$

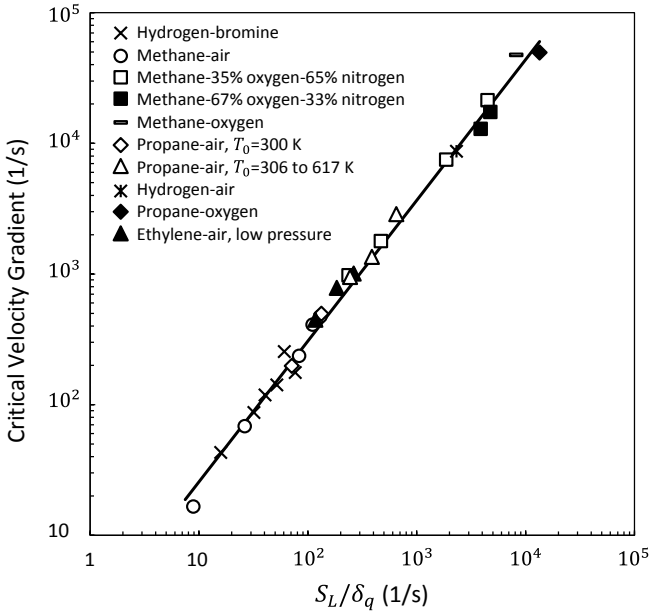

Figure 2.11: Critical velocity gradient variation using Eq. 2.22, reproduced from [69].

The effect of sub-atmospheric pressure on flashback was studied by Wohl [61]. The dependency of critical velocity gradient on pressure was determined from the original model developed in [47,48]. The

penetration distance is lower than the quenching distance and is approximated by the magnitude of the planar flame thickness δ_f as previously presented in Eq. 2.11.

$$g_c = \frac{S_L}{\delta_f} \qquad \text{Eq. 2.23}$$

The variation of the laminar flame speed and the flame thickness with pressure are described in Eq. 2.24 and Eq. 2.25 [61] using the similar approach developed by Spalding [143], Mallard and Le Chatelier [144]:

$$S_L \propto P^{(n-2)/2} \qquad \text{Eq. 2.24}$$

$$\delta_f \propto P^{-n/2} \qquad \text{Eq. 2.25}$$

in which n is the global reaction order. As a result, the variation of critical velocity gradient with pressure according to Eq. 2.23 would be [61]:

$$g_c \propto P^{n-1} \qquad \text{Eq. 2.26}$$

Assuming the reaction order of $1 < n < 2$, increasing pressure causes a decrease in burning velocity and flame thickness, while increases the critical velocity gradient.

The Damköhler number, defined as the flow time scale to the combustion time scale (Eq. 2.27), was also used as a non-dimensional parameter in numerical modeling of the laminar boundary layer flashback [90,94]. This non-dimensional group has been used in the literature to characterize flashback propensity of laminar as well as turbulent flames [90,94,110,138].

$$Da = \frac{S_L^2}{\alpha g_c} \qquad \text{Eq. 2.27}$$

An increase in the laminar flame speed increases the Damköhler number which corresponds to higher flashback propensity. For laminar flows, the critical velocity gradient is small compared to turbulent flows.

Section 2.3.1 has summarized the key basic models developed for boundary layer flashback of laminar premixed flames. The main underlying assumption of predictive models is that the flame and flow do not interact. As a result, the laminar velocity profile is presumed to remain undisturbed at onset of flashback and is therefore known from the analytical solution of fully developed laminar flows in a circular tube or two-dimensional channel. In addition, flame characteristics are described by one-dimensional flame propagation theory. By combining the premixed flame and flow characteristics, the critical condition at which flashback occurs is obtained.

2.3.2 Effect of Burner Diameter and Temperature

In their original work, Lewis and Von Elbe also investigated the effect of burner diameter on flashback behavior of fully developed laminar flows of natural gas air mixtures [47]. The tube burner was constructed from Pyrex with inner diameters varying from 0.315 to 1.55 *cm*. Between each test the burner was cooled down to the room temperature as the cooling effect was found an important parameter for obtaining consistent data. The inner surface of the Pyrex burner was also coated with various salts and metals to examine the effect of the surface material inside the tube. Because the heat conductivity of the burner is several times larger than that of a gas, the overall heat loss to the atmosphere is determined by the gas conductivity, not that of the burner. Hence, it was concluded that the wall temperature (up to 100 °C) had little effect on flashback propensity [47]. This is in good agreement with the study by Miller and Setzer [74], who concluded that the effect of premixer wall temperature is negligible below 115 °C. They did note that higher tip temperatures cause a strong effect on flashback limits. The effect of burner material on the tip temperature is discussed in more detail in Section 2.4.2.

Figure 2.12 presents the critical flow rates at which flashback occurs as a function of the mixture composition for burner diameters from 0.333 to 1.55 *cm*. The dashed curve shows the data at the beginning of the flame upstream propagation and the solid curve indicates “full flashback.” The data

between these two curves (solid points) represents situations in which the flame cone was partially drawn into the tube. It was concluded that this resulted from some local high temperature regions on the burner rim due to “some irregularity” that was not further defined or discussed. The partially propagated flame increases the pressure inside the tube and causes a deflection of the streamlines in the opposite direction. The flame at this condition was described as a “tilted flame” in which the dynamic symmetry of the flame was destroyed. The flame can propagate upstream unless the flame is quenched because of the tube cooling. The velocity gradient in this region, where the flame propagates into the burner, decreases due to the streamline distortion and consequently the flame flashes back below the critical flashback value. The velocity gradient of laminar flow in Eq. 2.5 was modified for tilted flames in [47] and later used by Grumer for predicting turbulent flashback limits [77].

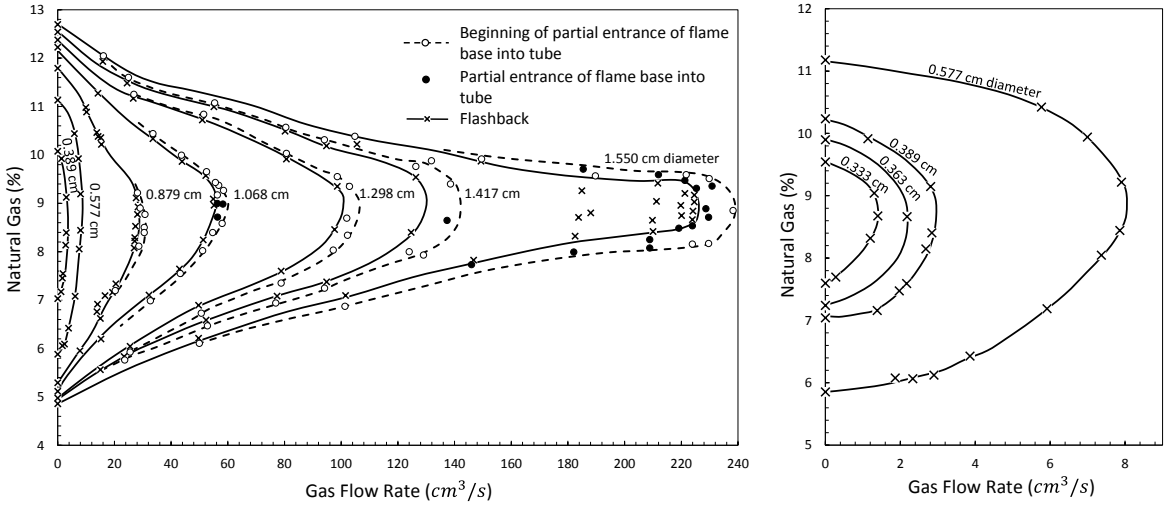

Figure 2.12: Flashback limit of natural gas as a function of volumetric flow rate for different burner diameters, reproduced from [47].

The flow velocity at which flashback occurs increases with an increase in the burner diameter. Indeed, for a given volumetric air flow rate, the flow bulk velocity decreases with square of the diameter resulting in lower equivalence ratio or fuel percent. The points at zero flow rate show the inflammability limit of natural gas for upstream propagation.

The variation of critical velocity gradient calculated from Eq. 2.5 is illustrated in Figure 2.13 as a function of natural gas concentration in air. The critical velocity gradient can correlate the effect of burner diameter for the diameter range studied. However, some discrepancy for the burner diameter of 1.55 *cm* is observed near stoichiometric conditions. This might be due to incipient turbulence at these conditions causing an increase the burning velocity [47]. The flame propagation is fully arrested for the limiting diameter for 0.315 *cm*. It is also observed that the burners with small diameters close to this value (0.333 and 0.389 *cm*) do not follow the general trend. This was explained by the fact that that the flow velocity profile within the wall and the penetration distance for small burner diameters is not linear.

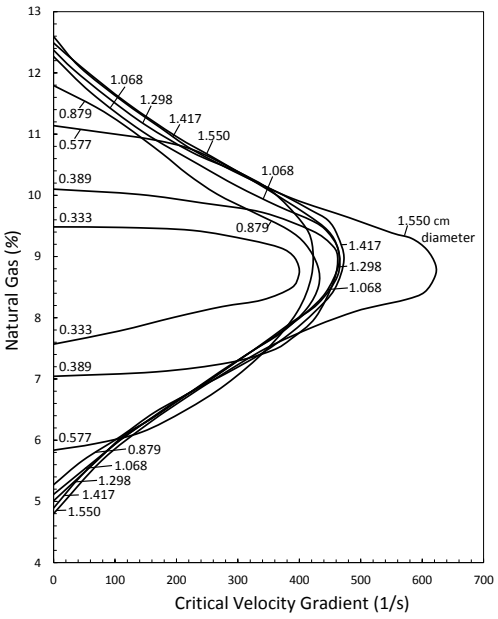

Figure 2.13: Critical velocity gradient of boundary layer flashback for natural gas at different burner diameters, adapted from [47].

Figure 2.14 presents another view of the effect of the burner diameter on flashback propensity at a lean condition (7.5% natural gas) [47]. At sufficiently large diameter, the critical velocity gradient remains approximately constant. The lack of diameter dependence was also observed by Kurz [73] for laminar flames for various hydrocarbon air mixtures shielded with inert gases of helium and nitrogen. However, the ratio of penetration distance to the burner diameter increases as the burner diameter decreases and

finally reaches a point at which this value is no longer small enough to apply one of underlying assumptions made for the critical velocity gradient concept. An underlying assumption of the critical velocity gradient concept is based on estimating the flow velocity at the penetration distance by the tangent to the velocity profile at the wall. This assumption is not valid when the penetration distance is comparable to the burner diameter; hence, the effect of the velocity profile curvature should be considered. With further decrease in burner diameter, the laminar burning velocity across the exit is entirely affected by the quenching distance. For burner diameters less than 0.389 *cm* in Figure 2.14, the burning velocity is reduced, even at the burner axis, leading to a sudden decrease of critical velocity gradient. The flame is eventually quenched by the smallest diameter as indicated in Figure 2.14.

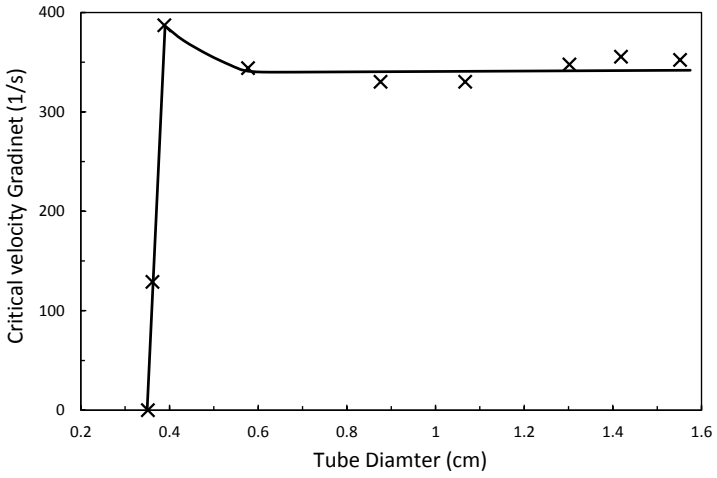

Figure 2.14: Critical velocity gradient variation of natural gas as a function of burner diameter at 7.5% natural gas-air mixture, reproduced from [47].

The qualitative effect of the burner diameter on critical velocity gradient shown in Figure 2.13 depends on the fuel concentration. For instance, the critical velocity gradient slightly increases with an increase in burner diameter at rich conditions. Hence, a general conclusion for variation of the critical velocity gradient with the burner diameter cannot be made regardless of the fuel percentage in the mixture. Furthermore, observations obtained from different studies are not entirely consistent. Figure 2.15 shows the flashback propensity of methane/air mixtures for two burner diameters at atmospheric pressure and

room temperature [93]. The critical velocity gradient decreases with an increase in burner diameter at rich conditions. The burner tip temperature in the experiment [93] was not controlled during each test and values were not reported. This may be the main reason for such a difference in flashback limits compared to Figure 2.13.

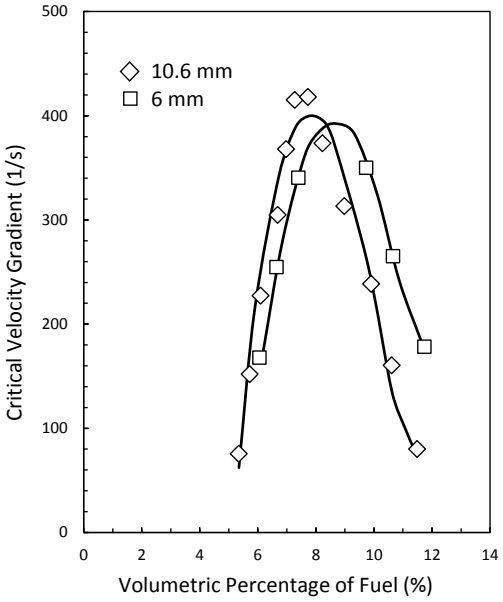

Figure 2.15: Critical velocity gradient of methane/air flames for two burner diameters, reproduced from [93].

In other work from von Elbe's group, the flashback limit of methane and propane with the mixture of oxygen and nitrogen was determined for laminar flames at atmospheric pressure and room temperature [51]. The flow was fully developed and the fuel/air mixture was injected through a Pyrex tube unless a constraint due to the flame temperature occurred. Near stoichiometric conditions for cases with oxygen used as an oxidizer, quartz, porcelain or copper were used interchangeably. The burner tube was cooled frequently between tests to avoid an increase in the temperature. Figure 2.16 indicates the variation of critical velocity gradient with the methane concentration in nitrogen/oxygen mixtures at burner diameters ranging from 1.397 to 18.07 *mm*. The burner diameter range was selected such that the Reynolds number remained less than 2000 for all cases. For methane/air reaction (labeled by the ratio of 0.21 in Figure 2.16), results of different burner diameters match well with the general trend line. However,

when the burner diameter is comparable to the flame quenching distances, the deviation is pronounced as seen from the top curve in Figure 2.16. An increase of oxygen in the mixture does not change the dependency of the critical velocity gradient on burner diameter.

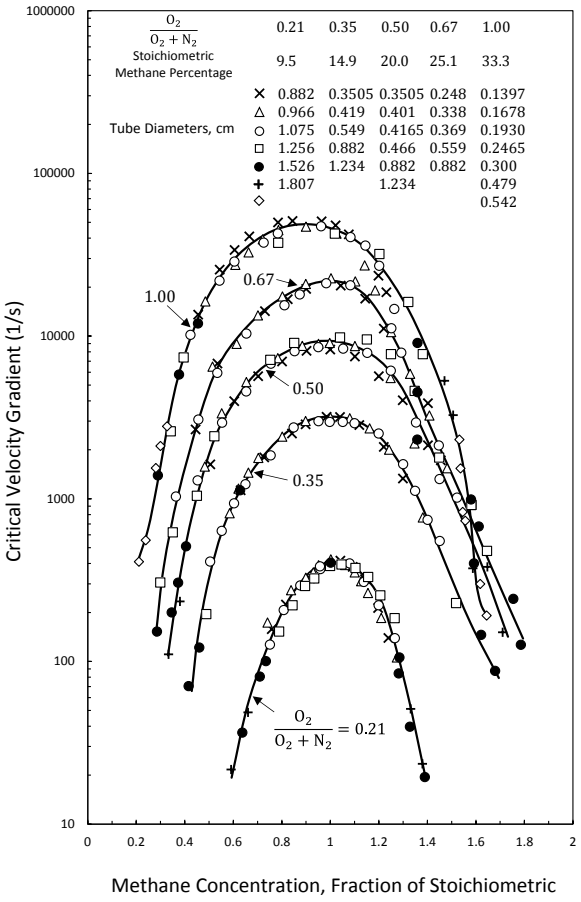

Figure 2.16: Critical velocity gradient variation of methane/oxygen-nitrogen mixtures at different tube burner diameters, reproduced from [51].

Figure 2.17 illustrates the variation of critical velocity gradient for propane/oxygen-nitrogen mixtures with different burner diameters. The propane/air mixture is not significantly influenced by changing the burner diameter. However, when the diameter decreases to a sufficiently small value, the quenching effect becomes more important. As discussed relative to Figure 2.13, for small diameters, the physical assumption of the linear velocity profile close to the wall used in the critical velocity gradient concept is not valid. A significant deviation from the solid curve (shown by diamond and cross shapes) is observed

for propane/oxygen mixture in Figure 2.17. The effect of dilution at the burner rim for fuel rich mixtures becomes more important as oxidizer other than air is used.

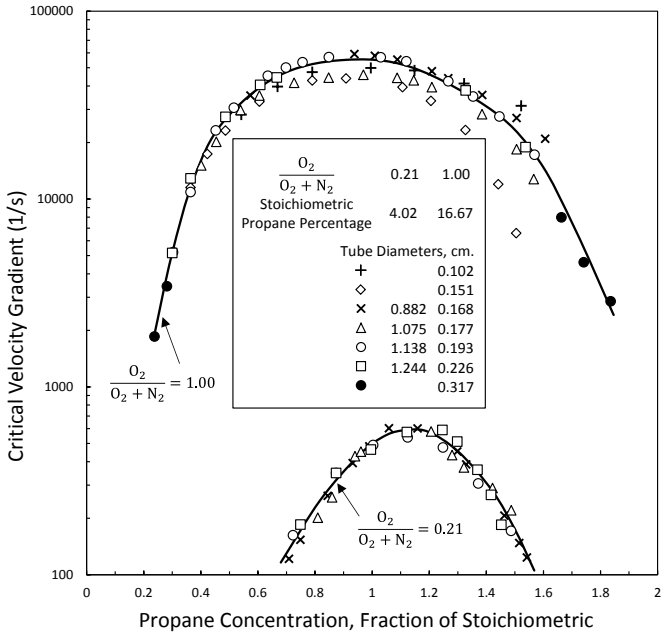

Figure 2.17: Critical velocity gradient variation of propane/oxygen-nitrogen mixtures at different tube burner diameters, reproduced from [51].

A more recent experiment studied the effect of burner diameter on laminar flashback of H_2-CO and H_2-CH_4 mixtures with variation of hydrogen from 5% to 25% in both mixtures [96]. Figure 2.18(a) indicates the variation of the critical velocity gradient of 25%H_2–75%CO mixture at three different burner diameters, i.e., 6, 7, and 10.6 *mm*. In this study, the effect of burner diameter is negligible at lean conditions and becomes more pronounced as the equivalence ratio increases. Furthermore, the largest diameter in Figure 2.18(a) has the lowest critical velocity gradient for fuel rich mixtures. This observation was not reported by Lewis and Elbe [47] for methane/air mixtures and may be due to the thermal coupling effect between the burner head and flame.

The effect of burner diameter observed by Dam et al. on flashback propensity of 25%H_2–75%CH_4 mixture is also illustrated in Figure 2.18(b). The effect of diameter is pronounced at lean condition. In addition, the

7 *mm* burner tube has the lowest critical velocity gradient. It is noted that the addition of 25% H_2 to the carbon monoxide or methane (Figure 2.18(a) and (b)) does not show the similar behavior. The methane mixture is less affected by the hydrogen addition for fuel rich mixtures. The results suggest that the heat transfer to the burner rim and the quenching distance are complicated functions of fuel composition and influenced by the burner diameter at small diameters. The description of such a different characteristic is described in Section 2.3.4. It appears that no general conclusion can be made regarding the variation of critical velocity gradient with diameter according to the study by Dam et al. [96].

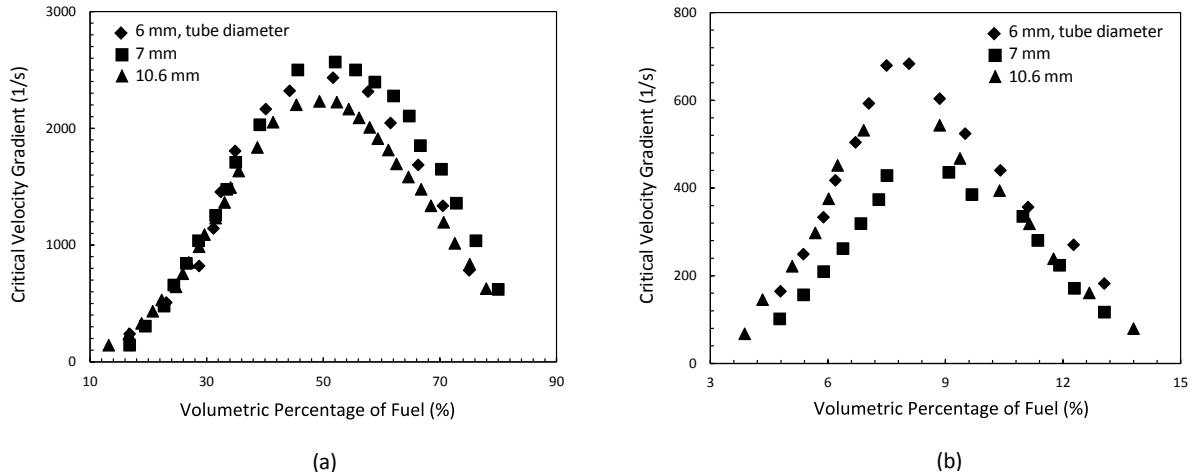

Figure 2.18: Critical velocity gradients as a function of fuel concentration for different burner diameters (a) 25%–75% H_2–CO mixtures and (b) 25%–75% H_2–CH_4 mixtures, reproduced from [96].

Early studies concluded that the critical velocity gradient is independent of burner diameter for sufficiently large values. However, it is noted that the effect of burner diameter cannot simply be extended to all equivalence ratio ranges and various fuel compositions. The size of the burner has an important effect on heat transfer between the burner rim and flame front. The complicated heat balance at the burner rim including convection of the gas flow mixture, radiation of products, and conduction of the burner material cannot be predicted by the simple critical velocity gradient model. Consequently, the variation of the burner diameter impacts differently on flashback limits for various fuel/air compositions. Furthermore, the heat balance between the burner rim and flame front is significantly affected by the equivalence ratio,

determining the temperature of the stabilized flame. This is the main reason why experiments examining different fuel compositions do not show consistent results. In order to isolate the effect of the burner diameter, the burner tip temperature needs to be monitored or controlled carefully. A small disturbance in flame front shape such as tilted flame can significantly change the tip temperature resulting in a different flashback limit. The size of burner (at sufficiently large values) does not significantly influence the flashback limits in terms of critical velocity gradient if the burner is cooled during the experiment and flashback is gradually approached such that the burner rim temperature remains at quasi-steady heat balance. However, this behavior changes when the quenching distance is comparable to the burner with small diameters.

2.3.3 Effect of Preheat Temperature and Operating Pressure

Dugger studied the effect of preheat temperature on flashback propensity of propane/air flames under laminar conditions [63]. The temperature of the reactants was varied from 300 to 620 *K*. The burner tube was constructed from brass with an inner diameter of 1.56 *cm*. The tube wall temperature was controlled such that it approximately remained constant at the temperature of the reactants. The Reynolds number values were less than 2000. Figure 2.19 presents the variation of critical velocity gradient with equivalence ratio at four different preheat temperatures of 306, 422, 506, and 617 *K* and illustrates that the critical velocity gradient increases with an increase in the preheat temperature. The laminar flame speed increases with temperature raised to an exponent which is a function of fuel composition [145–147]. Furthermore, the quenching distance decreases as the preheat temperature increases [44] and this effect is more pronounced in the experiment of Dugger [44] since the burner wall temperature was controlled to be the same as the preheat temperature.

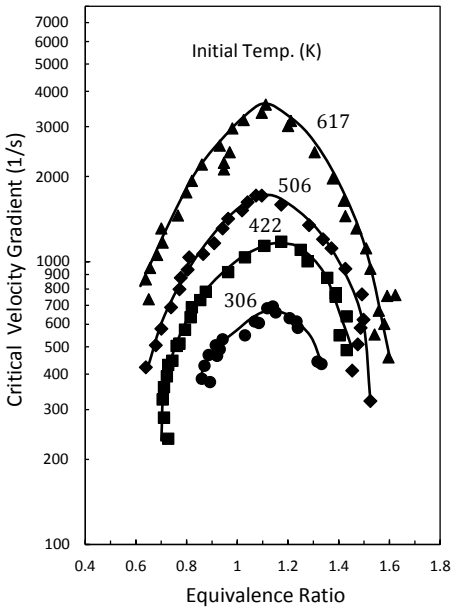

Figure 2.19: Effect of preheat temperature on flashback propensity of propane/air mixture, reproduced from [63].

To isolate the effect of laminar flame speed on flashback propensity, laminar propane/air mixture burning velocities are calculated from Eq. 2.28 as proposed by Metghalchi and Keck [145]. This expression is valid in the pressure range from 0.4 to 40 *atm*:

$$S_L = S_{L0}\left(\frac{T_u}{T_{u0}}\right)^{\alpha}\left(\frac{P}{P_0}\right)^{\beta} \qquad \text{Eq. 2.28}$$

in which $T_{u0} = 298\ K$ and $P_0 = 1\ atm$. S_{L0}, α, and β are fitted constants presented in Table 2.1 [145]. Assuming an equivalence ratio of 1.2 in Figure 2.19, critical velocity gradients at four preheat temperatures are $g_{c0} = 640$, $1.79g_{c0}$, $2.426g_{c0}$ and $4.87g_{c0}$, respectively. Using Eq. 2.3 (in which $g_c \propto S_L$) and the laminar flame speed in Eq. 2.28, critical velocity gradient values can be calculated with respect to the reference preheat temperature of $T_0 = 306\ K$ and the refrence critical velocity gradient of $g_{c0} = 640$.

Table 2.1: Constant values in Eq. 2.28 [145].

Equivalence ratio	$S_{L0}\ (cm/s)$	α	β
1.2	33.8	2.02	-0.17

Based on Eq. 2.29, the critical velocity gradients at three preheat temperatures of 422, 506, and 617 *K* are $1.91g_{c0}$, $2.76g_{c0}$ and $4.12g_{c0}$, respectively. These predicted values at 422 and 506 K preheat temperatures are higher than the actual values obtained from measurements, while the predicted value at 617 *K* is lower. Consequently, the effect of preheat temperature on laminar burning velocity alone does not account for an increase in critical velocity gradient as its impact on quenching distance must also be accounted for.

$$g_c = g_{c0}\left(\frac{T}{T_0}\right)^{\alpha} \qquad \text{Eq. 2.29}$$

A similar approach was used by Khitrin et al. [82] to study flashback propensity of methane/oxygen and methane/air mixtures with the preheat temperature varied from 20 to 400 ℃. The study was conducted for quartz and metal tube burners with different diameters ranging from 18 to 25 *mm*. The temperature of the burner rim was maintained at the mixture preheat temperature to within 10 ℃. Figure 2.20 illustrates the variation of the critical velocity gradient with equivalence ratio at five preheat temperatures. The slope of the critical velocity gradient is a function of equivalence ratio and exhibits more sensitivity as preheat increases.

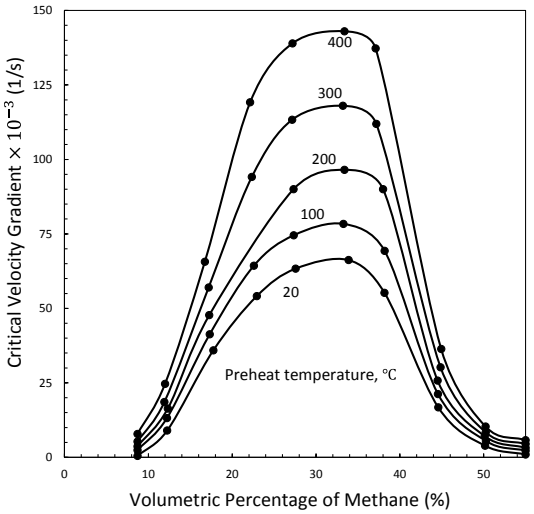

Figure 2.20: Critical velocity gradient of the methane/oxygen mixture at different preheat temperatures, reproduced from [82].

The measured data from Khitrin [82] are plotted in Figure 2.21 using the Peclet number (Eq. 2.13) as a non-dimensional parameter. The solid line shows the variation of $Pe_{flow} = 0.01\left(Pe_{flame}\right)^2$, in which the constant differs from the dashed line suggested by Putnam and Jensen [52] representing $Pe_{flow} = 0.0125\left(Pe_{flame}\right)^2$. Nevertheless, good agreement between the data obtained from various preheat temperatures and the correlations developed in previous studies is noted. This illustrates that the critical velocity gradient model is able to predict the preheat temperature effects. The difference between these two constants (i.e., 0.01 and 0.0125) may be due to the laminar flame speed measurement and its calibration.

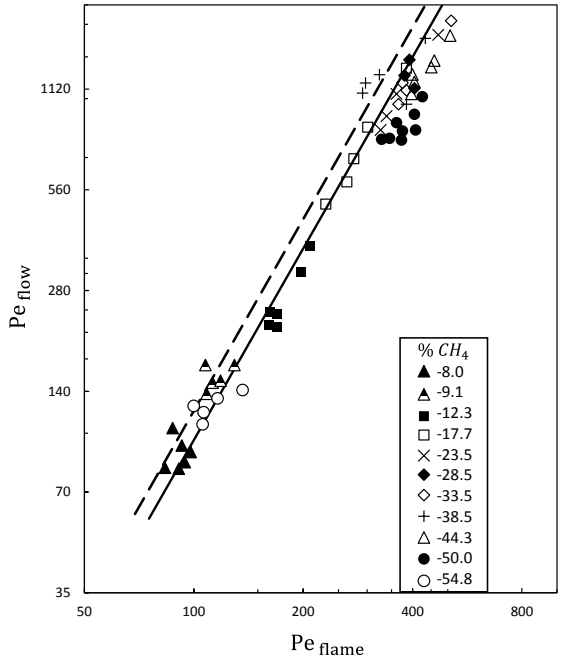

Figure 2.21: Relation between Pe_{flow} and Pe_{flame} for flashback propensity of methane/oxygen and methane/air mixtures, reproduced from [82].

The effect of preheat temperatures on flashback limit of methane/air mixtures was studied by Grumer and Harris [62] for sharp-edged short ports, which are common in gas appliances. Figure 2.22 shows the variation of critical velocity gradient as a function of preheat temperature for mixtures with given fractions of stoichiometric F (i.e., the fuel percentage divided by the stoichiometric fuel percentage). The velocity

profile for this burner was not fully developed and the critical velocity gradient was determined using an experimentally derived equation from [59,148]. It is noted that the variation of critical velocity gradient with preheat temperature shown in Figure 2.22 is better captured by exponential function rather than power law relation, which is generally used for laminar burning velocity correlations.

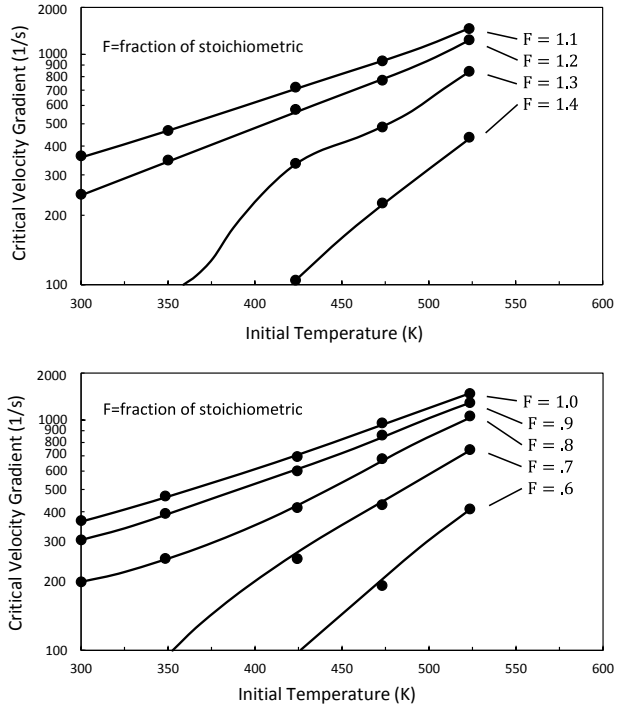

Figure 2.22: Critical velocity gradient of methane/air mixtures as a function of preheat temperature at various fractions of stoichiometric mixtures, reproduced from [62].

Fine conducted boundary layer flashback experiments for hydrogen/air mixtures at sub-atmospheric pressures varied from 0.15 to 1 *atm* [67,71]. The original model by Lewis and Von Elbe [47] was modified to take into account the effect of pressure. Flames were stabilized at the burner rim using burners with diameters of 0.546, 1.016, and 1.459 *cm*. The flow was fully developed at the exit section. The tip temperature was noted as a contributor to flashback and was thus controlled by water cooling to eliminate its effect. The pressure was increased slowly to approach flashback at constant mass flow rate and preheat temperature. The burning velocity was measured by determining the total flame area from

Schlieren images. The equivalence ratio was varied from 0.8 to 2.25. These tests were mainly obtained for rich conditions due to the high uncertainty at lower mass flow rates and characteristic of hydrogen flames.

Figure 2.23 shows the variation of the critical velocity gradient with pressure at equivalence ratio of 1.8 for three burner diameters studied by Fine [67,71]. The critical velocity gradient increases as the ambient pressure increases, resulting in higher flashback propensity. The critical velocity gradient dependency on pressure can be described as:

$$g_c \propto P^{n_f} \qquad \text{Eq. 2.30}$$

in which n_f is the pressure exponent of critical velocity gradient variation. n_f varied between 1.27 and 1.42 for equivalence ratios of $0.95 \leq \phi_f \leq 2.25$. Fine observed that Eq. 2.30 was in better agreement with data points at equivalence ratios between $1.3 \leq \phi_f \leq 1.8$. The variation of critical velocity gradient is not linear at the very low pressures shown in Figure 2.23, which is due to the enhanced quenching effect.

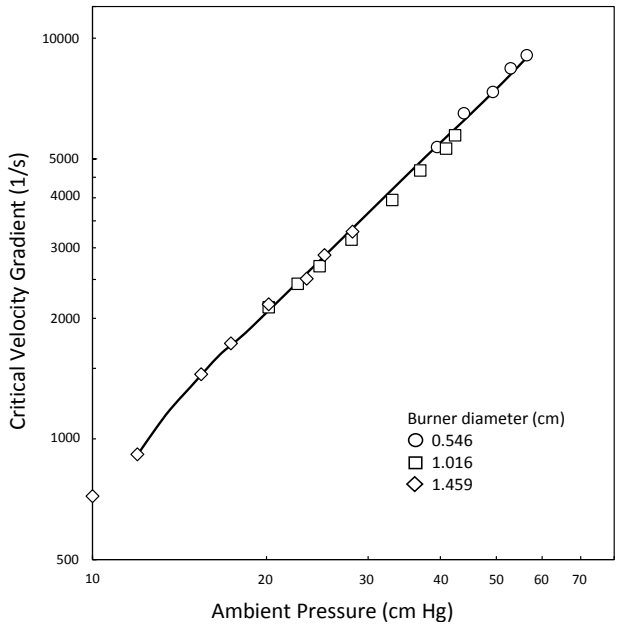

Figure 2.23: Critical velocity gradient variation as a function of ambient pressure for hydrogen/air flames at equivalence ratio of 1.8, reproduced from [67,71].

Fine [67,71] also measured burning velocity as a function of pressure at different equivalence ratios and a similar relation to Eq. 2.30 was suggested:

$$S_L \propto P^{n_u} \qquad \text{Eq. 2.31}$$

n_u varied between 0.208 and 0.256 for the equivalence ratio between $1.10 \leq \phi_f \leq 1.9$. This correlation suggests that the laminar burning velocity increases with an increase in pressure. This is consistent with other studies of the burning velocity of hydrogen/air flames at sub-atmospheric pressure in the literature. For example, Figure 2.24 illustrates the variation of laminar flame speed with pressure at different hydrogen concentrations [149]. For equivalence ratios less than 0.79 ($X_{H_2O} = 0.25$), the reaction order is less than 2 and a negative pressure dependence is observed, while for equivalence ratio higher than 0.79, the reaction order is larger than 2 with positive pressure dependence. This indicates that the laminar flame speed increases with an increase of sub-atmospheric pressure at fuel rich conditions [149] consistent with the positive exponents proposed by Fine for Eq. 2.31.

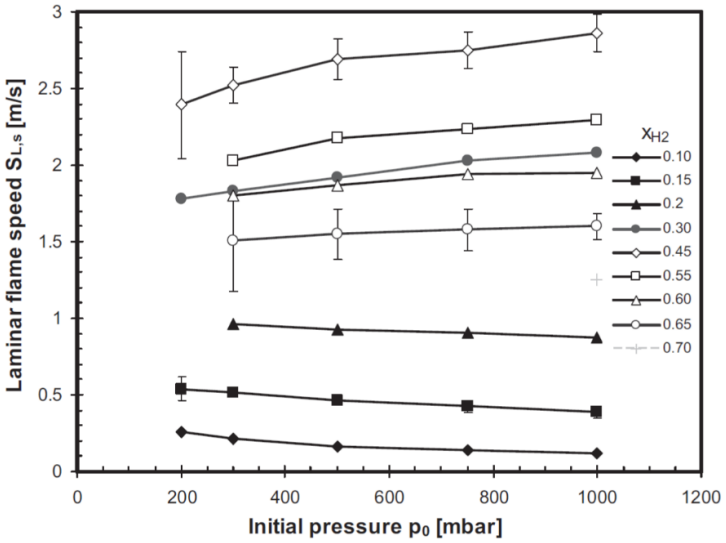

Figure 2.24: Laminar flame speed of hydrogen/air mixtures vs pressure at various hydrogen mole fractions [149].

Based on equations Eq. 2.30, Eq. 2.31 and using Eq. 2.3, the variation of the quenching distance with pressure would be:

$$\delta_q \propto P^{n_q} \qquad \text{Eq. 2.32}$$

in which n_q is equal to $n_u - n_f$. Considering the average values for pressure exponents of critical velocity gradient and laminar flame speed, $n_q = -1.12$ was suggested [67,71]. The comparison of the pressure exponent of quenching distance ($n_q = -1.12$) to the experimental results of Drell and Belles [75] for parallel plates indicates good agreement as illustrated in Figure 2.25. Drell and Belles reported pressure exponents of 1.051, 1.138, and 1.097 for the quenching distance between two parallel plates at equivalence ratios of 0.5, 1, and 2, respectively [75].

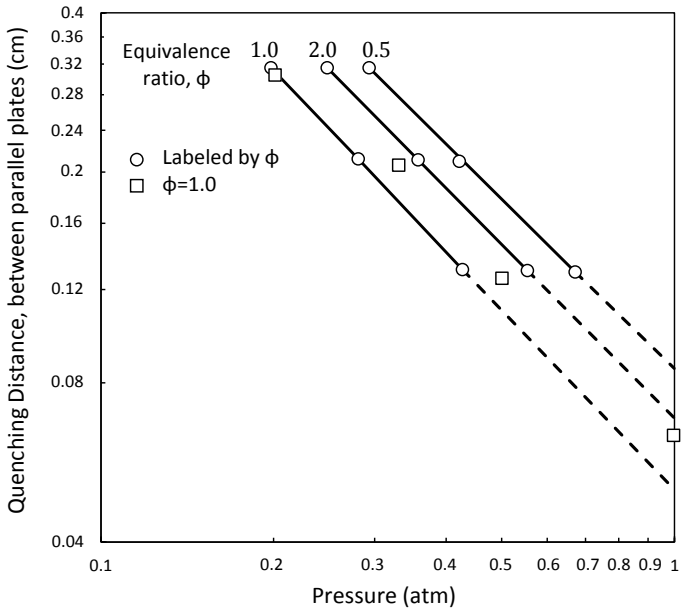

Figure 2.25: Effect of pressure on quenching distance of hydrogen/air mixtures, circle (data from [113]), square (data from [85]), reproduced from [75].

The variation of critical velocity gradient with equivalence ratio at different pressures found by Fine is indicated in Figure 2.26 [67,71]. The slope of the critical velocity gradient variation increases with an increase in pressure. This indicates that the flashback propensity is more sensitive to equivalence ratio variation at higher pressures. A general correlation was found to fit all the measured data of hydrogen/air flames at reduced pressures:

$$g_c = 2.6\frac{S_L}{\delta_q} \qquad \text{Eq. 2.33}$$

In this equation, δ_q is the quenching distance between two parallel plates. The quenching distance of hydrogen/air mixture in Eq. 2.33 was obtained from the tabulated data in [120]. The constant coefficient in Eq. 2.33 was found to be 3 from the study by Von Elbe at al. [48].

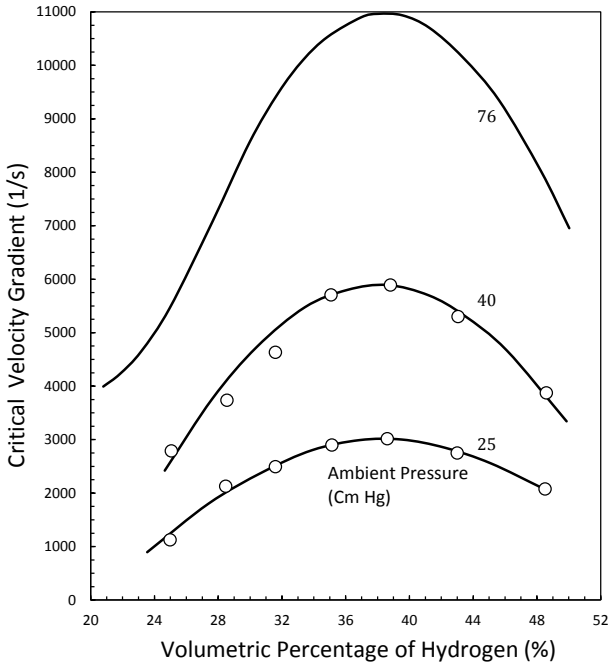

Figure 2.26: Critical velocity gradient as a function of fuel concentration for hydrogen/air flames at different pressures, top curve (atmospheric data from [48]), reproduced from [67,71].

Further work by Fine [70] investigated the effect of pressure on flashback propensity of hydrogen/oxygen-argon and hydrogen/oxygen-helium in which the concentrations of oxygen, argon, and helium were 20.6, 79.4, and 79.4, respectively. The experiment setup was similar to that used in previous studies [67,71]. The equivalence ratio was varied in the range of $0.9 \leq \phi \leq 2.25$ for the hydrogen/oxygen-argon mixtures and $1.1 \leq \phi \leq 1.5$ for the hydrogen/oxygen-helium mixtures. The burner head diameter used in this experiment was 0.546 and 1.016 *cm*. Figure 2.27 presents the variation of critical velocity gradient as a function of pressure for hydrogen/oxygen argon and hydrogen/oxygen-helium. The flashback data of

argon diluted mixture are in a good agreement with results for helium diluted mixture. The pressure exponents of critical velocity gradients for hydrogen/oxygen-argon mixtures are 1.59 and 1.49 at equivalence ratios of 1.1 and 1.5 respectively. The exponent values are 1.50 and 1.48 for the hydrogen/oxygen-helium mixtures at these same equivalence ratios, respectively, which are slightly different compared to the hydrogen/oxygen-argon mixtures. The average pressure exponent for equivalence ratios between $0.9 \leq \phi \leq 2.25$ was 1.51 for both argon and helium diluted mixtures.

The burning velocity of the mixture diluted by helium is much larger than the burning velocity of the hydrogen/oxygen-argon mixtures [70,150]. This suggests that the quenching distance of the helium diluted mixture increases in a manner that the critical velocity gradient remains approximately constant. This is consistent with the observation that the flame for the hydrogen/oxygen-helium mixture anchored at a larger distance from the burner rim [70]. Furthermore, results for two burner diameters follow the same trend line as indicated in Figure 2.27, except at richest condition with equivalence ratio of 2.25 (see Figure 2.28). For the 1.016 *cm* diameter tube, a transition from laminar to turbulent flow for the hydrogen/oxygen-argon mixture occurs at critical velocity gradient about 8000 resulting in a departure from the trend line as shown in Figure 2.27(a).

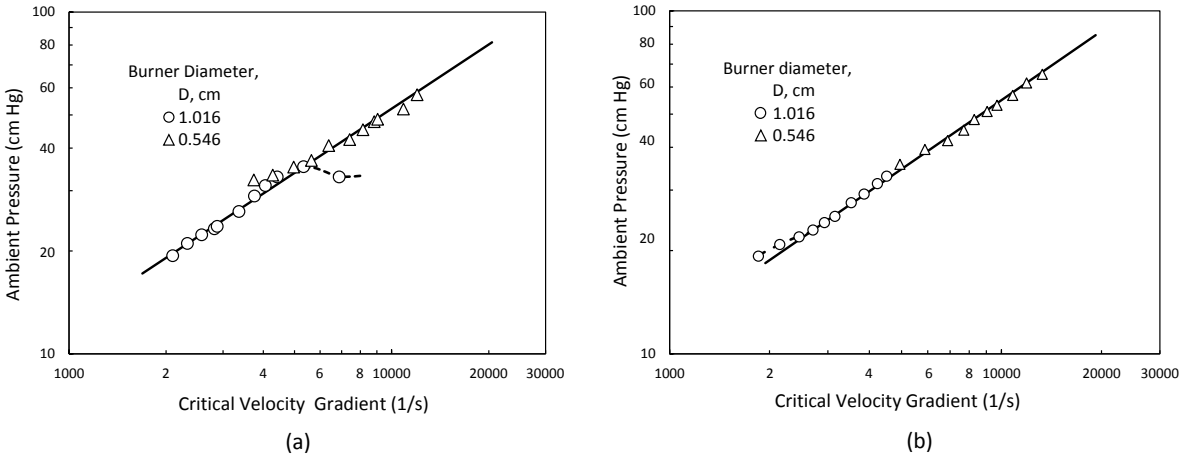

Figure 2.27: Variation of critical velocity gradient vs pressure at equivalence ratios of 1.1 (a) hydrogen/oxygen-argon and (b) hydrogen/oxygen-helium, reproduced from [70].

The variation of critical velocity gradient with equivalence ratio for hydrogen/oxygen-argon observed by Fine [70] is shown in Figure 2.28. An increase in pressure increases the velocity gradient at which flashback occurs, as previously mentioned. Data points for both burner diameters are coincident as no significant different was observed with the exception of equivalence ratio of 2.25. The diameter dependence at the richest condition is attributed to diffusion effects at the burner rim. The maximum critical velocity gradient occurs at about 39 percent hydrogen for both helium and argon diluted mixtures. This value agrees well with previous studies conducted for hydrogen-air flames [47,67,71].

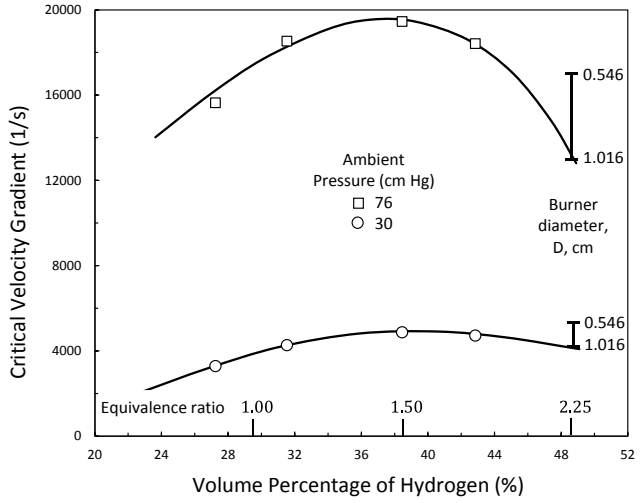

Figure 2.28: Critical velocity gradient of hydrogen/oxygen-argon mixture as a function of fuel concentration at two different pressures, reproduced from [70].

The results from the literature indicate that flashback limits are strongly affected by the preheat temperature and operating pressure. An increase of preheat temperature increases the laminar flame speed causing flashback to occur at higher air flow rate for a given equivalence ratio. Furthermore, the propagation of the flame front into the tube is a function of the burner tip temperature. Since the burner temperature remains approximately constant at the preheat temperature, the quenching distance significantly decreases at high preheat temperatures. In order to determine the effect of preheat temperature on flashback propensity, both laminar flame speed and quenching distance need to be considered for various fuel compositions.

All laminar flame flashback studies in the literature are limited to one atmosphere or sub-atmospheric operating pressures. The effect of sub-atmospheric pressure on critical velocity gradient is primarily determined by the fuel composition and equivalence ratio. In fact, the laminar flame speed of different fuels can increase or decrease with an increases of pressure at lean or rich conditions, and this pressure dependence is weak in many cases [149,151,152]. As a result, the quenching distance plays a crucial role in changing the flashback limit. The quenching effect can be significant when determining the overall variation of flashback limits regardless of an increase or decreases of laminar burning velocity with pressure. Despite the insight offered by the studies discussed in this section, for practical devices operating at elevated pressure or with high hydrogen content fuels, the flow is usually turbulent, hence application of these results is dubious.

2.3.4 Fuel Composition

With the general ability of flashback tendencies of laminar flames to be characterized with the critical velocity gradient concept, experimental efforts were directed towards using the concept to help determine the stability limits of various fuel compositions.

2.3.4.1 Hydrocarbon Fuels

Early comprehensive studies were conducted by Grumer to investigate the effect of individual fuels and their mixtures at room temperature and atmospheric pressure [54,64]. The measured flashback data were later used by Grumer to predict the interchangeability of fuels [58]. Boundary layer flashback was investigated for natural gas, methane, ethane, and propane with air as an oxidizer. Burner diameters ranging from 0.390 to 1.358 *cm* were used. The laminar flow was fully developed at the burner exit and the burner head temperature was controlled to remain at room temperature before starting each test.

Figure 2.29 indicates the variation of critical velocity gradient as function of “fraction of stoichiometric” (i.e., the fuel percentage divided by the stoichiometric fuel percentage) for natural gas, methane, ethane,

and propane. Flashback curves in Figure 2.29 qualitatively peak at the same fraction of stoichiometric for methane, natural gas, and ethane. However, the flashback curve of propane slightly shifts to the right as previously verified by Harris et al. [51] and shown in Figure 2.17.

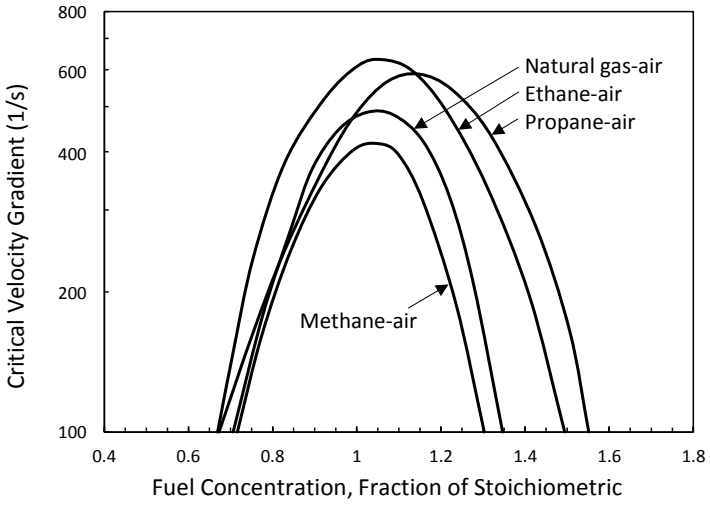

Figure 2.29: Flashback limits of different hydrocarbons as a function of fuel concentration, reproduced from [54,64].

Methane/air mixtures have the lowest flashback propensity of the hydrocarbon fuels studied. The critical velocity gradient for natural gas is slightly higher than that of methane due to the presence of higher hydrocarbons in the mixture. Ethane has a higher critical velocity gradient than propane at lean conditions, while the opposite is true at rich conditions. In order to interpret the difference in flashback limits, the laminar burning velocity of these fuels, as determined by Davis and Law [153] are compared in Figure 2.30. As shown, the laminar burning velocity of methane is lower than other fuels. The laminar burning velocity of ethane is slightly higher than propane within the stoichiometric and rich conditions, which can be also observed in [154,155]. Therefore, the critical velocity gradient behavior shown in Figure 2.29 does not follow the qualitative variation of the laminar burning velocity for propane, and ethane.

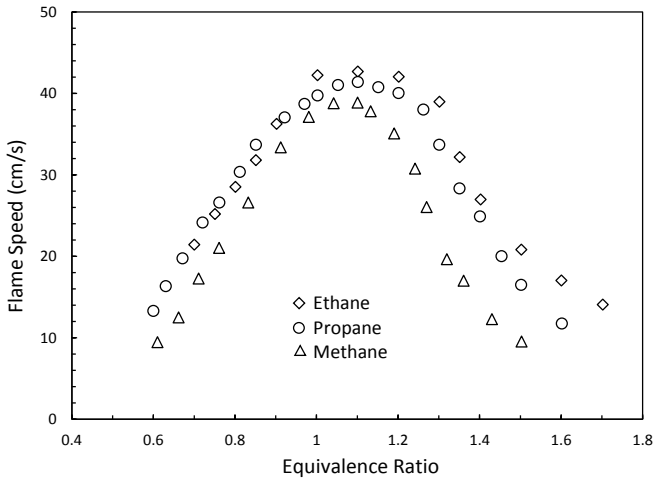

Figure 2.30: Laminar burning velocity of methane, ethane, and propane at atmospheric pressure and room temperature, reproduced from [153].

Figure 2.31 shows the flashback propensity of methane-propane and methane-ethane as a function of fuel volume concentration as studied by Davu et al. [93]. The addition of 25% propane to methane increases the maximum critical velocity gradient from 400 1/s to 490 1/s. Similarly with an addition of 5% ethane, the critical velocity gradient has the same amount of increase. This is consistent with the previous observation associated with Figure 2.29 regarding the higher peak of critical velocity gradient for ethane.

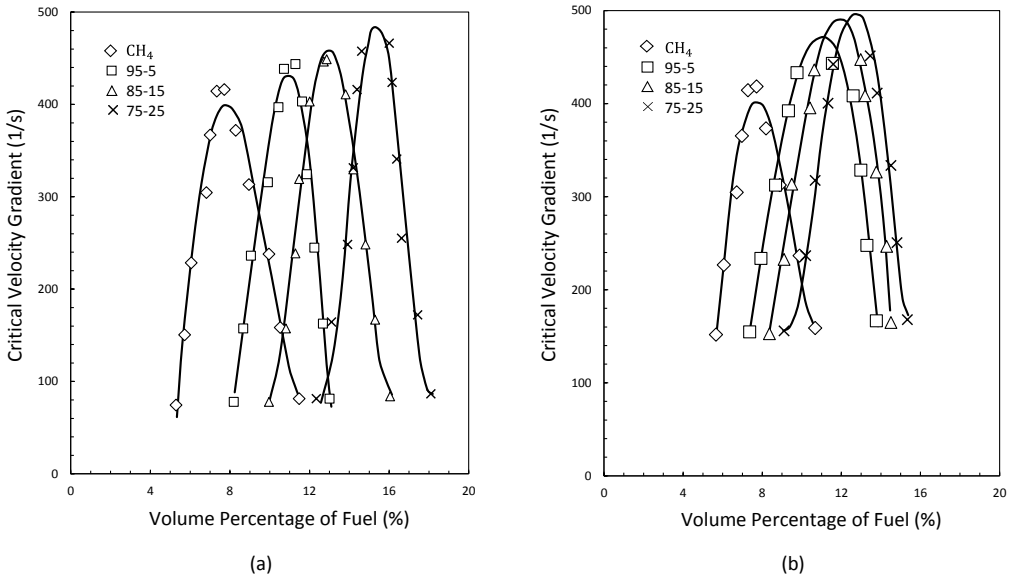

Figure 2.31: Variation of critical velocity gradient for (a) methane-propane mixtures and (b) methane-ethane mixtures, reproduced from [93].

2.3.4.2 Hydrogen Rich Fuels

Further discussion is now directed at hydrogen/air mixtures owing to the known high flashback propensity of hydrogen. Hydrogen has higher burning velocities and a smaller quenching distance than hydrocarbons [68,156]. The thermal and mass diffusivity of hydrogen are considerably larger compared to those for hydrocarbon fuels. Furthermore, reaction kinetics of hydrocarbons are basically limited by $CO \rightarrow CO_2$, which is relatively slow. The reaction kinetics of hydrogen is fast due in part to the lack of this step which must occur in all hydrocarbons fuels [141,157]. As a result, the flashback propensity of hydrogen is generally much higher than hydrocarbon fuels.

Von Elbe and Mentser [48] were the first to measure the flashback propensity of hydrogen at atmospheric pressure for different burner diameters varied from 0.108 to 0.33 *cm*. Water-cooling was used to control the temperature of the burner head. Figure 2.32 indicates the critical velocity gradient variation of hydrogen for the laminar flame [48]. The solid curve shows the flashback limit where the flame fully propagates upstream. The region between the dashed curved (beginning of partial entrance) and solid curve represents the partial entrance of the flame front into the burner, described as a tilted flame in [47]. The region of tilted flame is more extensive than that observed for natural gas flames as previously discussed in Section 2.3.2. These regions invoke perturbations to the stable flame and consequently led to flashback except at very lean or rich conditions [48]. Critical velocity gradient values of hydrogen shown in Figure 2.32 are significantly larger than those for methane shown in Figure 2.13. The maximum critical velocity gradient of hydrogen/air flames is more than twenty times that of methane/air flames and corresponds to ~40 percent hydrogen concentration (equivalence ratio of 1.59).

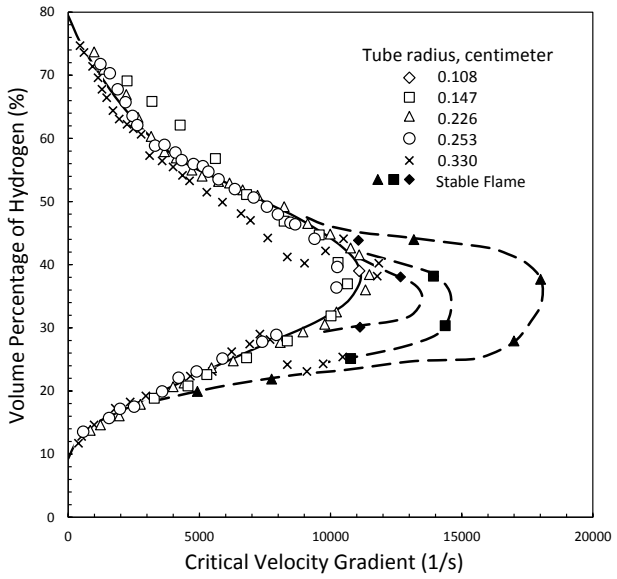

Figure 2.32: Critical velocity gradient of laminar hydrogen flame for different burner diameters, reproduced from [48].

Figure 2.33 illustrates the laminar burning velocity of hydrogen/air mixture at room temperature and atmospheric pressure obtained from Koroll et al [30]. The maximum laminar burning velocity occurs at 42 percent hydrogen concentration and is in good agreement with the maximum critical velocity gradient observed in Figure 2.32.

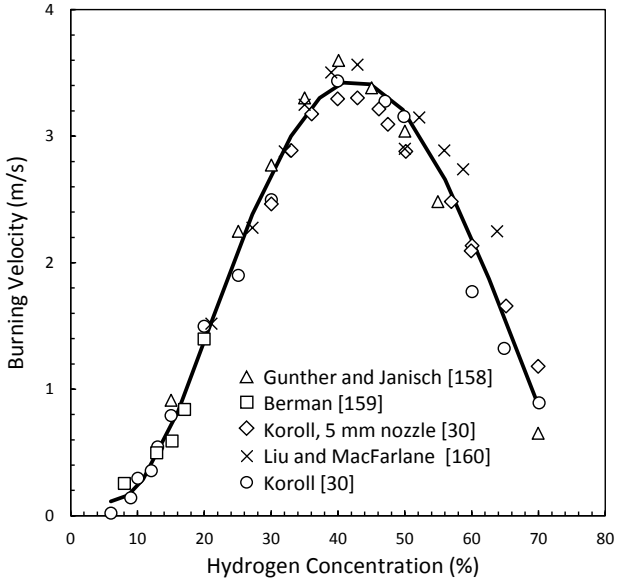

Figure 2.33: Laminar burning velocity of hydrogen/air mixture at 25 ℃ and atmospheric pressure measured by (Günther and Janisch [158]; Berman [159]; Liu and MacFarlane [160]), reproduced from [30].

2.3.4.3 Fuel Mixtures

Early studies demonstrated that the flashback propensity of binary mixtures is not generally a linear function of the individual components, especially when hydrogen or carbon monoxide is one of the components [55,57]. To better understand the behavior of binary mixtures, a comprehensive study was conducted by Grumer and Harris to investigate the flashback propensity of methane-hydrogen, carbon monoxide-hydrogen, and carbon monoxide-methane [57]. Experiments were carried out for several ratios of the two components. Since it was difficult to make a stability diagram for all different fuel compositions, results were presented in terms of critical velocity gradient variation as a function of hydrogen or carbon monoxide addition at given fraction of stoichiometric (F).

Figure 2.34 indicates the variation of critical velocity gradient for hydrogen-methane/air flames. From 0 to 50% hydrogen concentration, the ratio is defined by H_2/CH_4 and from 50 to 100% hydrogen the ratio is denoted by CH_4/H_2. The results are presented for both fuel lean and rich conditions as labeled by the fraction of stoichiometric in Figure 2.34. Adding a small amount of methane to hydrogen decreases flashback propensity significantly; however, adding a small amount of hydrogen to the methane does not drastically increase the critical velocity gradient.

This observation is consistent with the variation of the laminar flame speed for hydrogen-natural gas mixtures [161]. Figure 2.35 indicates the variation of the normalized laminar burning velocity as a function of hydrogen concentration in the mixture at equivalence ratio ranging from 0.6 to 1.4. Based on the definition in [161], the burning velocity increment can be defined as :

$$\frac{(S_{Mixture} - S_{NG})}{(S_{H_2} - S_{NG})} \qquad \text{Eq. 2.34}$$

in which, S denotes the laminar flame speed. For a given equivalence ratio, the laminar burning velocity increases exponentially (solid line). As a result, addition of methane to pure hydrogen fuel has more pronounced effect than the addition of hydrogen to pure methane according to Eq. 2.35 [161]:

$$\frac{(S_{Mixture} - S_{NG})}{(S_{H_2} - S_{NG})} = 0.00737 \exp\left(\frac{x}{20.38}\right) + 0.00334 \qquad \text{Eq. 2.35}$$

x is volume percent of hydrogen in the fuel mixture.

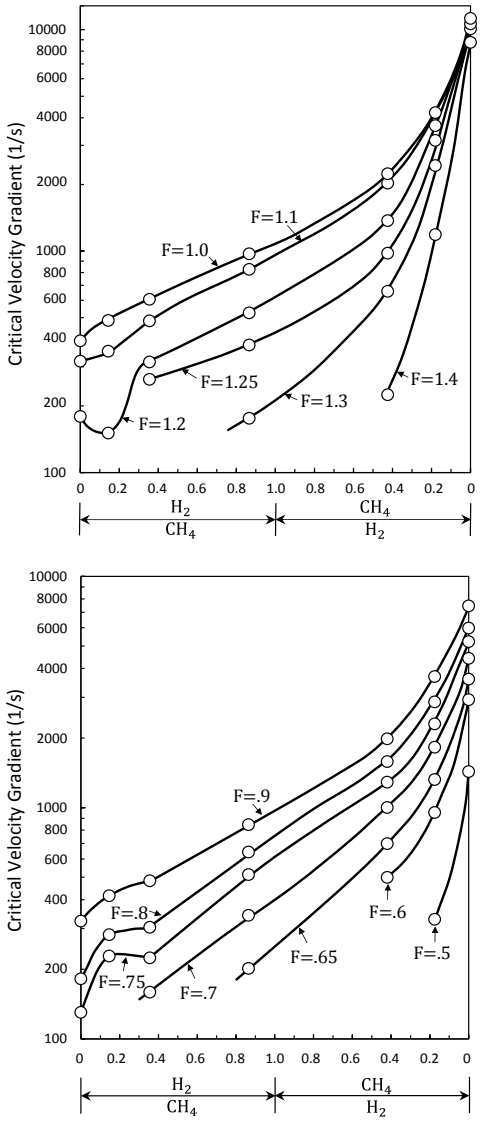

Figure 2.34: Critical velocity gradient of hydrogen-methane/air mixtures at different fuel concentrations (F), reproduced from [57].

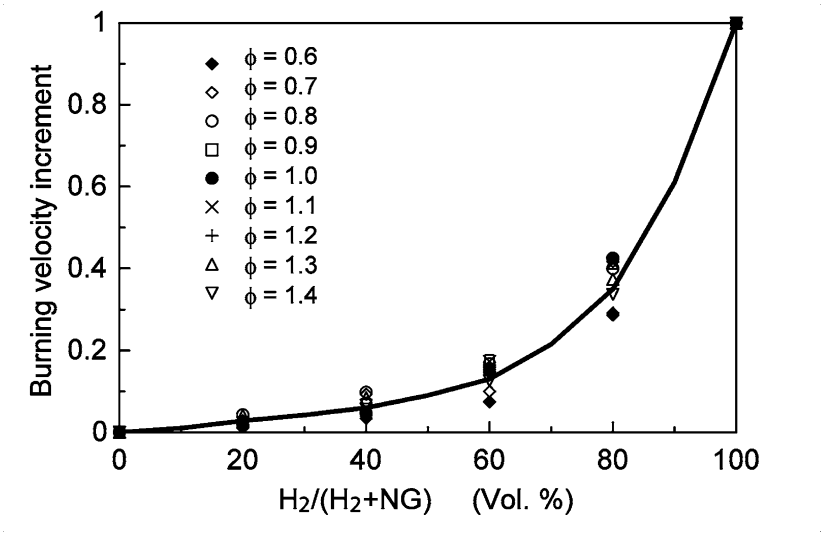

Figure 2.35: Normalized unstretched laminar burning velocity of hydrogen-natural gas/air mixture as a function of hydrogen concentration at different equivalence ratios [161].

Figure 2.36 illustrates the flashback propensity of carbon monoxide-hydrogen [57]. The flashback region of carbon monoxide-hydrogen mixture extends from stoichiometric fraction of 0.6 to 2.2, which is wider than that for hydrogen-methane mixtures (Figure 2.34). If Figure 2.36 is plotted in normal axis as a function of hydrogen concentration, the critical velocity gradient linearly varies for fraction of stoichiometric less than 1.4. However, when the hydrogen concentration is high, the critical velocity gradient increases rapidly with further increase in hydrogen content. This observation is consistent with the normalized laminar burning velocity measurement (see Eq. 2.36) by Dong et al. as shown in Figure 2.37 [162]. They concluded that the variation of laminar burning velocity is divided into three regions as seen in Figure 2.37: (1) rapid increase for hydrogen concentrations below 20%, (2) linear variation, and (3) rapid increase at hydrogen concentrations above 80%. Based on this study, the laminar burning velocity varies linearly for equivalence ratio from 0.7 to 2.1 [162]:

$$\frac{(S_{Mixture} - S_{CO})}{(S_{H_2} - S_{CO})} = -0.05914 + 0.00875x \qquad \text{Eq. 2.36}$$

in which, S denotes the laminar flame speed. The variation of critical velocity gradient at some rich conditions in Figure 2.36 is different from the overall trend, which is not predicted by the laminar burning velocity variation. There is no explanation for this observation in [57].

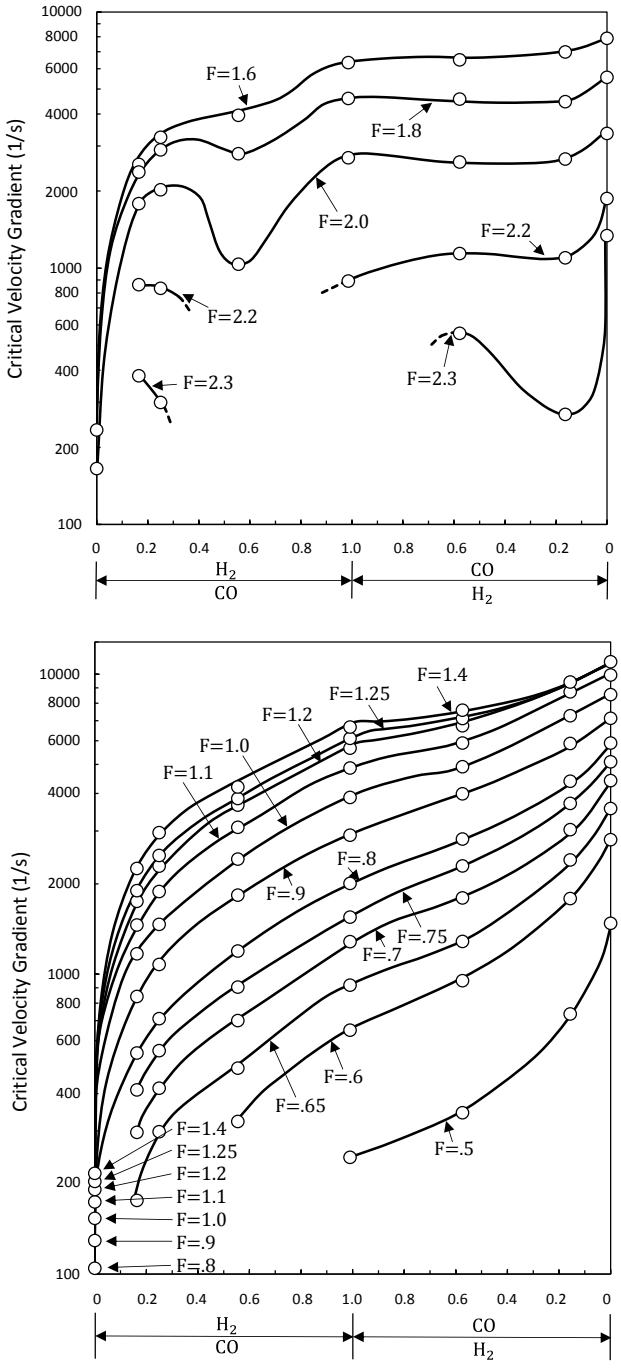

Figure 2.36: Critical velocity gradient of carbon monoxide-hydrogen/air mixtures at different fuel concentrations (F), reproduced from [57].

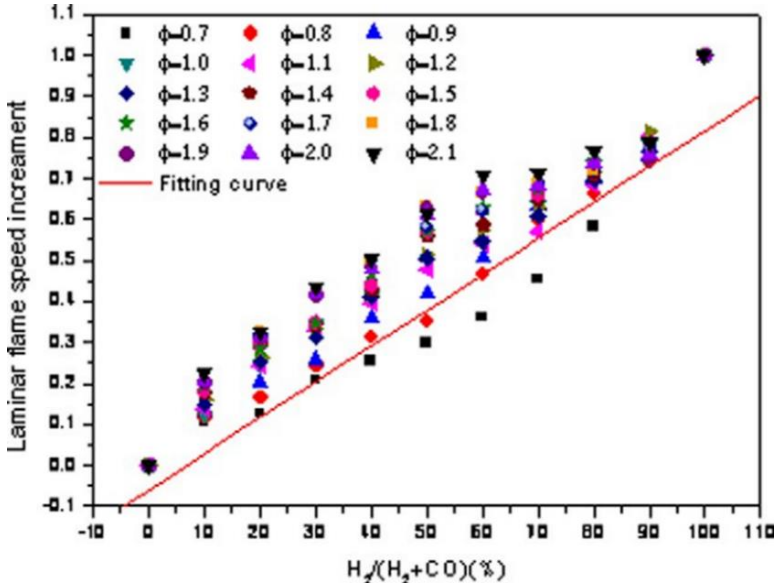

Figure 2.37: Normalized laminar burning velocity of carbon monoxide-hydrogen/air mixture vs hydrogen concentration at different equivalence ratios [162].

To further explore the subtleties of fuel mixture effects, Figure 2.38 presents the variation of critical velocity gradient for carbon monoxide-hydrogen/air mixtures as a function of fuel volume concentration. The addition of hydrogen to carbon monoxide significantly increases the critical velocity gradient. The effect of hydrogen concentration on critical velocity gradient is pronounced at lean conditions according to Figure 2.38(a) (data from Grumer and Harris [57]). However, this conclusion is not consistent with the recent experimental study by Dam et al. [96]. Indeed, as indicated in Figure 2.38(b), the effect of hydrogen addition in lean mixtures is small compared to its effect when added to fuel rich conditions. Furthermore, the addition of hydrogen shifts the peak of critical velocity gradient to lean conditions in Figure 2.38(a), while the opposite is observed in Figure 2.38(b). It is noted the maximum critical velocity gradient of hydrogen occurs at 40% fuel concentration as previously observed in Figure 2.32 [48], which is in agreement with the qualitative trend observed in Figure 2.38(a).

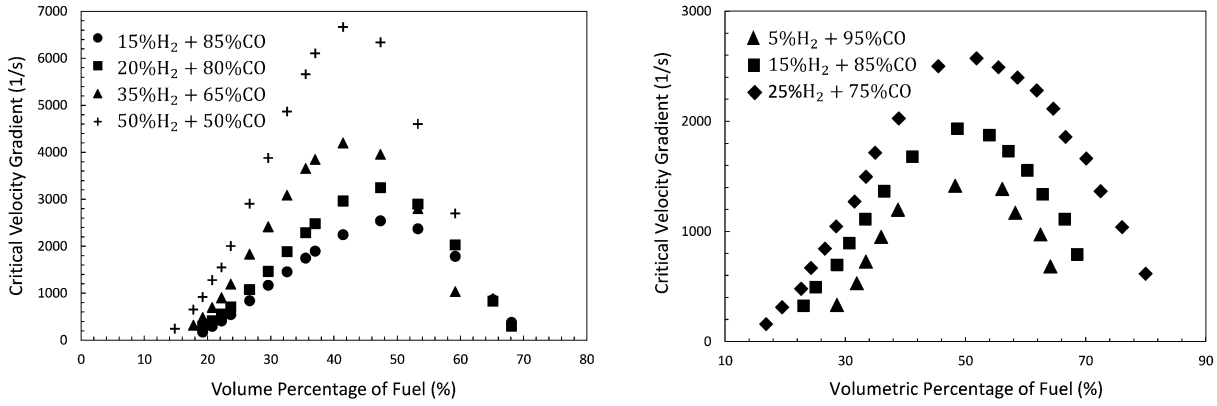

Figure 2.38: Critical velocity gradient variation as a function of fuel concentration for carbon monoxide-hydrogen/air mixtures (a) data from Grumer and Harris [57] and (b) reproduced from Dam et al. [96].

Figure 2.39 presents the critical velocity gradient variation of carbon monoxide-methane/air mixtures. Adding small amount of methane to carbon monoxide increases the flashback propensity drastically. However, the addition of small amounts of carbon monoxide to methane has only a slight effect. The molecular weight of methane is smaller than that of carbon monoxide and the addition of methane would be even smaller in terms of mass fraction. This illustrates that the dissimilar behavior resulting from adding a second fuel component to a single gas cannot be explained by difference in mass fraction [57].

The critical velocity gradient variation in Figure 2.39 is in accordance with the laminar burning velocity measurements by Scholte and Vaags [163] (shown in Figure 2.40). Figure 2.40 shows the burning velocity of methane-carbon monoxide mixtures as a function of the fuel/air ratio. An addition of a small amount of methane significantly increases the laminar burning velocity. With adding more methane, the laminar burning velocity peaks at about 90%CO-10%CH_4 and finally drops to the methane burning velocity. It is interesting to note that a similar point exists in Figure 2.39 (i.e., $CH_4/CO = 0.1$) at which the critical velocity gradient is maximum. Furthermore, Figure 2.39 illustrates that methane has a higher flashback propensity than carbon monoxide for fraction of stoichiometric less than 1.2, which is consistent with the laminar burning velocity variation reported in [163].

To create a stability diagram for a specific fuel binary compositions, one can select the fuel component ratios in Figure 2.34, Figure 2.36, Figure 2.39 and obtain critical velocity gradient at different fuel concentrations (see Figure 2.38a).

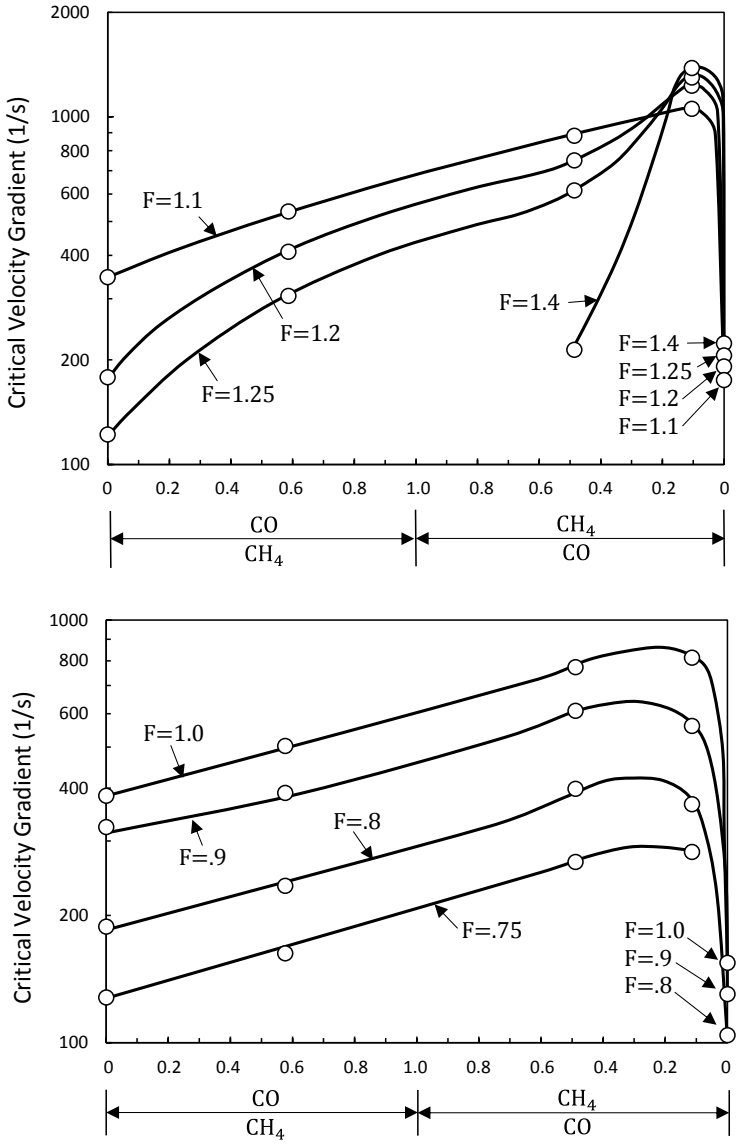

Figure 2.39: Critical velocity gradient of carbon monoxide-methane/air mixtures at different fuel concentrations (*F*), reproduced from [57].

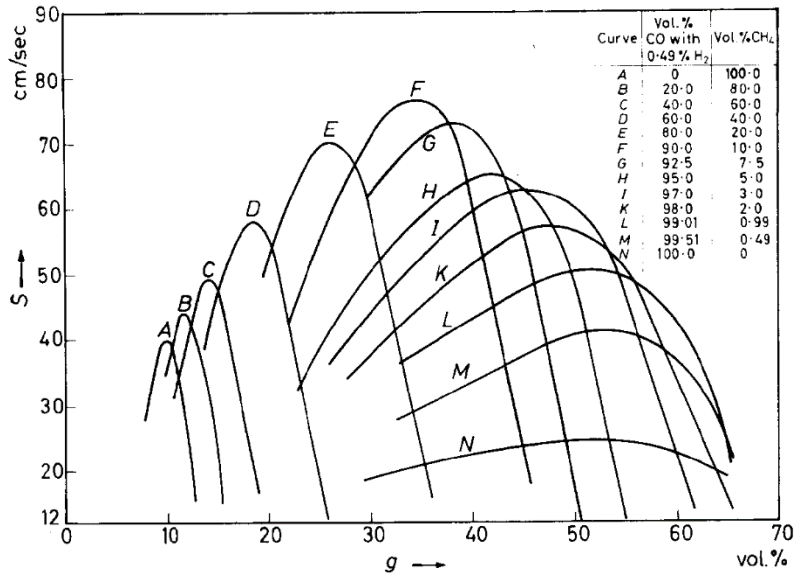

Figure 2.40: Burning velocity of carbon monoxide-methane/air mixtures as a function of fuel/air ratio [163].

The flashback propensity of air mixed with hydrogen-ethylene, propane-hydrogen, and hydrogen diluted with nitrogen was also investigated by Grumer et al. [65]. Figure 2.41 and Figure 2.42 present experimental results for these mixtures. Adding small amounts of ethylene or propane to hydrogen significantly decreases the flashback propensity of the mixture. Adding small amount of hydrogen to ethylene or propane increases the critical velocity gradient to a small extent.

Figure 2.43 illustrates the variation of laminar burning velocity for propane-hydrogen/air mixtures as a function of equivalence ratio at various hydrogen concentrations [164]. X_h denotes the volume percent of hydrogen in the fuel mixture. For a given equivalence ratio, small increase of propane in the pure hydrogen results in a significantly lower laminar flame speed and consequently much lower flashback limit as concluded in [55,65].

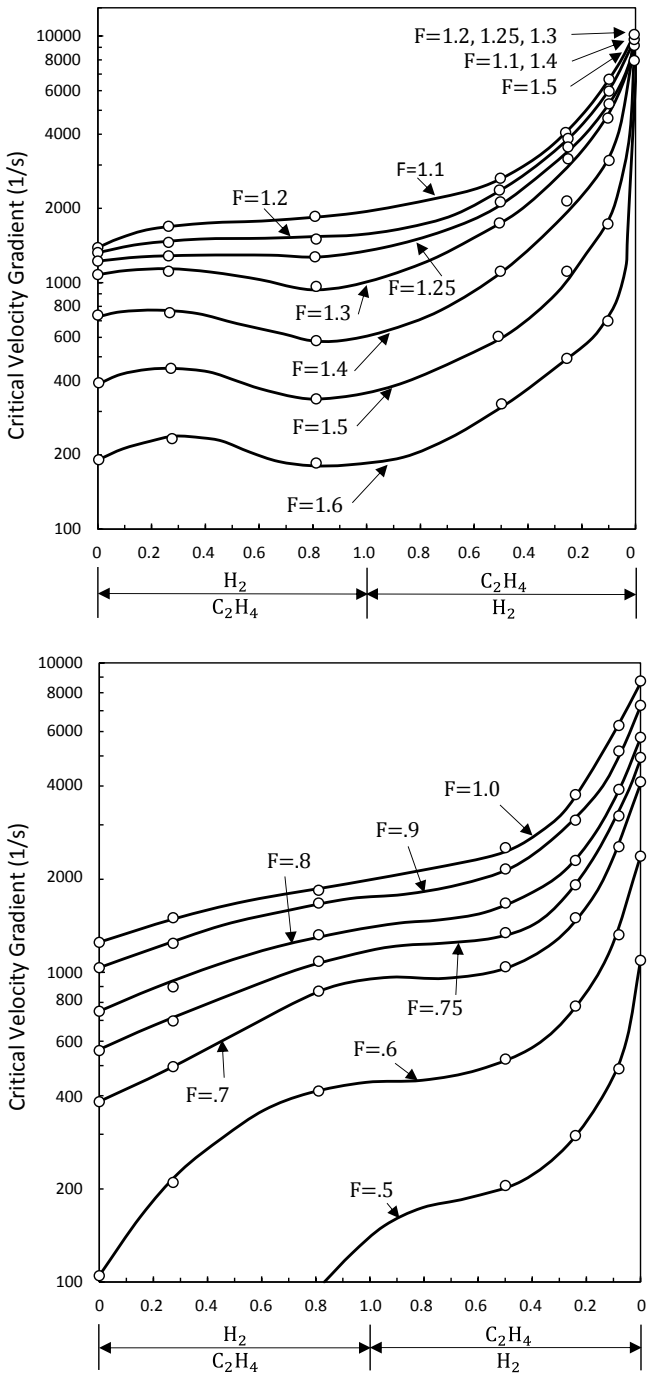

Figure 2.41: Critical velocity gradient of ethylene-hydrogen/air mixtures at different fuel concentrations (*F*), reproduced from [65].

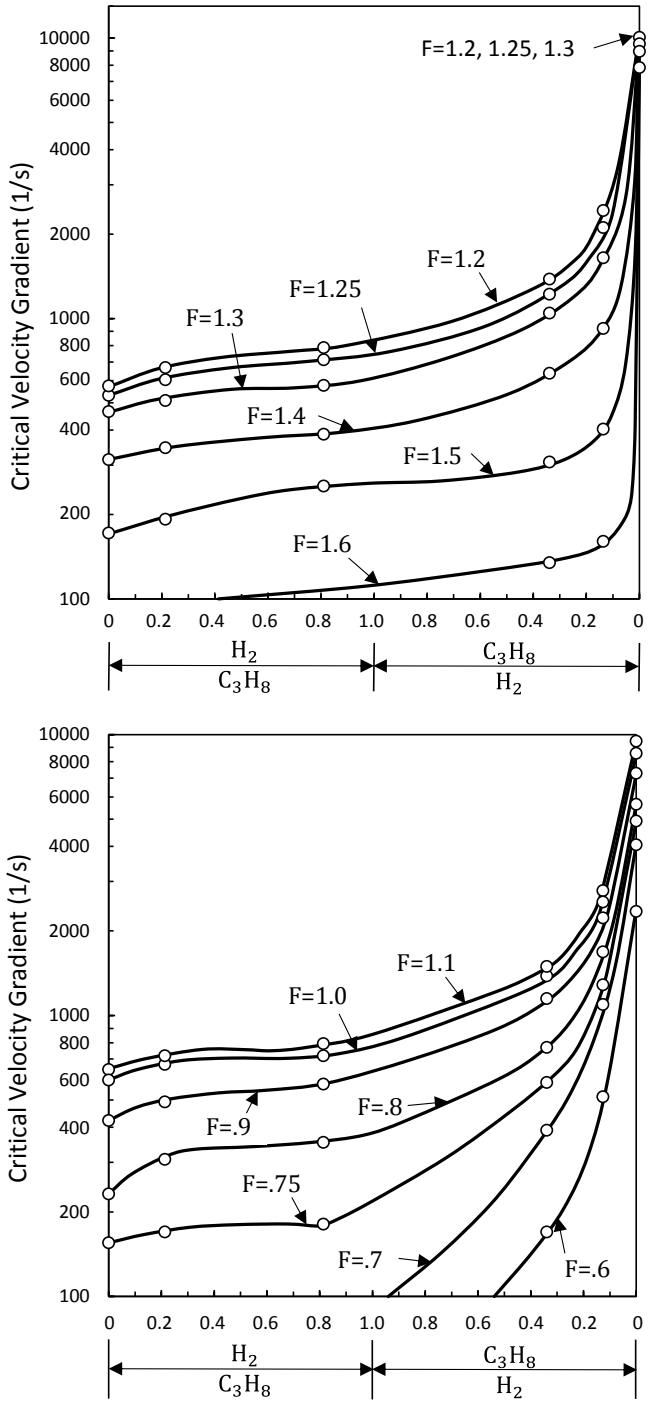

Figure 2.42: Critical velocity gradient of propane-hydrogen/air mixtures at different fuel concentrations (F), reproduced from [65].

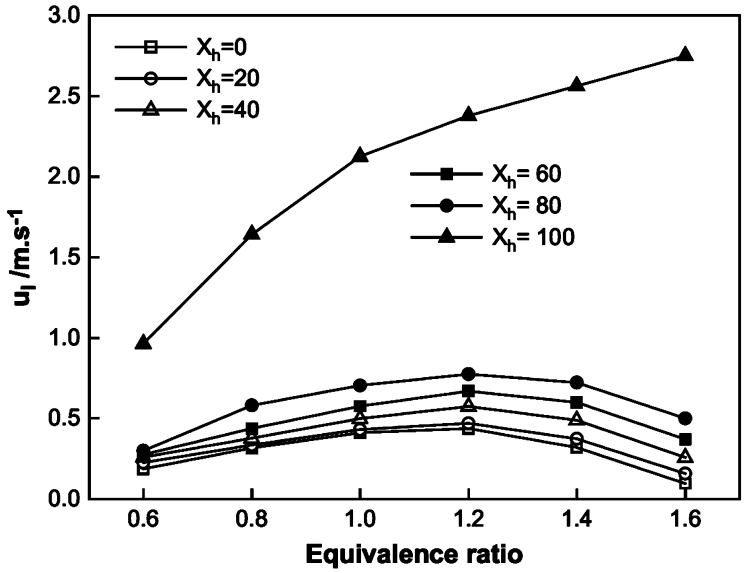

Figure 2.43: Laminar burning velocity of propane-hydrogen/air mixtures as a function of equivalence ratio at different hydrogen concentrations [164].

These results again indicate that the flashback propensity of multicomponent fuels is not a linear combination of the critical velocity gradient of single components involving hydrogen or carbon monoxide [57]. What has been observed is that for certain fuel components, a weighted average critical velocity gradient can been successfully applied. These fuels include binary and ternary hydrocarbon fuels including mixtures of alkanes and alkenes such as methane, ethane, propane, butane, and ethylene as studied in [65,72]. Figure 2.44 illustrates the flame stability diagram of mixture containing 79.4% methane-20.6% ethylene. The solid curve represents the calculated data from the linear combination of critical velocity gradients (Eq. 2.37), which is in a good agreement with experimental results. This method was also used for and 78.6 ethylene and 21.4% methane and a good agreement was obtained. Based on this conclusion, the critical velocity of a multicomponent mixture can be calculated from Eq. 2.37.

$$g_{y+z+\cdots} = n_y g_y + n_z g_z + \cdots \qquad \text{Eq. 2.37}$$

in which, *y* and *z* are fuel components and *n* is fractional volume concentration of each component. Values of g_y , g_z are obtained from critical velocity gradients of single component fuels.

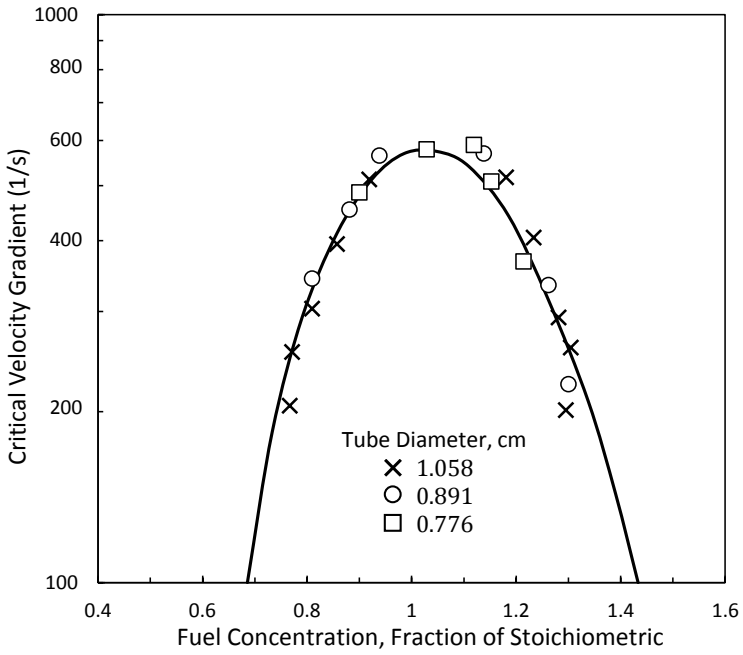

Figure 2.44: Boundary layer flashback propensity of 79.4% methane-20.6% ethylene vs fuel concentration, reproduced from [65].

When hydrogen and carbon monoxide are present in multicomponent fuels, a modified version of Eq. 2.37 was developed to calculate the critical velocity gradient of ternary fuel mixtures. Indeed, the critical velocity gradient of a multicomponent fuel is calculated from flashback limits of binary fuel mixtures, which are available for different fuel compositions as previously discussed. For a mixture including three gases α, β, and γ, a combination of two binary fuels $\alpha + \beta = n_y$ and $\alpha + \gamma = n_z$ are considered in which the value of α is devide between β and γ in the ratio of β/γ. The selection of α, β, and γ for a ternary fuel mixture was based on experimental results. For a fuel mixture containing hydrogen, carbon monoxide, and methane, the binary fuel components are selected as CO-CH_4 and H_2-CH_4. Figure 2.45 illustrates the evaluation of the implemented method for three fuel components. The curve lines represent calculated values from Eq. 2.37 and predict experimental results fairly well as shown in Figure 2.45(a). But, clear deviation is observed in Figure 2.45(b) at rich condition.

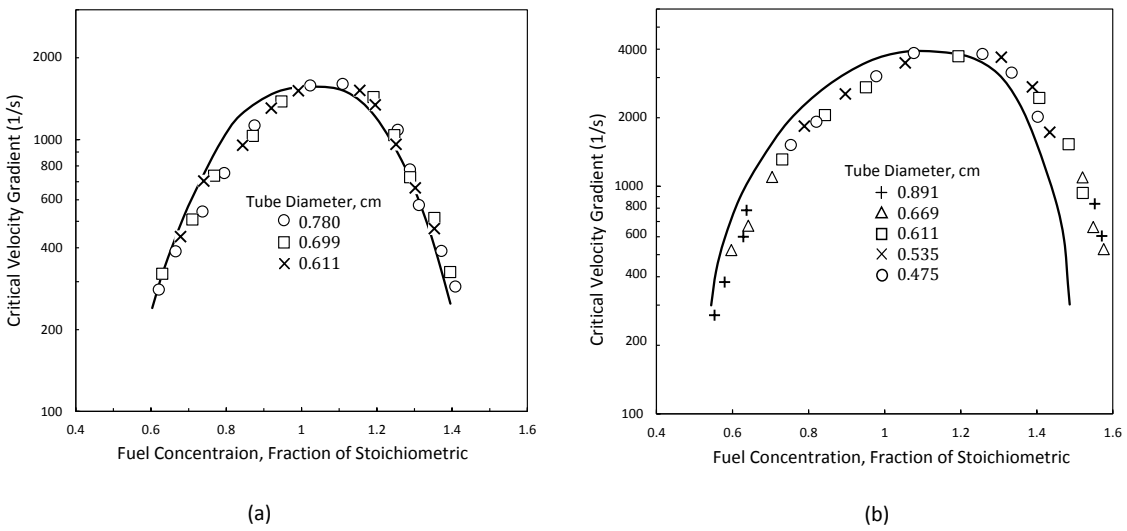

Figure 2.45: Boundary layer flashback limit for different burner diameters (a) 29.4% CH_4, 31.7% CO, 38.7% H_2 mixture and (b) 10.3% CH_4, 34.0% CO, 55.7% H_2 , reproduced from [57].

Eq. 2.37 was also implemented to predict the flashback propensity of multicomponent fuels as summarized in Table 2.2. Carbon dioxide and nitrogen were treated as diluents. This means that associated critical velocity gradients of these constituents are considered to be zero in Eq. 2.37. The critical velocity gradients of these fuels were calculated by assuming different single and binary mixtures as indicated in Table 2.3. As mentioned earlier, the selection of α was not arbitrary and determined experimentally. Since the critical velocity gradient of these single and binary mixtures are known from [57,65], the flashback propensity of the multicomponent mixture can be calculated. The comparison of calculated results with those from the experiment showed a good agreement [65].

A similar correlation was developed in [87] to calculate the critical velocity gradient of a fuel mixture consisting of hydrogen, methane, carbon monoxide, carbon dioxide, and nitrogen. The final equation was presented based on the volume fraction of fuel components in the mixture, in which coefficient and exponents were obtained from the experimental data obtained. The error of the correlation was less than 6 percent for studied cases.

Table 2.2: Composition of multicomponent fuels studied in [65].

	Fuel 1	Fuel 2	Fuel 3	Fuel 4	Fuel 5
Methane	37.4	29.1	32.1	42.6	37.5
Ethane	-	-	-	2.2	-
Ethylene	33.4	26.2	28.4	18.1	20.4
Propane	-	22.1	-	1.9	-
Propylene	-	0.2	-	0.2	-
Butane	-	-	-	0.2	-
Butylene	-	-	-	0.1	-
Hydrogen	15.2	11.8	12.5	17	17.5
Carbon monoxide	-	-	-	9.1	3.9
Nitrogen	14.0	10.6	27.0	3.4	13.3
Carbon dioxide	-	-	-	5.2	7.4

Table 2.3: Listing of complexes for use in Eq. 2.37 [65].

	Flashback complexes
Fuel 1	(C_2H_4 + H_2) and (CH_4)
Fuel 2	(C_2H_4 + H_2) and (CH_4) and (C_3H_8)
Fuel 3	(C_2H_4 + H_2) and (CH_4)
Fuel 4	(C_2H_4 + H_2) and (CH_4 + CO)
Fuel 5	(C_2H_4 + H_2) and (CH_4 + CO)

A systematic study of fuel composition effects on flashback was conducted by Van Krevelen et al. [78]. They developed a method to provide a generalized flame-stability diagram for all fuel mixtures. A generalized flashback diagram was introduced in Figure 2.46 by using (1) non-dimensional critical velocity gradient, and (2) reduced gas concentration. Based on this model, the critical velocity gradient (g_c) is normalized by the peak value of the flashback curve $(g_c)_M$ in Eq. 2.38 (see Figure 2.46).

$$(g_c)_R = \frac{g_c}{(g_c)_M} \qquad \text{Eq. 2.38}$$

The reduced gas concentration (F_R) is obtained from Eq. 2.39 to create a scaled parameter for fuel variation.

$$F_R = 1 + \alpha(F - F_M) \qquad \text{Eq. 2.39}$$

in which, F is the fuel gas concentration (fraction of stoichiometric) and F_M corresponds to the location at which critical velocity gradient is maximum. α is defined as a reduction factor, which is equal to the reciprocal of the width of flashback curve and normalized such that it is equal to one for methane.

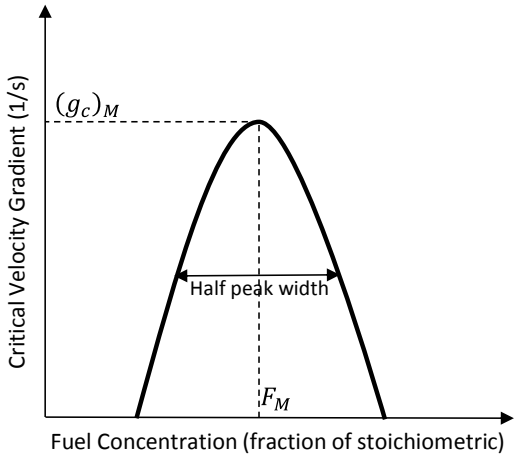

Figure 2.46: Schematic of boundary layer flashback curve for a fuel/oxidizer mixture, adapted from [78].

Measured values of $(g_c)_M$, F_M, and α for various fuels are summarized in Table 2.4 (data obtained from [57,65,78]). The generalized flashback curve has a peak value $(g_c)_R = 1$ at $F_R = 1$. Using characteristic values in Table 2.4 and generalized flashback curve in Figure 2.47 (semi-log plot), one can obtain the critical velocity gradient at desired fuel concentration for studied fuels using Eq. 2.38 and Eq. 2.39.

This method was extended to characterize the flashback propensity of mixtures diluted with inert gases including nitrogen and carbon dioxide. The characteristic values of binary and multicomponent fuels $(g_c)_M$, ϕ_M, and α were determined as functions of inert-free mixture and diluents concentrations. Some correlation were developed for hydrogen, carbon monoxide, methane, ethane, ethylene, and propane with combination of either nitrogen or carbon monoxide [78].

A similar approach was used by Van Krevelen et al. for binary and multicomponent fuel mixtures and characteristic values were tabulated in [78]. As previously pointed out, the characteristic parameters for mixtures of hydrocarbons are additive [57,65]. Consistent with earlier studies, it was concluded that this

cannot be extended to mixtures of carbon monoxide and hydrogen with hydrocarbons [78]. Furthermore, the behavior of the carbon monoxide was mentioned to be abnormal in many respects. Hence, "depression factors" were defined to capture this effect.

Table 2.4: Characteristic flashback values of different fuel compositions [78].

Fuel gas	$(g_c)_M\ (1/s)$	F_M	α
CH_4	400	1.00	1.00
C_2H_6	650	1.13	0.80
C_3H_8	580	1.12	0.60
C_2H_4	1400	1.10	0.63
C_3H_6	800	1.14	0.68
C_6H_6	720	1.09	0.63
H_2	10500	1.20	0.46

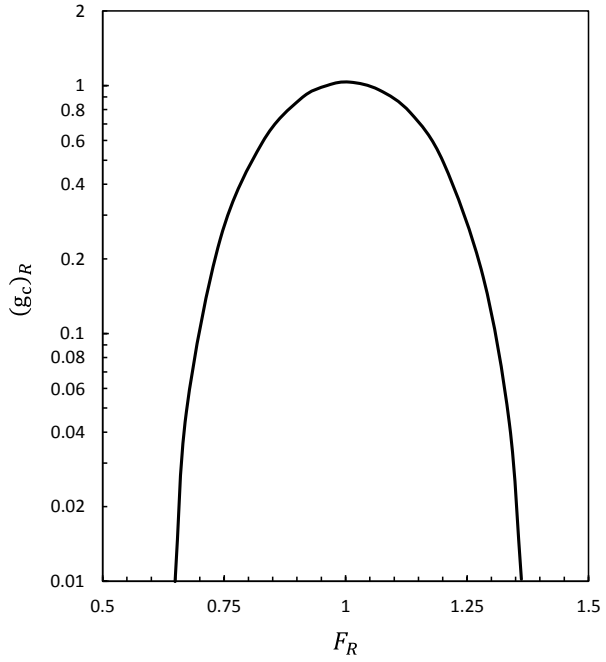

Figure 2.47: Generalized boundary layer flashback curve, reproduced from [78].

In further work to predict fuel composition effects when hydrogen is present, Caffo and Padovani developed a simpler method to predict the flashback propensity in multicomponent fuels [81]. In their correlation, the critical velocity gradient of multicomponent fuels was calculated by assigning a constant

coefficient to hydrocarbons and a variable coefficient to hydrogen. Thus, the critical velocity gradient of inert-free mixtures was introduced as:

$$g_c = a_{H_2} \times \%H_2 + \sum a_i \times \%C_i \qquad \text{Eq. 2.40}$$

where a_i is a coefficient for hydrocarbons present in the mixture. a_i is fixed for each component depending on the equivalence ratio. a_{H_2} is the hydrogen coefficient represented as a function of the mixture stoichiometric air coefficient (A_s) and the concentration of other hydrocarbons ($\%C_i$) accompanying the hydrogen. Based on the experimental results, a_{H_2} was presented in the form of:

$$a_{H_2} = \sum K_i \times \%C_i \qquad \text{Eq. 2.41}$$

in which K_i is determined from the mixture stoichiometric air coefficient (A_s). This variation is indicated in Figure 2.48 for various fuels and nitrogen as a diluent. The overall value of a_{H_2} is primarily affected by (A_s) according to Eq. 2.41. The values of a_i are also tabulated in Table 2.5. This result was also extended to carbon monoxide and different coefficients were tabulated in [81]. It is noted that all coefficients in Table 2.5 and reference [81] were obtained for stoichiometric conditions and cannot be generally extended to other equivalence ratios. The study by Caffo and Padovani indicates that the critical velocity gradient of the hydrogen and hydrocarbons mixtures can be expressed as a function of the mixture stoichiometric air coefficient. This method was evaluated for various fuel compositions at stoichiometric condition with hydrogen concentration varied from 8% to 56% in the fuel mixture and the results matched experimental data within 5% [81].

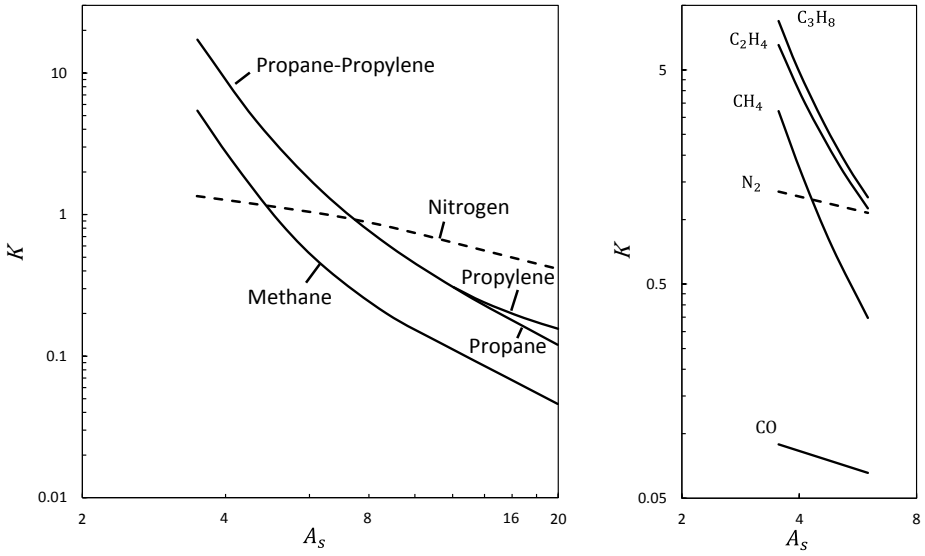

Figure 2.48: Coefficient *K* as a function of stoichiometric mixture coefficient, reproduced from [81].

Table 2.5: Values of a coefficient for hydrocarbons [81].

Hydrocarbon	CH_4	C_3H_8	C_3H_6
a coefficient	4.54	6.06	7.01

Correlations for flashback propensity of multicomponent fuel mixtures under laminar conditions were also developed by Putnam et al. [85]. They examined different fuel compositions as summarized in Table 2.6 [85]. Flashback propensity of each mixture was determined for various equivalence ratios and the value of $g_c\delta_q/S_L$ was calculated for each case and reported in Table 2.6. Each group labeled by (a, b, and c) has a constant adiabatic flame temperature and a constant product composition at stoichiometric condition. The burning velocity was measured by determining the flame front angle stabilized above the burner rim. Quenching distance was reported as the minimum width between two plates in which the flame can propagate. The critical velocity gradient was calculated from Eq. 2.5. The equivalence ratio corresponding to the peak critical velocity gradient also corresponded to the minimum quenching distance value However, the peak of the burning velocity (S_L) occurred at lower equivalence ratios compared to that corresponding to the maximum g_c and minimum δ_q condition. This deviation was

attributed to the burning velocity measurement procedure for the atmospheric test conditions. The further details of this experiment including the burning velocity and quenching distance data can be found in [84].

Table 2.6: Fuel compositions studied for boundary layer flashback in [85].

Mixture number	CO	H_2	CH_4	$C0_2$	O_2	N_2	$g_c\delta_q/S_L$
1a	0.590	0.295	0	0.115	0	0	2.36
b	0.566	0.147	0.096	0.151	0.039	0	2.40
c	0.542	0	0.193	0.187	0.078	0	1.90
2a	0.295	0.590	0	0.115	0	0	3.20
b	0.147	0.373	0.205	0.191	0.083	0	2.52
c	0	0.156	0.410	0.268	0.166	0	1.90
3a	0.442	0.442	0	0.115	0	0	2.50
b	0.360	0.221	0.171	0.179	0.069	0	2.40
c	0.277	0	0.342	0.243	0.138	0	1.92
4a	0.257	0.128	0	0.115	0	0.500	2.60
b	0.245	0.064	0.042	0.140	0	0.511	2.58
c	0.232	0	0.083	0.164	0	0.521	2.15
5a	0.128	0.257	0	0.115	0	0.500	2.60/2.35
b	0.064	0.162	0.087	0.167	0	0.521	2.85
c	0	0.067	0.173	0.218	0	0.541	1.80
6a	0.192	0.192	0	0.115	0	0.500	2.35
b	0.155	0.096	0.073	0.158	0	0.518	2.75
c	0.118	0	0.145	0.201	0	0.535	-

The final results were plotted in the form of concentrations ratio defined by $(H_2 - CH_4)/(H_2 + CH_4 + CO)$ as shown in Figure 2.49. The value of $g_c\delta_q/S_L$ approaches 2 as methane concentration increases and reaches 2.5 with an increases of hydrogen. Since the measured quenching distance between two parallel plates is around twice of the penetration distance [47], $g_c\delta_p/S_L$ would be 1-1.25, which is consistent with that obtained by Lewis and Elbe [47].

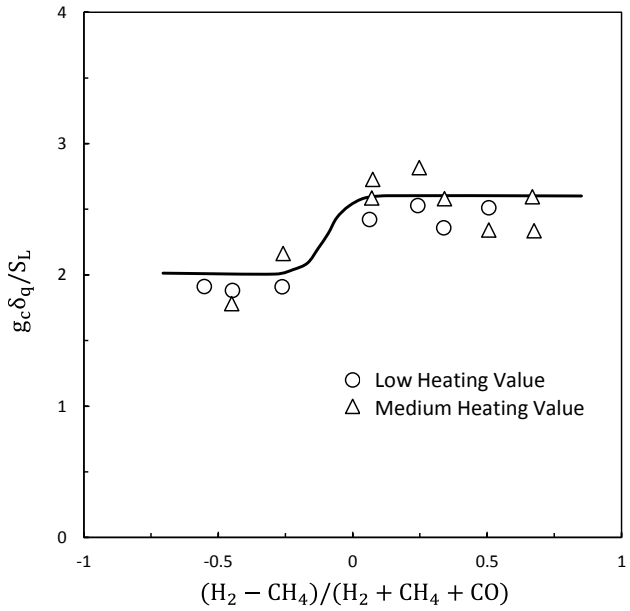

Figure 2.49: Variation of $g_c\delta_q/S_L$ as a function of fuel concentration ratio (see Table 2.6), reproduced from [85].

In summary, fuel composition can significantly impact the flashback limit as illustrated for single, binary, and multi-component fuels. A direct relationship between laminar burning velocity and flashback propensity is clearly observed for all fuel mixtures as predicted by simple models. Different studies have developed various correlations for the flashback limit of multicomponent fuels. Many of the studies observed that special consideration is required when hydrogen or carbon monoxide is present in the mixture. The empirical equations include various coefficients which are not known or validated for all operation conditions and experiment configurations. However, qualitative comparisons made in Section 2.3.4 can be served as a tool to investigate the interchangeability of fuel gases [54,58].

2.3.5 Numerical Analysis

Numerical simulations of boundary layer flashback have provided important details about the influence of the flame on the flow field. One-dimensional numerical simulations have been conducted for flame propagation normal to the wall (see head-on quenching in Figure 2.7) by different studies [123,125,165–

169]. However, only a few studies have addressed laminar boundary layer flashback, and these are summarized in this section.

The first numerical study was performed by Lee and T'ien [86] in 1982 for propagation of a premixed laminar flame through a tube. The analysis was limited to small diameters due to the computational cost. This pioneering simulation showed the importance of the flame back-pressure due to flame-flow interaction. The steady state Navier-Stokes and energy equations were solved numerically for the laminar flow with one-step chemical reaction and second order finite rate Arrhenius kinetics. A parabolic velocity profile for fully developed laminar flow was assumed at inlet condition with a variable magnitude in order to produce stationary flame representing the flashback condition. The wall temperature was considered equal to the unburned mixture temperature ($T_0 = 298$). The effect of the tube radius on flashback limits was studied for ten cases at equivalence ratio of 1 as indicated in Figure 2.50. The reference length (L) was defined by the flame thickness, which is the ratio of thermal diffusivity to the one-dimensional laminar burning velocity ($^{\alpha}/_{S_L} = 4.629 \times 10^{-3}\ cm$). The reference value of $S_L = 38\ cm/sec$ was used as a scaling parameter. As the tube radius decreases, the critical velocity gradient increases and then abruptly reduces. This trend line is similar to the experimental results of Lewis and Elbe [47] in Figure 2.14. At first, when the tube diameter decreases, the quenching distance moves closer to the tube axis and the critical velocity gradient assumption based on the linear velocity profile close to the wall is not valid. With further decrease of the tube diameter, the flame within the entire tube is influence by the quenching effect.

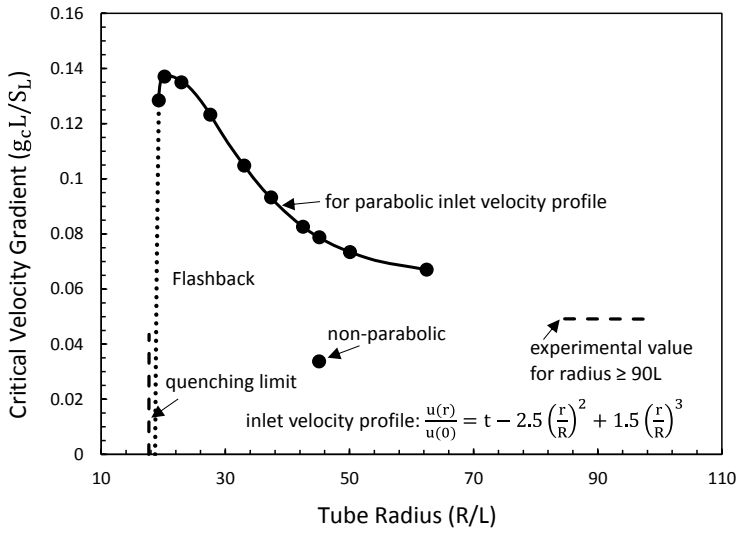

Figure 2.50: Critical velocity gradient as a function of tube radius, reproduced from [86].

Figure 2.50 also shows that the calculated critical velocity gradient reaches a plateau independent of the tube radius since the flame stabilization zone remains approximately unchanged at sufficiently large diameters. This value seems slightly high compared to measured critical velocity gradient value in the experimental data of [113] (denoted by dashed line in Figure 2.50). The quenching limit was interpolated from calculated results (indicated by dotted line) and the tube radius at which quenching occurs is lower than reported experimental values in [113]. It is noted that the experimental data in [47,113] were obtained for an unconfined flame stabilized in ambient air, while the numerical analysis was conducted for a confined flame.

The flame front is bent towards the unburned reactants through nearly the entire channel since the tube size was relatively small (recall the smallest diameter used by Lewis and Elbe). The shape and characteristic of the flame front are similar to the observation based on experimental results in Figure 2.5 [47,48,63]. The flame front is strongly curved inside the tube and one-dimensional flame sheet cannot provide a realistic values for the laminar flame speed, especially close to the tube wall (see the isothermal line in Figure 2.51).

The static pressure increases normal to the flame front and then decreases, which is in agreement with velocity vectors in Figure 2.51. The unburned mixture decelerates as it approaches the flame front in Figure 2.51. When the temperature of the mixture increases across the flame front, the density decreases and flow velocity increases accordingly. Interaction between velocity, pressure, and heat release leads to the distortion of the streamline before entering the flame zone, previously observed in experimental results of [170,171]. Divergence of the velocity vectors continues through the reaction zone and, as the flow passes the flame, the streamlines become parallel to the tube axis. The calculated burning velocity along the tube axis was higher than the one-dimensional laminar flame speed due to the interaction of the flame and pressure field [86].

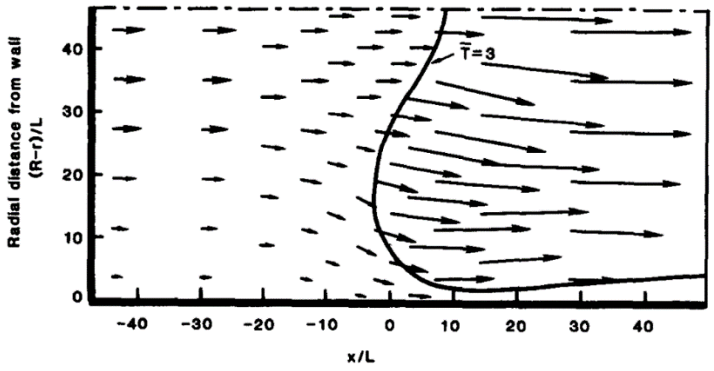

Figure 2.51: Velocity vectors at $T_0 = 298$ for the tube radius of $R = 46.5\ L$ [86].

Lee and T'ien [86] only considered the confined flame configuration. However, in practical applications, the flame is generally stabilized downstream of the burner rim. Mallens and Goey conducted a numerical study for unconfined methane/air flames and compared results with the experimental data [89]. The experimental setup by Mallens and Goey consisted of a rectangular slit burner with cross section of $55\ mm \times 2b$, in which 2b was varied from 4 to 10 *mm*. . The burner rim temperature was kept constant at 50 ℃ by water cooling. A similar setup was used to measure the flashback propensity of flames stabilized downstream of circular tubes with diameters from 4 to 10 *mm*. The tip temperature was not controlled during this experiment as it was believed to have a negligible effect on flashback limits. The

range of equivalence ratio covered in both experiment was between 0.9 and 1.1 and flow was fully developed at the burner exit.

Mallens and Goey also conducted a steady two-dimensional simulation of both laminar premixed flames considered in their experimental study. Governing equations of motion of motion and energy were formulated with stream-vorticity functions and solved considering one-step chemical reaction with the Arrhenius type source tem. A parabolic velocity profile was used at inlet condition. The detailed description of the numerical method implemented is available elsewhere [89,172–174]. In order to simulate the flashback limit by the steady code, the bulk flow velocity was decreased incrementally (5 percent reduction at each step) to reach the condition when the flame did not stabilize at the burner rim and propagated upstream. This critical flow rate was reported as a flashback limit for numerical results.

The comparison of numerical and experimental results is illustrated in Figure 2.52. The critical velocity gradient variation as a function of burner width and diameter are shown for both slit and tube burners. The experimental data agree well with the numerical results and the difference is less than 10% for all widths and diameters studied [89]. The deviation is more significant for the tube burner, possibly due to the low mass flow rate and associated uncertainty in measurements which can be up to 15 percent. The experimental results of Harris et al. [51] are shown as solid squares for two tube burner diameters of 8.82 and 9.66 *mm*. As suggested by the numerical results in Figure 2.52, the slit burner has a lower critical velocity gradient than the tube burner, which is consistent with the conclusion made by Putnam and Jensen [52]. The difference between the two burner configurations reduces to less than 5 percent for burner diameters larger than 6 mm. This trend is not predicted by experimental results probably due to the measurement uncertainty. Furthermore, the effect of tip temperature can be significant for the tube burner since it was not cooled in this experiment.

The critical velocity gradient decreases with an increases of burner diameter or channel width, which is consistent with the numerical results by Lee and T'ien [86]. As the burner diameter decreases, the quenching distance is comparable to the burner diameter and consequently the velocity at which flashback occurs can no longer be estimated by a linear velocity profile.

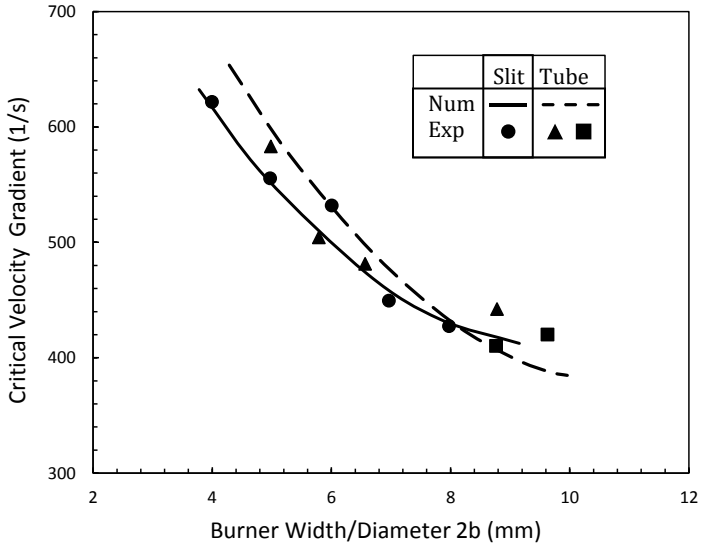

Figure 2.52: Critical velocity gradient variation as a function of burner width/diameter: the solid triangle and circle show experimental results for the tube burner and slit burner, respectively. Solid squares are experimental results by Harris et al. [51], reproduced from [89].

Figure 2.53 presents the variation of critical velocity gradient as a function of equivalence ratio for the 5 *mm* diameter burner. The numerical results match well with experimental data within equivalence ratio of 0.9 and 1.1. However, the numerical model does not follow the experiment trend line outside this interval. The deviation between numerical and experimental results is significant for the lowest and highest equivalence ratios studied. This is attributed to inaccuracies in the calculated burning velocity resulting from the one-step chemical reaction as well as inaccuracies in flow rates when setting the equivalence ratio in the experiment. The maximum critical velocity gradient occurs at equivalence ratio of 1, corresponding to experiment by Harris et al. [51].

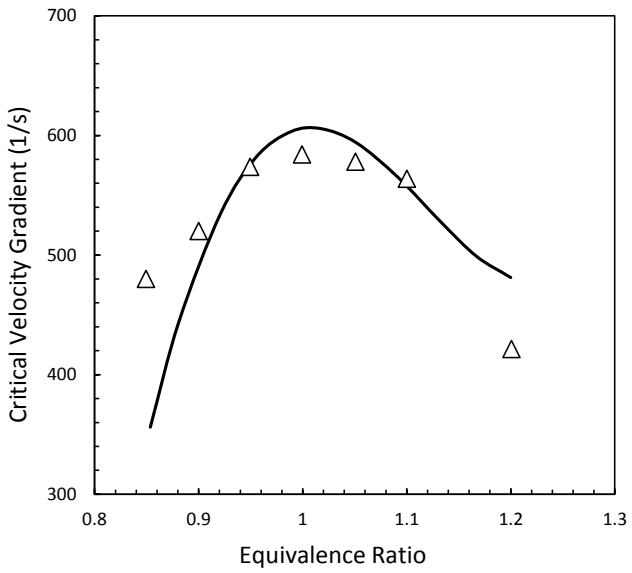

Figure 2.53: Critical velocity gradient variation with equivalence ratio for 5 *mm* burner diameter, experimental results are shown by triangles, reproduced from [89].

Kurdyumov et al. [90] carried out a simplified analysis of boundary layer flashback. They investigated the propagation of a flame close to the wall inside a tube, the diameter of which was much larger than the preheated flame thickness. With this condition, the computational domain was modeled by the flow over a flat plate and the so-called thermal-diffusive approximation was used. Neglecting the density and viscosity variation with temperature, the laminar velocity profile ($u = Ay, v = 0$) remains undisturbed through the entire domain. As a result, energy and deficient reactant mass conservations were solved without fluid dynamic coupling in non-dimensional forms for adiabatic and isothermal wall boundary conditions. A one-step chemical reaction with Arrhenius kinetics was used while taking into account the effect of Lewis number of different fuels. The Karlovitz number was used to present flashback limits and defined as ($\alpha g/S_L^2$), which is inversely proportional to the Damköhler number ($Ka = 1/Da$). Based on this definition, flashback occurs if the velocity gradient drops below a critical value. For Lewis number less than unity, the diffusion of the fuel is enhanced, resulting in an increase in flame temperature and, consequently, higher burning velocity. Hence, the critical velocity gradient increases with a decrease in

Lewis number leading to higher Karlovitz number. The Lewis number effect is more pronounced for the adiabatic wall boundary condition.

As pointed out, the governing equations of motion were not solved in this analysis and consequently the flame-flow interaction was not captured by the simulation. The interaction of heat release, pressure, and velocity distribution plays a crucial role in boundary layer flashback inside a tube or channel as discussed in 2.4.4.

A two-dimensional simulation of the flame propagation in a tube was also carried out in [91,92] considering the thermo-diffusive approximation. Figure 2.54 shows the flame propagation velocity in a tube normalized by the planar laminar burning velocity for various Lewis numbers [92]. The isothermal and adiabatic boundary conditions are denoted by solid and dashed lines, respectively. The circle symbols show the tube radius at which the flame quenching occurs. For Lewis number less than unity, the calculated flame speed is larger than that of the adiabatic planar burning velocity due to the cellular flame structure. It is noted that two solutions exist for the isothermal wall, upper branch (stable) and lower branch (unstable), separated by the quenching radius. For Lewis number larger than unity, the flame propagation approaches the planar burning velocity monotonically by an increase of the tube radius. For unity Lewis number, the curve has a “mushroom-shaped” as observed in [88,175] and the stable branch approaches the planar flame speed asymptotically. When the tube diameter is sufficiently large compared to the quenching radius, three dimensional analysis is required and calculated burning velocity changes significantly [92]. However, if the tube diameter is similar to the quenching diameter, two dimensional analysis successfully predicts the results since the flame structure is essentially two dimensional.

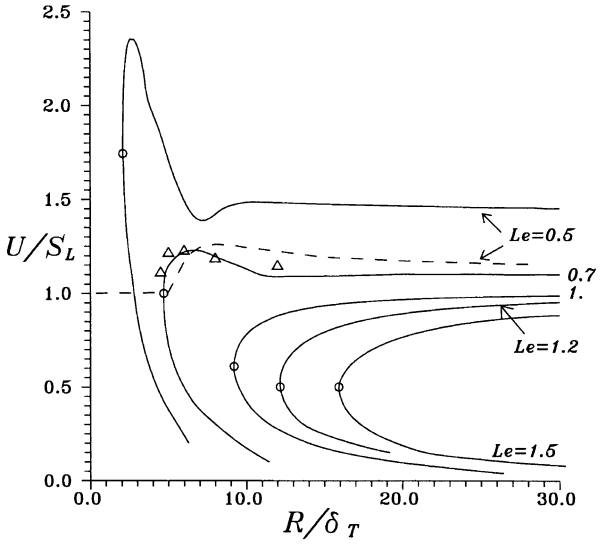

Figure 2.54: Non-dimensional flame velocity as a function of tube radius normalized by preheat zone thickness, solid line (isothermal wall), dashed line (adiabatic wall), circle (flame quenching), triangle (three-dimensional solution for isothermal wall and Le=0.7)[92].

Flame propagation in the boundary layer was studied numerically and experimentally by Kurdyumov et al. [94] and qualitative agreement was observed. The experiment was conducted with propane/air and methane/air mixtures at equivalence ratio of 0.53 and 0.57, respectively. The tube diameter was 21.4 *mm* and laminar flow was fully developed with the Reynolds number less than 150 for all cases. The flame was stabilized downstream of the burner similar to the experiment by Lewis and Elbe [47]. Kurdyumov et al. implemented laser tomography to capture the streamlines through the steady flame [94]. A tilted flame flashback was observed in this experiment and Figure 2.8(b) indicates the flame anchoring inside the tube burner. The flame front is strongly curved close to the tube wall as previously illustrated in Figure 2.5 [47,48,63]. The flame thickness was estimated around 0.23 *mm* and since it is significantly smaller than the tube diameter, the flame structure was considered two-dimensional in the laser sheet plane near the wall. Figure 2.55(a) shows the tomographic cut of streamlines across the flame zone. The parabolic velocity profile is also indicated in Figure 2.55(a) within 9 *mm* from the tube wall. As the flow approaches the flame front, the streamline departs from the parallel path along the tube wall due to back pressure of the flame front.

The critical velocity gradient of methane/air mixture at equivalence ratio of 0.57 was 50 *1/s*, which is in good agreement with Lewis and Von Elbe's results [47] shown in Figure 2.13. The value for the propane/air mixture at equivalence ratio of 0.53 was found to be 39 *1/s*, which is in agreement with results from [113].

The steady Navier-Stokes and energy equations were solved numerically along one-step chemical reaction and Arrhenius law [94]. The two dimensional numerical simulation was similar to the study in [86], but final equation were simplified by asymptotic techniques for scale parameters of the problem. The effect of Lewis number was studied as a parameter, while the Prandtl number was assumed to be a constant value at 0.72. The dependency of viscosity, thermal conductivity, and fuel diffusivity on the temperature were represented by a power law function. Streamlines obtained from numerical results is similar to the experimental results as indicated in Figure 2.55(b). Streamlines are deviated as approaching the flame front and then become parallel to the tube wall, which is consistent with observation in Figure 2.55(a).

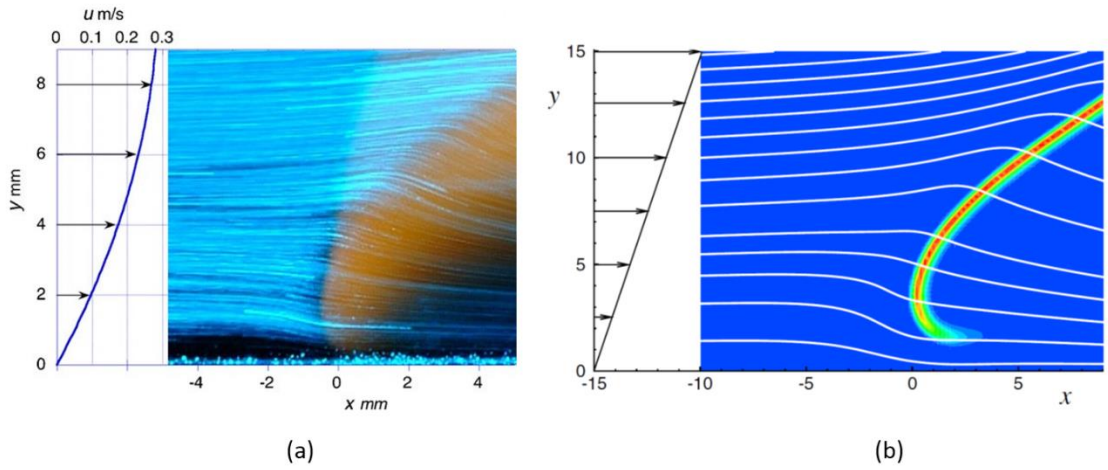

Figure 2.55: (a) Tomographic visualization of streamlines across the laminar flame and upstream velocity profile and (b) streamlines pattern and flame front location for the stabilized flame near the tube wall [94].

Figure 2.56 illustrates the critical Damköhler number as a function of Lewis number for isothermal and adiabatic wall boundary conditions. The experimental results are shown in Figure 2.56 for comparison. With a decrease in the Lewis number, the Damköhler number decreases, corresponding to increased flashback propensity. The experimental results of methane/air with $Le \approx 1.8$ and propane/air with $Le \approx$

0.97 mixture show that the flashback occurs at critical conditions of $Da = 9.8$ and $Da = 6.5$, respectively, which are in agreement with the numerical results shown in Figure 2.56. For Lewis numbers less than unity, the differential diffusion and curvature effects cause a higher flame temperature and burning velocity. It is important to realize that the real boundary condition of the tube wall is the combination of both isothermal and adiabatic cases and the experimental data fall within these two limits (i.e., solid and dashed lines) as indicated in Figure 2.56.

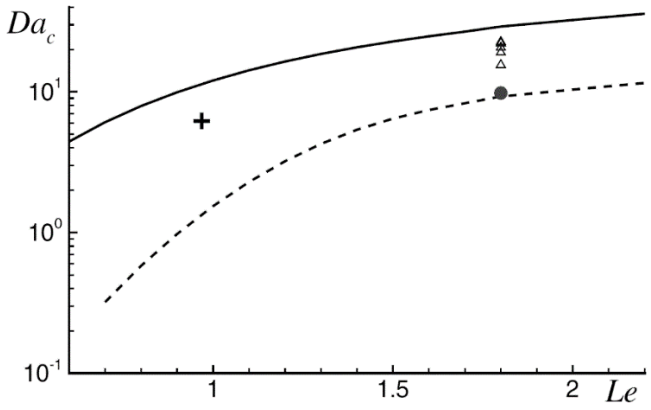

Figure 2.56: Critical Damköhler number as a function of Lewis number: solid line (isothermal wall), dashed line (adiabatic wall), triangle (experimental data points from [113]), circle (experimental result for propane), cross (experimental result for methane) [94].

The flame-wall interaction of the laminar flow has been numerically studied in the literature through one-dimensional and multidimensional analyses. The one-dimensional numerical modeling of laminar flame-wall interaction was mainly focused on head-on quenching in which the premixed flame propagates perpendicular to the wall. However, these studies cannot be applied to boundary layer flashback since the flame propagates parallel to the wall and the sidewall quenching occurs. In addition, reaction mechanisms used in most of these studies are limited to the single-step model, which is not able to provide realistic results due to the lack of recombination reactions near the wall.

The multidimensional numerical simulation of wall-flame interaction is expensive in terms of computational time. As a result, much of the existing research in the literature feature single-step

chemical reaction mechanisms or are simplified by the thermal-diffusive approximation. The latter case neglects fluid dynamics coupling in which the flow is not affected by the thermal expansion resulting from the presence of the flame.

2.3.6 Key Points and Status: Laminar Flames

Section 2.3 has summarized the literature relative to flashback of laminar flames under various conditions and the key points are as following:

- For unconfined flames, the interaction between the approaching reactants and the flame is small which is a major assumption underlying the critical velocity gradient concept. In this case, the critical velocity gradient concept to be successfully applied to predict flashback. The flow-flame interaction is significant in confined flames and thus the concept is less able to capture the behavior and a new physical framework is needed to account for these cases. Work in recent years has established this framework (e.g., [99]).

- Generalization of the concept to flows that are not fully developed has yet to be completely evaluated. Most studies specifically generate fully developed flow to allow analytical expressions to be used to estimate the velocity gradient near the wall. The role of developing flow in impacting flashback remains an open question.

- The role of the quenching distance is very important and yet different concepts are used to establish the value of this parameter. The quenching distance is measured between two parallel plates (inside a tube) or approximated by the flame thickness. These concepts may not be able to provide realistic values for the boundary layer flashback in which sidewall quenching occurs.

- Burner diameter plays a role in flashback once it falls below a certain diameter, which is comparable to the quenching distance. Above this diameter, burner diameter appears to be

unimportant based on studies isolating this parameter. From a practical view, for uncooled burners, thermal coupling between the flame and the burner results in a complex interaction between factors impacting heat transfer (e.g., flame temperature, flame proximity to the burner rim, product composition, and burner diameter). This interaction is not captured by models of the flashback process in any comprehensive manner.

- The reactant temperature plays a strong role in flashback of laminar flames. This is due to temperature effect on both the flame propagation rates (they increase with temperature) and quenching distance (reduces with increased temperature). The relative changes in these two parameters is a function of fuel composition which leads to difficulty in generalizing the effect in a manner that can be readily captured with a simple model. These effects, when also considered in the heat transfer impacts mentioned in regards to burner diameter effects, require careful consideration in any general model.

- Only a few studies have considered the impacts of operating pressure on laminar flame flashback. The laminar flame speed dependence on pressure has been established for many conditions in recent years and generally decreases weakly with an increase of pressure. The quenching distance, which is proportional to the flame thickness, decreases roughly linearly with pressure and plays the main role for increased flashback propensity at high pressure.

- Fuel composition plays a complex role in flashback behavior, but straightforward correlations have been developed to capture these effects especially for burners with controlled temperature. If hydrogen or carbon monoxide is involved in the mixture, additional consideration is required. The addition of small amounts of these species can have a strong impact on flashback propensity for a given condition.

- Numerical simulation of flashback in laminar jet flames has been carried out on a limited basis. Highly simplified chemistry and two dimensional approaches have been used with some success, but general agreement with experimental results is not as close as desired.

2.4 Turbulent Flames

As discussed in Section 2.3, boundary layer flashback of laminar flames has been extensively investigated in the literature and the critical velocity gradient concept is able to capture the overall behavior. However, the flame-wall interaction in turbulent flows is significantly more complex [176]. Considering the nature of turbulent flashback which, to a large degree, is a function of turbulent Reynolds number, spatially and temporally resolved diagnostics are required to capture the detailed processes. Due to computational complexity and the inherent temporal nature of turbulent flashback, simulations of the phenomena are relatively few with recent direct numerical simulations by Gruber et al. [100,108] one notable example. Due to the lack and/or cost of appropriate computational and experimental resources, many researchers have relied on the basic theory developed for laminar flames by Lewis and Von Elbe [47] in an attempt to estimate flashback in turbulent flames. As is discussed in this section, application of the basic theory has been made with some success although some completely new approaches have been considered in recent years.

2.4.1 Prediction Models

The laminar burning velocity and quenching distance can be measured by different techniques [177,178] as implemented by many researchers. However, extending laminar boundary layer flashback results to turbulent flames requires additional consideration. Also, in practice, the velocity profile at the burner head is not always fully developed due to the short length of premixer or presence of a nozzle or other feature in the premixer passage. The simple critical velocity gradient concept may not apply to such cases as evidenced by the study of Yamazaki and Tsuji [80] for a converging nozzle with different perforated

plates. Nevertheless, the concept of critical velocity gradient originally developed for laminar flames has been frequently used for characterizing turbulent boundary layer flashback propensity in the literature.

Khitrin et al. studied the turbulent flashback propensity for methane-air, methane-oxygen, and hydrogen-air mixtures [82]. Figure 2.57 presents the flashback velocity of laminar and turbulent flames as a function of hydrogen concentration in the mixture. Different points on the solid line show various burner diameters as labeled in Figure 2.57. Two dashed lines represent the flashback of laminar hydrogen flame from [48]. The velocity at which flashback occurs is much higher for turbulent flames. According to Figure 2.57, flashback velocity under turbulent conditions is not strongly affected by burner diameter while the flashback velocity of laminar flame is a function of diameter which is also consistent with Figure 2.12 and Eq. 2.5.

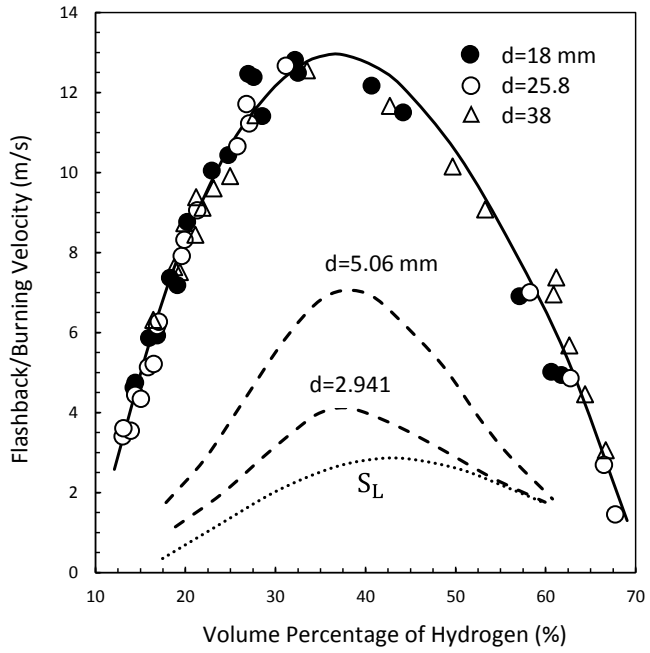

Figure 2.57: Flashback propensity of turbulent hydrogen flame (solid curve) and laminar hydrogen flame (dashed curves [48]). Dotted line shows the laminar burning velocity, reproduced from [82].

Using Eq. 2.3 and the calculated critical velocity gradient at the wall from Eq. 2.8, the following non-dimensional equation is obtained:

$$Pe_{flame} = \left(\frac{\delta_p}{D}\right) Re^{1.8} Pr \qquad \text{Eq. 2.42}$$

in which $Pe_{flame} = DS_L/\alpha$ and Pr is the Prandtl number of the unburned mixture. This equation was obtained based on the laminar critical velocity gradient model neglecting flame-flow interaction. The extension of critical velocity gradient model to turbulent flame was justified by assuming that the flashback of turbulent flame occurs in the viscous sublayer ($y^+ < 5$) where the velocity profile is linear. This basic model was applied to the experimental data for methane/oxygen and methane/air mixtures under turbulent conditions [82]. A Prandtl number of 0.9 was assumed for methane/oxygen and methane/air mixtures and the penetration distance was considered proportional to the one-dimensional flame thickness ($\delta_p = K\alpha/S_L$) [82]. With these considerations, the final form of Eq. 2.42 is reduced to:

$$Re = \text{const.}\, Pe_{flame}^{1.11} \qquad \text{Eq. 2.43}$$

Figure 2.58 illustrates the experimental data with respect to the critical velocity gradient model on a log-log plot. While the trends are captured to some extent, the deviation from the solid line (Eq. 2.43) is fairly significant in terms of predicting flashback propensity.

In this case, the critical velocity gradient model is not able to correctly predict the turbulent boundary layer flashback due to the simplifying assumptions used in the original for the model, including (1) linear velocity profile near the wall and (2) use of the unstretched laminar burning velocity. However, the velocity gradient at the wall can still characterize the local flow velocity and can be used along with the local turbulent burning velocity for boundary layer flashback prediction as discussed in Section 2.4.4.2.

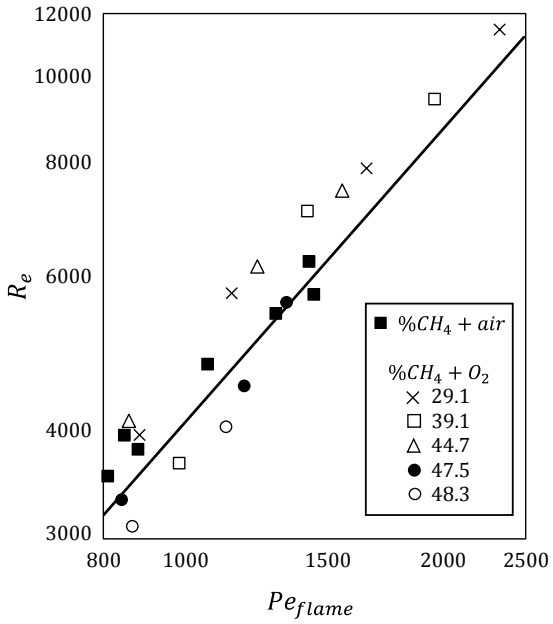

Figure 2.58: General prediction model (Eq. 2.43) for turbulent flashback propensity of methane/oxygen and methane/air mixtures, reproduced from [82].

2.4.2 Effect of Flame Configuration and Boundary Layer Heating

The effect of thermal coupling between the burner and flame front was noted in the literature even in the in the initial experiments conducted by Lewis and von Elbe [47]. To reach flashback limits, the equivalence ratio is required to be gradually increased such that the burner rim temperature remains in balance with the heat transfer from flame front, i.e., a quasi-steady process. It has been observed that, if flashback is approached quickly in an uncooled burner rim, the critical velocity gradient determined may be significantly different from the result with a slow approach. The first comprehensive study to investigate the effect of tip temperature on turbulent boundary layer flashback was conducted by Bollinger and Edse [66]. The experiment was carried out for hydrogen/oxygen flames at atmospheric pressure. The effect of burner material, burner diameter, and tube wall thickness were studied. Experiments for burners with small diameter were carried out in a closed room. Some other tests with larger diameter tubes were conducted in an open firing pit. The tip temperature was monitored using thermocouples mounted on

the burner head. The flashback was approached slowly to ensure that the thermal equilibrium was maintained as the equivalence ratio increased.

Figure 2.59 indicates the variation of critical velocity gradient as a function of hydrogen concentration for various burner diameters and thicknesses. Curves 2, 3, and 5 represent the effect of the burner diameter on critical velocity gradient. Results from burner tubes with diameters of 0.483 and 0.613 *cm* are similar at lean conditions. However, the dilution of the excess hydrogen with surrounding air leads to a significant deviation between results of curve 3 and 5 at rich condition. Also, the trend line of curve 2 differs significantly from two other burner tube diameters. This effect is more pronounced for the curve 1 with thinner wall as illustrated in Figure 2.59. The ratio of quenching distance to burner diameter increases as the burner diameter decreases. Indeed, once the quenching distance magnitude is comparable to the burner diameter, the velocity at which flashback occurs cannot be approximated by the linear velocity profile close to the wall. This observation is consistent with previous studies [47,48] for laminar flames.

The critical velocity gradient of burners with thicker walls (0.025 *in*) is consistently higher than that for burner tubes with thinner walls (0.009 *in*), i.e., curve 2 vs 1, curve 3 vs 4 in Figure 2.59. The effect of dilution via entrainment is stronger for thinner tube walls, leading to lower burning velocity at the burner rim and consequently a more stable flame. Hence, while the thicker tube wall may decrease tip temperature, they are more prone to flashback due to the reduced dilution effect according to [66].

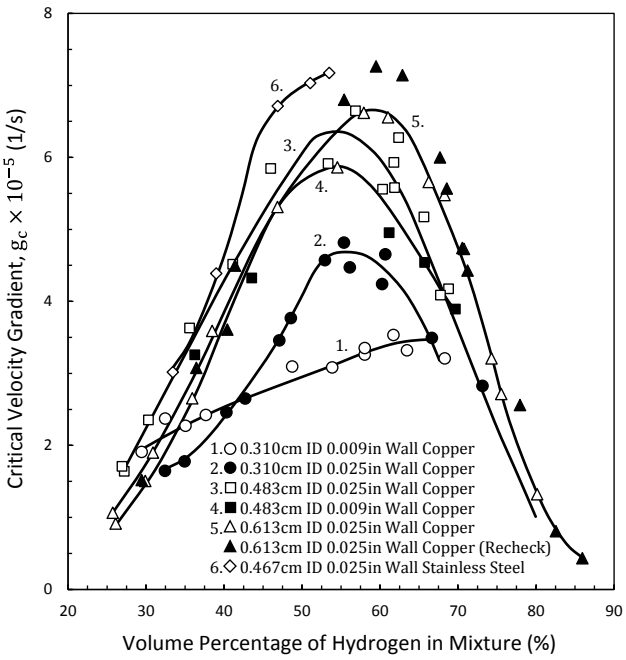

Figure 2.59: Effect of burner diameter on critical velocity gradient of hydrogen-oxygen flames for uncooled burners in closed room, reproduced from [66].

Figure 2.60 and Figure 2.61 illustrate the effect of the burner tube material on critical velocity gradient and tip temperature for a constant burner thickness. The flashback propensity for the copper burner is much lower than the other studied burner materials. This is due to the significantly lower tip temperature of the copper burner as indicated in Figure 2.61. Comparing the thermal conductivity of burner materials studied in [179], it is observed that the tip temperature is proportional to the thermal conductivity as indicated in Figure 2.61. The heat transfer from the flame to the burner balances with the heat loss to the ambient air and the incoming unburned mixture. The heat conduction along the tube wall is determined by the burner material and consequently the heat loss increases with an increase in thermal conductivity of the burner head, leading to lower burner tip temperature. However, the critical velocity gradient variation does not simply follow the thermal conductivity and tip temperature variations for stainless steel, Inconel, and Monel as illustrated by Figure 2.60. The thermal conductivity of these materials is approximately the same order of magnitude. The nickel burner has much higher thermal conductivity than stainless steel, Inconel, and Monel resulting in lower tip temperature and critical velocity gradient.

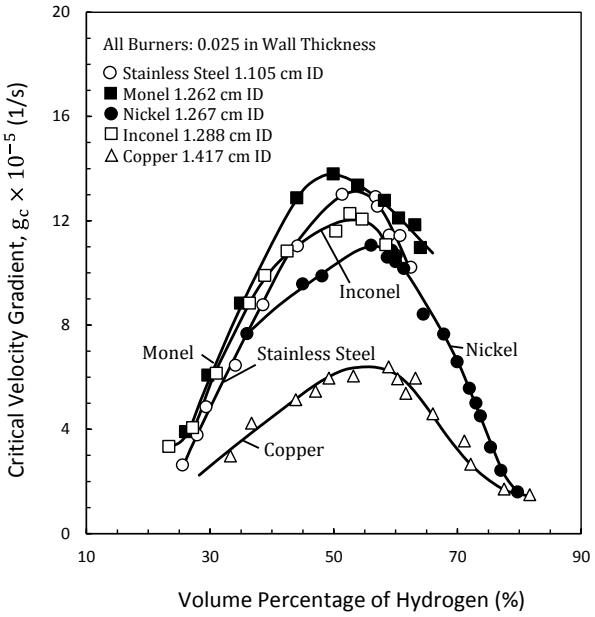

Figure 2.60: Critical velocity gradient variation with hydrogen concentration for uncooled burners constructed from different materials, reproduced from [66].

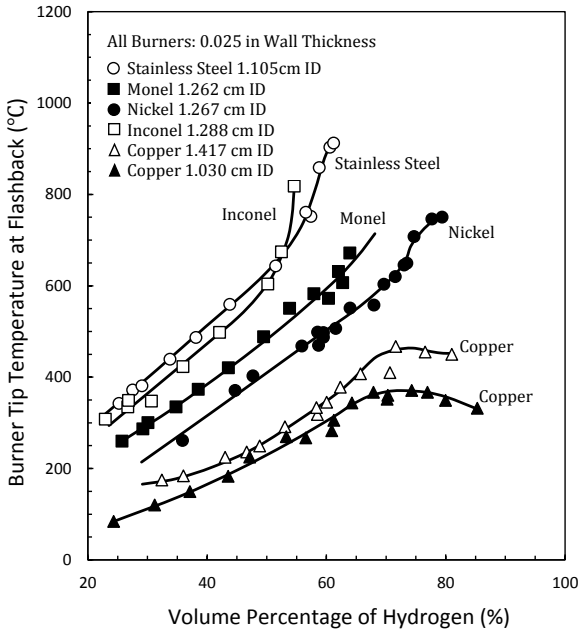

Figure 2.61: Tip temperature variation as a function of hydrogen concentration for uncooled burners constructed from different materials, reproduced from [66].

Flashback propensity of high hydrogen content fuels was studied for an unconfined flame (recall Figure 2.8) by Shaffer et al. [102]. Different fuel compositions including hydrogen, carbon monoxide, and

methane were investigated. The experiment was carried out at atmospheric pressure and room temperature for two constant adiabatic flame temperatures of 1700 and 1900 *K*. The flow was fully developed at the burner exit. The premixed reactants were injected through a quartz tube and flame was stabilized inside a quartz liner. To approach flashback, the fuel and air mass flow rates were decreased simultaneously such that the equivalence ratio remained constant, corresponding to a given adiabatic flame temperature.

The hydrogen data were obtained without an enclosure for comparison with results from [82,98]. A significant difference was observed for hydrogen with open flames and mainly attributed to the burner material of the injector as burner cooling was not implemented in this study. A quartz tube used in this experiment, while the flame in [98] was stabilized on top of a brass pilot burner. Final results of this study were presented in the form of a least squares best fit correlation based on fuel compositions and adiabatic flame temperatures as:

$$g_c = (2.401.\mathrm{H}_2 + 5.318.CO - 1.632.CH_4 - 0.264.AFT + 0.604.H_2.CH_4 + 0.00264.CH_4.AFT)^2 \quad \text{Eq. 2.44}$$

in which, the fuel concentration and adiabatic flame temperature are in percent and Kelvin, respectively. The effect of fuel composition can be isolated in this correlation and some conclusions were made by varying the fuel component concentration in Eq. 2.44. As carbon monoxide or methane are added to the pure hydrogen, the flashback propensity decreases to a different degree, which is consistent with the conclusion in [103]. The hydrogen-carbon monoxide mixture is found to be more prone to flashback than the hydrogen-methane for a given volume concentration of hydrogen in the mixture. This is in agreement with laminar flashback results shown in Figure 2.34 for H_2-CH_4 and Figure 2.36 for H_2-CO. It is noted that the addition of the methane to hydrogen decreases the laminar burning velocity exponentially (see

Figure 2.35), while the laminar burning velocity of H_2-CO mixture decreases linearly with an increase of carbon monoxide (see Figure 2.37).

A similar correlation Eq. 2.45 was also developed for tip temperature variation as a function of fuel composition and adiabatic flame temperature [102]. The hydrogen content has a significant impact on increasing the tip temperature and, for constant hydrogen concentration, added CO content increases flashback propensity more than added CH_4.

$$T_{tip} = -1.58.\mathrm{H_2} - 3.63.CO - 4.28.CH_4 - 0.264.AFT + 0.38.AFT \qquad \text{Eq. 2.45}$$

The thermal coupling between the burner and flame was investigated in more detail by Duan et al. [103]. The flashback propensity of enclosed flames was studied for the mixtures of hydrogen, methane, and carbon monoxide. Different preheat temperatures of 300, 450, 588, and 810K were examined for all fuel compositions mentioned. To investigate the effect of tip temperature on flashback propensity, burner heads constructed from stainless steel and quartz were used. Comparing the critical mass flow rate for stainless steel and quartz burners for a given fuel composition, it was concluded that the quartz burner head increases the flashback propensity. This is attributed by Duan et al. [103,104] to an increase of tip temperature, resulting from the lower thermal conductivity compared to the stainless steel. A simple analytical heat transfer solution was derived to show the dependency of the burner tip temperature on thermal conductivity for non-preheated mixtures. Based on this analysis, the tip temperature is proportional to square root of the thermal conductivity for a jet flame operating at room temperature.

Some correlations were developed in [103] based on statistical analysis of the data to predict the critical velocity gradient as a function of fuel contents, thermal properties, laminar flame speed, thermal properties, and quenching distance. The quenching distance was approximated by the one-dimensional-flame thickness taking into account the effect of wall temperature.

Duan et al. studied the influence of burner materials and geometrical flame configurations on flashback propensity of hydrogen/air jet flames [104]. Different burners were investigated including open, confined, and enclosed flames (recall Figure 2.8). Two enclosures with inner diameters of 44.45 and 63.5 *mm* were used to evaluate the effect of enclosure size on tip temperature and flashback limits. Furthermore, a ceramic block with a slightly larger inner diameter than the injector diameter was connected to the injector, resembling the confined flame.

The tip temperature of the enclosed flame was significantly higher than the open flame as the recirculation of hot products influences the burner rim temperature. Comparison of the associated critical velocity gradient indicated higher flashback propensity of the enclosed flame for metal and quartz burner heads. The difference between flashback limits of open and enclosed flames is more pronounced for the quartz burner with lower thermal conductivity. As a result, the difference in flashback limits is mainly due to boundary layer heating, which can induce the upstream flame propagation.

Duan et al. [104] also concluded that enclosure size has a negligible effect on tip temperature of the stainless steel burner, while it significantly affects the quartz burner. The quartz burner has a higher tip temperature for a given adiabatic flame temperature and is more sensitive to the enclosure size. Hence, the critical velocity gradient remains approximately constant for the stainless steel burner and decreases with an increase of enclosure size for the quartz burner. This indicates that the variation of critical velocity gradient is a result of change in the tip temperature and consequently the boundary layer heating. It also illustrates that a complex interaction between burner geometry and materials exists.

Figure 2.62 summarizes all results in terms of critical velocity gradient as a function of equivalence ratio. Note that the confined flame has significantly higher flashback propensity than unconfined flames regardless of the burner size and material. This conclusion was noted in [98] as will be discussed later. It was observed in [99] that the flashback mechanism for confined flames is affected by the flame-flow

interaction in the near-wall region at the onset of flashback. Indeed, a recirculation region exists in the boundary layer before the flashback occurrence, enhancing the flame regression into the burner (further discussed in Section 2.4.4). Cooling the burner decreases the flashback propensity as seen from results of stainless steel burner in Figure 2.62. Furthermore, the injector diameter has a negligible effect on flashback limits of hydrogen flames, consistent with the findings of Khitrin et al. [82].

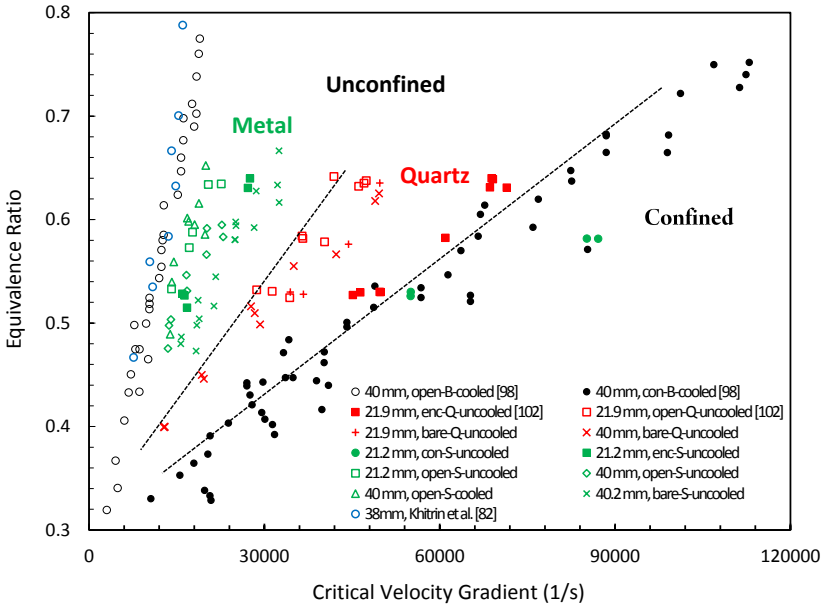

Figure 2.62: Summary of results for various injector configurations, burner diameters and materials [104].

Turbulent boundary layer flashback of methane-hydrogen/air in a channel with the presence of an adverse pressure gradient was investigated by Eichler and Sattelmayer [97]. The final results were presented in terms of critical velocity gradient and compared to the previous data in the literature for a tube burner. A diffuser with rectangular cross section was considered and the lower diffuser wall was adjusted to the 4 degree slope. The flow was fully developed at the burner exit.

The temperature of the lower diffuser wall was controlled by impinging the air though three jets and monitored by three thermocouples.

The flame tip location in the boundary layer was captured by OH* images. It was observed that the flame tip was strongly curved towards the wall channel as previously indicated in Figure 2.5. The critical velocity gradient was then calculated from the wall friction by the Reynolds averaged numerical simulation (RANS) of a 2D model.

The final results are summarized in Table 2.7 for methane and hydrogen at different mass flow rates. g_c denotes the mean critical velocity gradient calculated from the friction factor obtained by numerical simulation. Another set of experiments were conducted for each case to evaluate the effect of the wall heating on flashback propensity.

The critical velocity gradient results for confined flames are significantly higher than previous results in the literature for unconfined flames. The critical velocity gradient of natural gas at equivalence ratio of 0.8 in [77] was reported to be less 2000 1/s for turbulent flame, which is three times smaller than the value reported in Table 2.7 [97]. Such a significant difference reveals that the flashback characteristic is influenced by the flame configuration (i.e., confined and unconfined flames in Figure 2.8).

Table 2.7: Critical velocity gradient at different mass flow rates for methane and hydrogen, diffuser angle of 4 degree [97].

Fuel	$\dot{m}_{air}$ (g/s)	ϕ_f	$g_c(1/s)$
CH4	40	0.8	5329
CH4	50	0.8	6952
H2	50	0.25	8098
H2	60	0.25	10,047
H2	100	0.29	31,899
H2	120	0.29	42,576

The significantly different flashback limit for confined flames was further studied by Eichler et al. [98] for hydrogen/air mixtures. A setup similar to that shown in Figure 2.63 was used [98]. The metal channel was followed by a ceramic tile and another ceramic block. Three configurations were studied. In the first and second configurations, the ceramic tile is flush with the lower wall of the channel and the ceramic block is offset by 4 mm. The corner of the ceramic tile in configuration 2 is replaced by the stainless steel

material. In configuration 3, two small steps are formed between the channel, tile, and ceramic block with different heights, 0.5 and 3.5 *mm*; 2 and 2 *mm*.

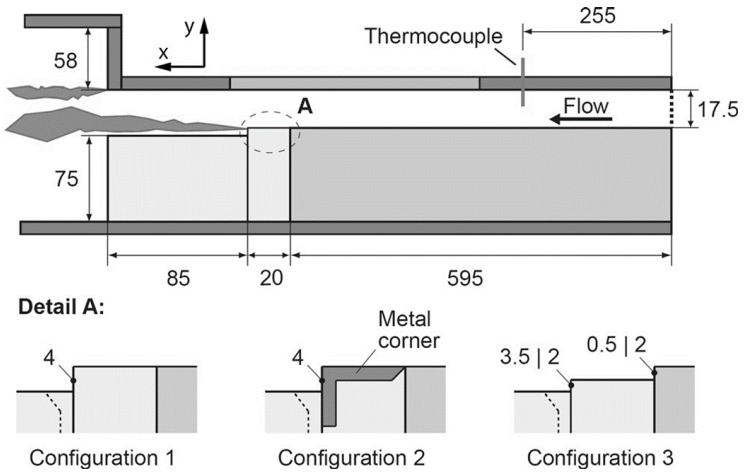

Figure 2.63: A schematic of boundary layer flashback setup used by Eichler et al. [98].

The channel length was less than the minimum value to create a fully developed flow at the exits section. As a result, the critical velocity gradient was calculated from a log law approximation in Eq. 2.47, in which the bulk flow velocity is related to the friction velocity [114].

$$u_\tau = \sqrt{\frac{\tau_w}{\rho}} \qquad \text{Eq. 2.46}$$

$$\bar{u} = u_\tau \left(\frac{1}{\kappa}\right) \ln \frac{h u_\tau}{\upsilon} + B - \frac{1}{\kappa} \qquad \text{Eq. 2.47}$$

Where h is half channel height and constants $\kappa = 0.41$, $B = 5$ are given from Coles and Hirst [180].

As mentioned earlier, the flashback propensity of confined flames in a channel was significantly higher than the existing data for unconfined tube burners. However, this was only validated for the channel, and it was not clear if the confinement is the main reason for such an increase. Hence, a confined flame was also studied in [98] for a tube burner to compare results from both experiments. A pilot burner made from brass was used to stabilize the flame. A ceramic block was used above the pilot burner and caused the

flame to creep upstream along the ceramic wall and finally stabilized at the burner rim, resembling the condition when the flame already exists in the tube. The pilot burner surface was air cooled to keep the temperature between 40 and 60 ℃. Fully developed flow was not achieved and consequently the velocity profile was verified by PIV measurement and RANS simulations. It was verified that the velocity gradient at the tube wall can be estimated by the Blasius correlation in Eq. 2.8 with less than 4% error from the measured values.

Figure 2.64 presents all results obtained for flashback limits in the channel and tube burner at different equivalence ratios. The first key observation is that the flashback data points of the unconfined tube burner lie significantly lower than those for all confined cases. Furthermore, the results for confined flames in either the channel or the tube are qualitatively similar. These two observations suggest that the higher flashback limit of confined flames is a result of different flashback characteristics and can be verified by both channel and tube burners.

The flashback limit of configuration 1 (recall Figure 2.63) is generally higher for all ranges of equivalence ratio covered. The second configuration with 0.5 *mm* step has a lower flashback limit than the first configuration, but this difference vanishes as the equivalence ratio increases to 1. A few data points were obtained for the configuration 3 with 2 mm step and the trend line indicates a lower flashback propensity compared to 0.5 *mm* step. Hence, an increase in step size decreases the flashback limit as indicated in Figure 2.64. For very lean conditions with equivalence ratio less than 0.4, the flame did not flashback through the entire channel and the flame oscillated between the intersection of ceramic tile and steel block, so this was mentioned as a reason for an offset of data points for three first sets. The flashback limit of the channel with metal corner is similar to results for the ceramic block and no clear difference was observed. It was also noted that the flashback data of the metal corner was limited due to observed

thermoacoustic instabilities, which was a result of lower surface temperature compared to the ceramic case.

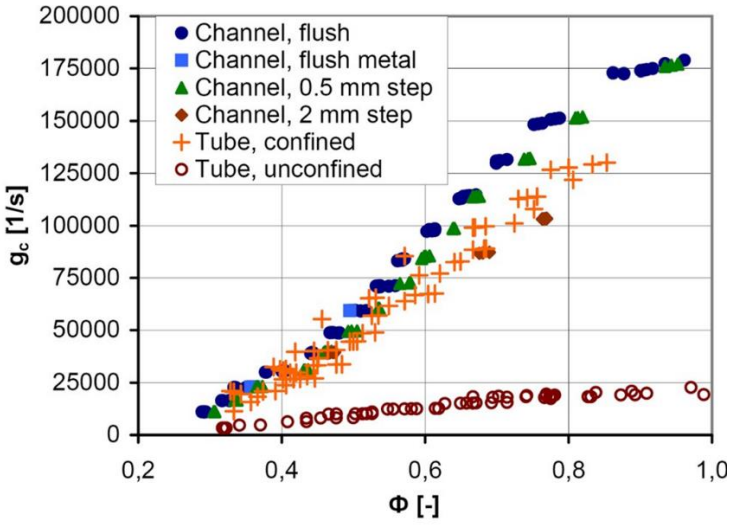

Figure 2.64: Boundary layer flashback limits of turbulent hydrogen flame for confined and unconfined configurations [98].

The thermal coupling between the burner rim and flame front plays an important role in boundary layer flashback of unconfined flames. As a result, an increase in tip temperature can significantly affect the boundary layer heating and triggering the flashback. Burners constructed from different materials show variation in flashback propensity limits when the burner is not cooled. The presence of the flame enclosure increases the tip temperature and consequently results in higher flashback propensity. Furthermore, a decrease of the enclosure size reduces the heat loss to the ambient air and the entrainment of the fresh oxidizer, leading to higher tip temperatures. The flashback propensity of confined flames is consistently higher than unconfined flames as experimentally verified for flame propagation through circular tubes and channels. The significant difference in flashback limit reveals that the flame-flow interaction near the wall-region cannot be predicted by the critical velocity gradient concept for confined flames. This observation has been the main objective of recent numerical and experimental studies in the literature [99,100,106,108], discussed in Section 2.4.4.

2.4.3 Effect of Operating Pressure and Preheat Temperature

Only a handful of studies of turbulent flashback propensity for mixtures at elevated pressures have been reported in the literature. Edse carried out the first flashback experiments using a Bunsen burner flame at pressures up to 100 *atm* for hydrogen/oxygen mixtures [56]. The other few studies that exist are discussed in this section.

The effect of sub-atmospheric pressure on the flashback propensity of hydrogen was studied for laminar flow, transitional, and turbulent flows by Fine [71,76]. Air and 20.6% oxygen-79.4% argon were used as oxidizers in these experiments with hydrogen as the fuel and flashback propensity was examined for equivalence ratios between 0.8 and 3. The experiment setup by Fine [71,76] was similar to the previous work by the same group carried out under laminar conditions [67]. Burner tubes of 0.546, 1.016, 1.459, and 1.890 *cm* diameters were used. The turbulent flame speed was calculated by determining the mean flame surface from the captured images as explained in [71,181]. The longitudinal velocity fluctuation was measured at the center of the burner to find the range of Reynolds number at which the transition to turbulent flow occurred. This measurement was made in the absence of the flame and the transition range was found to be occurring between $1500 \leq Re \leq 2500$. In addition, the flashback data show a clear transition from a laminar regime to the turbulent regime at similar range of Reynolds numbers. The critical velocity gradient in transition regime was calculated using the laminar approach in Eq. 2.5.

Figure 2.65 indicates the variation of critical velocity gradient for hydrogen/air mixtures as a function of pressure at an equivalence ratio of 0.95. The pressure exponents of the critical velocity gradient (slope of solid lines in Figure 2.65) are 1.28 and 1.22 for laminar and turbulent flames, respectively. It was observed that the pressure exponent remained approximately constant for both laminar and turbulent flames and it was independent of the burner diameter. The average pressure exponent of critical velocity gradient for turbulent flashback was 1.31, which is similar to the 1.35 ± 0.08, previously found for laminar

conditions (Section 2.3.3). The pressure value stays constant at transitional region (horizontal dashed lines in Figure 2.65), while the Reynolds number is increased. The value of critical velocity gradient corresponding to the transition regime increases with a decrease in diameter. This transition for the diameter of 1.016 occurs at critical velocity gradient of 4,000, which is higher than the measured value for the cold flow.

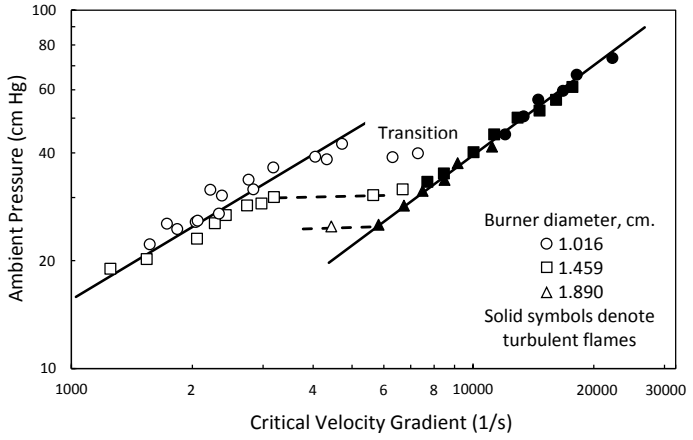

Figure 2.65: Critical velocity gradient of hydrogen/air mixture as a function of pressure at equivalence ratio of 0.95, reproduced from [71].

The critical velocity gradient of the turbulent flames was found to be approximately 2.8 times that of laminar flames [76]. Hence, the constant coefficient in Eq. 2.33 (Section 2.3.3) is multiplied by this value, resulting in 7.3 in the expression:

$$g_c = 7.3\frac{S_L}{\delta_q} \qquad \text{Eq. 2.48}$$

The comparison of the laminar and turbulent velocities indicated that the ratio of turbulent burning velocity to the laminar burning velocity is always less than 1.3 for this study. Consequently, an increases in critical velocity gradient of turbulent flames is not solely a result of higher flame speed. Indeed, the penetration distance of turbulent flame also decreases according to the Eq. 2.48 and thus also plays an important role in increasing flashback propensity for turbulent conditions.

Figure 2.66 illustrates the variation of critical velocity gradient for hydrogen/20.6% oxygen-79.4% argon at equivalence ratio of 1.5. The pressure exponent of critical velocity gradient is about 1.52 for turbulent flames, which is equal to the value reported for the laminar flame in [70] as discussed in Section 2.3.3.

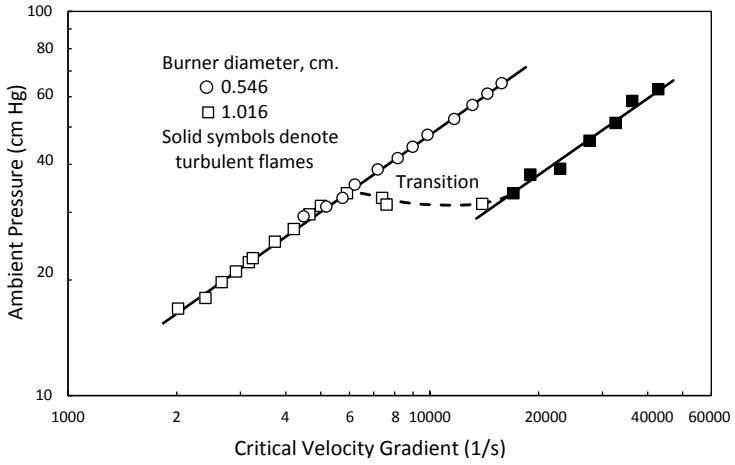

Figure 2.66: Critical velocity gradient of hydrogen/20.6% oxygen-79.4% argon as a function of pressure at equivalence ratio of 1.5, reproduced from [76].

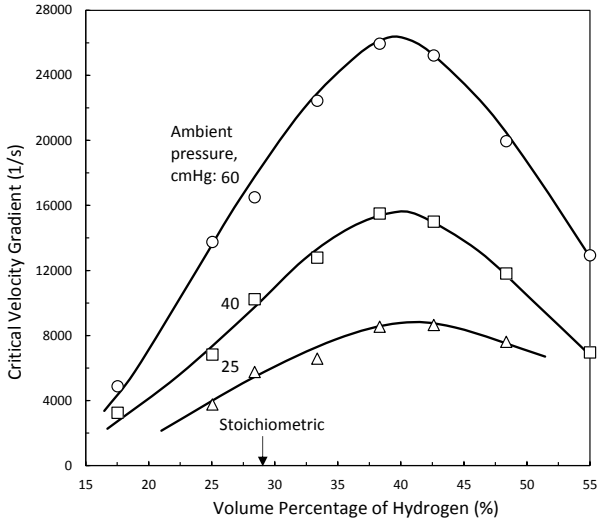

Figure 2.67: Critical velocity gradient of turbulent hydrogen/air flame as a function of fuel percentage at different pressures, reproduced from [71].

Figure 2.67 illustrates the variation of critical velocity gradient as a function of fuel percentage for hydrogen/air at different sub atmospheric pressures. For a given hydrogen concentration, the critical velocity gradient increases with an increase in pressure. Furthermore, the slope of critical velocity gradient

variation increases with an increases of pressure at lean and rich conditions. An important observation is that the maximum critical velocity gradient is independent of pressure and diluents, and remains constant at equivalence ratio of 1.5. The laminar flame speed also peaks at the same equivalence ratio of 1.5 according to [67] (see Figure 2.26), stating that the critical velocity gradient is proportional to the reaction rate.

A similar study was conducted by Fine to examine the effect of sub-atmospheric pressure on flashback propensity of propane/oxygen, propane/50%oxygen-50%nitrogen, and propane/20.6% oxygen-79.4% argon [70,76] using an experiment setup similar to their previous laminar studies [67,71]. The turbulent burning velocity was determined based on the mean surface of the flame front as previously pointed out. Again, burner tubes with inner diameters of 0.546, 1.016, 1.459, and 1.890 cm were examined. The range of equivalence ratio studied for propane/50%oxygen-50%nitrogen varied between 0.6 and 1.45. Propane/oxygen and propane/20.6% oxygen-79.4% argon were studied at equivalence ratios of 0.85 and 1, respectively. Critical velocity gradient data were independent of the burner diameter, except for the equivalence ratio larger than 1.25.

The laminar critical velocity gradient for propane/50%oxygen-50%nitrogen peaked at the equivalence ratio of 1.05, while the maximum critical velocity gradient for turbulent flame was not observed within the range of equivalence ratio studied.

Figure 2.68 illustrates the critical velocity gradient variation of propane/50%oxygen-50%nitrogen as a function of pressure at equivalence ratio of 1. The flashback data are divided to four regions in Figure 2.68, including very low Reynolds number, laminar, transitional, and turbulent regimes. Laminar and turbulent flames shows a linear trend in logarithmic scales and the slope of these trends line (i.e., pressure exponent) are equal to 1.17 and 1.22, respectively. Furthermore, the data obtained at different burner diameter lie on the same line. In transition regime, the pressure remains constant (horizontal dashed

lines) while the Reynolds number is increased and the range of Reynolds number found to be similar; $1500 \leq Re \leq 2500$, as previously observed in [71]. The transition to the turbulent flow for the burner diameter of 0.546 was not observed at pressures below one atmosphere. At very low Reynolds numbers, the slope of critical velocity gradient for the laminar flame drops below the slope of solid line as indicated in Figure 2.68. This is mainly due to the fact that the velocity gradient cannot be calculated by the linear velocity profile as the quenching effect is enhanced.

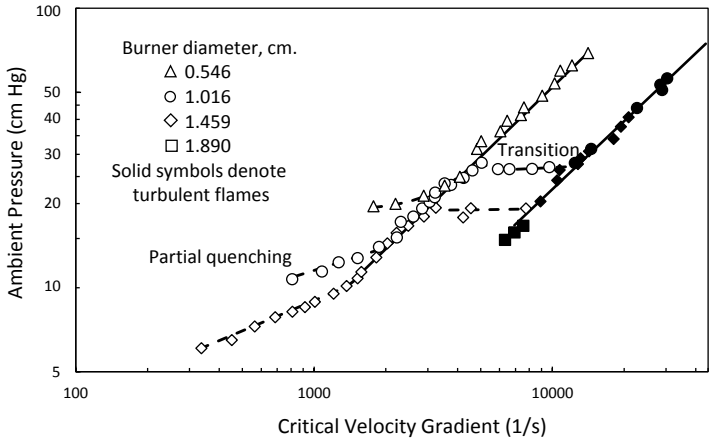

Figure 2.68: Critical velocity gradient of propane/50%oxygen-50%nitrogen mixtures as a function of pressure, reproduced from [70,76].

The average pressure exponents of critical velocity gradient for propane/50%oxygen-50%nitrogen in laminar and turbulent regimes were 1.13 and 1.11, respectively. These values are slightly lower than those of hydrogen flames as previously mentioned from [71]. For propane/oxygen, the pressure exponent of 1.4 was found for both laminar and turbulent flames. Propane/20.6% oxygen-79.4% argon data points were not sufficient to find the pressure exponent under turbulent conditions, while the pressure exponent of 0.91 was found for the laminar flames.

Using the measured burning velocity and quenching distance in [182], the critical velocity gradient can be represented as the ratio of the laminar burning velocity to the quenching distance. This ratio for the laminar flame at equivalence ratio of 1 is written as:

$$g_c = 3.1 \frac{S_L}{\delta_q} \qquad \text{Eq. 2.49}$$

The constant value of 3.1 is higher than the coefficient of 2.6 found for the laminar hydrogen flames. The ratio of critical velocity gradients $(g_c)_{turbulent}/(g_c)_{laminar}$ increases from 2.2 to 3.5 with variation of equivalence ratio from 0.6 to 1.25. Assuming the average value of 2.8, Eq. 2.49 for the turbulent flame would be:

$$g_c = 8.7 \frac{S_L}{\delta_q} \qquad \text{Eq. 2.50}$$

The effect of preheat temperature (300 to 620 *K*) and sub-atmospheric pressure was studied by Fine [79]. Different fuels were examined in this experiment including hydrogen/air, propane/oxygen-nitrogen, ethylene/oxygen-nitrogen, and ethylene/air. Oxygen-nitrogen mixture contains 50% oxygen and 50% nitrogen by volume. A brass tube burner head with 1.016 *cm* in diameter was used. The tip temperature was kept within $\pm 10\ K$ of the preheated gas temperature. For high heating value mixtures (such as propane) at high equivalence ratio, the tip temperature was higher than some low preheat temperatures. Hence, the burner was connected to the chamber to decrease the tip temperature through increasing the conduction heat loss.

Figure 2.69 illustrates the variation of critical velocity gradient as functions of pressure and temperature for hydrogen/air and ethylene/air. Each figure presents results for an equivalence ratio at which the corresponding critical velocity gradient is about the maximum. Flashback curves at a given preheat temperature are divided into three sections including laminar($R < 1500$), transition($1500 < Re < 2500$), and turbulent regimes ($Re > 2500$). In Figure 2.69(a), dashed line represents the non-preheat data studied in [70,71,76], obtained for water-cooled burner head. The room temperature data in Figure 2.69(b) represent the experimental results from [49]. The pressure exponent of critical velocity gradient is independent of preheat temperature for the different mixtures studied. The trend line in

Figure 2.69(b) has some curvature for low Reynolds numbers. This is due the enhanced flame quenching effect at these particular conditions. The variation of the critical velocity gradient as a function of preheat temperature is also independent of pressure. The average temperature exponent of critical velocity gradient, i.e., slope of the trend line in Figure 2.69(a) and Figure 2.69(b), are 1.52 and 1.59, respectively.

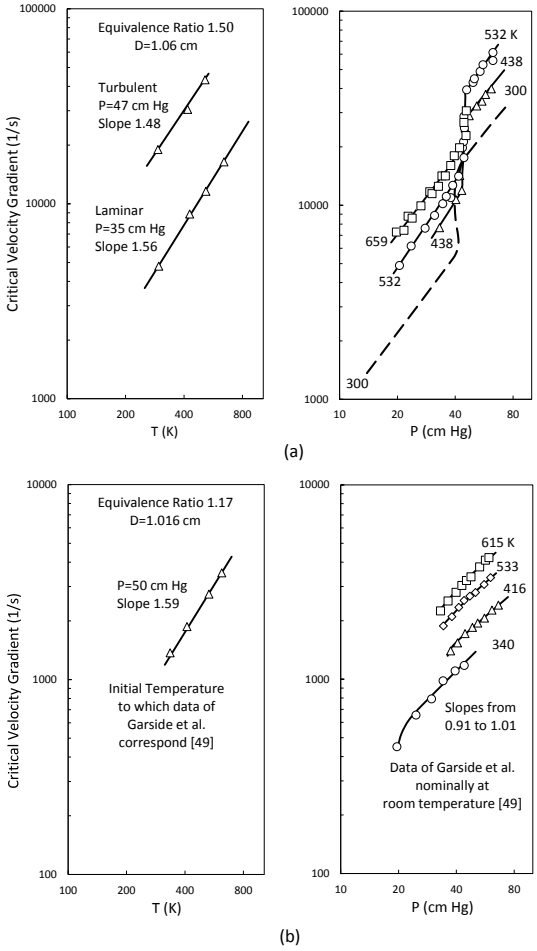

Figure 2.69: Critical velocity gradient as functions of pressure and preheat temperature for (a) H_2/air at $\phi = 1.50$ and (b) C_2H_4/air at $\phi = 1.17$, reproduced from [79].

The flashback propensity of hydrogen-carbon monoxide flames was studied by Daniele at al. [95] at elevated pressures up to 15 *atm*. H_2-CO mixtures in equal volumetric concentration were studied at equivalence ratios between 0.2 and 0.7. Fuel/Air mixtures were preheated between 577 K and 674 K and were injected into the combustor by a pipe with the inner diameter of 25 *mm*. The complete description of the high pressure facility used in this experiment can be found elsewhere [95,183]. Flashback was

approached by gradually increasing equivalence ratio while the preheat temperature and pressure remained constant. Furthermore, mass flow rate was adjusted to obtain a constant velocity for each set of data. Flashback was controlled by both active and passive mechanisms. For passive control, nitrogen gas was injected into the boundary layer of the burner located 150 *mm* upstream of the injector outlet. The nitrogen mass flow rate remained constant at 1% of the air flow rate for all operating conditions such that the flame position was not affected in significant manner.

Figure 2.70 presents the equivalence ratio at which flashback occurs as a function of pressure. The velocity at the burner head was kept constant at 45, 60, and 65 m/s as labeled for each data set. An increase in pressure for a given preheat temperature and velocity at the burner head decreases the equivalence ratio at flashback significantly, corresponding to increased flashback propensity. The dependency of the equivalence ratio on the pressure can be represented by $\phi = P^{-0.5}$, which is the average of all pressure exponents in Figure 2.70. For a constant pressure and velocity, an increase in preheat temperature from 577 to 674 *K* decreases the equivalence ratio at flashback, indicating higher flashback propensity. It was noted that an increases of injector velocity from 45 to 60 *m/s* has a small effect on increasing flashback limit.

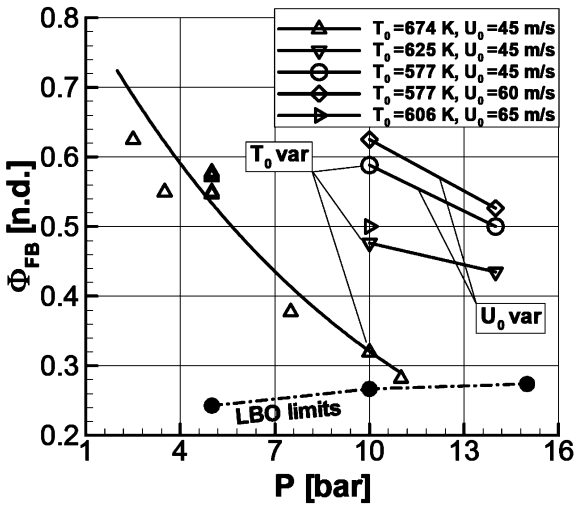

Figure 2.70: Flashback propensity of hydrogen-carbon monoxide mixture as a function of pressure at different preheat temperatures and velocities [95].

The turbulent burning velocity in this experiment was measured using the global consumption approach and it was observed that an increase in pressure had different impacts on turbulent flame speed depending on equivalence ratio [95]. Close to the flashback limit, the turbulent flame speed increases with an increase of pressure (pressure exponent of 0.12). Since this dependency is weak, the turbulent burning velocity alone cannot explain the significant increase in flashback propensity with an increase of pressure. Indeed, it was concluded that the dependency of flashback on pressure is mainly due to the quenching distance variation [95].

Lin et al. used the turbulent burning velocity to predict flashback propensity of high hydrogen content fuels at high pressure [105]. The experiment was conducted with hydrogen rich fuel gases including 70%H_2-30%N_2, 85%H_2-15%N_2, and pure hydrogen reacting with air. The bulk velocity at the injector and preheat temperature were kept constant at 40 *m/s* and 623 *K*., while the pressure was varied up to 10 *atm*. The experiment setup was similar to the previous studies by that group [95]. The turbulent flame speed was calculated using the global consumption rate definition [17].

Lin et al. [105] observed that the flame length can be a good indication of flashback. Indeed, flashback occurred when the flame length reduced to twice the diameter of the injector. Furthermore, the turbulent velocity correlated well with the flame length. The maximum turbulent burning velocity before flashback was on order of 10 m/s, which was close to the flow velocity in premixing tube at the boundary of viscous sublayer ($y^+ = 5$). As a result, the critical velocity gradient was used to predict flashback propensity. The laminar flame speed in Eq. 2.5 was replaced by the turbulent flame speed. Based on previous conclusions in the literature, the penetration distance was estimated by the quenching distance, which is proportional to the flame thickness (δ_f) [52]. The final correlation proposed by Lin et al. [105] to predict flashback limit is written as:

$$g_c = \frac{S_T}{Le \times \delta_f} \qquad \text{Eq. 2.51}$$

Flashback occurs when the velocity gradient of the flow (g_f), estimated by the Blasius correlation in Eq. 2.8, is equal to the value of g_c. Fully developed flow was not achieved in this experiment. Nevertheless, the velocity gradient of turbulent flow was calculated from Eq. 2.8. Lewis number is used in Eq. 2.51 to capture the influence of hydrogen in the mixture. This usage was based on the observation that the effect of Lewis number was significant on flashback propensity as described in [90,92,94].

The model by Lin et al. [105] (Eq. 2.51) was evaluated against the experimental flashback data for 50%H_2-50%CO in [95]. The model predicts the higher flashback propensity associated with higher preheat temperatures and pressures. The comparison of experimental results with predicted data shows a reasonable agreement. It should be noted that the experimental data were presented for 45 m/s, which is 5 *m/s* above the velocity of the predicted data. Considering this fact, the predicted data points would be slightly different.

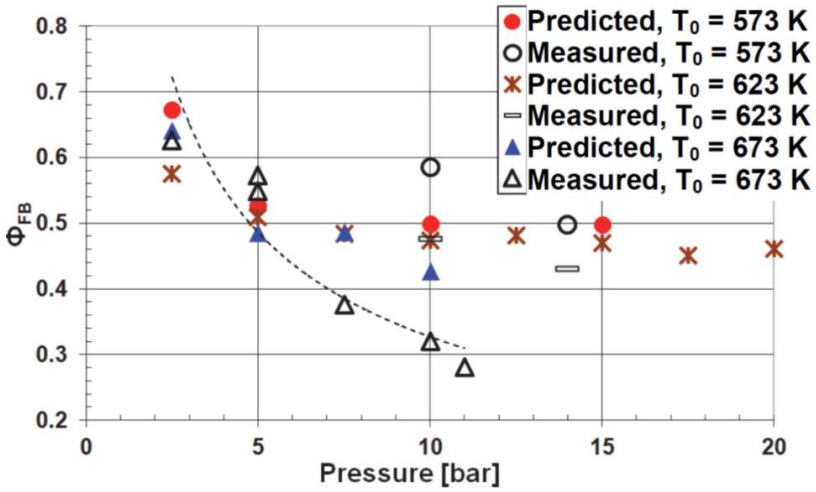

Figure 2.71: Predicted and measured equivalence ratios of 50%H2-50%CO mixture at flashback as functions of pressure and preheat temperatures [105].

The turbulent flashback propensity of a mixture increases at high pressure as experimentally observed for various fuel compositions. It is thus apparent that the laminar flame speed cannot be used to determine

the turbulent flashback limit and that the turbulent burning velocity is required to address the flame propagation at high Reynolds number. However, as pointed out in Section 2.1.1, turbulent burning velocity is a function of flow characteristics and can be determined based on different definitions [22]. While the ratio of turbulent burning velocity to laminar flame speed is considered a function of pressure based on consumption speed and flame angle methods [184–188], the dependency of the turbulent burning velocity magnitude on pressure was found to be weak in several studies [29,189,190]. Furthermore, the quenching distance decreases with an increase of pressure and was found to be an influential parameter for increased flashback propensity at high pressure.

2.4.4 Flame–Wall Interaction in Boundary Layer Flashback

A large number of experimental studies have investigated boundary layer flashback in the literature, primarily using the concept of critical velocity gradient for interpreting final results. In addition, a few numerical studies have been performed to study boundary layer flashback in more detail, mainly limited to laminar conditions. Until fairly recently, the underlying physics of the problem was based on the model (by Lewis and Elbe [47]) neglecting flame-flow interaction. However, the lack of experimental and numerical analyses taking into account high spatial and temporal resolution are still apparent. Section 2.4.4 discusses recent important studies having significant contributions to understanding of boundary layer flashback.

2.4.4.1 Confined flames

The confined flame situation refers to a condition in which the flame already exists in the boundary layer within a tube or channel. Flame can enter the premixing tube due to the operability issues such as pressure, velocity fluctuations, and auto ignition as indicated in Figure 2.8. The turbulent flame propagation through a channel has been studied experimentally and numerically with high spatial and temporal resolutions, achieved by micro-resolution particle image velocimetry (Micro-PIV) measurements

and direct numerical simulation (DNS). Since there is no mechanism for flame anchoring through a channel, the flame rapidly propagate upstream [99,100].

Eichler and Sattelmayer investigated boundary layer flashback of premixed flame for confined flames using simultaneous micro-PIV and chemiluminescence measurements [99]. Flame-flow interaction near the wall-region at the onset of flashback was studied in detail and presented conclusion were also verified by the numerical simulation of a laminar premixed flame stabilized on a flat plate using ANSYS CFX [99]. As discussed in prior work [98], the critical velocity gradient model cannot capture the characteristic of confined flames and temporally and spatially resolved measurements were used in this experiment to capture the onset of flashback. The setup used in this experiment was similar to configuration 1 in Figure 2.63. Both laminar and turbulent flames for hydrogen and methane were investigated in this study. The high spatial resolution required for capturing the structure of the near-wall region for the turbulent flame was achieved by spatial micron resolution PIV. Furthermore, Mie-scattering was also implemented to estimate the flame location in captured images. The detailed description of micro PIV setup and its alignments can be found in [99,191]. Since the channel length was not long enough, the flow did not reach a fully developed state.

Figure 2.72 presents the turbulent flame flashback behavior of hydrogen/air mixture by OH* chemiluminescence, Mie-scattering, and velocity contour images. The highly stochastic behavior of the turbulent flow is clear in this figure with presence of flame wrinkles. The concave wrinkles are formed into cusps, which can either travel upstream, move down stream, or stay at initial location. It was also observed that cusps in 40-50% of cases divided into new cusps, going through the same process of moving or remaining. The upstream movement comprising high fraction of formed cusps leads to the flame flashback. For first set of images at t=0, the flame tip is not located at the center of the channel (yellow line) and consequently the flame did not appear in Mie-scattering image. In the next three images, the

flame location can be estimated by the low density fluid. The white line represents the zero axial velocity in the flow field and the formation of back flow region. The back flow region was observed for cases in which the cups propagated upstream; however, backflow was not formed as the cusps were washed downstream of the flame. The boundary layer separation was also observed for laminar flashback of methane/air flames.

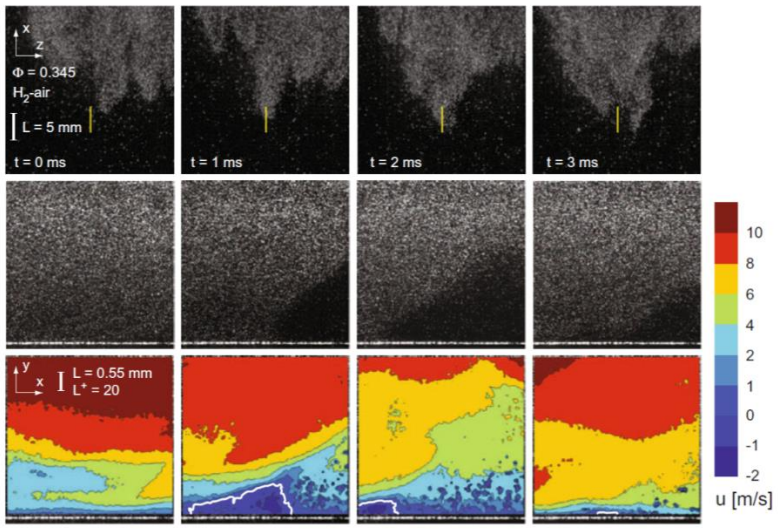

Figure 2.72: Micro-PIV and chemiluminescence measurements of turbulent boundary layer flashback for hydrogen/air [99].

This experiment shed some new light on the flame-flow interaction at the onset of flashback. An increase of pressure upstream of the flame front leads to the flow separation observed for both laminar and turbulent flames for studied cases. Hoferichter et al. recently developed a flashback prediction model for confined flames based on the separation of the turbulent boundary layer [111].

The boundary layer separation was further verified by numerical simulation of a laminar flame. In this model, the hydrogen/air mixture was stabilized on a flat plate with a hot wall segment used as a flame holder. The temperature of the mixture and the flat plate were kept constant at 293.15 *K*. The laminar premixed combustion was modeled by finite-rate chemistry with five species and three steps mechanisms based on Boivin et al. [192]. Full description of the implemented method can be found in [99].

An increase of pressure upstream of the flame front is a result of two dimension characteristics of the flame-flow interaction and was not predicted in simplified numerical models existing in the literature. The convex flame bulge towards reactants in the boundary layer results in the adverse pressure gradient and flow deceleration, which can potentially leads to the flow separation (see [138], chapter 7).

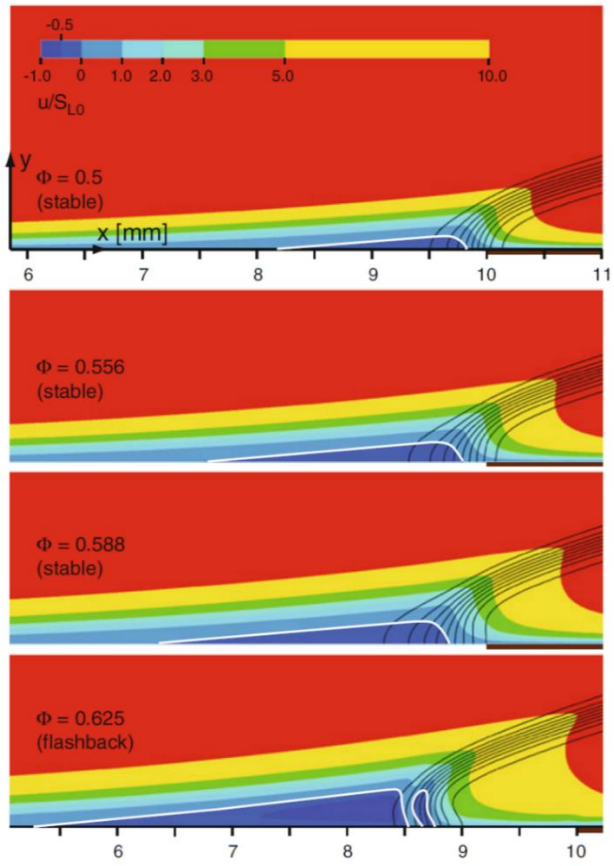

Figure 2.73: Axial velocity contour superimposed with isoline of hydrogen molar fraction for the laminar premixed flame at stable and flashback conditions [99].

The contour of axial velocity of the premixed flame is indicated in Figure 2.73, normalized by the laminar flame speed (S_{L0}). The three first contours represent the stable condition, while the last one shows the situation at flashback. The hot tile is indicated by a thick line at the right corner of the plate. The extension of the reaction zone can be seen from the black isoline of hydrogen molar fraction. As equivalence ratio increases the maximum height and length of back flow region increases. The ignition of the air/fuel mixture in the back flow region is a result of balance between the heat transfer from the flame front, heat

loss to the wall and external region. The height of back flow region is considerably larger than the quenching distance. As the maximum height of the back flow region reaches a certain value; which is dictated by energy balance, the reaction can sustain itself inside the back flow region and flashback occurs. The back flow region at the onset of flashback is continuously moved upstream by the adverse pressure in front of the flame.

Direct numerical simulation of boundary layer flashback in fully developed turbulent channel flow was carried out by Gruber et al [100]. The turbulent flame-wall interaction was studied for hydrogen/air with detailed chemical mechanisms developed by Li eta al. [193]. The simulation was obtained for Reynolds number of 3200 (friction Reynolds number, $Re_\tau = 180$) based on the channel half width, preheat temperature of 750 *K*, and equivalence ratio of 1.5. The rich mixture was examined at pressures of 1 and 2 *atm* for channel half widths of 1 and 0.5 *cm*, respectively. The compressible Navier-Stokes equations were solved in three-dimensional domain to simulate the freely propagation of non-anchored flame through turbulent planner channel flow.

Figure 2.74 indicates the upstream flame propagation inside the channel at different time steps. The laminar flame is initially present in the flow field with alternating streaks in the near-wall region which are the coherent structures of the turbulent boundary layer [194]. As shown in Figure 2.74, no back flow region is observed in the flow field initially simulated for the non-reactive mixture. Then, the high speed sweeps causes the formation of flame cusps, the convex flame region towards the products, while the low speed ejections lead to the formation of bulges, the convex flame towards the reactants (upstream leading edge in Figure 2.74). Darrieus-Landau hydrodynamic instability [195] induced by this mechanism enhances the interaction between the turbulent boundary layer and premixed flame. Consequently, the backflow region is generated upstream of the bulges shown by blue surfaces in Figure 2.74. Indeed, these

back flow pockets are results of the fluid expansion across the flame front occurring at the low-speed streaks locations.

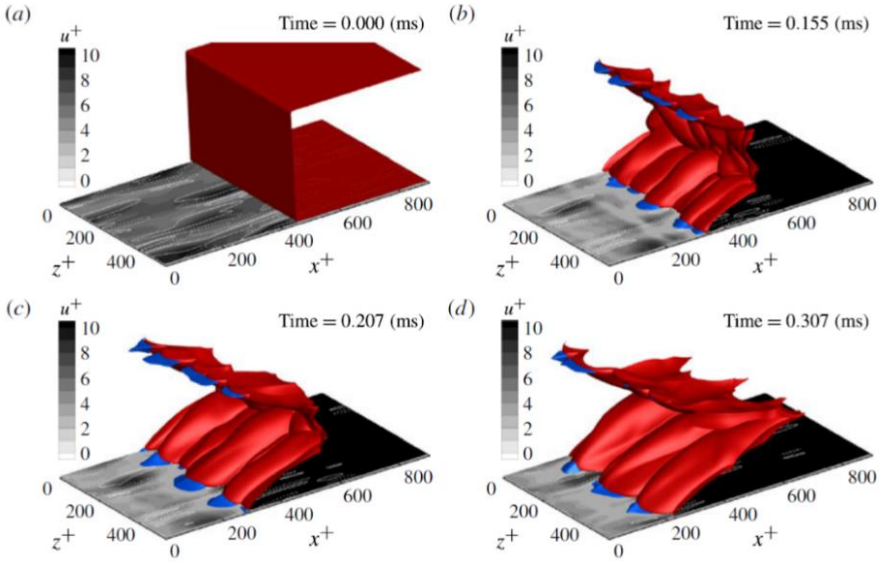

Figure 2.74: Temporal variation of the premixed flame (red color) in a channel, super imposed by the streamwise velocity contour (greyscale) on the $y^+ = 5$ plane, back flow region is shown by blue color [100].

These reverse flow regions are located near the wall with $y^+ < 20$ and extended up to 60-70 wall units in upstream direction. The height of backflow region reported in the experimental study by Eichler is $y^+ = 25$ to 30 [196]. The upstream propagation speed of the leading-edge flame is significantly enhanced by the presence of backflow pockets facilitating flashback. This is according to significantly higher critical velocity gradients associated with confined flames as shown in Figure 2.64 [98]. Figure 2.75 illustrates the streamwise velocity contour with location of the flame front (white line) relative to the back-flow region. The maximum negative velocity magnitude is $u^+ \sim -5$ or half of the laminar flame speed (Figure 2.75) and located at the wall distance of $y^+ = 9$, which matches well to the position of the upstream leading edge flame. It is noted that the flame is quenched at $y^+ = 2$, which is much smaller than the height of back flow region.

It was observed that the size of back flow region and the maximum strength of negative streamwise velocity are influenced by the mesh resolution of the boundary layer. Indeed, the course mesh suppresses

the formation of back flow region; as a result, the LES may not be able to capture the structure of flame-flow interaction in the near-wall region.

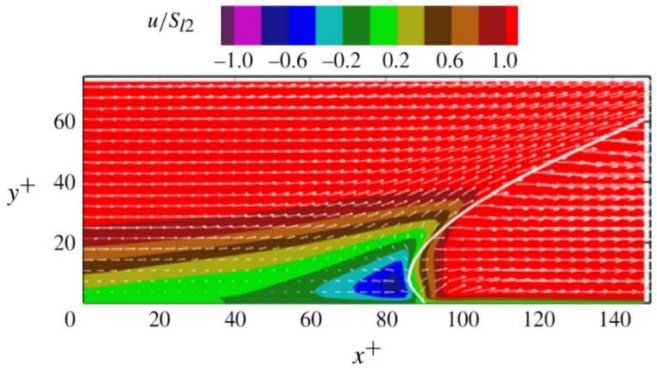

Figure 2.75: Streamwise velocity contours normalized by laminar flame speed. The flame is indicated by white line obtained from reaction progress variable of 0.7 [100].

2.4.4.2 Unconfined flames

In premixed combustors, the flame is generally stabilized downstream of the injector/premixer duct where the fuel/air mixture enters the combustion chamber with a larger cross sectional area. This sudden expansion is limited to the liner diameter, which is typically much larger than the premixer duct diameter. As this expansion ratio increases, the combustor resembles the case with free injection of the combustible mixture to the ambient air (Figure 2.8). Boundary layer flashback of jet flames has been extensively studied in the literature, but the detailed characteristics of the problem have not been well understood. The lack of numerical simulation addressing boundary layer flashback of jet flames is noted. Besides, all experimental studies in the literature are limited to investigating the flashback limits, in which the critical velocity gradient is used for comparison.

In order to the characterize the flame-flow interaction at the onset of flashback for unconfined jet flames, an experimental investigation at atmospheric pressure was conducted by Baumgartner et al. [106]. The high speed PIV, micro-PLIF along with chemiluminescence imaging were used to capture the spatial and temporal variations of the propagating hydrogen flame. The experimental setup includes a high aspect

ratio rectangular channel to resemble a two-dimensional flow through a planner channel. The flame is stabilized downstream of the burner exit to the ambient air.

Simultaneous OH* Chemiluminescence was used along the PIV or PLIF measurements. The temporal and spatial characteristics of the propagating flame were captured by the implemented high frequency lasers and long-distance microscopes. Further details of the laser diagnostics setup, measurement, and post processing of the data are found in [106].

Figure 2.76 presents the axial velocity contour with the propagation of the flame front at the onset of flashback for the bulk velocity of 7 m*/s*, equivalence ratio of 0.5, and temperature of the 293 *K*. The six images with the time interval of 0.33 *ms* show the flashback beginning and propagation of the flame front in which streamlines are indicated by white lines. The streamlines near the wall-region are highly deflected toward the expansion region, which is not observed for a jet flow without the reaction. The black dashed line in Figure 2.76 represent the approximate flame front location extracted from Mie scattering images. As the equivalence ratio is increased to the critical value, the leading flame tip is formed close to the edge of the lower wall and starts propagating upstream. With upstream propagation of leading flame, the flow decelerates as colored by red region in Figure 2.76. The upstream flame propagation through the duct enhances the reactants deceleration and can eventually lead to the boundary layer separation as previously observed from the experimental results for confined flames. This behavior is not observed in Figure 2.76 since the flame is partially confined by the lower wall.

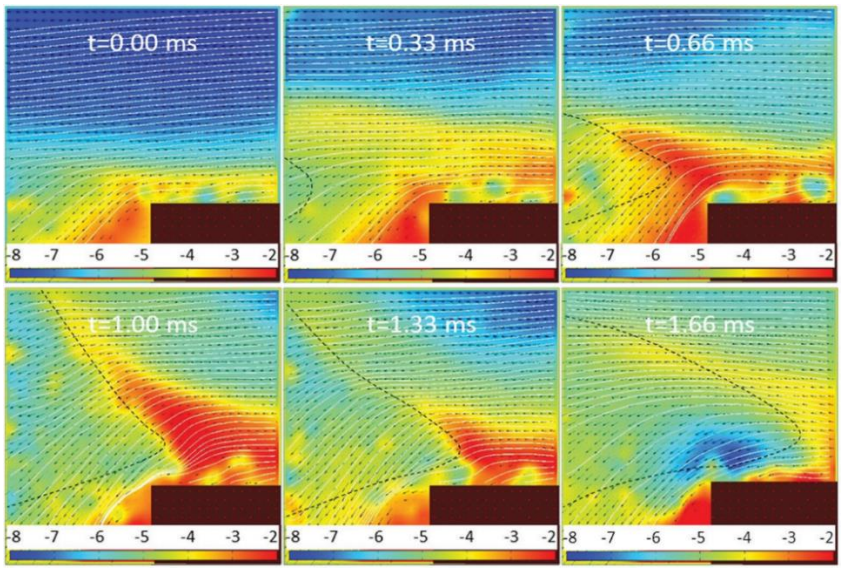

Figure 2.76: Flame propagation of boundary layer flashback for an unconfined flame (PIV measurement) [106].

The flame propagation in boundary layer flashback of an unconfined flame is not triggered by the immediate jump of the flame into the burner. Indeed, it initially starts with the formation of the leading flame front close to the wall appearing as a strongly curved flame tip towards the unburned mixture. This behavior is depicted with the schematic of flashback occurrence in Figure 2.77. The part of the flame anchored below the wall remains approximately undisturbed as the flame propagates upstream. The distance from the wall where the leading flame tip propagates is indicated by d_f and is approximately equal to 1 *mm* as reported in [106], which is in good agreement with the measured values (0.53-0.96 *mm*) for a confined flame in [196].

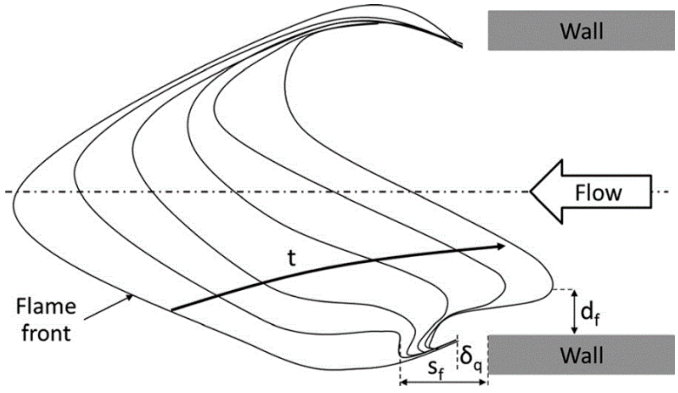

Figure 2.77: Schematic of flame front transition from the stable condition to flashback [106].

Based on this observation, a prediction model was proposed in [106]. Flashback starts at distance of s_f from the burner rim, which is larger than the head-on quenching distance (δ_q) as illustrated in Figure 2.77. At this location (s_f), the burning velocity is equal to the flow velocity providing the proper condition for the flame propagation. Based on experimental results, the streamline passing from the location (s_f) coincides with the distance (y_f) from the channel wall, which is slightly lower than the distance d_f in Figure 2.77. Assuming the axial velocity distribution inside the channel at the onset of flashback is not affected by the stable flame anchored downstream of the burner rim, the prediction model was proposed as following:

$$S_f(s_f) = u(s_f) \propto u(y_f) \qquad \text{Eq. 2.52}$$

This equation states that the prediction of boundary layer flashback for unconfined flames is a function of the undisturbed velocity profile of the flow inside the channel. Experimental results showed that the distance (y_f) is between 0.6 and 0.7 mm and almost independent of equivalence ratio. This range of (y_f) corresponds to $y^+ = 13$ and $y^+ = 21$ and falls within the buffer layer region, while the critical velocity gradient model assumption is that the flow velocity at flashback can be approximated by the linear velocity profile in the viscous sublayer. Hoferichter et al. further developed this flashback prediction model by assuming that the location at which flashback is triggered corresponds to the maximum streamwise turbulence intensity in a fully developed duct flow. This model includes a balance between the local turbulent burning velocity and the local flow velocity at $y^+ = 16.4$ [109].

The flame-flow interaction in unconfined configurations at the onset of flashback does not significantly impact the upstream flow field. As a result, the velocity profile remains approximately undisturbed upstream of the anchored flame. This is the main reason why the concept of critical velocity gradient has been able to predict various data in the literature for the onset of flashback. The presence of backflow region has been experimentally observed and numerically verified for both laminar and turbulent flame

propagation through a channel. But, it is important to realize that the backflow region occurs only if the necessary conditions are met. Otherwise, the presence of backflow pockets cannot be generally extended to all fuel compositions and operating conditions. Indeed, the flame expansion ratio needs to be large enough compared to the fluid velocity close to the wall, which determines the flow retardation in that region.

2.4.5 Key Points and Status: Turbulent Flames

Section 2.3 has summarized the literature relative to flashback of turbulent flames under various conditions and the key points are as following:

- Flashback limit is dictated by the turbulent boundary layer structure and the critical velocity gradient concept is less able to capture flashback behavior of turbulent flames compared to laminar flames. This is due in part to the breakdown of assumptions underlying the theory such as linear velocity profiles and no consideration of turbulent flame characteristics.

- The role of heat transfer between the flame and the burner is similar to that in laminar flames. The net result is strong interactions between parameters that affect heat transfer such as flame temperature and proximity of the flame to the burner. The boundary layer heating can potentially lead to the flow separation in the boundary layer, inducing the upstream flame propagation. As a result, incorporation of key heat transfer effects is required to generalize any predictive model for capturing flashback tendencies.

- Work done on turbulent configurations underscores the importance of considering which regime the flame is in, whether it be unconfined or confined. It is evident that once the flame transitions from outside the premixer tube to within it, the propagation rate greatly increases. If the flame issues into an enclosure (e.g., a combustor), the impact on flow field and heat

transfer again impacts the flashback behavior. Thus applying models based on open flames may not provide accurate results for flames issuing into an enclosure.

- More work has been carried on the pressure effect on turbulent flame flashback than for laminar flames. Increased flashback propensity at high pressure is a result of higher turbulent burning velocity and lower quenching distance. But, the contribution of each parameter to the overall trend (i.e., flashback as a function of pressure) is not well understood due to limited studies at high pressure.

- Recent insights into the behavior of confined turbulent flames has established a new framework to develop new theories and models for addressing flame propagation in these cases. These insights have been established with both detailed experiments (e.g., [99,104]) and high fidelity simulations (e.g., [100]). New approaches have been developed in light of these insights (e.g., [111]).

- The presence of backflow region for boundary layer flashback of confined flames has been observed. The backflow region occurs only if the flame expansion ratio is large enough compared to the fluid velocity in the near-wall region of a channel.

2.5 Summary

In the context of the present work emphasizing gas turbine conditions, several observations can be made in light of prior studies. First, laminar jet flames have been thoroughly studied for various fuel compositions, but generally not at elevated pressures or temperatures [197]. Relatively few studies have been conducted for turbulent jet flames, and even fewer for high hydrogen content fuels. Many experiments have been conducted to study flashback in swirl burners under turbulent conditions, while the lack of such studies for jet flame is apparent.

Despite the fact that experiments at gas turbine relevant conditions (i.e., elevated pressure and temperature) would be beneficial to robust design, no research that comprehensively examines flashback propensity in jet flames at these conditions has been conducted prior to the current study [197,198]. Although many correlations have been developed in the past, they have not been validated at elevated pressures and temperatures germane to gas turbine premixers. Furthermore, effects of various parameters such as the thermal coupling of the burner head are neglected. As a result, developing a design tool to predict boundary layer flashback is of great interest. The present work addresses these knowledge gaps by studying the boundary layer flashback of turbulent jet flames at gas turbine premixer conditions.

Chapter 3 - Approach

To address these knowledge gaps, the following approach is taken:

3.1 Task 1: Experimental Setup

To simulate the environment of combustion for gas turbine, the UCICL high pressure facility including two test rigs was implemented. The facility is capable of generating compressed air flow at temperatures up to 850 K and pressures up to 10 atm and providing the maximum air flow rate of 1.4 kg/s. The fuel and air were perfectly mixed through a premixer and the mixing performance at the burner exit was verified through CFD modeling. The premixing length was designed long enough to ensure that the flow field is fully developed, which was also validated by LDV measurements as well as CFD modeling.

Flashback experiments were conducted for (1) a tube burner, and (2) a commercially available injector using the primary test rig and alternate test rig, respectively (see Section 4.1). In both configurations, the turbulent hydrogen jet flame was stabilized at the burner rim where two thermocouples continuously measured the tip temperature. A pressure transducer was used to detect flashback occurrence, which was also confirmed by the thermocouples recording the variation in temperature at the burner head. The optical access allows for visually capturing the onset of flashback. Depending on a test rig, a YAG laser or a spark igniter was used for the mixture ignition.

3.2 Task 2: Flashback Data Acquisition

Flashback is a highly dynamic process in which many parameters are involved. The operating pressure in a gas turbine premixer plays a significant role in triggering flashback. As a result, experiments were conducted at different operating conditions to further investigate the effect of pressure. In addition, burners constructed of different materials were used to determine the influence of variations in the tip temperature. It is noted that all these parameters are strongly coupled and isolating the effect of each parameter would be complicated, considering the highly stochastic behavior of flashback at elevated

pressures. Air temperature, operating pressure, differential pressure between premixer and combustor, burner tip temperatures, air and fuel mass flow rates, and pilot fuel mass flow rate were recorded in this experiment.

3.3 Task 3: Data Analysis and Correlation Development

Results are first examined against the limited data available in the literature to ensure that the current setup is capable of reproducing previous results. The new data add insight towards understanding the pressure role in boundary layer flashback.

Many correlations have been developed in the past; however, they cannot be applied to gas turbines. Furthermore, effects of various parameters such as the thermal coupling between the burner and flame are neglected, while some of them are still crucial to study flashback. The lack of a comprehensive model is due to the fact that the existing correlations are not based on physical interpretations. To fully address effects of various parameters involved in flashback propensity, non-dimensional analysis has been applied to the current data as well as existing data in the literature. Non-dimensional analysis is developed based on Buckingham Pi theory, which is capable of capturing all effects encompassing operating pressure, preheat temperature, burner materials, burner diameter, fuel compositions, and thermal coupling. This approach provides a comprehensive model to predict flashback propensity under various conditions. In addition, the model is used to interpret flashback phenomena at high pressures and temperatures in the context of the engine conditions.

Chapter 4 - Experiment

4.1 Experiment Apparatus

Experiments were conducted at UC Irvine high pressure combustion facility. This facility includes a flow reactor used for ignition delays experiments and two combustor rigs used for simulating gas turbine combustors. The first combustor rig is located on the first floor with significant optical access for laser diagnostics as well as full traversing. The second combustor rig is located on the second floor with less optical access, which is primarily designed for long duration reacting experiments. The ancillary systems used for both test rigs are the same and include compressed air supply, fuel supply, electric heaters, back-pressure valve, and heat rejection system.

4.1.1 Test Rig I

Flashback experiments were carried out using the combustion facility shown in Figure 4.1. The high pressure combustion facility has been designed to simulate the actual gas turbine premixer conditions at pressures up to 10 atm and temperatures up to 850 K (1070 ^{o}F). The air is pressurized and heated to the desired temperature by passing through electrical resistance heaters. The air flow enters the vessel made from a 16 inch (40.64 cm) schedule-40 chrome-moly steel pipe and exits from through the bottom of vessel with 16 inch (40.64 cm) flange end. The hot exhaust gas is then quenched by a closed-loop water circuit. The vessel contains two circular and two oblong windows made from 50 mm thick fused silica as illustrated in Figure 4.1. This allows for optical access to the combustion chamber and enables experimenters to visually capture the flame regression as flashback happens.

A premixed model combustor, jet flame in the current experiment, was fitted into the vessel as shown in Figure 4.2. The premixed jet flame setup includes the venturi mixer, perforated plate, premixing tube, burner head, and quartz liner as illustrated in Figure 4.2.

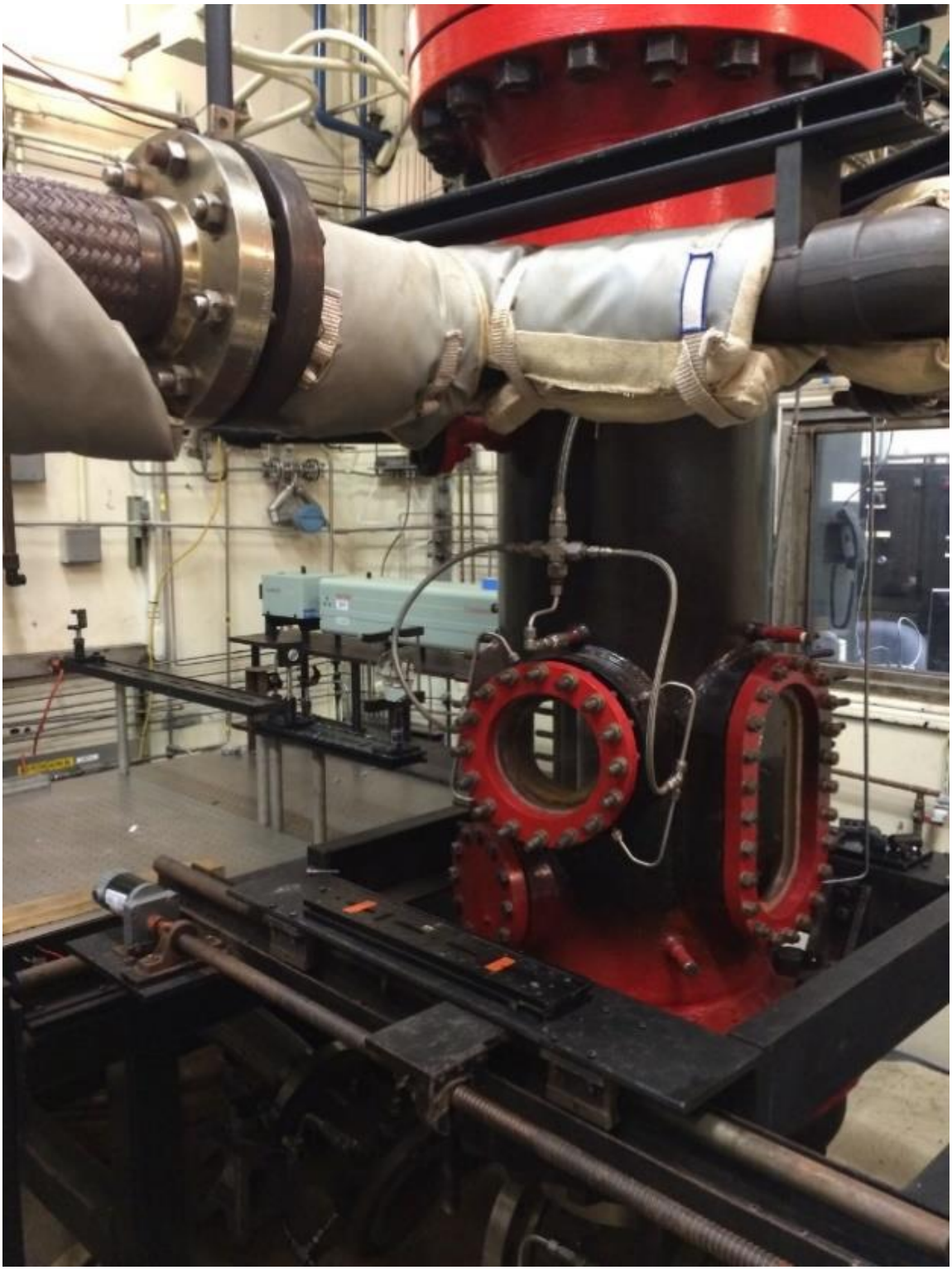

Figure 4.1: Flashback apparatus in the UC Irvine high pressure combustion facility.

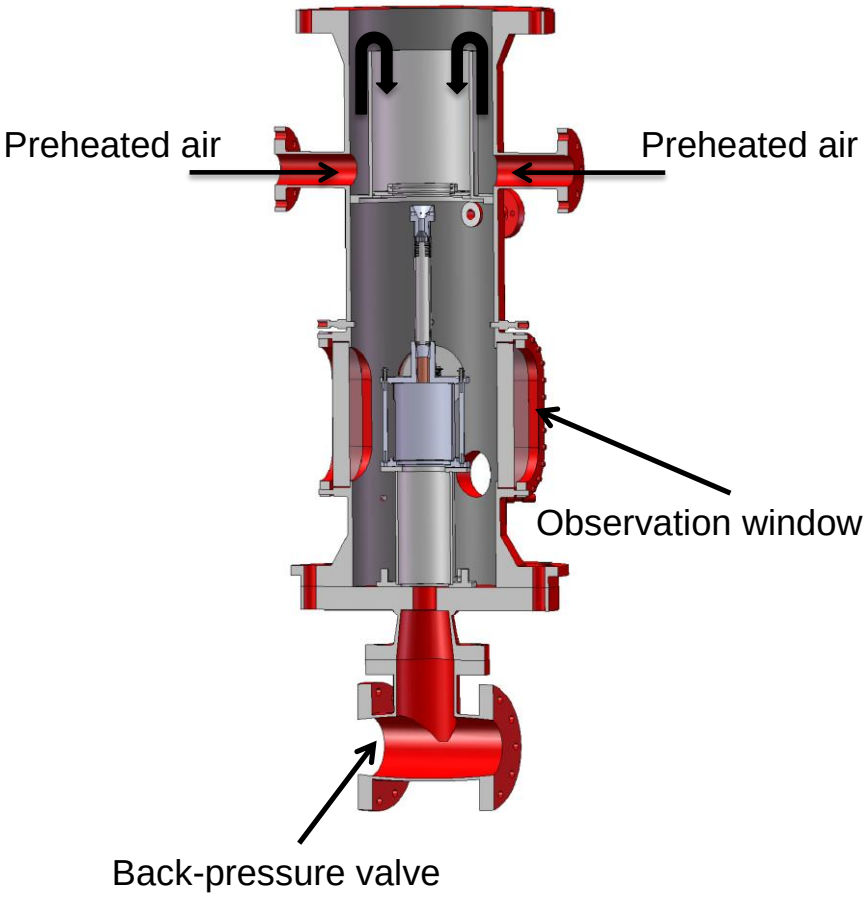

Figure 4.2: Schematic of high pressure apparatus and flashback test setup.

The fuel and air are mixed within a venturi as indicated in Figure 4.3, ensuring a uniform concentration profile. Fuel is injected through six inlet ports placed at the low pressure section of the venturi. The computational simulation was performed using ANSYS FLUENT to evaluate the mixing performance of the venturi (see Section 5.1.1).

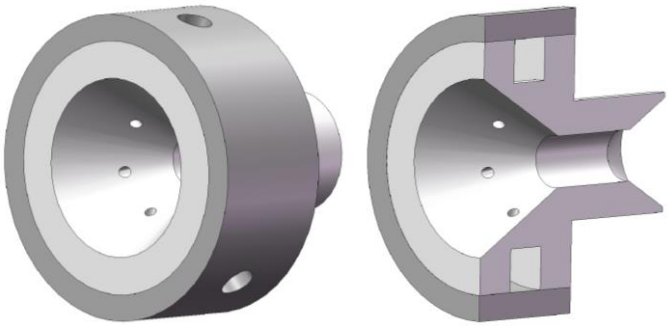

Figure 4.3: Schematic of venturi mixer.

A stainless steel perforated plate with the thickness of 12.7 mm and outer diameter of 36.83 mm is set immediately after the venturi to help create a uniform velocity profile. The perforated plate consists of 60 holes, 2.375 mm diameter which are designed in circular pattern (see Figure 4.4).

Figure 4.4: Perforated plate used to create uniform flow field.

After passing through the perforated plate, the flow enters a pipe with the inner diameter of 35 mm and length of 30 cm in order to ensure fully developed flow at the burner tip. The combustor liner is a quartz tube with 15 cm in inner diameter, 3 mm in thickness, and 19 cm in length. The quartz tube is held between two stainless steel plates that are supported by four metal posts as indicated in Figure 4.5 a and Figure 4.6. The spring located at the end of each post allows for pressure on the quartz tube (and thus sealing of the combustor) to be maintained during thermal expansion of the stainless steel posts while preventing the quartz from breaking. The fuel-air mixture enters the combustor through a burner head. Laser Doppler Velocimetry was performed in parallel to numerical modeling to verify the fully developed velocity profile at the exit of the burner head (discussed in Section 5.1.2).

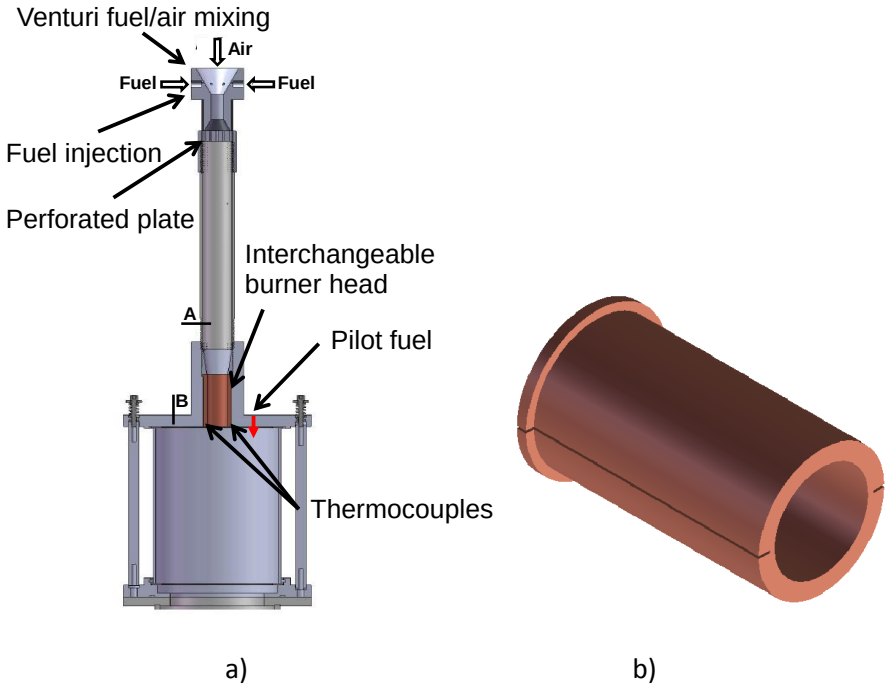

Figure 4.5: a) Cross section of mixing and combustor test sections and b) burner head.

Figure 4.6: Test section for premixed jet flame.

Two thermocouples shown in Figure 4.5 b are inserted into slots along the burner head to measure the burner tip temperature at the onset of flashback. A pressure transducer is also set such that it continuously records the pressure drop between the premixer and combustor corresponding to point A and B in Figure 4.5 a. Flame regression into the burner results in a clear peak in the pressure transducer reading and tip temperature amplitude which both serve as indicators of flashback.

Three burner heads constructed of different materials (stainless steel, copper, and zirconia ceramic) with an inner diameter of 25.4 mm (1 inch) were used to evaluate the flashback dependency on burner physical properties. In addition, a tube burner with the inner diameter of 30.48 mm (1.2 inch) was used to investigate the effect of burner diameter on flashback propensity (see Figure 4.7 and Figure 4.8).

Figure 4.7: Burner head constructed of copper.

Figure 4.8: Original (left) and enlarged (right) stainless steel burner heads.

4.1.2 Test Rig II

To validate the reliability and accuracy of experimental data, similar experiments were conducted for a commercially available injector from a micro turbine combustor. The facility shown in Figure 4.9 was used to investigate the flashback propensity of a factory built injector. Similar to the first test rig, flashback tests can be carried out at pressures up to 10 atm and temperatures up to 850 K (1070 ^{o}F). Both test rigs

have the same ancillary systems, which are discussed in other sections. The test vessel is equipped with two round windows made from 50 mm thick fused silica to allow for optical access to the combustion chamber.

Figure 4.9: Alternate flashback apparatus in the UC Irvine high pressure combustion facility.

The preheated air enters the test vessel from the top right as shown in Figure 4.9 and Figure 4.10. The incoming air in the test vessel passes through radial holes in a premixer section, where the fuel is axially injected as illustrated in Figure 4.10. The resulting fuel/air mixture enters the combustor liner, which is made from a quartz tube with 15 cm in inner diameter and 10 cm in length. The quartz tube is compressed between two stainless steel plates that are held by four posts as shown in Figure 4.10. Springs located at the end of each post allow for thermal expansion, while providing perfect sealing. The injector diameter is 2.54 cm (1 inch) and protrudes 1.27 cm below the combustor top plate.

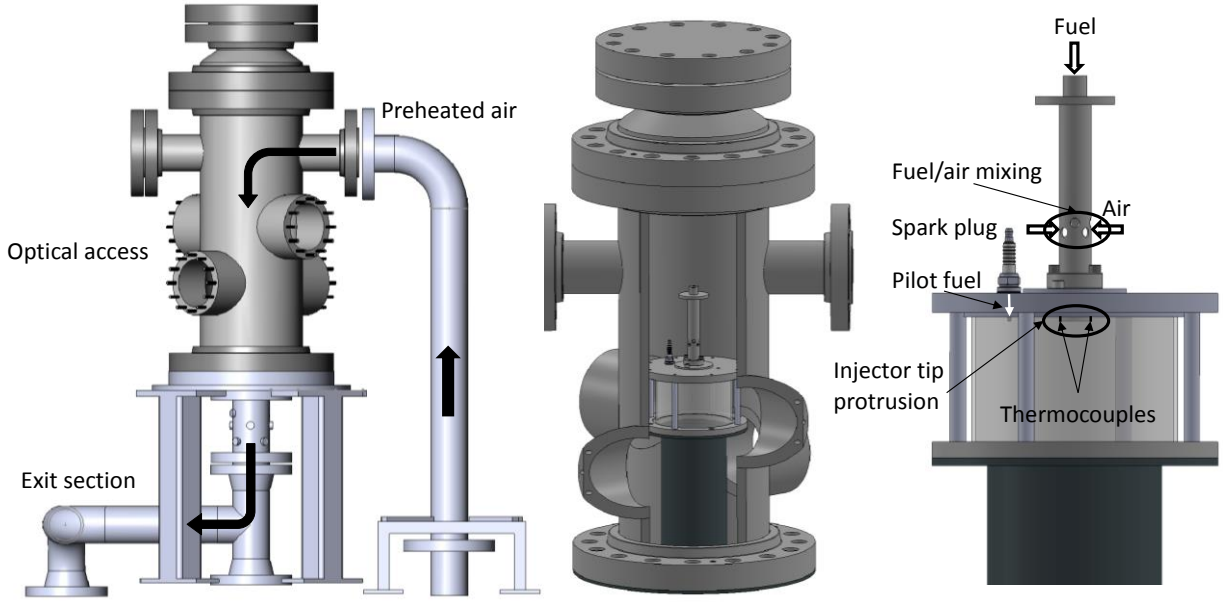

Figure 4.10: Schematic of high pressure apparatus and flashback test setup.

Figure 4.11 indicates the factory built injector from a commercial 60 kW microturbine generator (i.e., a Capstone C-60 MTG). Two thermocouples are attached to the injector head, indicated in Figure 4.11, to continuously record the tip temperature, a parameter found crucial in determining the flashback propensity. The pressure difference between the combustion chamber and premixer tube is also recorded by a pressure transducer. Two thermocouples along with the pressure transducer are used to detect flashback and confirm the direct visual observation.

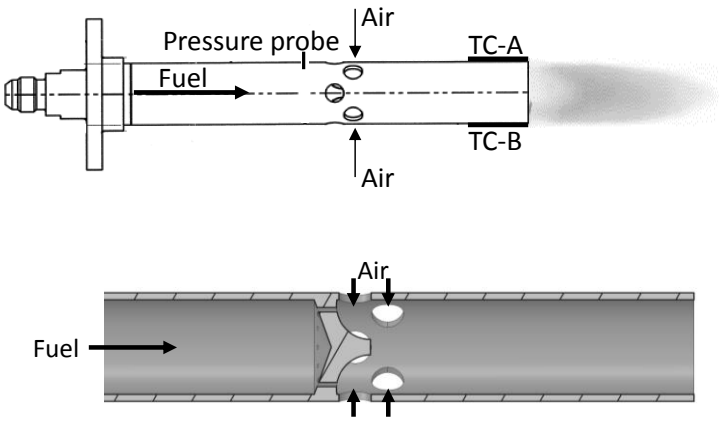

Figure 4.11: Factory built injector used in flashback setup.

4.2 Elevated Pressure and Temperature Facility Subsystems

Flashback experiments at gas turbine premixer conditions were achieved by implementing several subsystems as described in this section.

4.2.1 Air Circuit

Air enters the test cell via a 4-inch steel pipe at pressure of 10.5 atm (154 psi) from three Ingersoll-Rand air-compressors. The compressors can produce the maximum mass flow rate of 1.4 kg/s (3.1 lb/s). Air then passes through a water drop out tank, supplying dry air to the test rig. The air mass flow rate is measured by a thermal mass flow meter (Sierra model 780S-NAA-NC9-E2-P3-V4-NR-0) with a 2% uncertainty and controlled by a one inch pipe size Fisher V150 remote control valve. The mass flow meter and remote control valve interact with a Fisher DPR 900 PID (proportional-integral-derivative) process controller. The PID controller reads the actual mass flow rate and sends a signal to the remote control valve to adjust the air flow rate to the desired value.

The exhaust section is followed by a back pressure valve downstream, which is used to adjust the test rig operating pressure as shown in Figure 4.12. A six inch pipe size gate valve provides course adjustment of the back pressure, while fine adjustment is achieved by a 1.25 inch pipe size Fisher V200 remote control

valve. The remote control valve also interacts with a Fisher DPR 900 PID process controller to reach the required pressure.

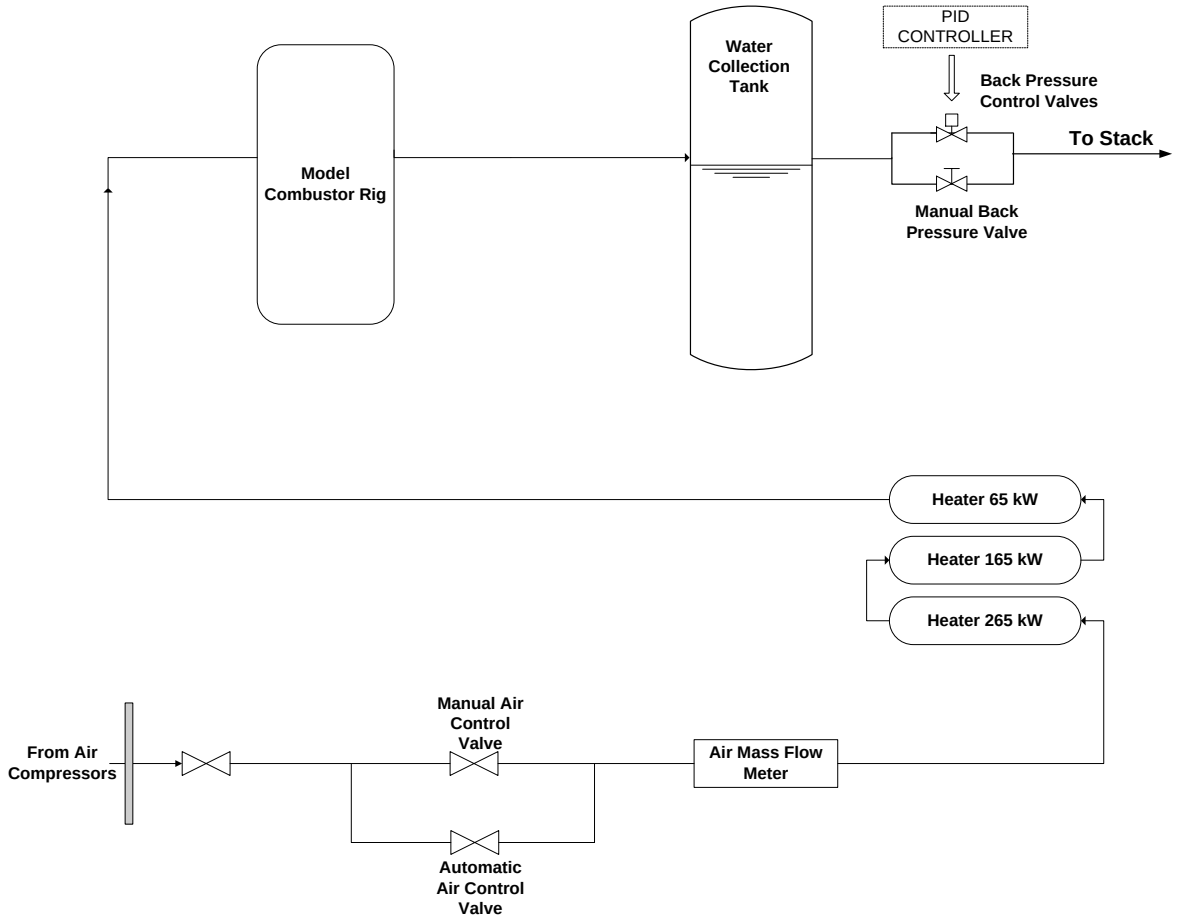

Figure 4.12: Schematic of compressed air circuit in the high pressure combustion facility.

4.2.2 Fuel Circuit

The fuel circuit can be connected to two different sources: (1) high pressure natural gas compressors and (2) bottled gas manifold. The high pressure facility is fed by two compressors, which are capable of providing natural gas at pressure of 10.5 atm (154 psi) and 28 atm (411 psi). The bottled gas manifold is used for hydrogen and different fuel blends including (H_2, CH_4, and CO), which are already prepared in certain concentrations. The fuel pipe line enters the test cell and passes through a solenoid shutoff valve, a rotary needle valve, and a second solenoid shutoff valve as indicated in Figure 4.13. The first shutoff

valve is primarily used to isolate the test rig after each test and ensures fuel does not enter the test rig, while a new component is being installed. The second shutoff valve is located immediately upstream of the test rig and is used to shut off the fuel in case of a flashback or an emergency occurring. The fuel flow rate is measured by a Micromotion CMF025 Coriolis flow meter, which has a 0.5% uncertainty. This allows for the mass flow rate measurement of various fuel mixtures without a need for recalibration. In Coriolis mass flow meter, fluid flows through an oscillating curved tube and causes a tube deflection, which can be measured. This deflection is proportional to the mass flow rate and is detected by a sensor outputting mA signal to the control system.

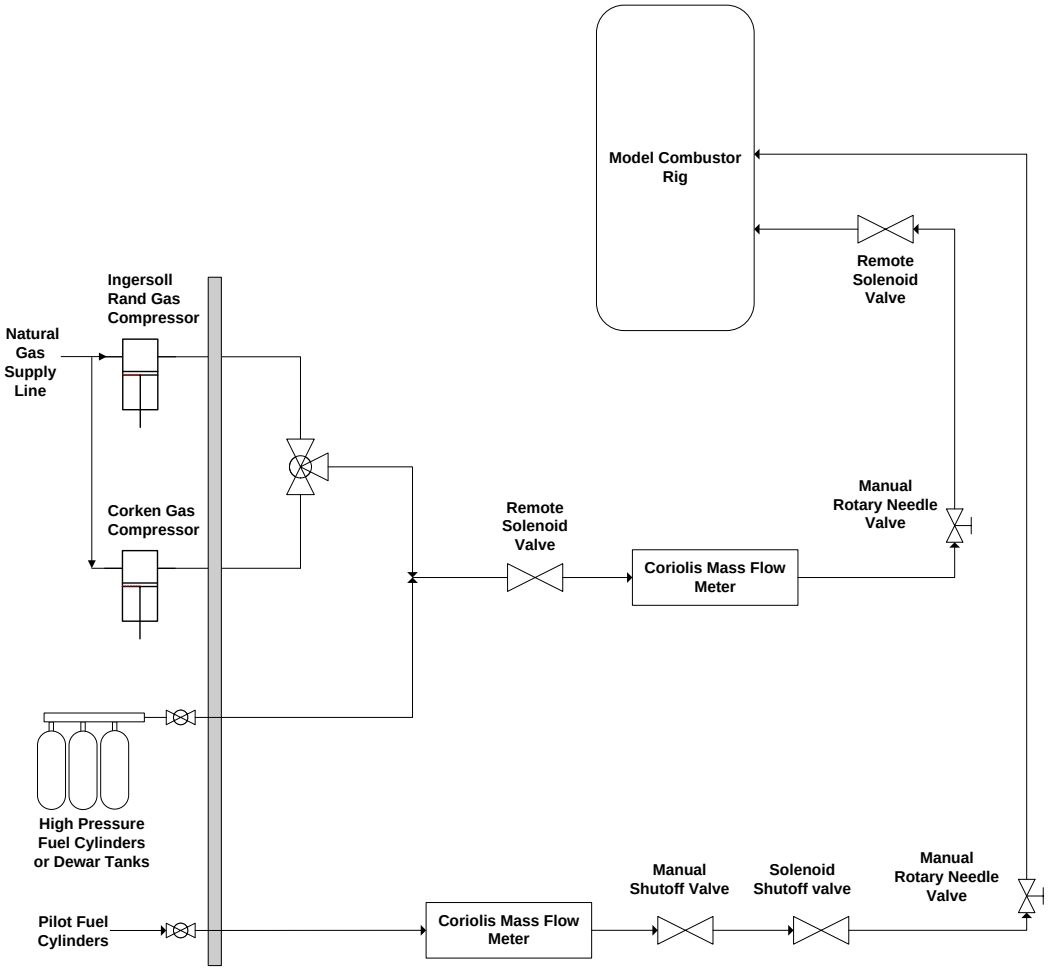

Figure 4.13: Schematic of fuel circuit in the high pressure combustion facility.

4.2.3 Electric Heaters

The air is heated to the desired temperature by passing through three Watlow® electrical resistance heaters shown in Figure 4.14. The first stage heater with the output power of 250 kW heats up the air to 700 K (800 ^{o}F). The second and third stages with the output power of 165 and 65 kW can provide a maximum exit temperature of 865 K (1097 ^{o}F) and 1000 K (1340 ^{o}F), respectively. The preheated air is delivered to the test rig through a four inch stainless steel corrugated flexible hose. Despite the insulation used to avoid heat loss between the heaters and the test rig, the maximum inlet temperature drops to 850 K (1070 ^{o}F).

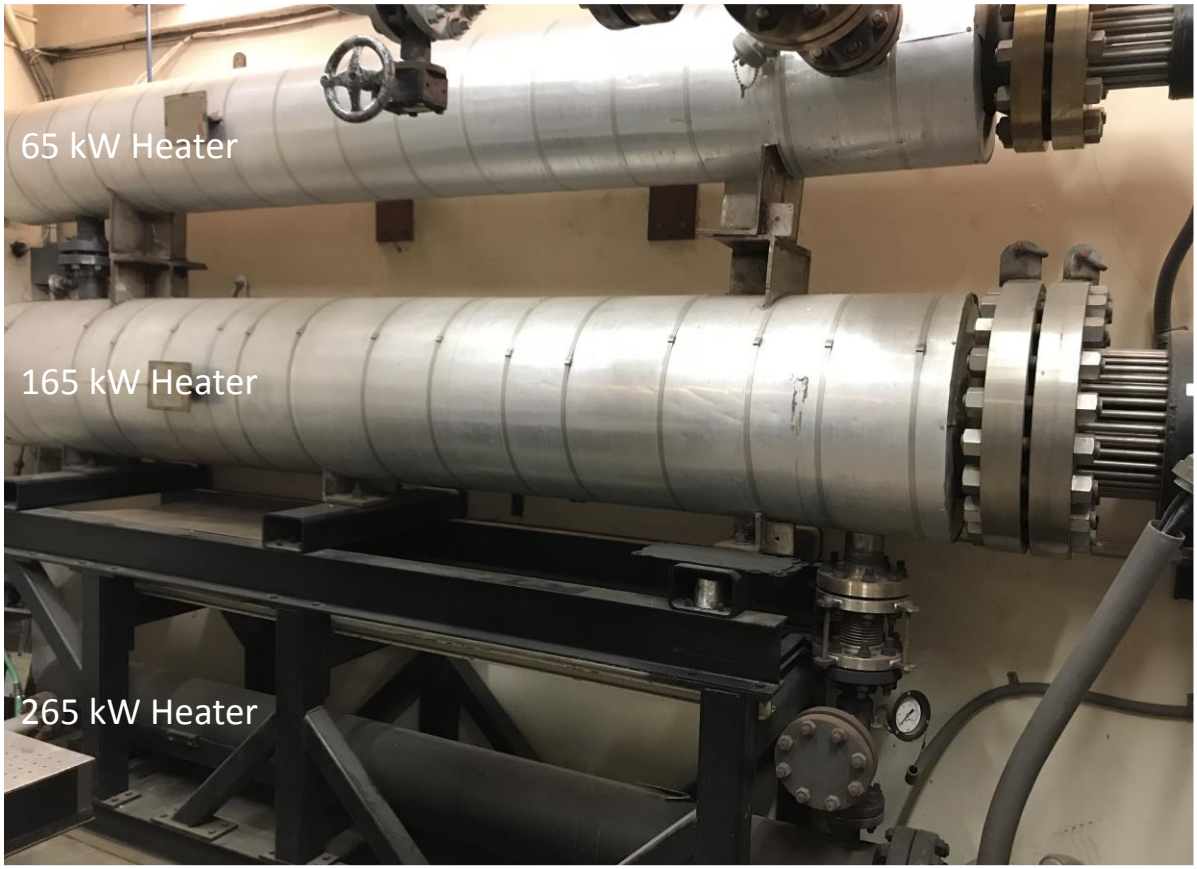

Figure 4.14: Electric heaters in the high pressure combustion facility.

4.2.4 Heat Rejection

The exhaust gas temperature is considerably high and can cause a severe damage to the back pressure valve, exit pipe lines, and stack. As a result, a closed-loop water circuit, capable of removing heat up to 400 kW during continuous operation, is implemented. The quench-water is continuously sprayed at the exhaust section upstream of the back pressure valve to reduce the temperature as shown in Figure 4.15. The water injectors are fed by a twenty horsepower water-quench pump at 27 atm (400 psi) pressure. The water is then returned to the collection tank and passes through fan-cooled radiators before entering the quenching pump. The makeup water is also supplied by two pumps (see Figure 4.15) as the water level drops in the collection tank.

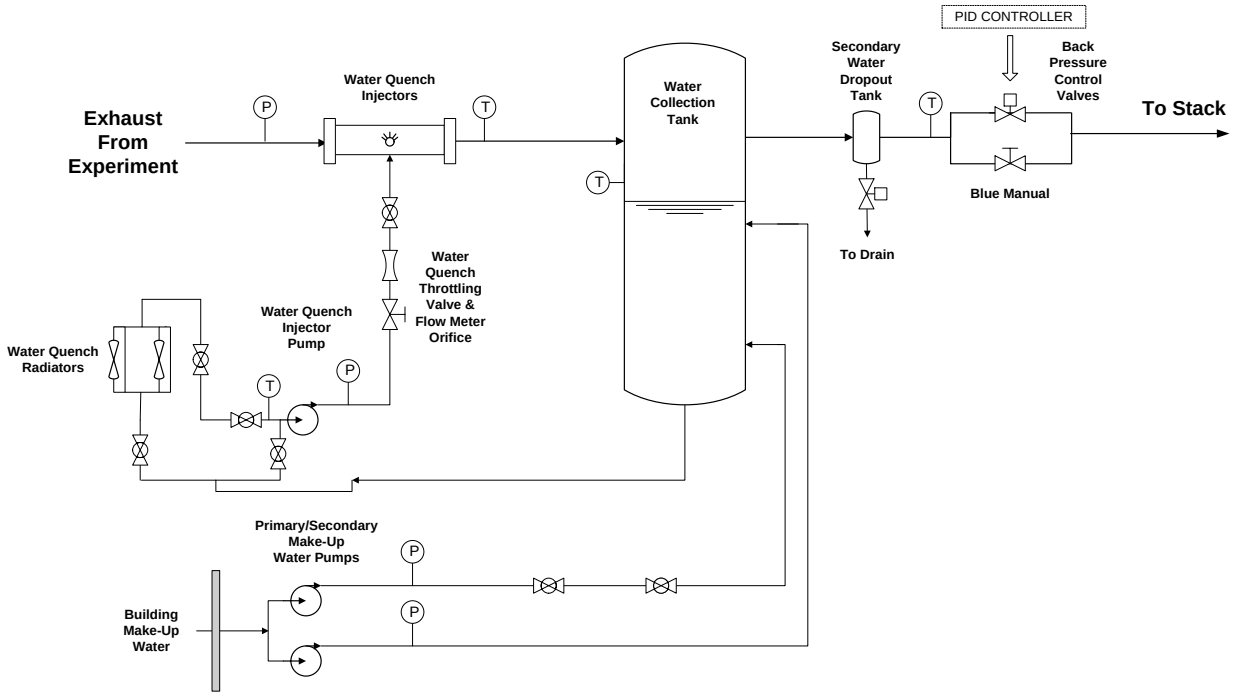

Figure 4.15: Water-quench system in the high pressure combustion facility.

4.2.5 Ignition

A hydrogen pilot torch is used for the ignition process of the main fuel/air mixture. For experiments carried out using the first test rig, the hydrogen pilot is ignited by a frequency doubled Nd:YAG laser (Continuum

Surelite III-10) fired into the combustor through one of the quartz windows as shown in Figure 4.16. The laser power and optical train is set to give rise to breakdown of air within the burner while not damaging the quartz windows or burner liner. The laser is used to ignite hydrogen pilot fuel which then assists in the ignition and stabilization of the jet flame. The laser is controlled with a computer running LabVIEW and this allows for remote control of the ignition laser for light off. For other experiments carried out using the second test rig, the hydrogen diffusion pilot is ignited with a spark igniter, which is flush with the combustor wall to prevent any disturbance to the flow field.

Figure 4.16: Nd:YAG laser ignition setup.

4.2.6 Video capabilities

A remote CCD (Charge-Coupled Device) camera was used to visually observe flame during each test and also connected to a desktop computer simultaneously recording video at 30 frames per second and 862 by 647 pixels.

The flame dynamic at the onset of flashback was observed by implementing intensified high speed OH* imaging. The images were taken by a Vision Research Phantom 7.1 high speed camera at 3000 fps with an exposure time of 330 µs using a UV CoastalOpt SLR Lens manufactured by Jenoptik Optical Systems, Inc. (105 mm, f/4.5). A high speed intensifier (HiCATT 18MM Gen 2 by Lambert Instruments) was used along with a 308 nm bandpass filter to isolate OH* emissions as indicated in Figure 4.17. The images were recorded with resolution of 800*600 and directly saved on a desktop computer.

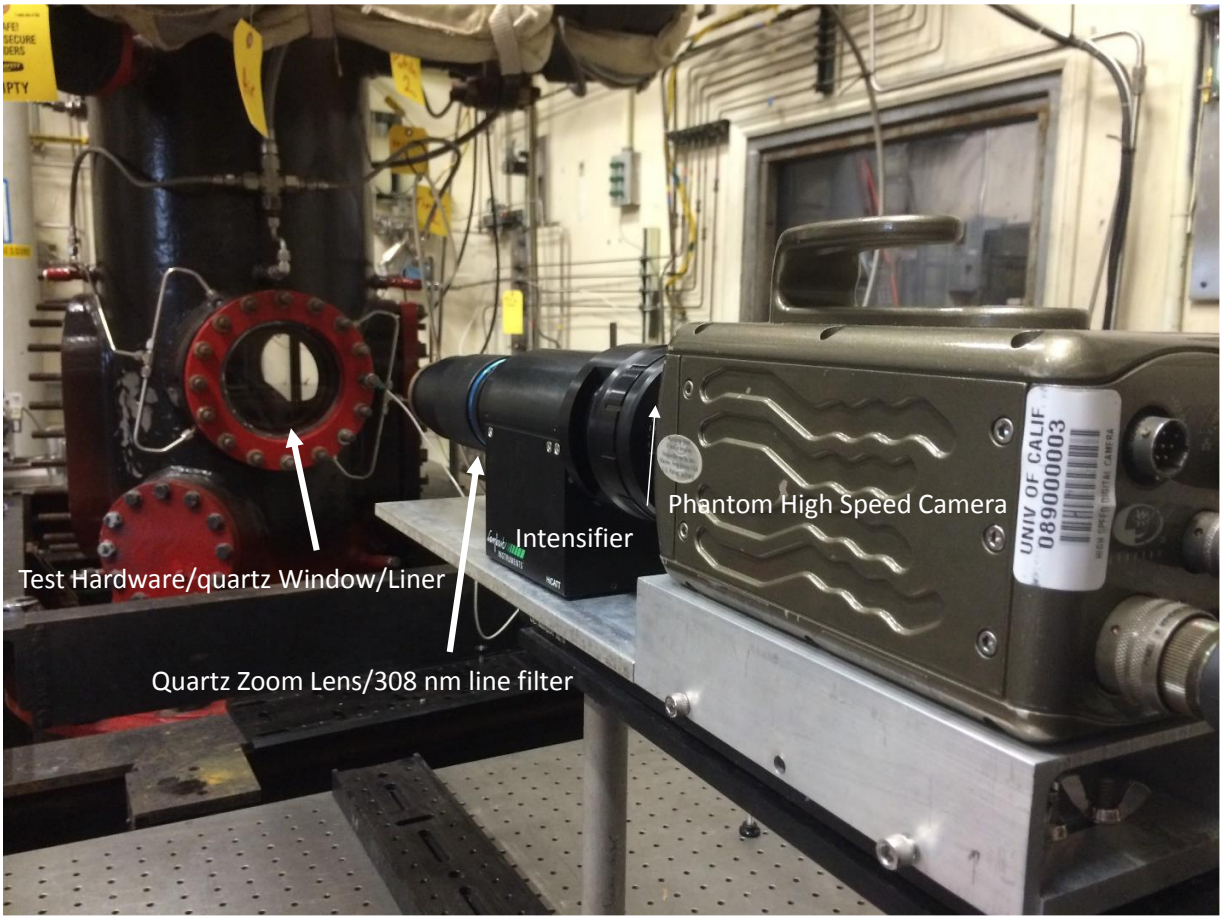

Figure 4.17: Intensified high speed OH* imaging setup.

4.2.7 Laser Doppler Velocimetry

LDV is a single-point velocimetry method with very high resolution. The flow is seeded by small particles that scatter light. The particles are illuminated at the measurement point by two crossing beams with the same wavelength λ. As a result of this interference, a fringe pattern (i.e., alternating brightness and

darkness) is generated at the same measurement point, indicated in Figure 4.18. The intensity of the scattered light varies as the illuminated particle crosses the fringe pattern and is recorded by the photodetector. The frequency of the measured signal (f_D) is proportional to the particle velocity component (V) perpendicular to the fringe pattern according to Eq. 4.1.

$$f_D = \frac{2V}{\lambda}\sin\left(\frac{\theta}{2}\right) \qquad \text{Eq. 4.1}$$

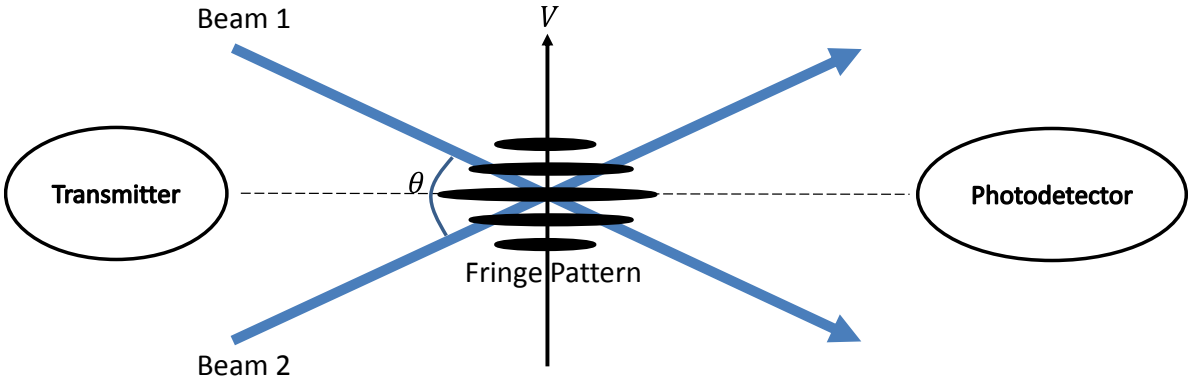

Figure 4.18: Fringe pattern generated by two beams intersecting at the measurement point.

Laser Doppler Velocimetry (LDV) was used to measure the velocity profile near the burner exit plane. In the LDV setup, air flows upward where small water droplets are added through a Y-shaped pipe fitting. Figure 4.19 indicates the setup for this experiment including a 4 watt Coherent Innova 90C-A4 argon-ion laser coupled with a TSI LDV system. The laser beam is separated by an Aerometrics Fiberlight multi-color beam separator for measuring three velocity components. In the current experiment, only axial and radial velocity components are measured. Transmitting and receiving optics are achieved by a LDV00302 backscatter transceiver, consisting of a 261 mm focal length, a PDM 1000 photodetector, and a FSA 4000 signal processor unit.

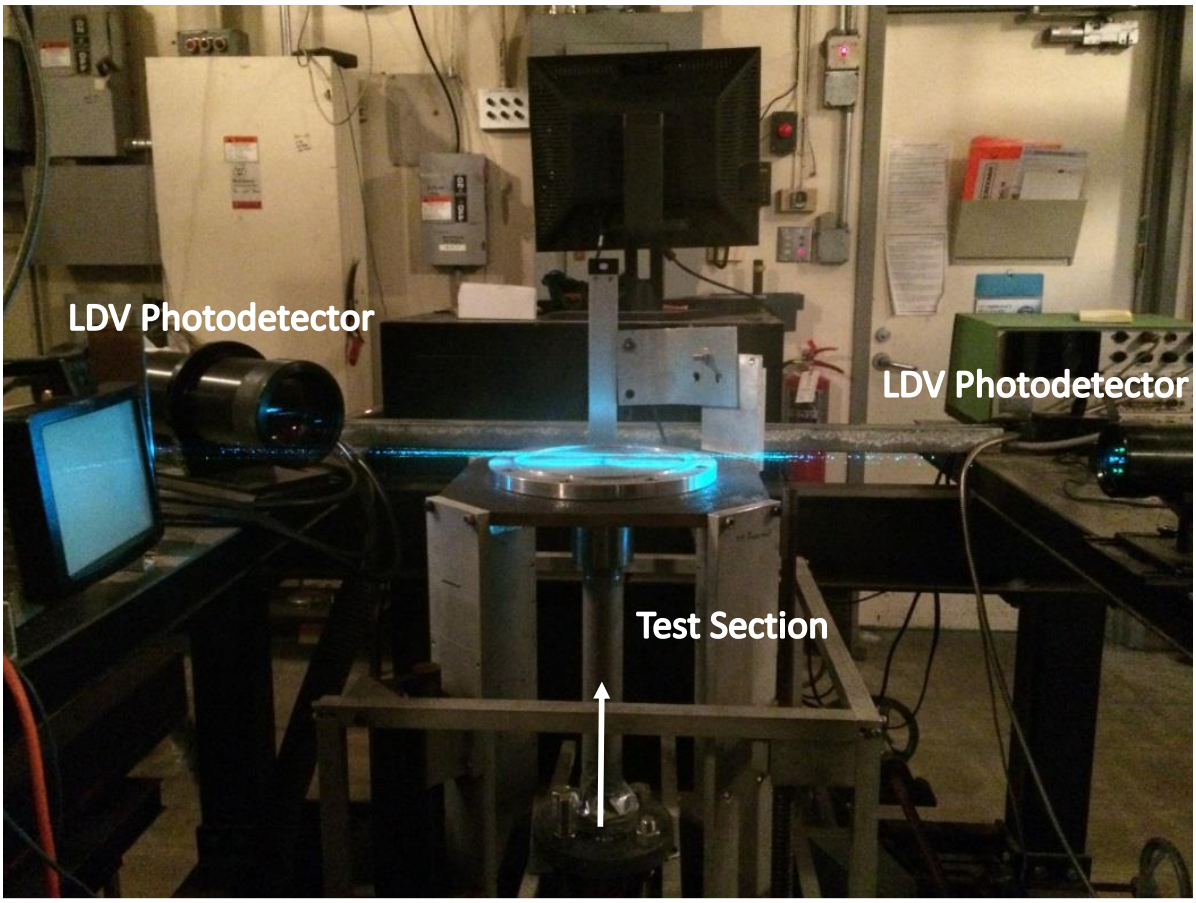

Figure 4.19: LDV setup for the atmospheric test.

4.2.8 Computer Controller

The data is recorded in a desktop computer by LabVIEW, which is connected to data acquisition boxes through National Instruments PCI. The recorded data include air temperature, operating pressure, differential pressure between premixer and combustor, burner tip temperatures, air and fuel mass flow rates, and pilot fuel mass flow rate. In addition, the calculated properties including bulk flow velocity at the burner exit and equivalence ratio of the mixture are displayed in the user interface (Figure 4.20) and also stored in a computer. Nd:YAG laser is also remotely controlled by LabVIEW for light off and the laser power is adjusted to induce breakdown of air within the burner.

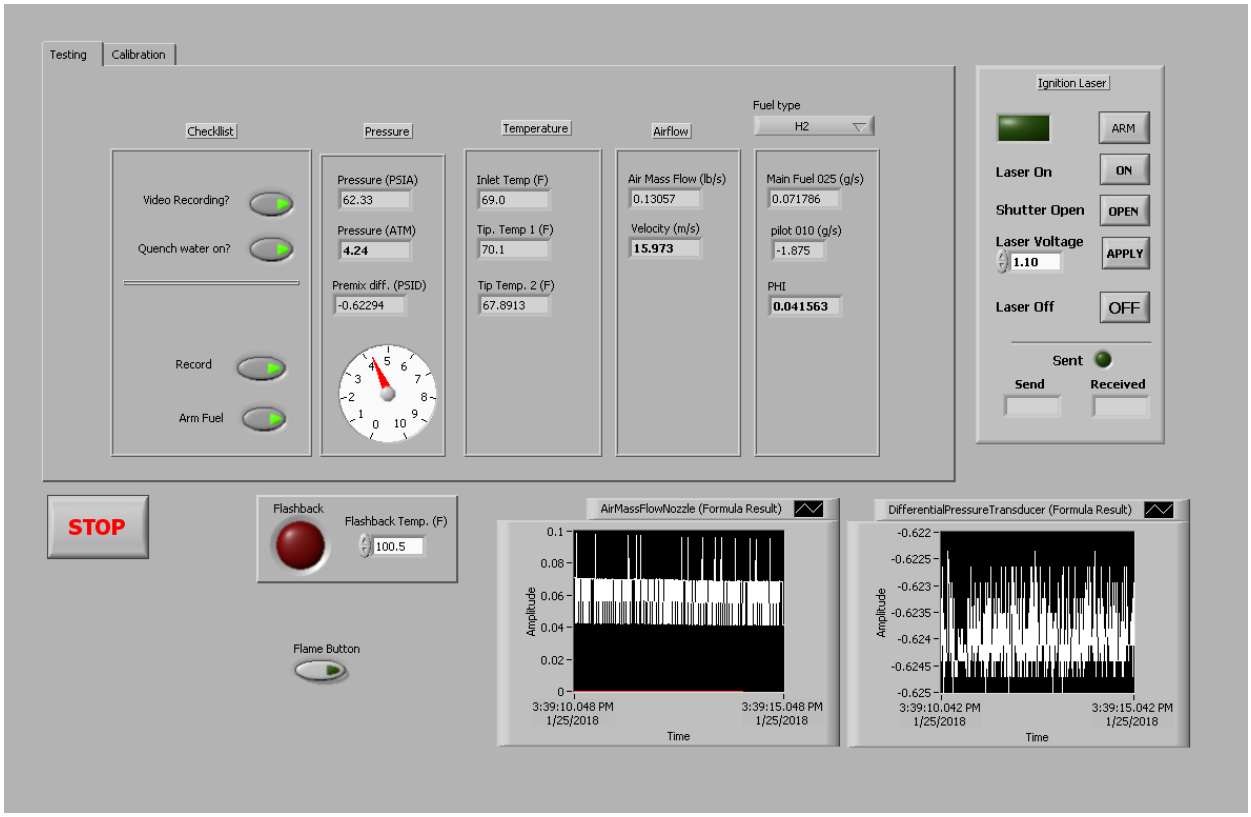

Figure 4.20: LabVIEW user interface designed for flashback testing.

4.2.9 Data Post Processing

Each data set corresponding to a flashback point was processed by a MATLAB code. Tip temperature and differential pressure variations are first plotted versus time and once flashback point is located, the associated data will be saved as an Excel file.

All thermodynamic and transport properties were calculated at given operating pressure and preheat temperature by in-house code. These properties consist of density, viscosity, specific heat capacity, thermal conductivity, and thermal diffusivity. All data base of thermodynamic and transport properties are from CHEMKIN and mixture properties are determined according to multicomponent analysis. The method used in the previously developed code is similar to other open source chemical kinetic software such as CANTERA. The laminar flame speed was calculated by CHEMKIN chemical kinetic software using GRI 3.0 chemical kinetics and transport mechanisms.

4.3 Flashback Testing

4.3.1 Test Rig I

The experiment has been conducted using hydrogen, 50% hydrogen and 50% methane (by volume), and natural gas at absolute pressures between 3-8 atm and preheat temperatures between 300-500 K. Measurements were performed at burner head bulk velocities between 30 and 40 m/s for hydrogen and 10 m/s and 20 m/s for natural gas and mixture of 50% hydrogen and 50% methane. The range of Reynolds number covered in this experiment is $5 \times 10^4 < Re_D < 3 \times 10^5$, which is considerably higher than previous studies in the literature. Three burner heads constructed of different materials (stainless steel, copper, and zirconia ceramic) were used to evaluate flashback dependency on burner physical properties. The thermal coupling effect between flame and burner rim was captured by tip temperatures measured by thermocouples. The standard procedure used to stabilize a flame in the combustor rig is as follows: the air mass flow rate is set to the desired value and hydrogen pilot is ignited by the laser. The main fuel rate is steadily increased until the flame stabilizes. At this point the pilot fuel is shut off and flashback can be approached. The air mass flow rate is held constant and fuel flow rate is increased gradually until flashback occurs.

4.3.2 Test Rig II

The boundary layer flashback of an injector from a commercial 60 kW microturbine generator (i.e., a Capstone C-60 MTG, see Figure 4.11) operated on hydrogen was studied at pressures and preheat temperatures between 2-7 atm and 390-610 K, respectively. The Reynolds number at the injector exit varied between $6 \times 10^4 \leq Re \leq 2 \times 10^5$. Tests were performed by setting the pressure, bulk flow velocity, and the preheat temperature at desired values. The pilot torch was then ignited by the spark igniter and the main fuel flow rate was increased until the main flame was stabilized. At this point, the pilot fuel was shut off and the main fuel flow rate was incrementally increased to approach flashback limit. The corresponding equivalence ratio and associated parameters were recorded and used for the analysis.

Chapter 5 - Results

5.1 Non Reacting Flow

Non reacting tests and numerical simulation were initially carried out to ensure a fully developed flow and a uniform fuel/air mixing at the burner exit. In addition, the ability of changing turbulence intensity at the flame front was investigated using different perforated plates.

5.1.1 Mixing Performance

5.1.1.1 Test Rig I

The computational simulation was performed using ANSYS FLUENT to evaluate the mixing performance of the venturi. The geometry was modeled in three dimensions using unstructured tetrahedral mesh with 10^6 elements (see Figure 5.1). A Reynolds-averaged Navier–Stokes (RANS) simulation was conducted using the k-epsilon turbulence model. A second-order scheme was used for all conservation equations. The turbulent Schmidt number was assumed to be 0.7, previously found to provide good agreement with experimental results for high hydrogen content fuels [199,200]. The air and fuel velocity vectors were considered perpendicular to all inlets and the fuel mass flow rate was uniformly distributed in fuel passages (see Figure 4.3 and Figure 5.1) such that the corresponding bulk velocities remained constant.

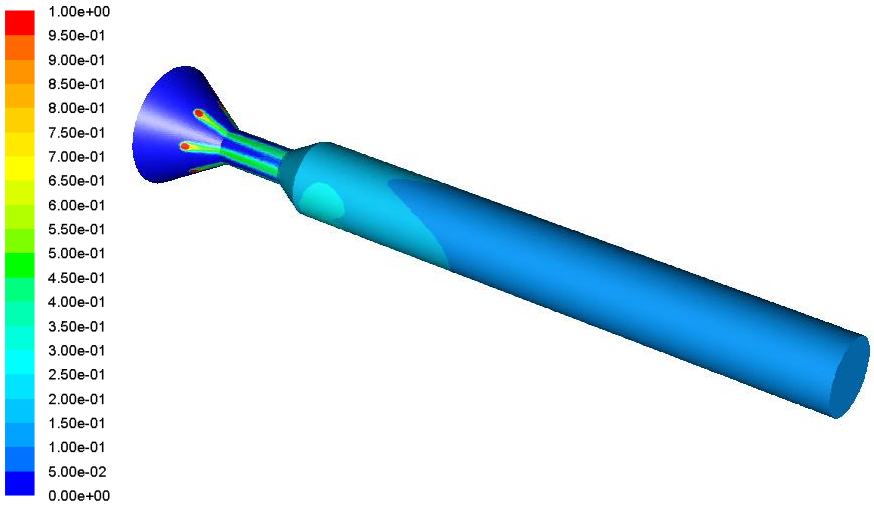

Figure 5.1: Hydrogen mole fraction in the mixture along the premixing tube.

The preheat temperature and operating pressure were set at 300 K and 1 atm, respectively. The average equivalence ratio of hydrogen/air mixture and bulk flow velocity at the burner exit were also set at 0.54 and 40 m/s, respectively. Figure 5.1 illustrates the contour of hydrogen mole fraction in the mixture along the premixing tube. The red color regions show the fuel injection point while the air is introduced upstream, denoted by the blue color. The result shows uniform concentration profiles at the exit section of the burner head.

Figure 5.2 illustrates the variation of hydrogen concertation in radial direction at different cross sections along the premixing tube. The horizontal axis is normalized by the injector radius. The location of each cross section is also illustrated in Figure 5.3. The hydrogen concentration at X=2.54 cm is minimum in the center and rapidly increases toward the wall where the fuel was initially injected. As the fuel/air mixture passes through the premixing tube, the variation of hydrogen concertation between the center and wall rapidly decreases. At X=12.7 cm, the hydrogen concentration is uniform along the radial direction, indicating a good mixing performance required for flashback tests.

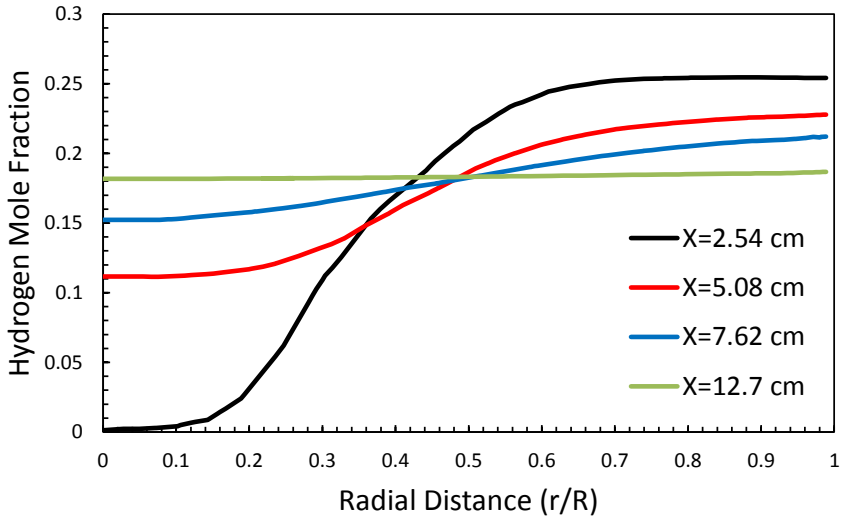

Figure 5.2: Variation of hydrogen mole fraction in radial direction at different cross sections (denoted by X).

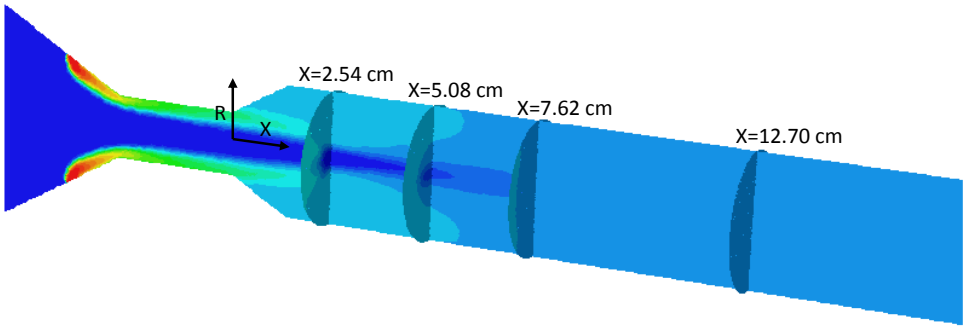

Figure 5.3: Cross sectional planes along the premixing tube.

5.1.1.2 Test Rig II

The fuel/air mixing performance of the injector was determined using ANSYS FLUENT. The 3D geometry shown in Figure 5.4 was modeled using an unstructured tetrahedral mesh with 2×10^6 grid points. A Reynolds-averaged Navier–Stokes (RANS) simulation was conducted using the k-epsilon turbulence model. A second-order scheme was used for all conservation equations.

The air velocity vector was considered perpendicular to all inlets and the air mass flow rate was uniformly distributed in air passages (see Figure 5.4) such that the corresponding bulk velocities remained constant. The turbulent Schmidt number was assumed to be 0.7, previously found to provide good agreement for high-rich fuels [199,200]. The preheat temperature and operating pressure were set at 600 K and 2 atm, respectively, corresponding to a test operating condition. The average equivalence ratio of hydrogen/air mixture at the injector exit was set at 0.4 with the Reynolds number 9.5×10^4.

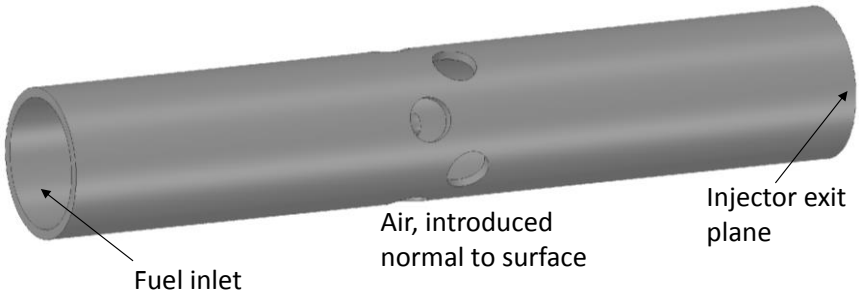

Figure 5.4: Injector geometry for numerical simulation.

Figure 5.5 indicates the hydrogen/air mass ratio along a diameter at the injector exit plane. The radial distance is horizontal axis, normalized by the injector radius. The variation of hydrogen/air concentration across the engine injector is less than 5%. Experimental results from [201] indicated that the variation of methane/air concentration is less than 11% for the engine injector operating in a special injector test rig that mimics all the geometry of the casing/liner in the engine (i.e., a Capstone C-60 gas turbine engine). The difference between these two values (5% versus 11%) may be a combined result of (1) non-uniform air flow distribution in the injector in the special test rig and (2) the relative diffusivity of hydrogen compared to methane. Nevertheless, both studies show a uniform fuel/air distribution at the injector exit.

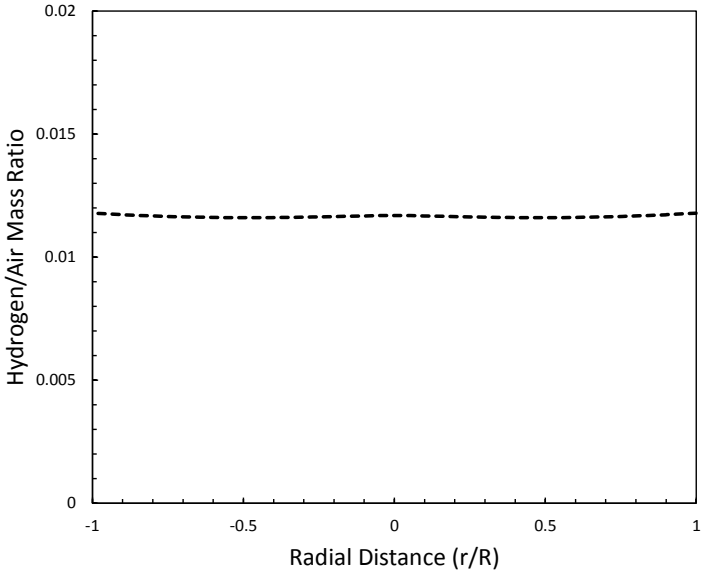

Figure 5.5: Hydrogen/air mass ratio across the injector exit plane (numerical simulation).

5.1.2 Fully Developed Flow

The numerical simulation was also carried out to determine the velocity profile at the burner exit as indicated in Figure 5.6. The numerical modeling approach is similar to details mentioned in Section 5.1.1. The simulation was performed at pressure of 1 atm and temperature of 300 K. The flow bulk velocity at the exit is 37 m/s, corresponding to $Re = 6 \times 10^4$.

Figure 5.7 indicates the mean axial velocity profile at the burner exit along a radial direction. The radial distance is normalized by the burner radius. It is noted that the velocity gradient is steep at the wall and the velocity profile is almost inform at the center, as also predicted for a fully developed turbulent flow. This ensures that the velocity gradient at the wall can be calculated by empirical equation (Eq. 2.8) rather than the numerical simulation for all data points.

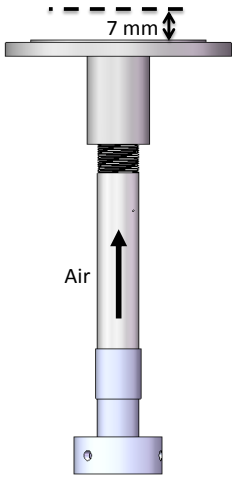

Figure 5.6: Schematic of experimental setup and 3D model used for numerical simulation.

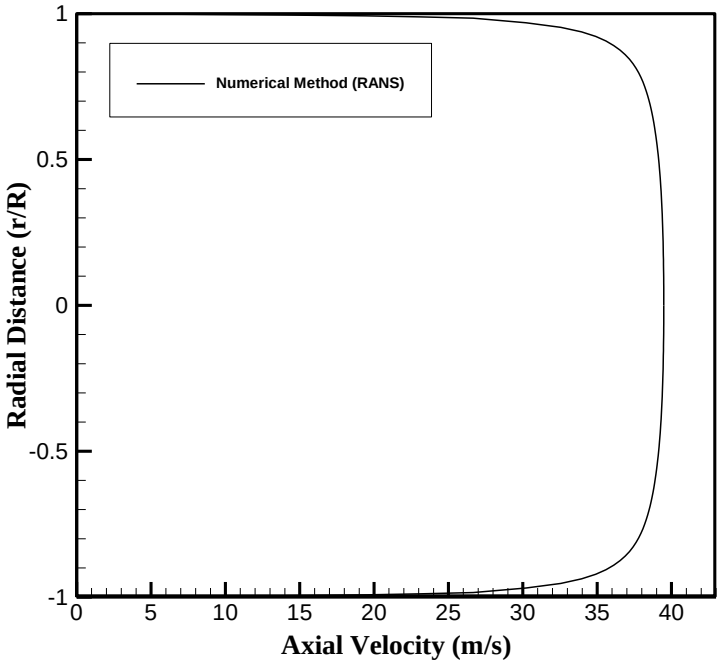

Figure 5.7: Mean axial velocity profile at the burner exit plane (numerical simulation).

Figure 5.8 illustrates the velocity profile obtained by LDV at a plane 7 mm above the burner exit (see Figure 5.6) for different mass flow rates. The radial distance is normalized by the tube radius. As the jet flow decays and spreads due to the sudden exposition at the burner, the mean velocity profile also changes. This is also seen from Figure 5.8 where the jet width expands beyond the burner diameter. The velocity profile is fully developed and almost uniform at the center, but it slightly decreases at one side. Considering the waters droplet seeding, the water spray point could not be moved farther upstream due to quick droplet accumulation at the burner exit. As a result, the velocity distribution was slightly disturbed by the water injection as clear from Figure 5.8.

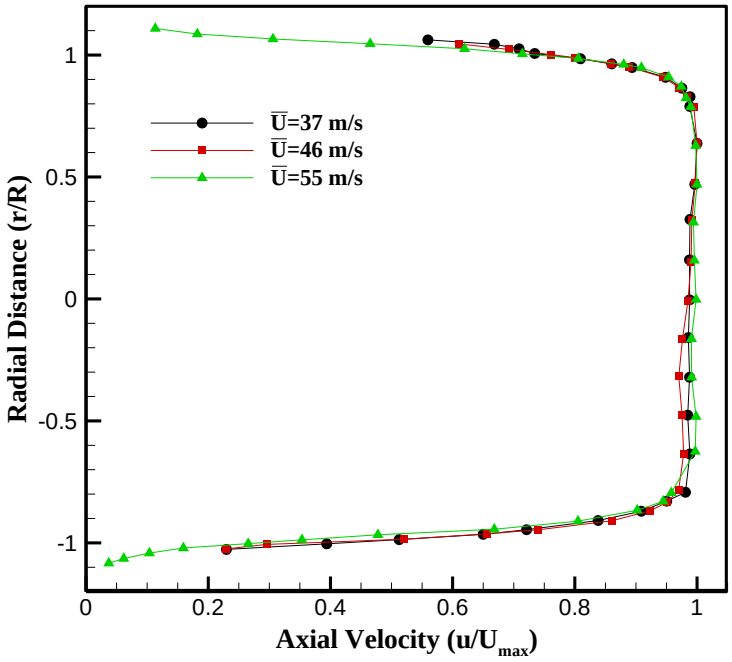

Figure 5.8: Velocity profile for different mass flow rates at the exit plane, obtained by LDV.

5.1.3 Turbulence Intensity

In an effort to establish impacts of turbulence levels, a number of perforated plates (7.62 mm width and 3.68 cm diameter) were designed and 3D printed as shown in Figure 5.9. Laser Doppler Velocimetry (LDV) was used to measure the turbulence intensity generated by the different perforated plates at the exit plane of the jet burner. The blockage ratio was varied systematically to determine the possibility of

changing turbulence intensity for a fully developed turbulent flow. Table 5.1 shows the measurement of axial turbulence intensity at the center for indicated patterns in Figure 5.9 as well as a honeycomb sheet. The bulk flow velocity was 25 m/s for all cases. The turbulence intensity variation is not significant since the turbulence intensity rapidly decays in a long pipe as flow approaches the exit section. Hence, the difference between measured turbulence intensity would not be sufficient to make a clear change in flashback limits. Further work is needed to establish an improved strategy for controlling turbulence intensities. Part of the challenge in the current approach is that, to apply analytical expressions to determine the velocity profile at the wall, fully developed flow is desired which is achieved with the long pipe upstream of the exit plane. This obviously conflicts with the ability to change turbulence levels with plates located well upstream of the burner exit.

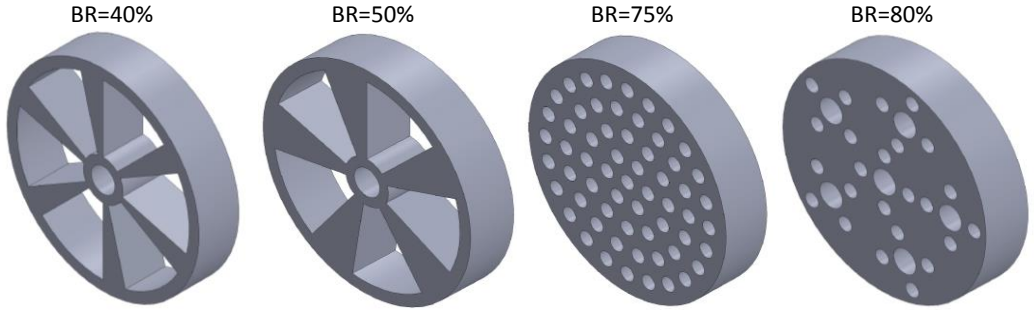

Figure 5.9: Perforated plates with different blockage ratios.

Table 5.1: Measured values of axial turbulence intensity for different perforated plates at the center.

Perforated Plates	Turbulence Intensity (%)
None	3
40% BR	3.2
50% BR	3.5
75% BR	5.5
80% BR	4
Honeycomb	5.5

5.2 Reacting Flow

After verifying the mixing performance and velocity distribution at the burner exit, boundary layer flashback tests were carried out and final results are presented in this section.

5.2.1 Flashback Diagnostic

The typical response of thermocouples measuring the tip temperature is illustrated in Figure 5.10. The tip temperature rises as the equivalence ratio increases and an abrupt increase in the measured tip temperature is observed when flashback occurs. The result represents the functionality of the tip thermocouples to measure the burner head tip temperature and to also serve as one sensor for confirming flashback. However, during some tests, fluctuations in the measured tip temperature were of the same order as the tip temperature rise due to flashback, making it difficult to determine the exact point at which flashback occurs. Consequently, differential pressure across the burner tip has been used along with tip temperature to ensure the precise flashback detection. This strategy has been successfully implemented as indicated in Figure 5.11. Clear peaks at the onset of flashback can be observed in both pressure transducer and thermocouple responses, which are coincident.

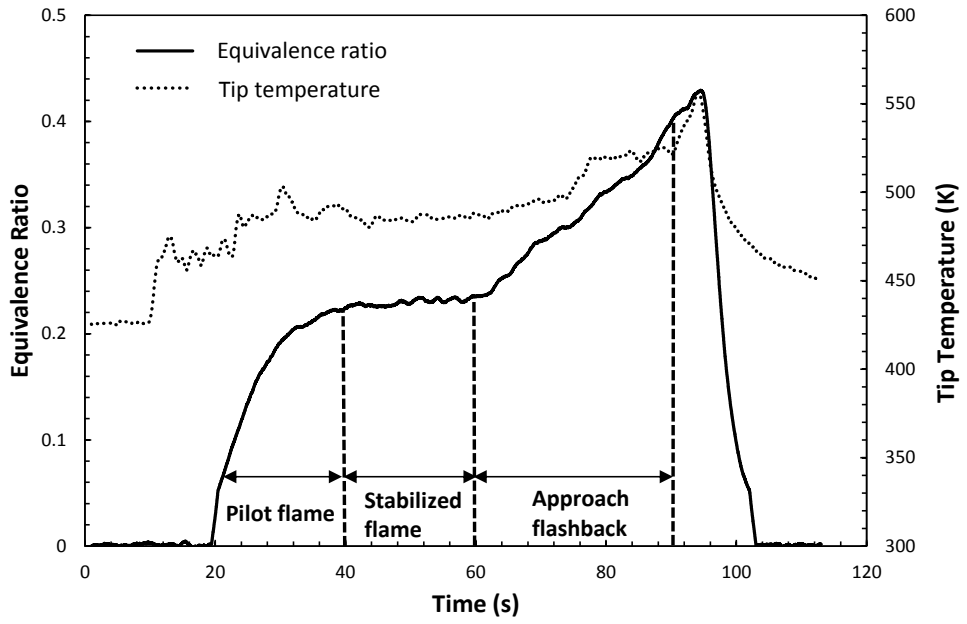

Figure 5.10: Variation of tip temperature and equivalence ratio with time.

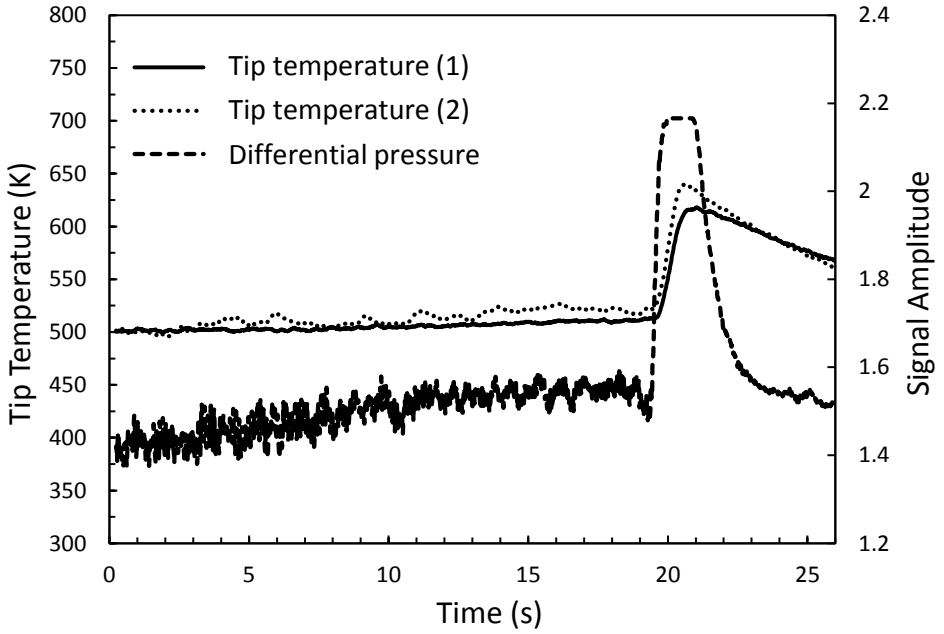

Figure 5.11: Tip temperature and pressure transducer responses as an indicator of flashback.

5.2.2 Flame Configuration

Figure 6 illustrates high speed intensified OH* consecutive images at the onset of boundary layer flashback. The exit of the burner diameter is shown by white lines. Further detail regarding the OH* imaging system are found in Section 4.2.6. The flame is initially stable (a) and starts propagating upstream from the left corner (b). Once the flame partially enters the injector (c), the full flashback occurs (d). The flame length decreases with an increase of equivalence ratio. When the flame length becomes shorter than a critical value, it can be used as an indication of flashback (see [95]). It is also noted that the OH* signal increases on the left near the injector exit as flame continues to regress into the injector. Similar observations were made in [98,102]. The OH* signal increases due to a larger local heat release where flashback occurs.

Figure 5.13 also illustrates the stabilized flame and the flame regression at the onset of flashback for hydrogen. Figure 5.13 b also justifies an increase in OH* signal as flashback occurs.

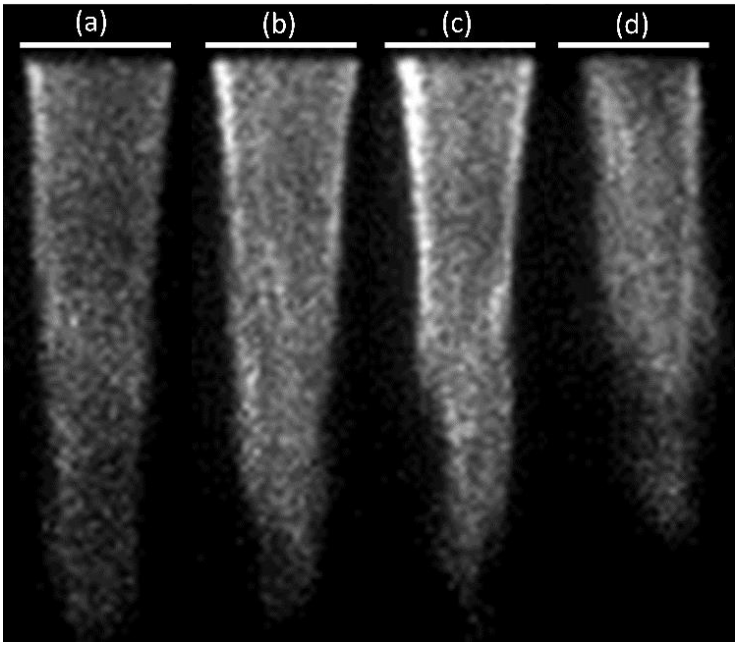

Figure 5.12: Flashback occurrence of hydrogen jet flame at operating pressure of 5 atm and preheat temperature of 400 K.

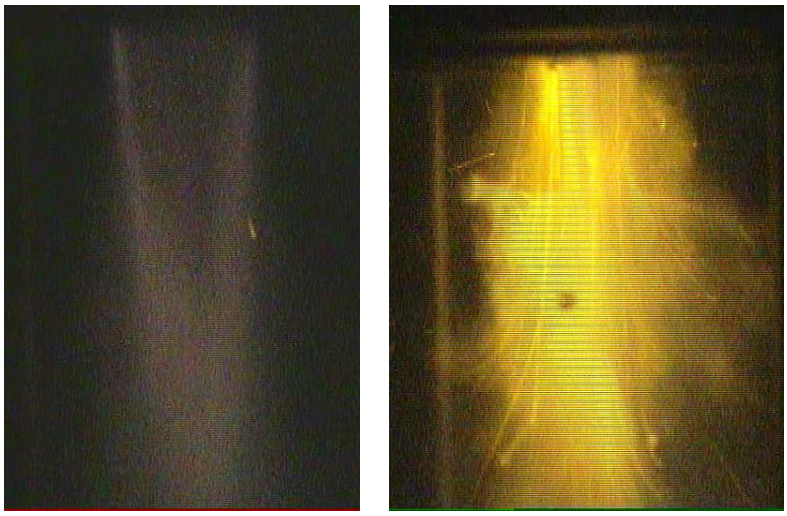

Figure 5.13: Hydrogen flame configuration at pressure of 5 atm and preheat temperature of 400 K: (a) stable flame and (b) flashback.

5.2.3 Flashback Tests

5.2.3.1 Test Rig I

Figure 5.14 shows the equivalence ratio at which flashback occurs (ϕ_{FB}) as a function of pressure for the stainless steel burner head and different preheat temperatures. An increase of preheat temperature for

a constant bulk velocity decreases the equivalence ratio (ϕ_{FB}). Furthermore, the higher velocity inlet results in the lower flashback propensity, but this effect is not significant. Trend lines in Figure 5.14 represent $\phi_{FB} = P^{-m}$, in which m is the pressure exponent and increases according to the direction of the indicated arrow. Daniele et al. reported the average pressure exponent of 0.5 for a fuel mixture of H_2 and CO in equal volumetric parts [95].

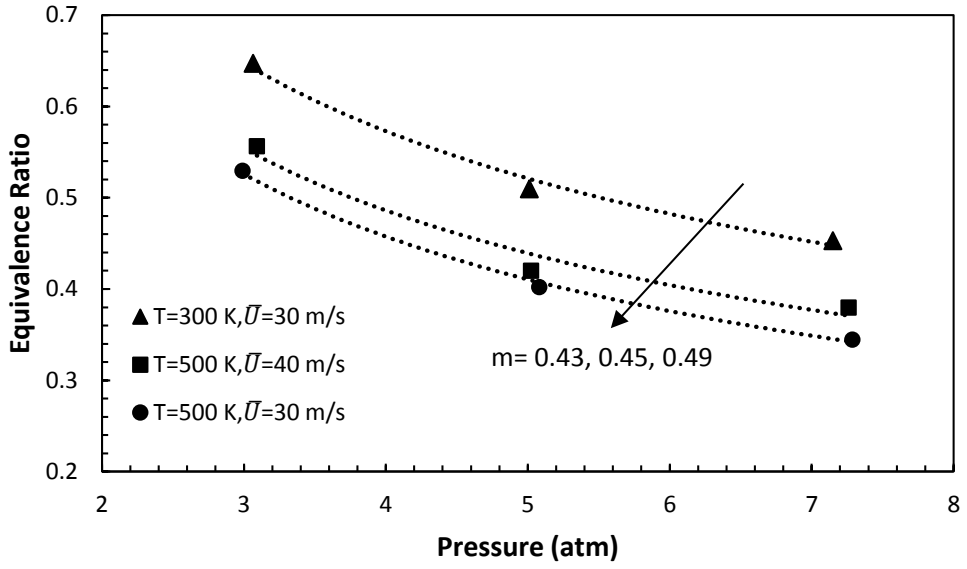

Figure 5.14: Variation of equivalence ratio as a function of pressure for the stainless steel burner head.

Using measured data, Figure 5.15 illustrates tip temperature variation as a function of equivalence ratio for a stainless steel burner head for different pressures, and inlet temperatures. For each set, three points along the trend line represent different flashback propensity of hydrogen according to the velocity at the burner head. At constant pressure, an increase of preheat temperature leads to flashback at a lower equivalence ratio and higher tip temperature. Lower equivalence ratio results in a lower adiabatic flame temperature, but an increase of preheat temperature compensates this effect and finally causes a higher tip temperature. At constant preheat temperature, an increase of pressure shifts the flashback point to lower equivalence ratios and higher tip temperatures. As the pressure increases, the quenching distance of the stabilized flame reduces and leads to higher tip temperature. As shown in Figure 5.15, an increase

of preheat temperature from 400 to 500 K caused a more significant increase in tip temperature at flashback than does an increase in pressure from 3 to 7 atm.

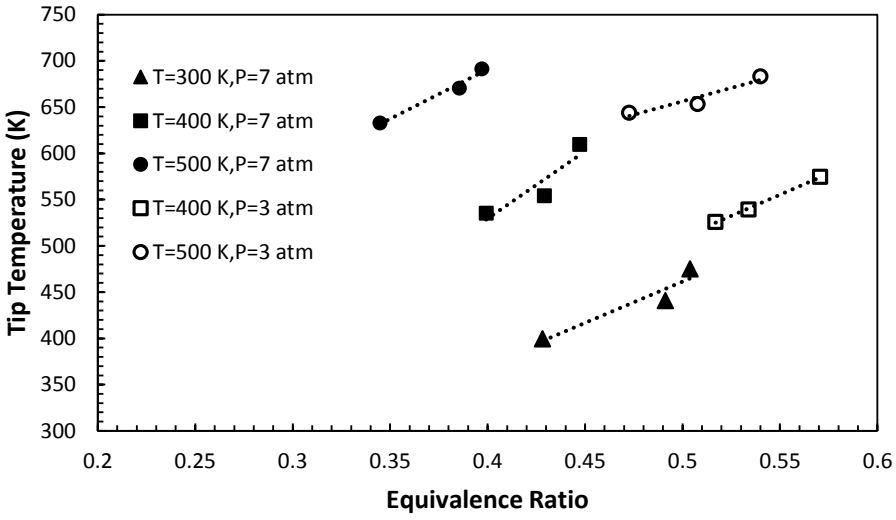

Figure 5.15: Variation of tip temperature with equivalence ratio at different preheat temperatures and pressures.

Experimental data obtained for hydrogen with the stainless steel burner head is shown in Figure 5.16 and illustrates the effect of pressure on critical velocity gradient. Each line of data represents a different velocity at the burner head. Higher velocities correspond to higher equivalence ratios at flashback for a given preheat temperature and pressure. At a constant preheat temperature, an increase of pressure causes a higher flashback propensity, i.e., higher critical velocity gradient and lower equivalence ratio. The critical velocity gradient variation rate increases with an increase of pressure. This observation is consistent with previous studies performed at sub atmospheric pressures. In fact, the effect of equivalence ratio is enhanced at higher pressure.

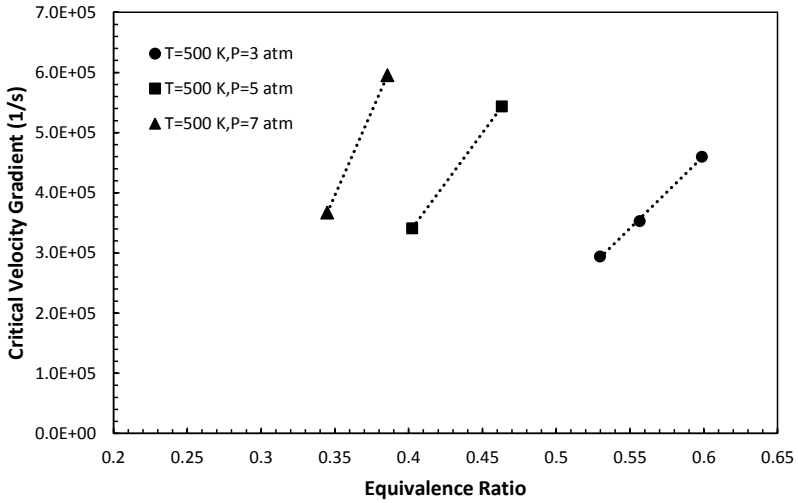

Figure 5.16: Critical velocity gradient variation as a function of equivalence ratio at different pressures.

5.2.3.2 Test Rig II

The equivalence ratio at flashback for the engine injector operated on pure hydrogen is indicated in Figure 5.17 as a function of pressure for various preheat temperatures. The bulk flow velocity at the injector is 50 m/s for all cases, nominally matching the condition in the actual engine. For a given preheat temperature, an increase of pressure decreases the equivalence ratio at which flashback occurs (dashed lines in Figure 5.17). This is mainly associated with the lower quenching distance and higher turbulent burning velocity at higher pressures.

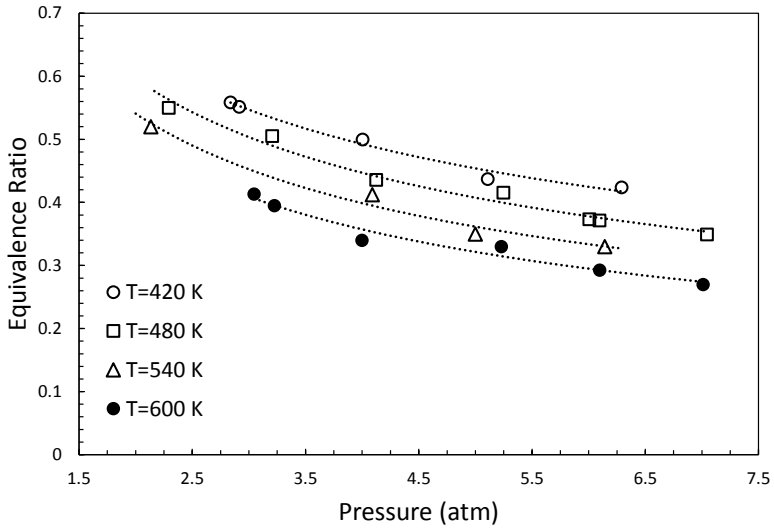

Figure 5.17: Effect of pressure on flashback propensity at various preheat temperature.

The average power law exponent in Figure 5.17 is 0.42, which is consistent with existing flashback results at high pressure. Average pressure exponent of 0.46 was found for experiments carried out in the first test rig. As the preheat temperature increases, the burning velocity also increases, resulting in higher flashback propensity. It is noted that the actual engine preheat temperature is about 850 K, which was not achieved in the experiment due to the large heat loss between the electric heaters and the test rig.

Chapter 6 - Analysis

6.1 Non-dimensional Analysis

Figure 6.1 illustrates the variation of critical velocity gradient with equivalence ratio for all the data at different test conditions. This figure incorporates effects of various parameters including pressures, preheat temperatures, bulk flow velocities, and burner materials; consequently, the equivalence ratio covers a wide range of data, i.e., (0.3, 0.7). As shown, no specific correlation is shown which is due to the challenge in changing only a single parameter at a time during the experiments. In the present study it was acknowledged at the outset that extensive analysis of the results would be needed to develop a model that could then be used to isolate the influence of parameters of interest.

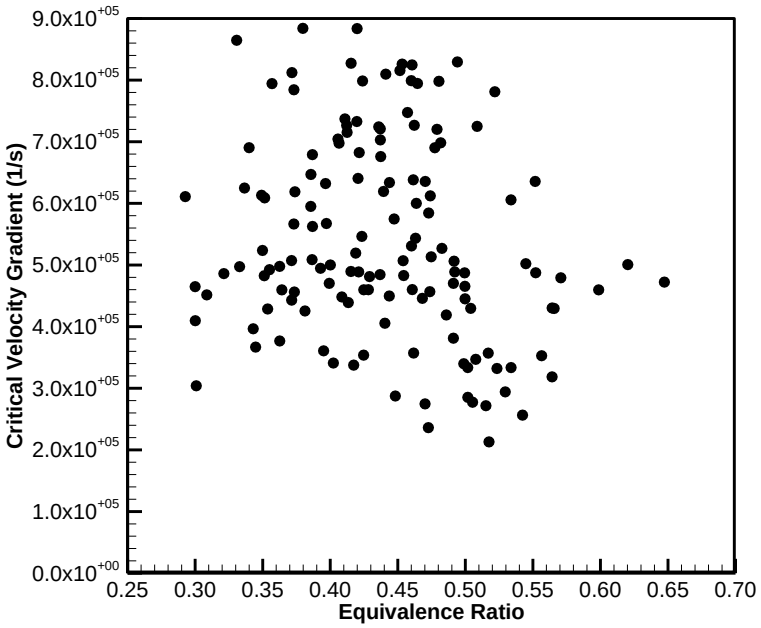

Figure 6.1: Critical velocity gradient versus equivalence ratio for all pressures, temperatures, bulk flow velocities and burner materials.

The critical velocity gradient can be represented as a ratio of the flame speed to penetration distance, Eq. 2.3. This approach has been frequently used in the literature to characterize the boundary layer flashback propensity and thus worth considering as an initial correlating approach. The penetration distance is defined as a height above the wall at which the laminar flame speed is equal to the flow

velocity. Penetration distance is considered proportional to quenching distance and can be calculated based on the flame thickness. Both flame speed and flame thickness are determined using one dimensional, adiabatic, and laminar flame assumptions. This method has been used to characterize the flashback propensity of the current data as shown in Figure 6.2. While some trends may be evident (compared to Figure 6.1), they are not particularly strong. Hence, it is evident that this strategy cannot capture the effects of various parameters including pressure, preheat temperature, inlet bulk velocity, and burner material. As a result, it is apparent that a comprehensive model is needed to take into account all parameters which are effective in flashback propensity.

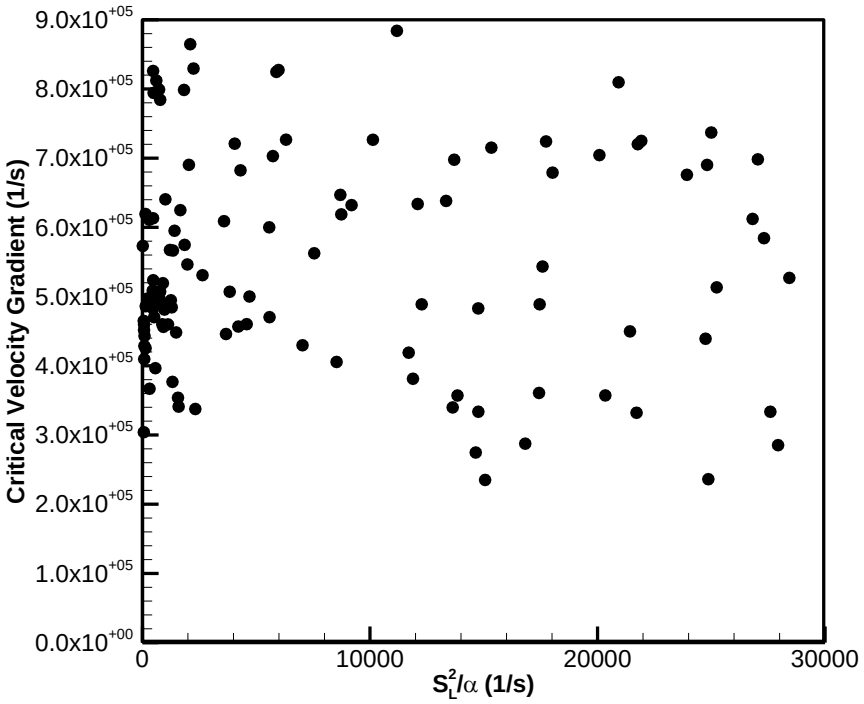

Figure 6.2: Critical velocity gradient variation as a function of $S_L{}^2/\alpha$ for all pressures, temperatures, bulk flow velocities, and burner materials.

Boundary layer flashback occurs when the turbulent burning velocity (S_T) exceeds the local flow velocity (u) in the near-wall region, according to Eq. 6.1:

$$S_T(y_f) = u(y_f) \qquad \text{Eq. 6.1}$$

y_f is the distance from the wall at which the burning and flow velocities are equal. Parameters involved in boundary layer flashback (i.e., Eq. 6.1) are categorized into three groups [197]: (1) flow and combustion characteristics, (2) operating conditions, and (3) flame configuration and boundary layer heating. The local flow velocity (u) in the near-wall region for an unconfined flame is mainly a function of the velocity gradient at the wall. The turbulent burning velocity S_T and flashback location y_f are functions of side-wall quenching distance, laminar flame speed, flame stretch, pressure, preheat temperature, and turbulence intensity. For instance, the turbulent burning velocity of syngas including hydrogen, carbon monoxide, and methane has been correlated by Eq. 6.2 [188]. The ratio of the turbulent flame speed (using global consumption method) to the laminar flame speed was represented as functions of turbulence intensity (u'), turbulence integral length scale (L_T), laminar flame thickness (δ_f), pressure (P_u), and unburned mixture temperature (T_u). The turbulence characteristics in this correlation were measured for non-reactive flow at the flame location [188].

$$\frac{S_T}{S_L} = a\left(\frac{u'}{S_L}\right)^{0.63}\left(\frac{L_T}{\delta_f}\right)^{-0.37}\left(\frac{P_u}{P_0}\right)^{0.63}\left(\frac{T_u}{T_0}\right)^{-0.63}, \qquad a = 337.5 \qquad \text{Eq. 6.2}$$

The turbulent burning velocity in the near- wall region is also affected by the flame stretch since the flame leading edge is convex towards the reactants (recall Figure 2.5). In addition, the upstream flame propagation is strongly affected by hydrogen-rich fuels, which have lower Lewis number. Hence, Eq. 2.51 proposed by Lin et al. takes into account the effect of Lewis number for predicting flashback propensity of hydrogen-rich fuel gases [105]. The final form of this correlation by substituting Eq. 6.2 in Eq. 2.51 is as following:

$$g_c = a\frac{S_L\left(\frac{u'}{S_L}\right)^{0.63}\left(\frac{L_T}{\delta_f}\right)^{-0.37}\left(\frac{P_u}{P_0}\right)^{0.63}\left(\frac{T_u}{T_0}\right)^{-0.63}}{Le \times \delta_f} \qquad \text{Eq. 6.3}$$

The laminar flame thickness δ_f is proportional to α/S_L. Using Damköhler number as a non-dimensional parameter, Eq. 6.3 reduces to:

$$Da = Const.Le\left(\frac{u'}{S_L}\right)^{-0.63}\left(\frac{L_T}{\delta_f}\right)^{0.37}\left(\frac{P_u}{P_0}\right)^{-0.63}\left(\frac{T_u}{T_0}\right)^{0.63} \quad \text{Eq. 6.4}$$

The length and time scales of the wall flashback should be defined properly in order to take into account the location of the anchored flame inside the boundary layer [99,100]. The streamwise turbulence intensity plays the dominant role in determining the total value of the turbulent kinetic energy in the near-wall region. Hence, the magnitude of the near-wall peak in the streamwise turbulence intensity is used as a scaling parameter and is proportional to the shear stress velocity (u_τ) in Eq. 6.5 [202,203]. τ_w is a function of Reynolds number and can be directly related to the critical velocity gradient according to Eq. 6.6. The turbulence length scale is also defined based on the size of vortices placed near-wall region [204]. As a result, both turbulence intensity and turbulence length scale in Eq. 6.4 can be represented by the critical velocity gradient for a fully developed flow.

$$u_\tau = \sqrt{\frac{\tau_w}{\rho}} \quad \text{Eq. 6.5}$$

$$g = \frac{\tau_w}{\mu} \quad \text{Eq. 6.6}$$

Figure 6.3 indicates the application of Eq. 6.4 to the current data. Eq. 6.4 developed by Daniele et al [95] provides poor agreement with the experimental results. Accurate estimation of the turbulence intensity and turbulence length scale in the near-wall region is not trivial, when they are not directly available from measurements. This is a possible reason why Eq. 6.4 is not able to predict the current flashback data. In addition, the thermal coupling between the burner and flame front in Eq. 6.4 is neglected. Hence, a more comprehensive design tool is developed in the present work without a need for such estimations.

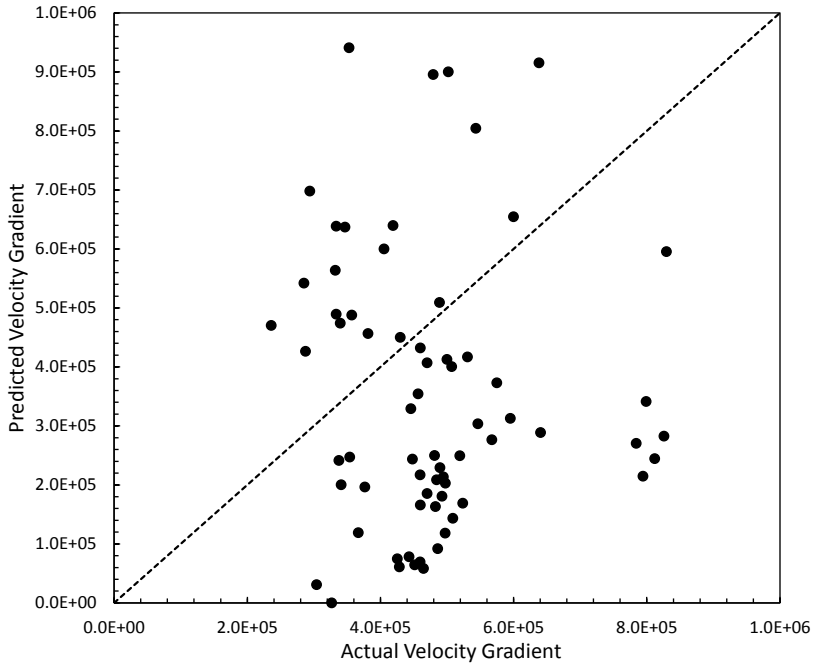

Figure 6.3: Application of Eq. 6.4 to the current data for predicting flashback.

In the present work, a similar non-dimensional analysis based on Buckingham Pi theorem has been conducted to develop a correlation that fits all of the data for various preheat temperatures, pressures, burner materials, and inlet bulk velocities. All effective parameters in flashback propensity can be characterized by following non-dimensional groups:

$$\Pi_1 = Da = \frac{{S_L}^2}{\alpha \cdot g_c}, \Pi_2 = \frac{T_u}{T_0}, \Pi_3 = Le, \Pi_4 = \frac{T_{tip}}{T_0}, \Pi_5 = \frac{D \cdot S_L}{\alpha}, \Pi_6 = P_u/P_0 \qquad \text{Eq. 6.7}$$

Π_1 denotes the Damköhler number (*Da*). It is selected as the indicator of flashback propensity because it contains terms generally associated with flashback, namely the critical velocity gradient and the flame speed. *Da* is defined as a ratio of the turbulent time scale to the chemical time scale. The turbulent timescales have been defined based on the conditions near the burner wall at flashback. Higher *Da* values indicate less mass flow is required to avoid flashback for a given equivalence ratio, i.e., greater flashback resistance. The next step, then, is to develop a correlation for Π_1 in terms of other factors.

$$\Pi_1 = f(\Pi_2, \Pi_3, \Pi_4, \Pi_5, \Pi_6) \quad \text{Eq. 6.8}$$

The ratio of unburnt and reference temperature (Π_2) is used to capture the properties of the bulk flow. The Lewis number (Π_3) compares two diffusivities: thermal and molecular. When molecular diffusion is stronger than thermal diffusion, heat released from the reaction is easier to accumulate locally, creating hot spots. This case is predominant when the fuel is high in hydrogen. The effect of thermal coupling is estimated by using ratio of tip temperature to the reference temperature (Π_4). It increases when more heat is transferred from the reaction region to the upstream mixture. Tip temperature was found to define the controlling kinetics at the onset of flashback and to be a crucial factor in determining flashback propensity. Higher tip temperature leads to a lower quenching distance and consequently higher flame speed at a given height close to the wall. Additionally, this parameter accounts for the effect of burner head materials. Π_5 denotes the flame stretch effect. The burner diameter is divided by flame thickness (α/S_L). It should be noted that Π_5 can also be written as flame Peclet number (Pe_f). The pressure effects are represented by Π_6. The laminar flame speed varies with pressure exponentially and the pressure exponent is a function of equivalence ratio. For lean conditions which are the case in the current study, the laminar flame speed decreases as the pressure increases. Consequently, the higher flashback propensity that is observed at higher pressure is mainly associated with the penetration distance variation based on Eq. 2.24 to Eq. 2.26.

Experimental results showed that the pressure exponent of the critical velocity gradient is also a function of equivalence ratio and cannot be considered constant [95]. The developed correlation takes into account the effect of equivalence ratio.

The correlation based on this analysis for the current high pressure data can be represented as:

$$Da = Const.Le^{1.68}.{Pe_f}^{1.91}.\left(\frac{T_u}{T_0}\right)^{2.57}.\left(\frac{T_{tip}}{T_o}\right)^{-0.49}.\left(\frac{P_u}{P_0}\right)^{-2.1} \quad \text{Eq. 6.9}$$

Hoferichter et al. used flame angle theory and developed a prediction model for boundary layer flashback of hydrogen [109]. It is worth mentioning that a similar correlation was derived from their analysis, as presented in Eq. 6.10. The results have been published in a joint paper with collaboration of Technical University of Munich (TUM) [205].

$$Da = Const.Le.{Pe_f}^2.\left(\frac{T_u}{T_0}\right)^{0.47}.\left(\frac{P_u}{P_0}\right)^{-1.75} \quad \text{Eq. 6.10}$$

6.2 Test Rig I

Figure 6.4 shows application of the developed model to the current data at different pressures, preheat temperatures, and bulk flow velocities. A good agreement is observed between the predicted values and experimental data.

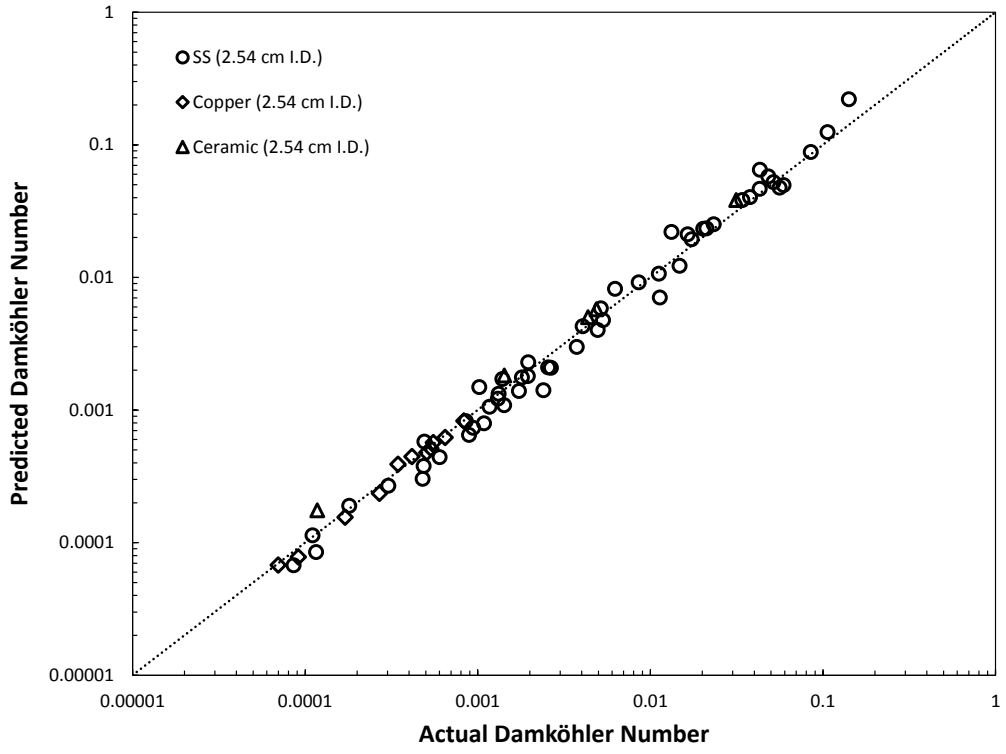

Figure 6.4: Predicted Damköhler number based on the correlation.

The correlation was first developed based on the high pressure data for a 2.54 cm (1 inch) burner diameter and examined against the existing data in the literature as well as the experimental data obtained from a practical combustor (see Section 6.3). Previous work (largely conducted at 1 atm) suggested that burner diameter did not play a significant role in the flashback behavior. In an effort to further validate the developed correlation for the boundary layer flashback prediction, a tube burner with the diameter of 3.05 cm (1.2 inch*)* was used (see Figure 4.8). With an increases in burner diameter, the heat transfer from the flame front to the burner rim changes and can influence the flashback propensity, but this effect is captured in the developed correlation by using the burner tip temperature in Eq. 6.9. As a result, the new data for the larger diameter are in good agreement with the correlation, Figure 6.5. Hence the generality of Eq. 6.9 has been demonstrated to a reasonable extent.

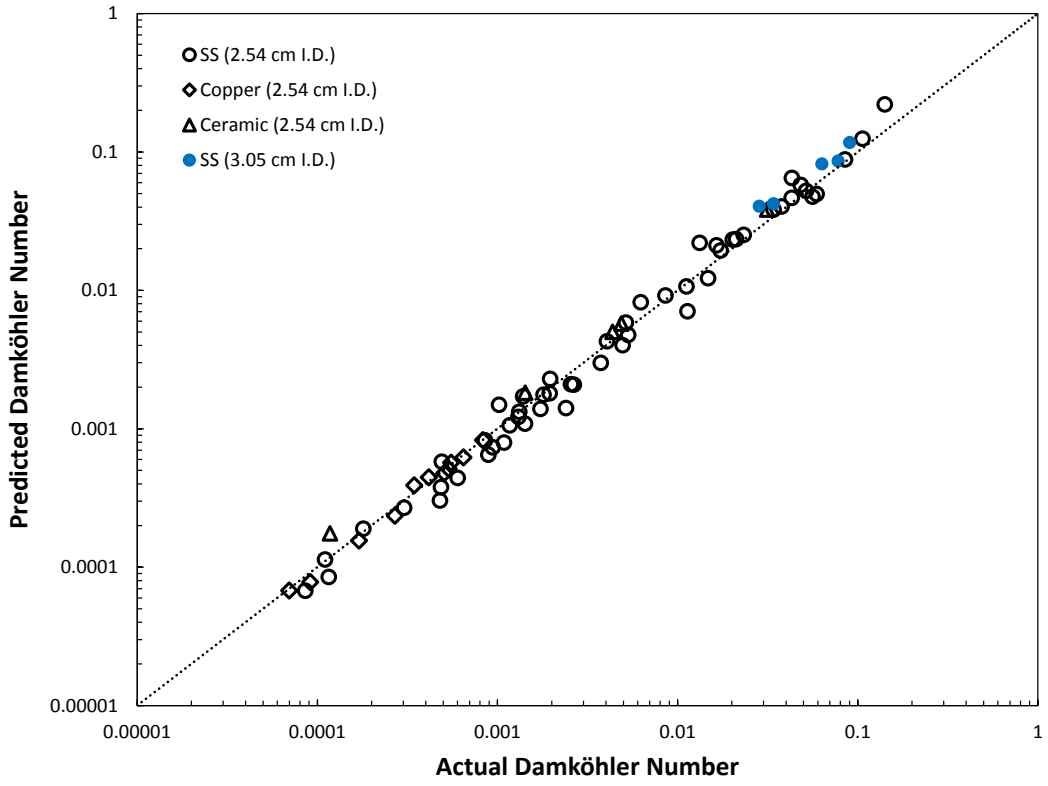

Figure 6.5: Application of the developed correlation (Eq. 6.9) to the larger burner diameter.

6.3 Literature Data

In order to validate Eq. 6.9, literature data were sought out. As discussed in the background, only one study presented boundary layer flashback data under elevated temperature and pressure conditions [95]. Daniele et al. [95] reported limited flashback data for a fuel mixture of 50% H_2 and 50% CO at elevated temperatures (up to 674 K) and pressures (up to 15 atm). A jet burner with the dimeter of 2.5 cm used in flashback experiments. Non-dimensional groups have been determined by calculating physical properties of gas mixture and implementing CHEMKIN. Because Daniele et al. [95] did not explicitly measure tip temperatures, this non-dimensional group has been estimated for the comparison. Assuming the burner head was made from stainless steel, the tip temperature was estimated using the current data and taking into account the effect of adiabatic flame temperature. Figure 6.6 presents the results and illustrates that Eq. 6.9 can capture the trends for flashback observed for all cases.

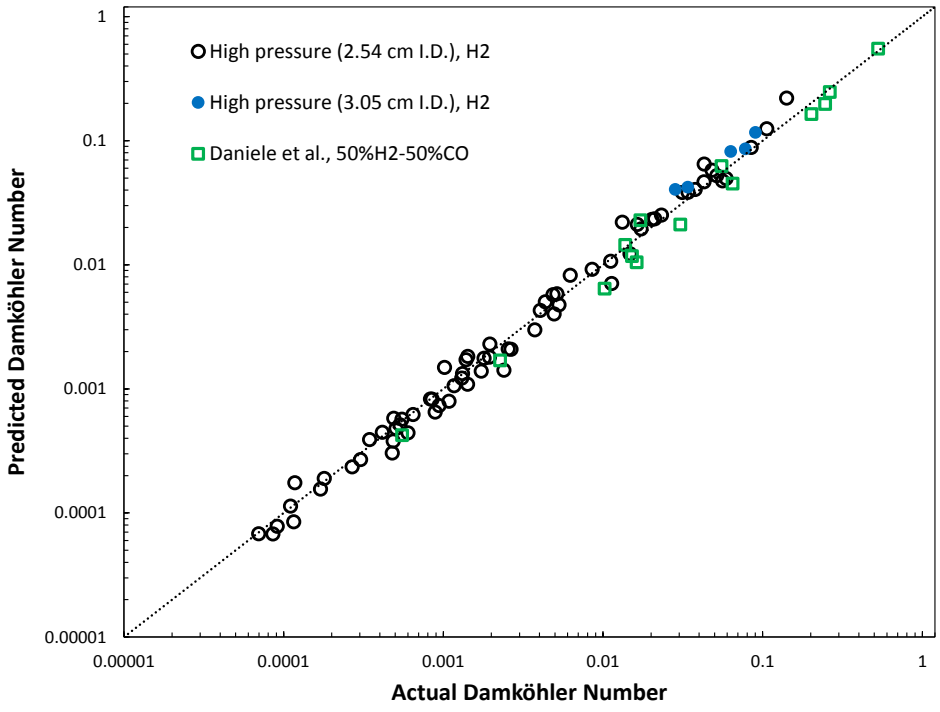

Figure 6.6: Application of the developed correlation (Eq. 6.9) to literature data.

The correlation has also been applied to an existing data set that varied pressure by reducing pressure. For this case, the results are not well described by Eq. 6.9. Reasons are several fold. First, the data of Fine were obtained at pressures which were sub atmospheric [70]. While pressure was varied, the data of Fine are reported for Reynolds number in the range of transitional flow, i.e., $1800 \leq Re \leq 3000$, which is approximately thirty times smaller than the data used to develop the current correlation. As a result, the combustion regime associated with Fines data is the wrinkled flamelets zone. Besides, the experiment conducted by Fine mainly focused on rich conditions. For these reasons, Eq. 6.9 does not accurately predict Fine's data.

6.3.1 C-60 Combustor

The correlation was also verified against the existing data for a combustor from a Capstone C-60 Microturbine, indicated in Figure 6.7 (studied by Page et al. [101]). The combustor was adapted to be operated at one atmosphere and to provide visual access to the reaction. To achieve this goal, the combustor was extracted from the engine and some turbo machinery parts required for operation in the engine were removed to make the annular combustor visually and physically accessible. The engine normally operates on natural gas at a pressure of approximately four atmospheres. A manifold was developed to feed air to the combustor as it would be in the engine and a fuel blending system was utilized to vary the fuel content and flow rate fed to the combustor.

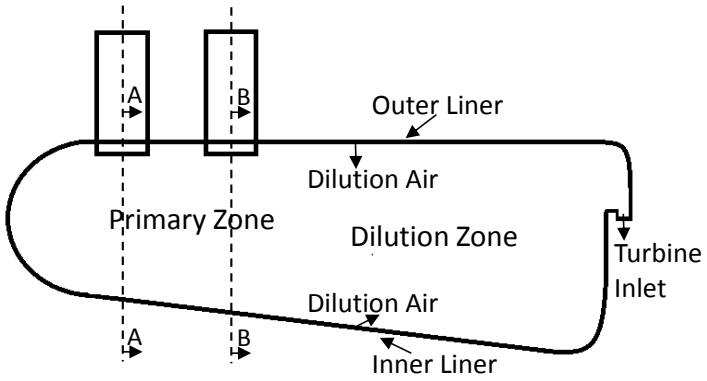

Figure 6.7: Schematic of capstone C-60 microturbine combustor.

The fuel/air mixture enters the combustor through the six injectors located tangentially at two different planes along the combustor axis according to Figure 6.8. The inner diameter of the burner head for all injectors is 2.54 cm with Reynolds number varied between $1 \times 10^4 < Re_D < 3 \times 10^4$. Air inlets ports were adapted to simulate the actual flow field and primary zone structure found in the mictoturbine generator. The incoming air was heated to reach the desired preheat temperatures of 300 *K* and 672 K. Two sets of experiments were conducted with two injectors on the plane A (Figure 6.8 a), while other injectors on the plane B (Figure 6.8 b) were not fueled and preheated air constantly entered through them. Air mass fractions entering from different holes in the primary and dilution zones were modified to represent the actual values for this gas turbine engine.

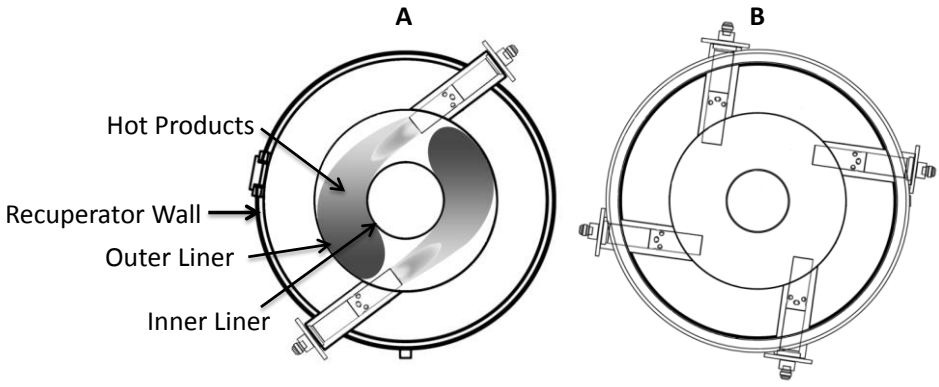

Figure 6.8: (a) Plane A with two injectors and (b) plane B with four injectors.

For the first case, natural gas was injected through one injector at constant equivalence ratio of 0.7, while the equivalence ratio of the other injector was varied for two fuel mixtures; H_2/CO and H_2/NG, to approach flashback. For the second case, the equivalence ratio of the two injectors were varied simultaneously to reach the onset of flashback. In this case, both injectors were instrumented and whichever flashed back first was considered as flashback for the test.

Fuel/air mixtures were prepared by four Alicat® mass flow controllers, enabling the operator to independently adjust the equivalence ratio of the two injectors. Control of the fuel/air mixing was done

with the existing C-60 injector basically designed for natural gas, as it is illustrated in Figure 6.9. The air mass flow rate and preheat temperature were independently controlled by PID controllers.

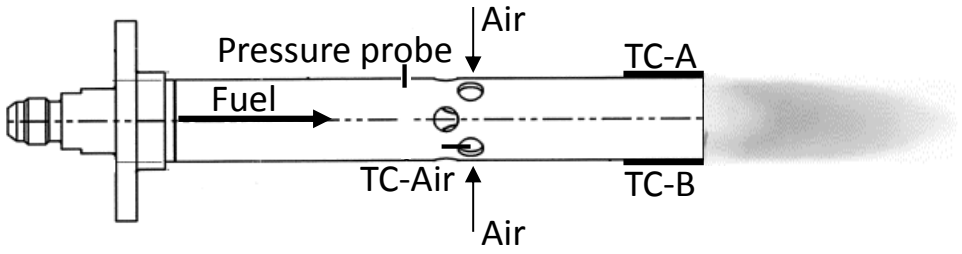

Figure 6.9: Factory built injector used in the combustor.

Two thermocouples (TC-A and B) were placed at the burner head to continuously report the tip temperature. Two measured tip temperature at opposite sides were different due to the location of the burner rim relative to the primary zone. Indeed, the side of the burner which is closer to the primary zone is exposed to the higher temperature, while the opposite side located close to the combustion liner experiences a lower temperature. Tip temperature is a crucial parameter in triggering flashback and can also be used to detect flashback by reporting a sudden increase in its value. The TC-Air is placed in injector air hole (Figure 6.9) to report the temperature of the mixture right before the injection and was also used as a flashback indicator.

Furthermore, a pressure probe was used to measure the pressure at indicated location inside the premixing tube, Figure 6.9. Flame propagation into the burner head results in a pressure rise, used as the second method along with tip temperature measurements to detect flashback. Additionally, since this experiment is conducted at atmospheric pressure, the audible sound with a clear pitch can be used as an indicator of flashback for the operator. The experiment was conducted at two preheat temperatures of 300 *K* and 672 *K* with various fuel compositions, i.e., H_2/CO with variation of CO from 0 to 70% H_2/NG with variation of NG from 0 to 60% based on the volume concentration.

Figure 6.10 presents the application of the developed correlation to the atmospheric annular combustor data presented above. The “high pressure” data include the current results for pure hydrogen used with three burners (inner diameter of 2.54 cm) constructed from stainless steel, copper, and ceramic with preheat temperatures from 300 to 500 *K* and pressures from 3 to 8 *atm*. Furthermore, the high pressure data obtained for the stainless steel burner with the inner diameter of 3.05 cm at preheat temperature of 400 *K* and pressure of 3 *atm* is indicated. Also shown are the results from Daniele et al. [95], who reported the flashback propensity of H_2/CO at pressure up to 15 *atm*, and preheat temperature between 577 *K* and 674 *K*. As shown in Figure 6.10, the correlation captures the effects of various fuels, pressures, preheat temperature, and burner materials and is able to collapse the results from the atmospheric annular combustor study. It should be noted that the effect of burner diameter on flashback propensity might be significant due to the tip temperature variation when the burner is not cooled during the experiment. As a result, the presence of tip temperature term in Eq. 6.9 is crucial to take into account the heat transfer between the burner rim and flame front. The solid points above the dashed line in Figure 6.10 represent the atmospheric data with a preheat temperature of 672 *K*. The solid points below the dashed line represent the 300 *K* inlet temperature cases. As shown, the deviation from Eq. 6.9 increases for the non-preheated case. The actual velocities in that experiment were calculated based on an assumed constant airflow splits between the fuel injectors, the dilution jets and leakage paths. In reality this flow split likely changes with temperature, accounting for the deviation of the predicted and measured flashback values. The deviation is more pronounced for H_2/NG mixtures.

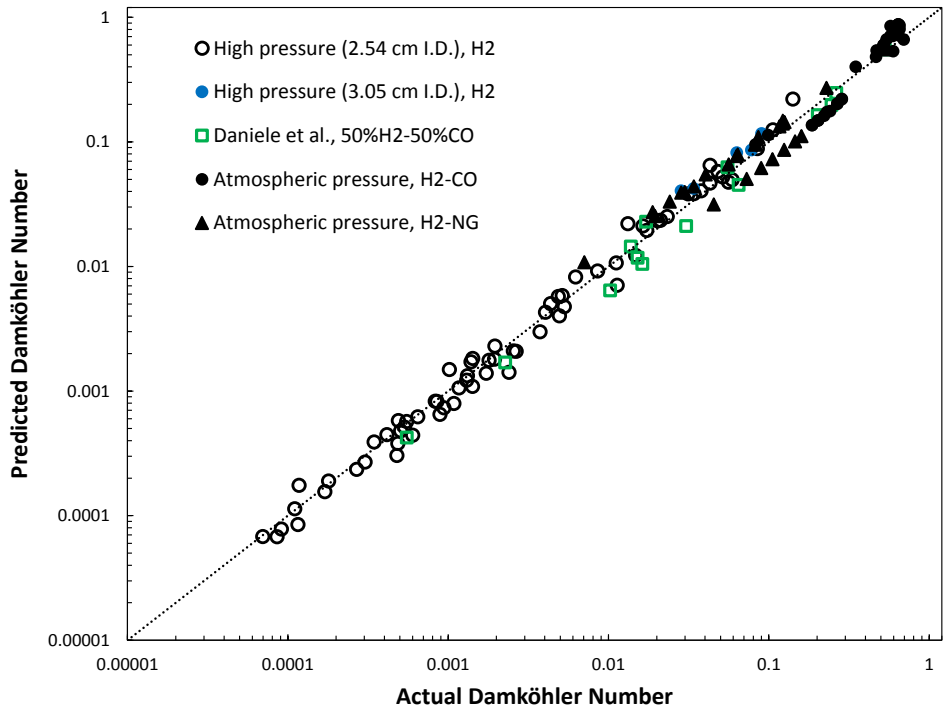

Figure 6.10: Application of the developed correlation (Eq. 6.9) to atmospheric combustor data.

6.3.2 C-60 Engine Data

Data were also gathered from a commercial Capstone C-60 60-kW natural gas fired microturbine generator (MTG) as shown in Figure 6.11 [112]. The same combustor configuration used for the atmospheric studies was also used in the full engine tests. Experiments were conducted for H_2/CO with variation of CO from 60 to 90% and H_2/NG with variation of NG from 30 to 70% at operating conditions summarized in Table 6.1. The engine operated at Reynolds number of $3 \times 10^4 < Re_D < 6 \times 10^4$ in this experiment. The engine control system automatically varies the fuel flow rate in order to maintain combustion temperatures and control engine speed, therefore equivalence ratio could not be varied during these tests to induce flashback. To approach flashback, the concentration of hydrogen in the fuel was increased until flashback occurred. More details regarding the engine test bed can be found elsewhere [206,207].

For the engine tests, the same instrumented injectors shown in Figure 6.9 were used in the engine. Data from the thermocouples were used to detect flashback and to monitor injector tip temperature. A specially developed fuel mixing system was used to blend mixtures of natural gas and hydrogen as well as hydrogen and carbon monoxide. Additional details on the mixing system can be found elsewhere [206,207].

Figure 6.11: C-60 MTG.

Table 6.1: Test conditions for C-60 microturbine generator.

Power (kW)	Equivalence ratio	Pressure (atm)	Preheat temperature (K)	Injector velocity (m/s)
20-60	0.3-1	2.4-4.3	800-850	55-65

Like the results for the 1 *atm* annular combustor, the results from the engine test are difficult to analyze since many parameters must vary together according the engine "cycle deck"[207]. Hence it is impossible to simply fix inlet temperature and pressure and maintain the injector bulk velocity due to the parameters imparted by the engine control system. However, since all of these parameters were monitored as tests were conducted by slowly adding hydrogen to either natural gas or carbon monoxide until flashback was

noted, it is possible to apply the correlation to the data obtained. Noteworthy for the engine results is that the injector tip temperature was monitored as a means to detect flashback. In the engine tests, no optical access to the combustor was available, hence the injector temperatures were the means of detecting flashback. For some cases, emissions measurements were also being obtained and when flashback was indicated by the injector temperatures, NOx levels were also observed to spike.

Results for the engine data are shown in Figure 6.12. As shown, the agreement is quite good. The data shown represent different engine loads from 20 to 60 *kW* conditions for various amounts of hydrogen added to either natural gas or carbon monoxide. The inlet pressures and temperatures corresponding to the set engine load conditions are used along with the measured injector tip temperature at flashback as inputs to Eq. 6.9. The injector bulk velocity is determined from the air flow corresponding to the engine load condition. As shown in Figure 6.12, Eq. 6.9 is able to capture the impact of various effects on flashback propensity.

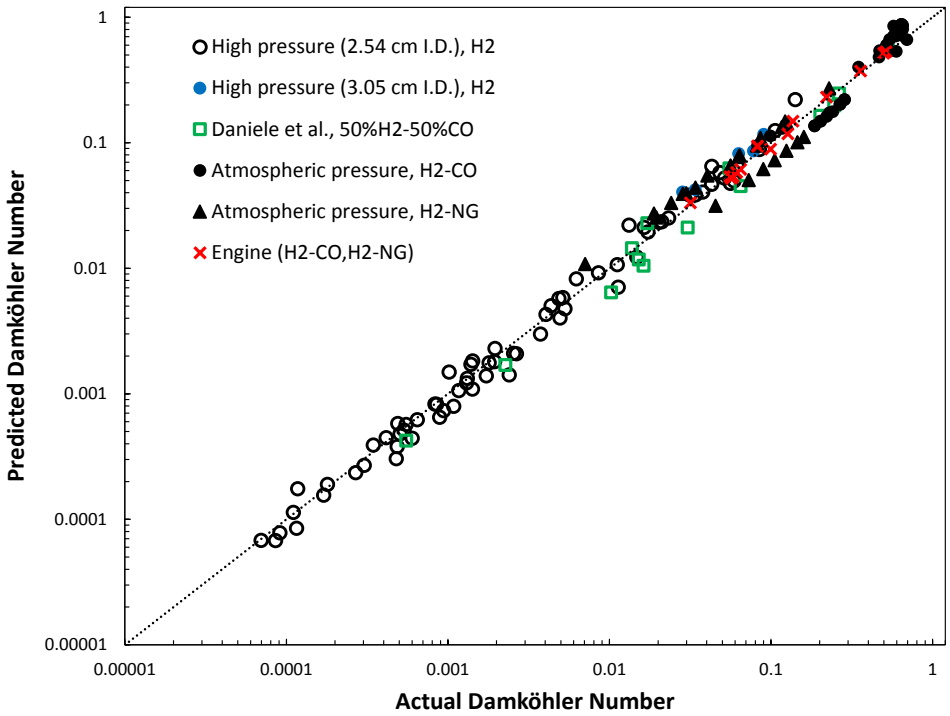

Figure 6.12: Application of the developed correlation (Eq. 6.9) to engine data (previous data shown for reference).

6.4 Test Rig II

Figure 6.13 shows the application of Eq. 6.9 to predict the flashback propensity [208]. The predicted Damköhler number represents the bulk flow velocity at which flashback occurs. The dashed line in Figure 6.13 shows the ideal case (i.e., 100% agreement). Previous flashback data at high pressure [95,110,112] are shown for reference. The red open circles in Figure 6.13 predict the engine injector flashback data. The good agreement illustrates that the flashback model is independent of the experimental setup and can be directly applied to the actual injector of a gas turbine combustor.

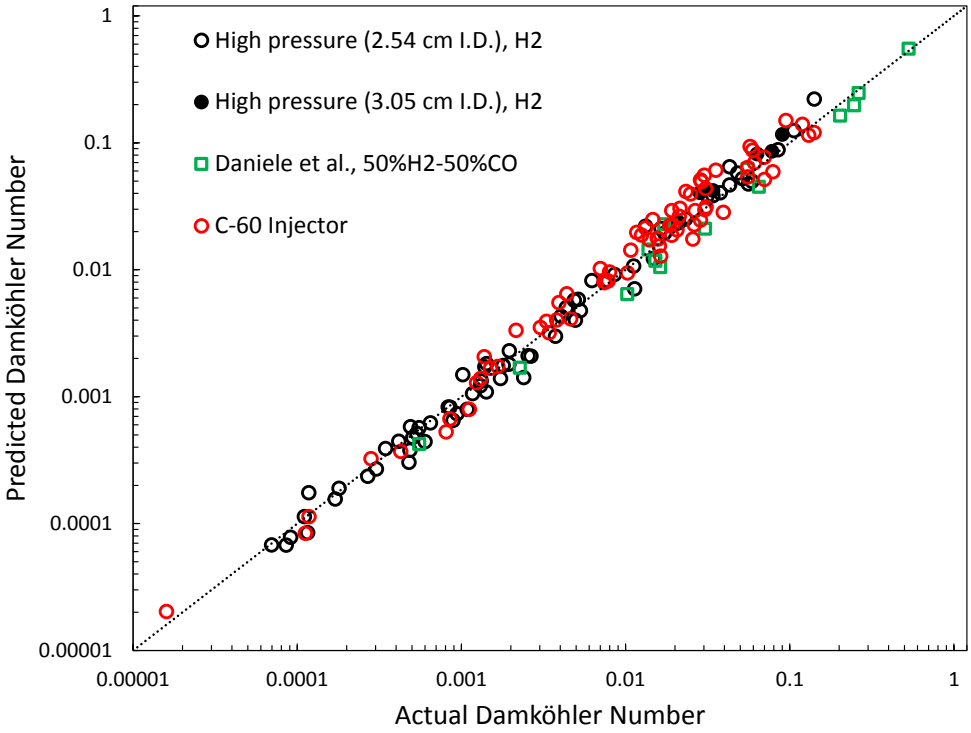

Figure 6.13: Application of Eq. 6.9 to the engine injector flashback data.

6.5 Uncertainty

Figure 6.14 indicates the percent uncertainty based on difference between the predicted velocity (Eq. 6.9) and actual velocity at flashback divided by the actual velocity. As shown, the percent uncertainty is a function of bulk velocity at which flashback occurs. The range of velocities covered in all of the

experimental data used varies from 20 to 65 m/s. The objective of the current research was to study flashback at gas turbines premixer conditions (i.e., elevated pressures and temperatures), consequently higher Reynolds numbers. As a result, it is expected that the accuracy of the correlation decreases for lower Reynolds numbers as clear from Figure 6.14. The main reason is that the turbulent combustion regime is different at low Reynolds numbers, influencing on the flame-turbulence interaction.

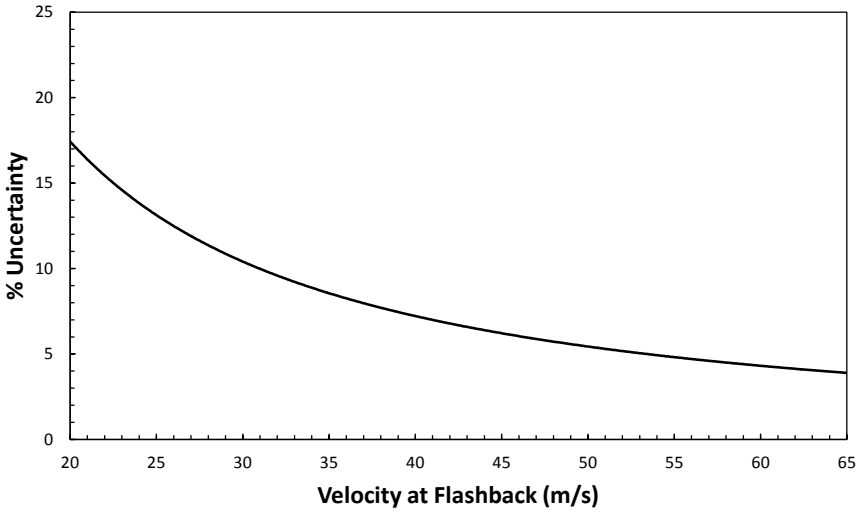

Figure 6.14: Percent uncertainty of the correlation as a function of bulk velocity at flashback.

6.6 Application of Correlation

The effects of various parameters on flashback propensity can be estimated by implementing the developed correlation. For instance, the variation of critical velocity gradient as a function of pressure has been depicted in Figure 6.15. Each line represents a constant equivalence ratio at 500 K preheat temperature. Critical velocity gradient varies with pressure to the power of 1.09 for equivalence ratio of 0.4. As the equivalence ratio increases to 0.6, the power approaches to the value of 1.15. Indeed, an increase of equivalence ratio increases the pressure exponent. The penetration distance and quenching distance have the same order of magnitude and both are functions of pressures (see Eq. 2.11). The pressure exponent magnitude of quenching distance increases as the equivalence ratio varies from fuel-lean towards stoichiometric while the pressure exponent value of laminar flame speed decreases [75,209–

211]. These two effects explain why the pressure exponent of the critical velocity gradient increases with equivalence ratio in Figure 6.15. Fine reported that the value of pressure exponent for the equivalence ratio between 0.8 and 2.25 varies in the range of 1.22 to 1.44 [76], whereas the present work suggests a slightly lower value of 1.1-1.15. Fine also reasoned that that an increase of ambient pressure at this range of equivalence ratio results in higher laminar flame speed. For the present range of equivalence ratios it has been demonstrated that the laminar flame speed actually decreases exponentially as a function of pressure [209]. Hence, in addition to being in the transitional Re regime, the results of Fine may not be relevant to the current study (focused on lean conditions) due to considerable differences at rich conditions. Nonetheless, the pressure dependency exponent is similar.

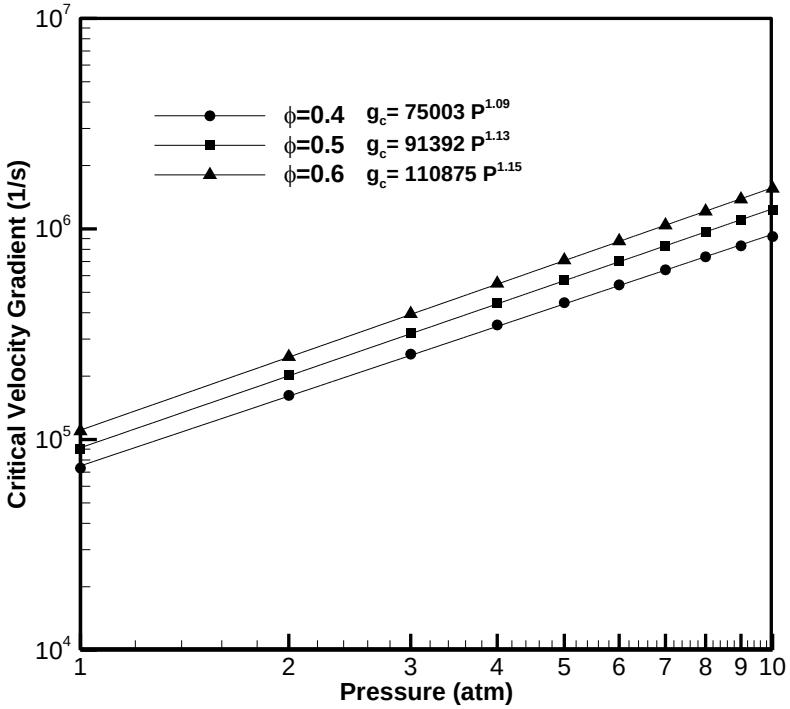

Figure 6.15: Critical velocity gradient as a function of pressure.

The flashback velocity variation with pressure is shown in Figure 6.16. For a given equivalence ratio, an increase of pressure leads to increased flashback propensity. In a similar way, the variation of flashback velocity increases as the pressure rises.

With the developed correlation it is possible to isolate the behavior of a given parameter whereas in the experiment it is quite challenging to accomplish this. Isolating the impact of a given parameter is quite difficult at high pressure because of challenges associated with keeping equivalence ratio constant at different pressures. In the two examples presented, the flashback behavior is consistent with intuition and expected behavior. As a result, the trends derived from the correlation appear promising.

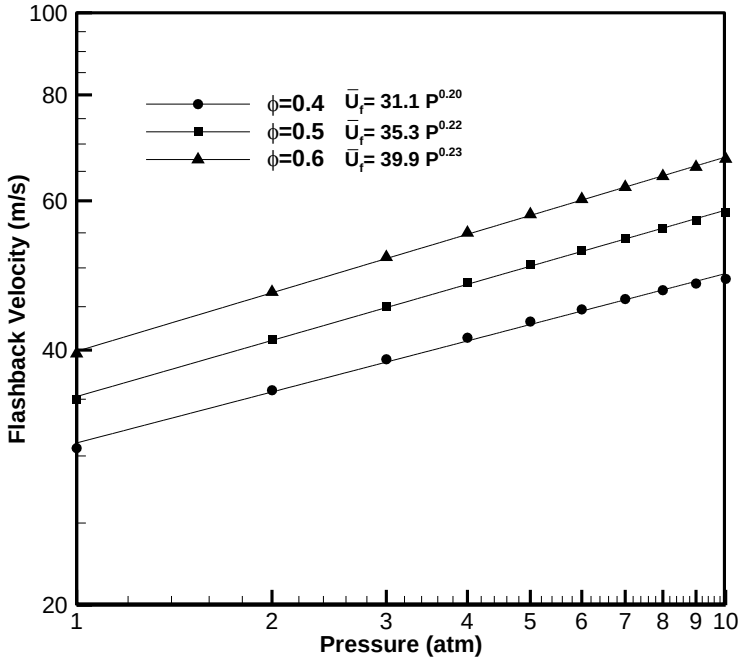

Figure 6.16: Flashback velocity as a function of pressure.

The critical velocity gradient has been predicted as a function of tip temperature for hydrogen using the further validated correlation at equivalence ratio of 0.5 and preheat temperature of 300 K, Figure 6.17. An increase of tip temperature leads to higher flashback propensity by reducing the quenching distance. The higher pressure enhances the effect of tip temperature, based on Figure 6.17, and this observation is similar to the experimental data depicted in Figure 5.15. Indeed, the slope of trend lines in Figure 5.15 increases with an increase of pressure for a constant preheat temperature. Hence, the correlation is able to predict the physical bases underlying the thermal coupling effect. The results above as well as those

from previous studies have noted the importance of the burner tip temperature as a means of instigating flashback.

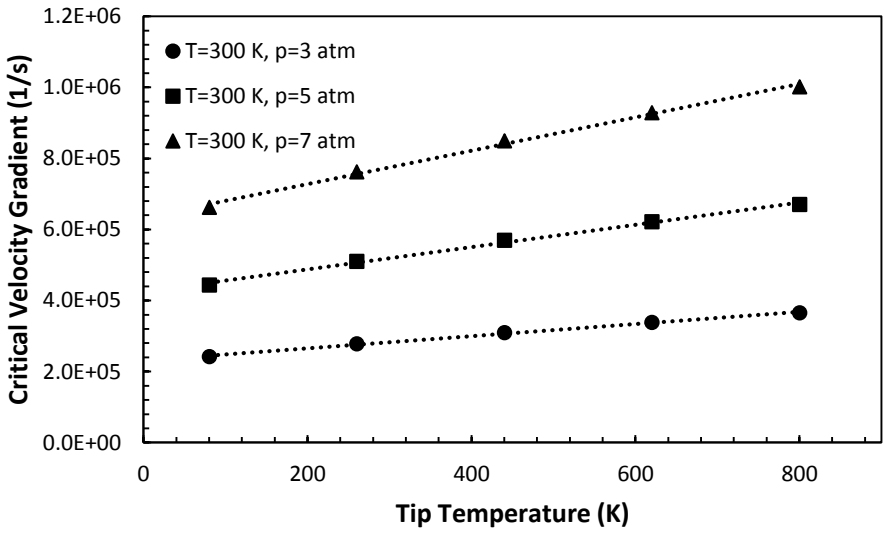

Figure 6.17: Critical velocity gradient variation as a function of tip temperature at different pressures.

Eq. 6.9 was also used to estimate the flashback limit of C-60 injector at preheat temperature of 850 K (i.e., the actual engine preheat temperature) and bulk velocity of 50 m/s. Figure 6.18 indicates the equivalence ratio at which flashback occurs as a function of pressure. The equivalence ratio is 0.26 at pressure of 2 atm, according to Eq. 1. Therefore, for the pressure range of 2-6 atm, the critical equivalence ratio is always less than 0.26, which indicates much higher flashback tendency compared to natural gas. Understanding this limit allows designs to be developed to keep the equivalence ratio below this limit in the boundary layer in order to avoid boundary flashback.

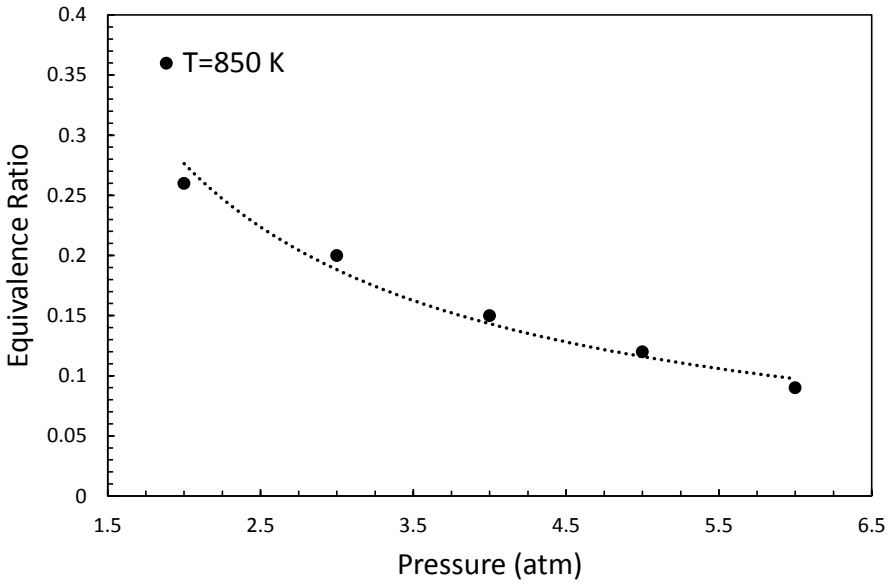

Figure 6.18: Variation of equivalence ratio at flashback with pressure at actual engine preheat temperature.

Different definitions of effective Lewis number exist in the literature including heat release, volume, and diffusion based approaches [134,135,212,213]. The effective Lewis number of hydrogen-hydrocarbon/air mixtures in the current analysis is defined based on the volumetric weighted (x_i) approach for bi-component fuels in Eq. 6.11. The volume-based effective Lewis number (Le_V) has been found to provide more accurate results compared to other approaches for lean H_2-HC/air flames [136].

$$Le_V = x_1 Le_1 + x_2 Le_2 = \alpha \left(\frac{x_1}{D_1} + \frac{x_2}{D_2} \right) \qquad \text{Eq. 6.11}$$

Le_i in Eq. 6.11 is calculated based on the diffusion of a single component fuel into the mixture [212]. Figure 6.19 indicates the variation of critical velocity gradient of hydrogen-methane mixture as a function of hydrogen volume concentration, using Eq. 6.9 at temperature of 300 *K*, equivalence ratio of 0.7, and burner diameter of 2.54 cm. With an increase of hydrogen in the fuel mixture, the critical velocity gradient increases for a given pressure. The 3 atm pressure shows a larger variation in flashback propensity with an increase of hydrogen. The Lewis number in Figure 6.19 varies from 0.4 to 0.97 for hydrogen and methane, respectively.

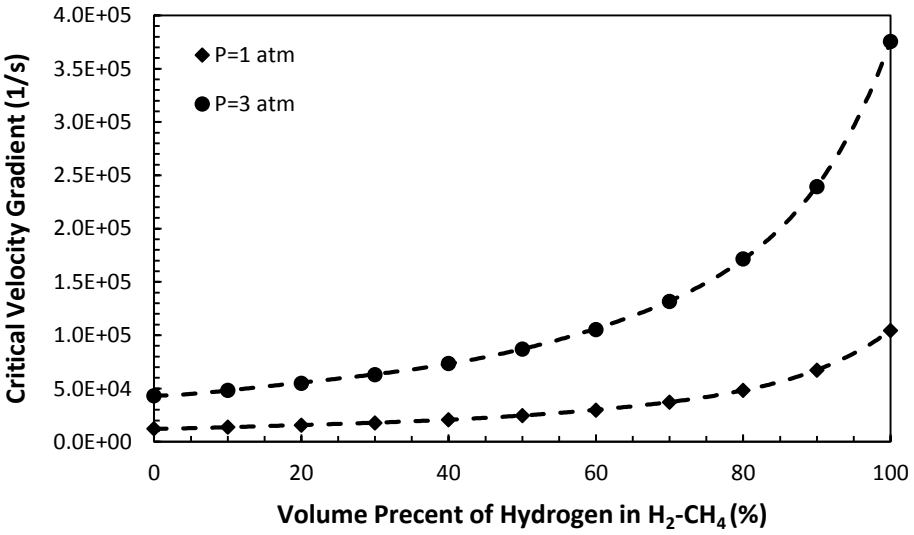

Figure 6.19: Variation of critical velocity gradient as a function of hydrogen in the hydrogen-methane mixture.

The comparison of flashback data with those predicted by Eq. 6.9 for hydrogen-carbon monoxide mixtures illustrates that the effect of hydrogen is dominant in the fuel mixture and the diffusion based Lewis number, Eq. 6.12 [134,136,213], is a better representative of the syngas flame stability [136].

$$Le_D = \frac{\alpha}{x_1 D_1 + x_2 D_2} \qquad \text{Eq. 6.12}$$

In which α and D are thermal and molecular diffusivity of a single component fuel. Figure 6.20 indicates the variation of critical velocity gradient of hydrogen-carbon monoxide mixture as a function of hydrogen concentration at preheat temperature of 400 *K*, equivalence ratio of 0.6, and burner diameter of 2.54 *cm*. The rate of flashback propensity variation for H_2-CO mixture is small with an increase of hydrogen in the mixture, while the addition of hydrogen to methane increases the flashback exponentially, shown in Figure 6.19. As pointed out, this effect is a result of difference in chemical properties of fuel compositions and has been observed for laminar boundary layer flashback [57] and laminar burning velocity [161,162,214] in the literature.

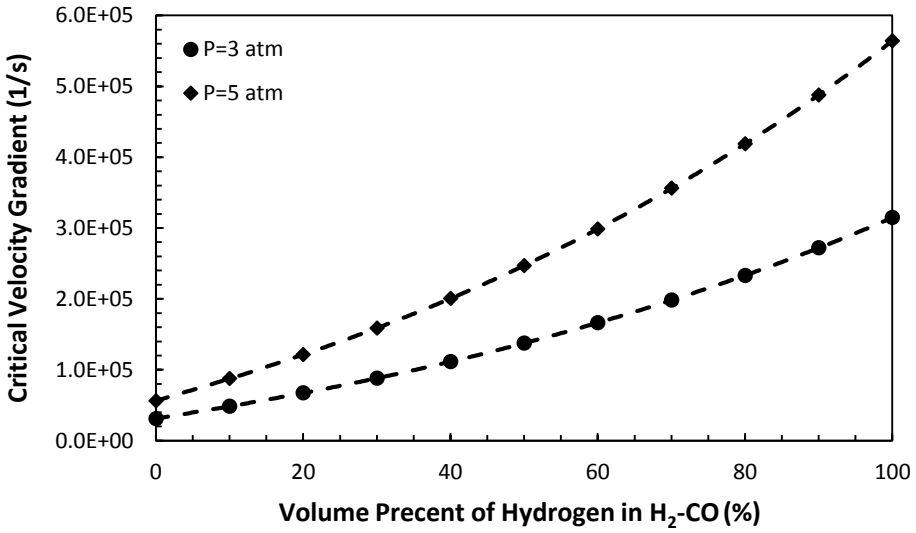

Figure 6.20: Variation of critical velocity gradient as a function of hydrogen in the hydrogen/carbon monoxide mixture.

Chapter 7 -Summary and Conclusions

7.1 Summary

The boundary layer flashback of turbulent hydrogen-air jet flames was studied at gas turbine premixer conditions, pressure up to 8 atm and temperature up to 600 K. The range of Reynolds number studied in this experiment was $5 \times 10^4 < Re_D < 3 \times 10^5$. The fuel and air were mixed through a venturi, far upstream of the burner exit to ensure a good mixing performance. This was verified using numerical simulation. In addition, the premixing tube length was designed long enough to achieve a fully developed flow at the exit, which was confirmed by laser Doppler velocimetry as well as numerical simulation.

Data for three burner materials including stainless steel, copper, and ceramic were gathered. The burner diameter was also varied to examine its impact on flashback propensity (I.D. 2.54 vs 3.05 cm). Intensified high speed OH* imaging was implemented to observe the flame dynamics at the onset of flashback. The effect of preheat temperature and pressure on flashback propensity were fully discussed. To validate the reliability of the results, similar experiments were also carried out at the same operating conditions for a commercially available injector from a micro turbine combustor.

The current work has extended this analysis and has resulted in a proposed correlation based on Buckingham Pi theorem. The tool accounts for the thermal coupling between the flame and burner rim and was derived using detailed studies carried out in a test rig at elevated temperature and pressure. The resulting correlation was applied to current data (tube burner and factory built injector) and found to provide reasonable ability to predict flashback tendencies for the parameters studied.

For a commercial 60 kW micro turbine generator (MTG), two sets of data were evaluated for various amounts of hydrogen added to either natural gas or carbon monoxide. One set was from the combustor, removed from the engine, which was configured to operate like it does in the engine but at atmospheric pressure and various preheat temperatures. The second set of data was from a combustor operated as it

normally would in the commercial engine. The previously developed model was able to capture the measured flashback tendencies in both configurations.

7.2 Conclusions

- **Flashback propensity is enhanced at high pressures due to the higher turbulent burning velocity and smaller quenching distance.**

  While the ratio of turbulent burning velocity to laminar flame speed is considered a function of pressure based on consumption speed and flame angle methods, the dependency of the turbulent burning velocity magnitude on pressure is weak. As a result, the quenching distance was found to be an influential parameter for increased flashback propensity at high pressure. However, the contribution of each parameter to the overall trend (i.e., flashback as a function of pressure) is not well understood due to limited existing data at high pressures.

- **The reactant temperature plays a strong role in flashback propensity.**

  With an increase of flame temperature, the flame propagation rate increases. Furthermore, the propagation of the flame front into the tube is a function of the burner tip temperature. Since the burner temperature is directly influenced by the reactant temperature, the sidewall quenching distance significantly decreases at high preheat temperatures.

- **Tip temperature at the onset of flashback was found to be a crucial factor for incorporating the thermal coupling between the flame and burner rim.**

  The dependency of the flashback propensity on the injector tip temperature is enhanced with an increase in pressure. Indeed, higher pressure increases the tip temperature by reducing the quenching distance for a given preheat temperature and velocity. Thermal coupling between the flame and the burner results in a complex interaction between factors impacting heat transfer (e.g., flame temperature, flame proximity to the burner rim, product composition, and burner diameter). As a

result, incorporation of key heat transfer effects is required to generalize any predictive model for capturing flashback tendencies.

- **For unconfined flames, the flame does not strongly impact the velocity and pressure distributions of the incoming flow and the reactant velocity profile upstream of the flame front remains approximately undisturbed.**

  The velocity gradient at the burner wall can be used as a parameter, representing turbulent flow characteristics for unconfined flames. However, the flow-flame interaction cannot be neglected in confined flames and the critical velocity gradient is not able to capture the flow behavior due to the presence of back flow region upstream of the propagating flame.

- **The model developed using the high-pressure test rig is able to predict flashback tendencies of premixed jet flames and can be used to evaluate the effect of various parameters involved.**

  The current study has confirmed the utility of the developed correlation for various test conditions, test setups, and actual engines and can thus serve as an effective design tool for identifying when flashback is likely to occur for a given geometry and condition.

- **The addition of a small amount of carbon monoxide or methane to hydrogen decreases the flashback propensity to a different extent.**

  For a given hydrogen percent (by volume) in the fuel mixture, hydrogen-carbon monoxide mixture is more prone to flashback compared to hydrogen-methane mixture.

7.3 Recommendations

It is apparent that more studies are required at gas turbine premixer conditions to investigate the effect of pressure and high Reynolds numbers on flashback propensity. The effect of pressure can be isolated by controlling the burner rim temperature under conditions of interest. Such effects have not been studied

at elevated pressure. In addition, laser diagnostic techniques such PIV, PLIF, and flame spectroscopy can be implemented to provide a better understanding of boundary layer flashback at high pressures.

The effect of turbulence intensity on flashback propensity, especially at elevated pressure, has not yet been studied in the literature. The strategy to alter the turbulence of the air/fuel mixture has proven difficult in narrow ducts as the fully developed flow needs to be attained, but with varying turbulence. It is noted that no numerical simulation has been conducted for the transition of the turbulent stabilized flame at burner rim to the injector as flashback occurs. Indeed, the numerical simulation addressing flame-wall interaction using detailed chemical kinetics for unconfined configurations is still required. These open questions warrant further work, but progress has been made in terms of design tool development as well as phenomenological understanding of the boundary layer flashback mechanism.

Chapter 8 - References

[1] Richards G., McMillian M., Gemmen R., Rogers W., Cully S. Issues for low-emission, fuel-flexible power systems. Prog Energy Combust Sci 2001;27:141–69. doi:10.1016/S0360-1285(00)00019-8.

[2] Lefebvre A, Ballal D. Gas turbine combustion 2010.

[3] Lieuwen T, McDonell V, Petersen E, Santavicca D. Fuel flexibility influences on premixed combustor blowout, flashback, autoignition, and stability. J Eng Gas Turbines Power 2008;130:011506. doi:10.1115/1.2771243.

[4] Bickerstaff K, Walker G. Public understandings of air pollution: the 'localisation' of environmental risk. Glob Environ Chang 2001;11:133–45. doi:10.1016/S0959-3780(00)00063-7.

[5] Bickerstaff K. Risk perception research: socio-cultural perspectives on the public experience of air pollution. Environ Int 2004;30:827–40. doi:10.1016/j.envint.2003.12.001.

[6] Lieuwen T, McDonell V, Santavicca D, Sattelmayer T. Burner development and operability issues associated with steady flowing syngas fired combustors. Combust Sci Technol 2008;180:1169–92. doi:10.1080/00102200801963375.

[7] Lieuwen T., Vigor Y. Combustion instabilities in gas turbine engines: Operational experience, fundamental mechanisms, and modeling. Prog Astronaut Aeronaut 2005. doi:10.2514/4.866807.

[8] Howarth RW, Ingraffea A, Engelder T. Natural gas: Should fracking stop? Nature 2011;477:271–5. doi:10.1038/477271a.

[9] Wang Q, Chen X, Jha AN, Rogers H. Natural gas from shale formation – The evolution, evidences and challenges of shale gas revolution in United States. Renew Sustain Energy Rev 2014;30:1–28. doi:10.1016/j.rser.2013.08.065.

[10] Demirbas A. Progress and recent trends in biofuels. Prog Energy Combust Sci 2007;33:1–18. doi:10.1016/j.pecs.2006.06.001.

[11] Rostrup-Nielsen JR, Sehested J, Nørskov JK. Hydrogen and synthesis gas by steam- and C02 reforming. Adv Catal 2002;47:65–139. doi:10.1016/S0360-0564(02)47006-X.

[12] Xu J, Froment GF. Methane steam reforming, methanation and water-gas shift: I. Intrinsic kinetics. AIChE J 1989;35:88–96. doi:10.1002/aic.690350109.

[13] Bolland O, Undrum H. A novel methodology for comparing CO2 capture options for natural gas-fired combined cycle plants. Adv Environ Res 2003;7:901–11. doi:10.1016/S1093-0191(02)00085-0.

[14] Descamps C, Bouallou C, Kanniche M. Efficiency of an integrated gasification combined cycle (IGCC) power plant including CO2 removal. Energy 2008;33:874–81. doi:10.1016/j.energy.2007.07.013.

[15] Minchener AJ. Coal gasification for advanced power generation. Fuel 2005;84:2222–35. doi:10.1016/j.fuel.2005.08.035.

[16] Haszeldine RS. Carbon Capture and Storage: How Green Can Black Be? Science (80-) 2009;325:1647–52. doi:10.1126/science.1172246.

[17] Herzog HJ. What Future for Carbon Capture and Sequestration? Environ Sci Technol 2001;35:148A–153A. doi:10.1021/es012307j.

[18] Turner JA. Sustainable Hydrogen Production. Science (80-) 2004;305:972–4. doi:10.1126/science.1103197.

[19] Chiesa P, Lozza G, Mazzocchi L. Using Hydrogen as Gas Turbine Fuel. ASME Turbo Expo, 2003, p. 163–71. doi:10.1115/GT2003-38205.

[20] Plee SL, Mellor AM. Review of flashback reported in prevaporizing/premixing combustors. Combust Flame 1978;32:193–203. doi:10.1016/0010-2180(78)90093-7.

[21] Thibaut D, Candel S. Numerical study of unsteady turbulent premixed combustion: application to flashback simulation. Combust Flame 1998;113:53–65. doi:10.1016/S0010-2180(97)00196-X.

[22] Driscoll JF. Turbulent premixed combustion: Flamelet structure and its effect on turbulent burning velocities. Prog Energy Combust Sci 2008;34:91–134. doi:10.1016/j.pecs.2007.04.002.

[23] Lipatnikov AN, Chomiak J. Molecular transport effects on turbulent flame propagation and structure. Prog Energy Combust Sci 2005;31:1–73. doi:10.1016/j.pecs.2004.07.001.

[24] Kido H, Nakahara M, Nakashima K, Hashimoto J. Influence of local flame displacement velocity on turbulent burning velocity. Proc Combust Inst 2002;29:1855–61. doi:10.1016/S1540-7489(02)80225-5.

[25] Borghi R. Turbulent combustion modelling. Prog Energy Combust Sci 1988;14:245–92. doi:10.1016/0360-1285(88)90015-9.

[26] Borghi R. On the structure and morphology of turbulent premixed flames. Recent Adv. Aerosp. Sci., Springer US; 1985, p. 117–38. doi:10.1007/978-1-4684-4298-4_7.

[27] Kwon O., Faeth G. Flame/stretch interactions of premixed hydrogen-fueled flames: measurements and predictions. Combust Flame 2001;124:590–610. doi:10.1016/S0010-2180(00)00229-7.

[28] Kobayashi H, Kawabata Y, Maruta K. Experimental study on general correlation of turbulent burning velocity at high pressure. Symp Combust 1998;27:941–8. doi:10.1016/S0082-0784(98)80492-X.

[29] Kobayashi H, Tamura T, Maruta K, Niioka T, Williams FA. Burning velocity of turbulent premixed

flames in a high-pressure environment. Symp Combust 1996;26:389–96. doi:10.1016/S0082-0784(96)80240-2.

[30] Koroll GW, Kumar RK, Bowles EM. Burning velocities of hydrogen-air mixtures. Combust Flame 1993;94:330–40. doi:10.1016/0010-2180(93)90078-H.

[31] Bradley D, Lawes M, Liu K, Mansour MS. Measurements and correlations of turbulent burning velocities over wide ranges of fuels and elevated pressures. Proc Combust Inst 2013;34:1519–26. doi:10.1016/j.proci.2012.06.060.

[32] Benim A, Syed K. Flashback mechanisms in lean premixed gas turbine combustion. Academic Press; 2014.

[33] Keller J 0., Vaneveld L, Korschelt D, Hubbard GL, Ghoniem AF, Daily JW, et al. Mechanism of Instabilities in Turbulent Combustion Leading to Flashback. AIAA J 1982;20:254–62. doi:10.2514/3.51073.

[34] Billant P, Chomaz J-M, Huerre P. Experimental study of vortex breakdown in swirling jets. J Fluid Mech 1998;376:S0022112098002870. doi:10.1017/S0022112098002870.

[35] Leibovich S. The structure of vortex breakdown. Annu Rev Fluid Mech 1978;10:221–46. doi:10.1146/annurev.fl.10.010178.001253.

[36] Konle M, Kiesewetter F, Sattelmayer T. Simultaneous high repetition rate PIV--LIF-measurements of CIVB driven flashback. Exp Fluids 2007;44:529–38. doi:10.1007/s00348-007-0411-2.

[37] Asato K, Wada H, Hiruma T, Takeuchi Y. Characteristics of flame propagation in a vortex core: Validity of a model for flame propagation. Combust Flame 1997;110:418–28. doi:10.1016/S0010-2180(97)00082-5.

[38] Duwig C, Fuchs L. Large eddy simulation of vortex breakdown/flame interaction. Phys Fluids 2007;19:075103. doi:10.1063/1.2749812.

[39] Konle M, Sattelmayer T. Interaction of heat release and vortex breakdown during flame flashback driven by combustion induced vortex breakdown. Exp Fluids 2009;47:627–35. doi:10.1007/s00348-009-0679-5.

[40] Ishizuka S. Flame propagation along a vortex axis. Prog Energy Combust Sci 2002;28:477–542. doi:10.1016/S0360-1285(02)00019-9.

[41] Konle M, Sattelmayer T. Time scale model for the prediction of the onset of flame flashback driven by combustion induced vortex breakdown. J Eng Gas Turbines Power 2010;132:041503. doi:10.1115/1.4000123.

[42] Dam B, Corona G, Hayder M, Choudhuri A. Effects of syngas composition on combustion induced vortex breakdown (CIVB) flashback in a swirl stabilized combustor. Fuel 2011;90:3274–84. doi:10.1016/j.fuel.2011.06.024.

[43] Sayad P, Schönborn A, Li M, Klingmann J. Visualization of different flashback mechanisms for H2/CH4 mixtures in a variable-swirl burner. J Eng Gas Turbines Power 2014;137:031507. doi:10.1115/1.4028436.

[44] Friedman R, Johnston WC. The wall-quenching of laminar propane flames as a function of pressure, temperature, and air-fuel ratio. J Appl Phys 1950;21:791. doi:10.1063/1.1699760.

[45] Bellenoue M, Kageyama T, Labuda SA, Sotton J. Direct measurement of laminar flame quenching distance in a closed vessel. Exp Therm Fluid Sci 2003;27:323–31. doi:10.1016/S0894-1777(02)00304-7.

[46] Boust B, Sotton J, Labuda SA, Bellenoue M. A thermal formulation for single-wall quenching of transient laminar flames. Combust Flame 2007;149:286–94. doi:10.1016/j.combustflame.2006.12.019.

[47] Lewis B, von Elbe G. Stability and structure of burner flames. J Chem Phys 1943;11:75. doi:10.1063/1.1723808.

[48] von Elbe G, Mentser M. Further Studies of the Structure and Stability of Burner Flames. J Chem Phys 1945;13:89. doi:10.1063/1.1724004.

[49] Garside JE, Forsyth JS, Townend DTA. The stability of burner flames. J Inst Fuel 1945;18:175–85.

[50] Markstein GH, Polanyi ML. Flame Propagation: Critical Review of Existing Theories. Cornell Aeronaut Lab Inc, Buffalo, NY, Rep No 61, 1947.

[51] Harris ME, Grumer J, von Elbe G, Lewis B. Burning velocities, quenching, and stability data on nonturbulent flames of methane and propane with oxygen and nitrogen: Application of theory of ignition, quenching, and stabilizationto flames of propane and air. Symp Combust Flame, Explos Phenom 1948;3:80–9. doi:10.1016/S1062-2896(49)80010-9.

[52] Putnam AA, Jensen RA. Application of dimensionless numbers to flash-back and other combustion phenomena. Symp Combust Flame, Explos Phenom 1948;3:89–98. doi:10.1016/S1062-2896(49)80011-0.

[53] Wohl K, Kapp NM, Gazley C. The stability of open flames. Symp Combust Flame, Explos Phenom 1948;3:3–21. doi:10.1016/S1062-2896(49)80005-5.

[54] Grumer J. Predicting burner performance with interchanged fuel gases. Ind Eng Chem 1949;41:2756–61. doi:10.1021/ie50480a023.

[55] Reiter SH, Wright CC. Stability of burner flames with propane-hydrogen mixtures. Ind Eng Chem 1950;42:691–4. doi:10.1021/ie50484a035.

[56] Edse R. Studies on burner flames of hydrogen-oxygen mixtures at high pressures. Wright Air Dev Cent Tech Rep 52-59, 1952.

[57] Grumer J, Harris ME. Flame-stability limits of methane, hydrogen, and carbon monoxide mixtures. Ind Eng Chem 1952;44:1547–53. doi:10.1021/ie50511a023.

[58] Grumer J, Harris ME, Schultz H. Predicting interchangeability of fuel gases. Interchangeability of oil gases or propane-air fuels with natural gases. Ind Eng Chem 1952;44:1554–9. doi:10.1021/ie50511a024.

[59] Grumer J, Harris ME, Schultz H. Flame stabilization on burners with short ports or noncircular ports. Symp Combust 1953;4:695–701. doi:10.1016/S0082-0784(53)80092-5.

[60] Phillips VD, Brotherton TD, Anderson RC. Physical characteristics and stability of some low-temperature flames: The hydrogen-bromine system. Symp Combust 1953;4:701–7. doi:10.1016/S0082-0784(53)80093-7.

[61] Wohl K. Quenching, flash-back, blow-off-theory and experiment. Symp Combust 1953;4:68–89. doi:10.1016/S0082-0784(53)80011-1.

[62] Grumer J, Harris MEM. Temperature dependence of stability limits of burner flames. Ind Eng Chem 1954;46:2424–30.

[63] Dugger GLG. Flame stability of preheated propane-air mixtures. Ind Eng Chem 1955;47:109–14. doi:10.1021/ie50541a038.

[64] Grumer J, Harris M, Rowe V. Fundamental flashback, blowoff, and yellow-tip limits of fuel gas-air

mixtures. US Deptartment Inter Bur Mines 5225, 1955.

[65] Grumer J, Harris ME, Schultz H. Flame–stability limits of ethylene, propane, methane, hydrogen, and nitrogen mixtures. Ind Eng Chem 1955;47:1760–7. doi:10.1021/ie50549a024.

[66] Bollinger LE, Edse R. Effect of burner-tip temperature on flash back of turbulent hydrogen-oxygen flames. Ind Eng Chem 1956;48:802–7. doi:10.1021/ie50556a040.

[67] Fine B. Stability limits and burning velocities of laminar hydrogen-air flames at reduced pressure. NACA TN 3833, 1956.

[68] Barnett HC, Hibbard RR. Basic Considerations in the Combustion of Hydrocarbon Fuels with Air. NACA Rept 1300, 1957.

[69] Berlad AL, Potter AE. Relation of boundary velocity gradient for flash-back to burning velocity and quenching distance. Combust Flame 1957;1:127–8. doi:10.1016/0010-2180(57)90040-8.

[70] Fine B. Stability limits and burning velocities for some laminar and turbulent propane and hydrogen flames at reduced pressure. NACA TN 4031, 1957.

[71] Fine B. Further experiments on the stability of laminar and turbulent hydrogen-air flames at reduced pressures. NACA TN 3977, 1957.

[72] Kurz PF. Stability limits of flames of ternary hydrocarbon mixtures. Combust Flame 1957;1:3–13. doi:10.1016/0010-2180(57)90026-3.

[73] Kurz PF. Some factors influencing stability limits of bunsen flames. Combust Flame 1957;1:162–78. doi:10.1016/0010-2180(57)90043-3.

[74] Miller E, Setzer HJ. Burning structure and stability of n-butane-nitrogen dioxide flames in air. Symp

Combust 1957;6:164–72. doi:10.1016/S0082-0784(57)80025-3.

[75] Drell IL, Belles FE. Survey of Hydrogen Combustion Properties. NACA TN 1383, 1958.

[76] Fine B. The flashback of laminar and turbulent burner flames at reduced pressure. Combust Flame 1958;2:253–66. doi:10.1016/0010-2180(58)90046-4.

[77] Grumer J. Flashback and blow off limits of unpiloted turbulent flames. Jet Propuls 1958;28:756–759.

[78] Van Krevelen DW, Chermin HAG. Generalized flame stability diagram for the prediction of interchangeability of gases. Symp Combust 1958;7:358–68. doi:10.1016/S0082-0784(58)80066-1.

[79] Fine B. Effect of initial temperature on flash back of laminar and turbulent burner flames. Ind Eng Chem 1959;51:564–6. doi:10.1021/ie50592a044.

[80] Yamazaki K, Tsuji H. An experimental investigation on the stability of turbulent burner flames. Symp Combust 1961;8:543–53. doi:10.1016/S0082-0784(06)80545-X.

[81] Caffo E, Padovani C. Flashback in premixed air flames. Combust Flame 1963;7:331–7. doi:10.1016/0010-2180(63)90208-6.

[82] Khitrin LN, Moin PB, Smirnov DB, Shevchuk VU. Peculiarities of laminar- and turbulent-flame flashbacks. Symp Combust 1965;10:1285–91. doi:10.1016/S0082-0784(65)80263-6.

[83] France DH. Flashback of laminar monoport burner flames. J Inst Fuel 1977;50:147–52.

[84] Ball DA, Putnam AA, Radhakrishnan E, Levy A. Relation to burning velocity, quenching distance, and flash-back velocity gradient for low-and intermediate-Btu gases. Battelle Columbus Labs Rept DOE/ET/10653-3, 1978.

[85] Putnam AA, Ball DA, Levy A. Effect of fuel composition on relation of burning velocity to product of quenching distance and flashback velocity gradient. vol. 37. 1980. doi:10.1016/0010-2180(80)90085-1.

[86] Lee ST, T'ien JS. A numerical analysis of flame flashback in a premixed laminar system. Combust Flame 1982;48:273–85. doi:10.1016/0010-2180(82)90134-1.

[87] Fox JS, Bhargava A. Flame speed and flashback gradient for simulated biomass gasification products. Proc., Intersoc. Energy Convers. Eng. Conf.;(United States), vol. 2, University of Hawaii at Manoa, Honolulu, Hawaii; 1984.

[88] Lee ST, Tsai CH. Numerical investigation of steady laminar flame propagation in a circular tube. Combust Flame 1994;99:484–90. doi:10.1016/0010-2180(94)90040-X.

[89] Mallens RMM, Goey LPH De. Flash-back of laminar premixed methane/air flames on slitand tube burners. Combust Sci Technol 1998;136:41–54. doi:10.1080/00102209808924164.

[90] Kurdyumov VN, Fernández E, Liñán A. Flame flashback and propagation of premixed flames near a wall. Proc Combust Inst 2000;28:1883–9. doi:10.1016/S0082-0784(00)80592-5.

[91] Daou J, Matalon M. Flame propagation in Poiseuille flow under adiabatic conditions. Combust Flame 2001;124:337–49. doi:10.1016/S0010-2180(00)00209-1.

[92] Kurdyumov VN, Fernández-Tarrazo E. Lewis number effect on the propagation of premixed laminar flames in narrow open ducts. Combust Flame 2002;128:382–94. doi:10.1016/S0010-2180(01)00358-3.

[93] Davu D, Franco R, Choudhuri A, Lewis R. Investigation on flashback propensity of syngas premixed flames. AIAA Pap 2005;3585.

[94] Kurdyumov V, Fernández-Tarrazo E, Truffaut J-M, Quinard J, Wangher A, Searby G. Experimental and numerical study of premixed flame flashback. Proc Combust Inst 2007;31:1275–82. doi:10.1016/j.proci.2006.07.100.

[95] Daniele S, Jansohn P, Boulouchos K. Flashback propensity of syngas flames at high pressure: diagnostic and control. ASME Turbo Expo, 2010, p. 1169–75. doi:10.1115/GT2010-23456.

[96] Dam B, Love N, Choudhuri A. Flashback propensity of syngas fuels. Fuel 2011;90:618–25. doi:10.1016/j.fuel.2010.10.021.

[97] Eichler C, Sattelmayer T. Experiments on flame flashback in a quasi-2D turbulent wall boundary layer for premixed methane-hydrogen-air mixtures. J Eng Gas Turbines Power 2011;133:011503. doi:10.1115/1.4001985.

[98] Eichler C, Baumgartner G, Sattelmayer T. Experimental investigation of turbulent boundary layer flashback limits for premixed hydrogen-air flames confined in ducts. J Eng Gas Turbines Power 2012;134:011502. doi:10.1115/1.4004149.

[99] Eichler C, Sattelmayer T. Premixed flame flashback in wall boundary layers studied by long-distance micro-PIV. Exp Fluids 2012;52:347–60. doi:10.1007/s00348-011-1226-8.

[100] Gruber A, Chen JH, Valiev D, Law CK. Direct numerical simulation of premixed flame boundary layer flashback in turbulent channel flow. J Fluid Mech 2012;709:516–42. doi:10.1017/jfm.2012.345.

[101] Page D, Shaffer B, McDonell V. Establishing operating limits in a commercial lean premixed combustor operating on synthesis gas pertaining to flashback and blowout. ASME Turbo Expo, 2012, p. 647. doi:10.1115/GT2012-69355.

[102] Shaffer B, Duan Z, McDonell V. Study of fuel composition effects on flashback using a confined jet

flame burner. J Eng Gas Turbines Power 2012;135:011502. doi:10.1115/1.4007345.

[103] Duan Z, Shaffer B, McDonell V. Study of fuel composition, burner material, and tip temperature effects on flashback of enclosed jet flame. J Eng Gas Turbines Power 2013;135:121504. doi:10.1115/1.4025129.

[104] Duan Z, Shaffer B, McDonell V, Baumgartner G, Sattelmayer T. Influence of burner material, tip temperature, and geometrical flame configuration on flashback propensity of H2 -air jet flames. J Eng Gas Turbines Power 2013;136:021502. doi:10.1115/1.4025359.

[105] Lin Y-C, Daniele S, Jansohn P, Boulouchos K. Turbulent Flame Speed as an Indicator for Flashback Propensity of Hydrogen-Rich Fuel Gases. J Eng Gas Turbines Power 2013;135:111503. doi:10.1115/1.4025068.

[106] Baumgartner G, Boeck LR, Sattelmayer T. Experimental Investigation of the Transition Mechanism From Stable Flame to Flashback in a Generic Premixed Combustion System With High-Speed Micro-Particle Image Velocimetry and Micro-PLIF Combined With Chemiluminescence Imaging. J Eng Gas Turbines Power 2015;138:021501. doi:10.1115/1.4031227.

[107] Duan Z, Kalantari A, McDonell V. Parametric analysis of flashback propensity with various fuel compositions and burner materials. ASME Turbo Expo, 2015, p. V04BT04A048. doi:10.1115/GT2015-43629.

[108] Gruber A, Kerstein AR, Valiev D, Law CK, Kolla H, Chen JH. Modeling of mean flame shape during premixed flame flashback in turbulent boundary layers. Proc Combust Inst 2015;35:1485–92. doi:10.1016/j.proci.2014.06.073.

[109] Hoferichter V, Hirsch C, Sattelmayer T. Analytic prediction of unconfined boundary layer flashback limits in premixed hydrogen–air flames. Combust Theory Model 2016:1–37.

doi:10.1080/13647830.2016.1240832.

[110] Kalantari A, Sullivan-Lewis E, McDonell V. Flashback Propensity of Turbulent Hydrogen–Air Jet Flames at Gas Turbine Premixer Conditions. J Eng Gas Turbines Power 2016;138:061506. doi:10.1115/1.4031761.

[111] Hoferichter V, Hirsch C, Sattelmayer T. Prediction of confined flame flashback limits using boundary layer separation theory. J Eng Gas Turbines Power 2017;139:021505. doi:10.1115/1.4034237.

[112] Kalantari A, Sullivan-Lewis E, McDonell V. Application of a turbulent jet flame flashback propensity model to a commercial gas turbine combustor. J Eng Gas Turbines Power 2017;139:041506. doi:10.1115/1.4034649.

[113] Lewis B, von Elbe G. Combustion, Flames and Explosives of Gases. Third Edit. Academic Press; 1987.

[114] White FM, Corfield I. Viscous fluid flow. vol. 3. McGraw-Hill New York; 2006.

[115] Green KA, Agnew JT. Quenching distances of propane-air flames in a constant-volume bomb. Combust Flame 1970;15:189–91. doi:10.1016/0010-2180(70)90030-1.

[116] Kim KT, Lee DH, Kwon S. Effects of thermal and chemical surface–flame interaction on flame quenching. Combust Flame 2006;146:19–28. doi:10.1016/j.combustflame.2006.04.012.

[117] Friedman R, Johnston WC. Pressure dependence of quenching distance of normal heptane, iso-octane, benzene, and ethyl ether flames. J Chem Phys 1952;20:919. doi:10.1063/1.1700600.

[118] Potter, A E J, Berlad AI. A thermal equation for flame quenching. NACA TN 1264, 1956:287–93.

[119] Ferguson CR, Keck JC. On laminar flame quenching and its application to spark ignition engines. Combust Flame 1977;28:197–205. doi:10.1016/0010-2180(77)90025-6.

[120] Potter AE, Berlad AL. The effect of fuel type and pressure on flame quenching. Symp Combust 1957;6:27–36. doi:10.1016/S0082-0784(57)80009-5.

[121] Berlad AL, Potter AE. Prediction of the quenching effect of various surface geometries. Symp Combust 1955;5:728–35. doi:10.1016/S0082-0784(55)80100-2.

[122] Enomoto M. Head-on quenching of a premixed flame on the single wall surface. JSME Int J Ser B 2001;44:624–33. doi:10.1299/jsmeb.44.624.

[123] Popp P, Baum M. Analysis of wall heat fluxes, reaction mechanisms, and unburnt hydrocarbons during the head-on quenching of a laminar methane flame. Combust Flame 1997;108:327–48. doi:10.1016/S0010-2180(96)00144-7.

[124] Sotton J, Boust B, Labuda SA, Bellenoue M. Head-on quenching of transient laminar flame: heat flux and quenching distance measurements. Combust Sci Technol 2005;177:1305–22. doi:10.1080/00102200590950485.

[125] Dabireau F, Cuenot B, Vermorel O, Poinsot T. Interaction of flames of H2 + O2 with inert walls. Combust Flame 2003;135:123–33. doi:10.1016/S0010-2180(03)00154-8.

[126] Enomoto M. Sidewall quenching of laminar premixed flames propagating along the single wall surface. Proc Combust Inst 2002;29:781–7. doi:10.1016/S1540-7489(02)80100-6.

[127] Poinsot TJ, Haworth DC, Bruneaux G. Direct simulation and modeling of flame-wall interaction for premixed turbulent combustion. Combust Flame 1993;95:118–32. doi:10.1016/0010-2180(93)90056-9.

[128] Gruber A, Sankaran R, Hawkes ER, Chen JH. Turbulent flame–wall interaction: a direct numerical simulation study. J Fluid Mech 2010;658:5–32. doi:10.1017/S0022112010001278.

[129] Veynante D, Vervisch L. Turbulent combustion modeling. Prog Energy Combust Sci 2002;28:193–266. doi:10.1016/S0360-1285(01)00017-X.

[130] Clavin P. Dynamic behavior of premixed flame fronts in laminar and turbulent flows. Prog Energy Combust Sci 1985;11:1–59. doi:10.1016/0360-1285(85)90012-7.

[131] Haworth DC, Poinsot TJ. Numerical simulations of Lewis number effects in turbulent premixed flames. J Fluid Mech 1992;244:405. doi:10.1017/S0022112092003124.

[132] Chen JB, Im HG. Stretch effects on the burning velocity of turbulent premixed hydrogen/air flames. Proc Combust Inst 2000;28:211–8. doi:10.1016/S0082-0784(00)80213-1.

[133] Bell JB, Cheng RK, Day MS, Shepherd IG. Numerical simulation of Lewis number effects on lean premixed turbulent flames. Proc Combust Inst 2007;31:1309–17. doi:10.1016/j.proci.2006.07.216.

[134] Dinkelacker F, Manickam B, Muppala SPR. Modelling and simulation of lean premixed turbulent methane/hydrogen/air flames with an effective Lewis number approach. Combust Flame 2011;158:1742–9. doi:10.1016/j.combustflame.2010.12.003.

[135] Muppala SPR, Nakahara M, Aluri NK, Kido H, Wen JX, Papalexandris MV. Experimental and analytical investigation of the turbulent burning velocity of two-component fuel mixtures of hydrogen, methane and propane. Int J Hydrogen Energy 2009;34:9258–65. doi:10.1016/j.ijhydene.2009.09.036.

[136] Bouvet N, Halter F, Chauveau C, Yoon Y. On the effective Lewis number formulations for lean hydrogen/hydrocarbon/air mixtures. Int J Hydrogen Energy 2013;38:5949–60. doi:10.1016/j.ijhydene.2013.02.098.

[137] Natarajan J, Lieuwen T, Seitzman J. Laminar flame speeds of H2/CO mixtures: Effect of CO2 dilution,

preheat temperature, and pressure. Combust Flame 2007;151:104–19. doi:10.1016/j.combustflame.2007.05.003.

[138] Lieuwen TC. Unsteady combustor physics. Cambridge University Press; 2012.

[139] Strakey P, Sidwell T, Ontko J. Investigation of the effects of hydrogen addition on lean extinction in a swirl stabilized combustor. Proc Combust Inst 2007;31:3173–80. doi:10.1016/j.proci.2006.07.077.

[140] Kröner M, Fritz J, Sattelmayer T. Flashback Limits for Combustion Induced Vortex Breakdown in a Swirl Burner. ASME Turbo Expo, 2002, p. 413–22. doi:10.1115/GT2002-30075.

[141] Law CK. Combustion physics. Cambridge university press; 2010.

[142] Simon DM, Belles FE, Spakowski AE. Investigation and interpretation of the flammability region for some lean hydrocarbon-air mixtures. Symp Combust 1953;4:127–38. doi:10.1016/S0082-0784(53)80016-0.

[143] Spalding D. Combustion and mass transfer. New York: Pergamon Press; 1979.

[144] Mallard E, Chatelier H Le. Combustion of explosive gas mixtures. Ann Mines 1883;8:274.

[145] Metghalchi M, Keck JC. Laminar burning velocity of propane-air mixtures at high temperature and pressure. Combust Flame 1980;38:143–54. doi:10.1016/0010-2180(80)90046-2.

[146] Bradley D, Hicks RA, Lawes M, Sheppard CGW, Woolley R. The Measurement of Laminar Burning Velocities and Markstein Numbers for Iso-octane–Air and Iso-octane–n-Heptane–Air Mixtures at Elevated Temperatures and Pressures in an Explosion Bomb. Combust Flame 1998;115:126–44. doi:10.1016/S0010-2180(97)00349-0.

[147] Andrews GE, Bradley D. The burning velocity of methane-air mixtures. Combust Flame 1972;19:275–88. doi:10.1016/S0010-2180(72)80218-9.

[148] Wilson CW. Lifting and blowoff of flames from short cylindrical burner ports. Ind Eng Chem 1952;44:2937–42. doi:10.1021/ie50516a046.

[149] Kuznetsov M, Kobelt S, Grune J, Jordan T. Flammability limits and laminar flame speed of hydrogen–air mixtures at sub-atmospheric pressures. Int J Hydrogen Energy 2012;37:17580–8. doi:10.1016/j.ijhydene.2012.05.049.

[150] Manton J, Milliken B. Study of pressure dependence of burning velocity by the spherical vessel method. Proc Gas Dyn Symp Aerothermochemistry 1955:151–7.

[151] Burbano HJ, Pareja J, Amell AA. Laminar burning velocities and flame stability analysis of syngas mixtures at sub-atmospheric pressures. Int J Hydrogen Energy 2011;36:3243–52. doi:10.1016/j.ijhydene.2010.12.001.

[152] Zhu DL, Egolfopoulos FN, Law CK. Experimental and numerical determination of laminar flame speeds of methane/(Ar, N2, CO2)-air mixtures as function of stoichiometry, pressure, and flame temperature. Symp Combust 1989;22:1537–45. doi:10.1016/S0082-0784(89)80164-X.

[153] Davis SG, Law CK. Determination of and fuel structure effects on laminar flame speeds of C1 to C8 hydrocarbons. Combust Sci Technol 1998;140:427–49. doi:10.1080/00102209808915781.

[154] Ranzi E, Frassoldati A, Grana R, Cuoci A, Faravelli T, Kelley AP, et al. Hierarchical and comparative kinetic modeling of laminar flame speeds of hydrocarbon and oxygenated fuels. Prog Energy Combust Sci 2012;38:468–501. doi:10.1016/j.pecs.2012.03.004.

[155] Bosschaart KJ, de Goey LPH. Detailed analysis of the heat flux method for measuring burning

velocities. Combust Flame 2003;132:170–80. doi:10.1016/S0010-2180(02)00433-9.

[156] Law CK, Kwon OC. Effects of hydrocarbon substitution on atmospheric hydrogen–air flame propagation. Int J Hydrogen Energy 2004;29:867–79. doi:10.1016/j.ijhydene.2003.09.012.

[157] Turns S. An introduction to combustion. 1996.

[158] Günther R, Janisch G. Measurements of burning velocity in a flat flame front. Combust Flame 1972;19:49–53. doi:10.1016/S0010-2180(72)80085-3.

[159] Berman M. Sandia Laboratories Report. Sandia Lab Rep 84-0689, 1984.

[160] Liu DDS, MacFarlane R. Laminar burning velocities of hydrogen-air and hydrogen-air steam flames. Combust Flame 1983;49:59–71. doi:10.1016/0010-2180(83)90151-7.

[161] Huang Z, Zhang Y, Zeng K, Liu B, Wang Q, Jiang D. Measurements of laminar burning velocities for natural gas–hydrogen–air mixtures. Combust Flame 2006;146:302–11. doi:10.1016/j.combustflame.2006.03.003.

[162] Dong C, Zhou Q, Zhao Q, Zhang Y, Xu T, Hui S. Experimental study on the laminar flame speed of hydrogen/carbon monoxide/air mixtures. Fuel 2009;88:1858–63. doi:10.1016/j.fuel.2009.04.024.

[163] Scholte TG, Vaags PB. Burning velocities of mixtures of hydrogen, carbon monoxide and methane with air. Combust Flame 1959;3:511–24. doi:10.1016/0010-2180(59)90057-4.

[164] Tang C, Huang Z, Jin C, He J, Wang J, Wang X, et al. Laminar burning velocities and combustion characteristics of propane–hydrogen–air premixed flames. Int J Hydrogen Energy 2008;33:4906–14. doi:10.1016/j.ijhydene.2008.06.063.

[165] Westbrook CK, Adamczyk AA, Lavoie GA. A numerical study of laminar flame wall quenching.

Combust Flame 1981;40:81–99. doi:10.1016/0010-2180(81)90112-7.

[166] Ezekoye O, Greif R, Sawyer RF. Increased surface temperature effects on wall heat transfer during unsteady flame quenching. Symp Combust 1992;24:1465–72. doi:10.1016/S0082-0784(06)80171-2.

[167] Egolfopoulos FN, Zhang H, Zhang Z. Wall effects on the propagation and extinction of steady, strained, laminar premixed flames. Combust Flame 1997;109:237–52. doi:10.1016/S0010-2180(96)00152-6.

[168] Popp P, Smooke M, Baum M. Heterogeneous/homogeneous reaction and transport coupling during flame-wall interaction. Symp Combust 1996;26:2693–700. doi:10.1016/S0082-0784(96)80105-6.

[169] Hocks W, Peters N, Adomeit G. Flame quenching in front of a cold wall under two-step kinetics. Combust Flame 1981;41:157–70. doi:10.1016/0010-2180(81)90049-3.

[170] Hirano T, Kanno Y. Aerodynamic and thermal structures of the laminarboundary layer over a flat plate with a diffusion flame. Symp Combust 1973;14:391–8. doi:10.1016/S0082-0784(73)80038-4.

[171] Hirano T, Kinoshita M. Gas velocity and temperature profiles of a diffusion flame stabilized in the stream over liquid fuel. Symp Combust 1975;15:379–87. doi:10.1016/S0082-0784(75)80312-2.

[172] De Lange HC, De Goey LPH. Numerical flow modelling in a locally refined grid. Int J Numer Methods Eng 1994;37:497–515. doi:10.1002/nme.1620370308.

[173] Lange HC de, Goey LPH de. Two-dimensional Methane/Air Flame. Combust Sci Technol 1993;92:423–7. doi:10.1080/00102209308907681.

[174] Smooke MD, Mitchell RE, Keyes DE. Numerical solution of two-dimensional axisymmetric laminar

diffusion flames. Combust Sci Technol 1986;67:85–122. doi:10.1080/00102208908924063.

[175] Hackert CL, Ellzey JL, Ezekoye OA. Effects of thermal boundary conditions on flame shape and quenching in ducts. Combust Flame 1998;112:73–84. doi:10.1016/S0010-2180(97)81758-0.

[176] Pope S. Turbulent premixed flames. Annu Rev Fluid Mech 1987;19:237–70. doi:10.1146/annurev.fl.19.010187.001321.

[177] Potter AE. Flame quenching. Prog. Combust. Sci. Technol., vol. 1, New York: Pergamon Press; 1960, p. 145–81.

[178] Rallis CJ, Garforth AM. The determination of laminar burning velocity. Prog Energy Combust Sci 1980;6:303–29. doi:10.1016/0360-1285(80)90008-8.

[179] Lange NA, Dean JA. Lange's handbook of chemistry. New York: McGraw-Hill; 1979.

[180] Coles DE, Hirst EA. Memorandum on data selection. Proc Comput Turbul Bound Layers, AFORS-IFP-Stanford Conf Proc 1968:47–55.

[181] Fine B, Wagner P. Space heating rates for some premixed turbulent propane-air flames. NACA TN 3277, 1956.

[182] Berlad A. Flame quenching by a variable-width rectangular-slot burner as a function of pressure for various propane-oxygen-nitrogen mixtures. NACA RM E53K30, 1954.

[183] Griebel P, Boschek E, Jansohn P. Lean blowout limits and NOx emissions of turbulent, lean premixed, hydrogen-enriched methane/air flames at high pressure. J Eng Gas Turbines Power 2007;129:404. doi:10.1115/1.2436568.

[184] Kobayashi H, Seyama K, Hagiwara H, Ogami Y. Burning velocity correlation of methane/air

turbulent premixed flames at high pressure and high temperature. Proc Combust Inst 2005;30:827–34. doi:10.1016/j.proci.2004.08.098.

[185] Kobayashi H, Kawazoe H. Flame instability effects on the smallest wrinkling scale and burning velocity of high-pressure turbulent premixed flames. Proc Combust Inst 2000;28:375–82. doi:10.1016/S0082-0784(00)80233-7.

[186] Venkateswaran P, Marshall AD, Seitzman JM, Lieuwen TC. Turbulent consumption speeds of high hydrogen content fuels from 1–20 atm. J Eng Gas Turbines Power 2013;136:011504. doi:10.1115/1.4025210.

[187] Marshall AD, Venkateswaran P, Seitzman JM, Lieuwen TC. Pressure effects on the turbulent consumption speeds of high H2 mixtures. ASME Turbo Expo, 2012, p. 231. doi:10.1115/GT2012-68305.

[188] Daniele S, Jansohn P, Mantzaras J, Boulouchos K. Turbulent flame speed for syngas at gas turbine relevant conditions. Proc Combust Inst 2011;33:2937–44. doi:10.1016/j.proci.2010.05.057.

[189] Lipatnikov AN, Chomiak J. Turbulent flame speed and thickness: phenomenology, evaluation, and application in multi-dimensional simulations. Prog Energy Combust Sci 2002;28:1–74. doi:10.1016/S0360-1285(01)00007-7.

[190] Beerer D, McDonell V, Therkelsen P, Cheng RK. Flashback and turbulent flame speed measurements in hydrogen/methane flames stabilized by a low-swirl injector at elevated pressures and temperatures. J Eng Gas Turbines Power 2013;136:031502. doi:10.1115/1.4025636.

[191] Kähler CJ, Scholz U, Ortmanns J. Wall-shear-stress and near-wall turbulence measurements up to single pixel resolution by means of long-distance micro-PIV. Exp Fluids 2006;41:327–41. doi:10.1007/s00348-006-0167-0.

[192] Boivin P, Jiménez C, Sánchez AL, Williams FA. An explicit reduced mechanism for H2–air combustion. Proc Combust Inst 2011;33:517–23. doi:10.1016/j.proci.2010.05.002.

[193] Li J, Zhao Z, Kazakov A, Dryer F. An updated comprehensive kinetic model of hydrogen combustion. Int J 2004;36:566–575. doi:10.1002/kin.20026.

[194] Robinson SK. Coherent motions in the turbulent boundary layer! Annu Rev Fluid Mech 1991;23:601–39. doi:10.1146/annurev.fl.23.010191.003125.

[195] Sivashinsky G. Instabilities, pattern formation, and turbulence in flames. Annu Rev Fluid Mech 1983;15:171–99. doi:10.1146/annurev.fl.15.010183.001143.

[196] Eichler C. Flame flashback in wall boundary layers of premixed combustion systems. 2011.

[197] Kalantari A, McDonell V. Boundary layer flashback of non-swirling premixed flames: Mechanisms, fundamental research, and recent advances. Prog Energy Combust Sci 2017;61:249–92. doi:10.1016/j.pecs.2017.03.001.

[198] Kalantari A, Sullivan-Lewis E, McDonell V. Development of Criteria for Flashback Propensity in Jet Flames for High Hydrogen Content and Natural Gas Type Fuels. US Dep Energy, Final Rep 2016. doi:10.2172/1357931.

[199] Akbari A, McDonell V, Samuelsen S. Statistical Evaluation of Rans Simulations Compared To Experiments for A Model Premixer. Eng Appl Comput Fluid Mech 2013;7:103–15. doi:10.1080/19942060.2013.11015457.

[200] Yeung PK, Xu S, Sreenivasan KR. Schmidt number effects on turbulent transport with uniform mean scalar gradient. Phys Fluids 2002;14:4178–91. doi:10.1063/1.1517298.

[201] Phi VM, Mauzey JL, McDonell VG, Samuelsen GS. Fuel Injection and Emissions Characteristics of a

Commercial Microturbine Generator. ASME Turbo Expo, 2004, p. 687–95. doi:10.1115/GT2004-54039.

[202] Hultmark M, Bailey SC, Smits AJ. Scaling of near-wall turbulence in pipe flow. J Fluid Mech 2010;649:103. doi:10.1017/S0022112009994071.

[203] Wu X, Moin P. A direct numerical simulation study on the mean velocity characteristics in turbulent pipe flow. J Fluid Mech 2008;608:81–112. doi:10.1017/S0022112008002085.

[204] Jiménez J. Near-wall turbulence. Phys Fluids 2013;25:101302. doi:10.1063/1.4824988.

[205] Hoferichter V, Hirsch C, Sattelmayer T, Kalantari A, Sullivan-Lewis E, McDonell V. Comparison of Two Methods to Predict Boundary Layer Flashback Limits of Turbulent Hydrogen-Air Jet Flames. Flow, Turbul Combust 2018;100:849–73. doi:10.1007/s10494-017-9882-2.

[206] Hack RL, McDonell VG. Impact of ethane, propane, and diluent content in natural gas on the performance of a commercial microturbine generator. J Eng Gas Turbines Power 2008;130:011509. doi:10.1115/1.2770493.

[207] U.S. Department of Energy, 2013, “Integrated Fuel Flexible Microturbine Generation and Gasification System,” Contract DE-EE0001732, Final Report. n.d.

[208] Kalantari A, McDonell V, Samuelsen S, Farhangi S, Ayers D. Towards Improved Boundary Layer Flashback Resistance of a 65kW Gas Turbine With a Retrofittable Injector Concept. ASME Turbo Expo, 2018.

[209] Bradley D, Lawes M, Liu K, Verhelst S, Woolley R. Laminar burning velocities of lean hydrogen–air mixtures at pressures up to 1.0 MPa. Combust Flame 2007;149:162–72. doi:10.1016/j.combustflame.2006.12.002.

[210] Ó Conaire M, Curran HJ, Simmie JM, Pitz WJ, Westbrook CK. A comprehensive modeling study of hydrogen oxidation. Int J Chem Kinet 2004;36:603–22. doi:10.1002/kin.20036.

[211] Aung KT, Hassan MI, Faeth GM. Flame stretch interactions of laminar premixed hydrogen/air flames at normal temperature and pressure. Combust Flame 1997;109:1–24. doi:10.1016/S0010-2180(96)00151-4.

[212] Kee RJ, Rupley FM, Miller JA. Chemkin-II: A Fortran chemical kinetics package for the analysis of gas-phase chemical kinetics 1989.

[213] Muppala SPR, Aluri NK, Dinkelacker F, Leipertz A. Development of an algebraic reaction rate closure for the numerical calculation of turbulent premixed methane, ethylene, and propane/air flames for pressures up to 1.0 MPa. Combust Flame 2005;140:257–66. doi:10.1016/j.combustflame.2004.11.005.

[214] Hu E, Huang Z, He J, Jin C, Zheng J. Experimental and numerical study on laminar burning characteristics of premixed methane–hydrogen–air flames. Int J Hydrogen Energy 2009;34:4876–88. doi:10.1016/j.ijhydene.2009.03.058.

Appendix-Example Problems

Example Problem 1

A gas turbine combustor is operating on hydrogen at equivalence ratio of 0.4, preheat temperature of 500 K, and operating pressure of 5 atm. To increase the output power, the equivalence ratio is increased to 0.6 at the same operating conditions. Calculate the minimum bulk velocity at the injector (I.D 2.54 cm) to avoid flashback?

Solution:

To obtain Da number from the correlation, all non-dimensional parameters are calculated as following:

$$Da = \exp(-12.06) \cdot Le^{1.68} \cdot {Pe_f}^{1.91} \cdot \left(\frac{T_u}{T_0}\right)^{2.57} \cdot \left(\frac{T_{tip}}{T_o}\right)^{-0.49} \cdot \left(\frac{P_u}{P_0}\right)^{-2.1}$$

Lewis number

$$Le = \frac{\alpha}{D} = 0.3985$$

α and D are calculated at preheat temperature and operating pressure by Transport Property Code.

$$\alpha_{(air/fuel\ mixture)} = 0.1825\ cm^2/s$$

$$D_{(hyrogen\ into\ mixture)} = 0.4580\ cm^2/s$$

Peclet Number

$$Pe_f = \frac{d \cdot S_L}{\alpha} = 1795.4$$

Laminar flame speed is calculated at preheat temperature and operating pressure by Chemical Kinetic Software such as CANTERA, CHEMKIN.

$$d = 2.54\ cm$$

$$S_L = 129\ cm/s$$

Temperature ratio

$$\frac{T_u}{T_0} = \frac{500}{300} = 1.67$$

Tip temperature ratio

$$\frac{T_{tip}}{T_o} = \frac{750}{300} = 2.5$$

Tip temperature is estimated by CFD.

Pressure ratio

$$\frac{P_u}{P_0} = 5$$

Minimum bulk velocity

$$Da = \frac{{S_L}^2}{\alpha \cdot g_c} = 0.1645 \rightarrow g_c = \frac{(129/100)^2}{(0.1825 \times 10^{-4}) \cdot 0.1643} = 554307.37/s$$

$$g_c = 0.03955\, Re_d^{0.75} \frac{\overline{U}}{d} \rightarrow g_c = 0.03955\, \frac{\overline{U}^{1.75}}{d^{0.25} \times \nu^{0.75}}$$

ν is calculated at preheat temperature and operating pressure by Transport Property Code.

$$\overline{U} = \left(\frac{d^{0.25} \times \nu^{0.75} \times g_c}{0.03955}\right)^{1/1.75} = \left(\frac{(2.54/100)^{0.25} \times (0.09345 \times 10^{-4})^{0.75} \times 554307.37}{0.03955}\right)^{1/1.75}$$

$$\overline{U} = 50\, m/s$$

Example Problem 2

A gas turbine combustor is operating on natural gas at equivalence ratio of 0.7, preheat temperature of 600 K, operating pressure of 7 atm, and injector bulk velocity of 40 m/s.

Hydrogen is now used at the same operating conditions, calculate the minimum bulk velocity at the injector to avoid flashback?

Solution:

To obtain Da number from the correlation, all non-dimensional parameters are calculated as following:

$$Da = \exp(-12.06) \cdot Le^{1.68} \cdot {Pe_f}^{1.91} \cdot \left(\frac{T_u}{T_0}\right)^{2.57} \cdot \left(\frac{T_{tip}}{T_o}\right)^{-0.49} \cdot \left(\frac{P_u}{P_0}\right)^{-2.1}$$

Lewis number

$$Le = \frac{\alpha}{D} = 0.4064$$

α and D are calculated at preheat temperature and operating pressure by Transport Property Code.

$$\alpha_{(air/fuel\ mixture)} = 0.1858\ cm^2/s$$

$$D_{(hyrogen\ into\ mixture)} = 0.4572\ cm^2/s$$

Peclet Number

$$Pe_f = \frac{d \cdot S_L}{\alpha} = 2378.7$$

Laminar flame speed is calculated at preheat temperature and operating pressure by Chemical Kinetic Software such as CANTERA, CHEMKIN.

$$d = 2.54\ cm$$

$$S_L = 174\ cm/s$$

Temperature ratio

$$\frac{T_u}{T_0} = \frac{600}{300} = 2$$

Tip temperature ratio

$$\frac{T_{tip}}{T_o} = \frac{850}{300} = 2.83$$

Tip temperature is estimated by CFD.

Pressure ratio

$$\frac{P_u}{P_0} = 7$$

Minimum bulk velocity

$$Da = \frac{{S_L}^2}{\alpha \cdot g_c} = 0.2147 \rightarrow g_c = \frac{{S_L}^2}{\alpha \cdot Da} = \frac{(174/100)^2}{(0.1858 \times 10^{-4}) \cdot 0.2147} = 758963.24\ 1/s$$

$$g_c = 0.03955\ Re_d^{0.75} \frac{\overline{U}}{d} \rightarrow g_c = 0.03955\ \frac{\overline{U}^{1.75}}{d^{0.25} \times \nu^{0.75}}$$

ν is calculated at preheat temperature and operating pressure by Transport Property Code

$$\overline{U} = \left(\frac{d^{0.25} \times \nu^{0.75} \times g_c}{0.03955}\right)^{1/1.75} = \left(\frac{(2.54/100)^{0.25} \times (0.09326 \times 10^{-4})^{0.75} \times 758963.24}{0.03955}\right)^{1/1.75}$$

$$\overline{U} = 60\ m/s$$

	Equivalence ratio	Velocity (m/s)
Natural gas	0.7	40
Hydrogen	0.7	60